World Renewable Energy Congress – Sweden

8–13 May, 2011
Linköping, Sweden

Editor

Professor Bahram Moshfegh

Copyright

Linköping Electronic Conference Proceedings, 57
Linköping University Electronic Press
Linköping, Sweden, 2011

http://www.ep.liu.se/ecp_home/index.en.aspx?issue=057
ISBN: 978-91-7393-070-3
ISSN 1650-3740 (online)
ISSN 1650-3686 (print)

Volume 15

Wind Energy Applications

Table of Contents

Wind energy resources of the South Baltic Sea

Charlotte Hasager[1,*], Jake Badger[1], Ferhat Bingöl[1], Niels-Erik Clausen[1], Andrea Hahmann[1], Ioanna Karagali[1], Merete Badger[1] Alfredo Peña[1]

[1] *Risø National Laboratory for Sustainable Energy, DTU, Roskilde, Denmark*
** Corresponding author. Tel: +45 46775014, Fax: +45 46775970, E-mail: cbha@risoe.dtu.dk*

Abstract: The wind resources of the South Baltic Sea in the area between latitude 54 and 58 degrees North and longitude 10 to 22 degrees East are quantified from state-of-the-art methods using a combination of long-term and short-term mesoscale modeling output and satellite-based methods. The long-term overall statistics based on the NCEP/NCAR re-analysis dataset will be used in combination with more than one year of real time simulations using the Weather Research and Forecasting (WRF) mesoscale model operated at Risø DTU. The satellite Synthetic Aperture Radar (SAR) ocean wind maps and scatterometer ocean wind maps from QuikSCAT will be used to evaluate the wind resource calculation. The advantage of including SAR wind maps for evaluation is the finer spatial detail. In some regions, the mesoscale model may not fully resolve the wind-producing atmospheric structures. The satellites, however, only provides information at 10 m above sea level, whereas the mesoscale model provide results at several heights.

Keywords: *Offshore wind, mesoscale model, satellite data*

1. Introduction

The wind energy resources in the South Baltic Sea are not known in much detail despite the fact that several wind farms are being planned at sea. The existing wind farms are located typically less than 10 km offshore whereas most new wind farms are planned further offshore, up to 80 km. There are plans to construct more than 12GW installed wind farm capacity in the South Baltic Sea. The countries Denmark, Sweden and Germany already have installed offshore wind farms whereas Poland, Russia (Kaliningrad), and the Baltic countries have plans to do so. The web-site http://www.4coffshore.com/windfarms/ provides a listing and map of existing and planned offshore wind farms. It is important to know the wind climate in the planning phase of wind farms, as the expected annual energy production will be proportional to the expected financial benefit of the investment.

The European Wind Atlas[1] covers land areas http://www.windatlas.dk/Europe/Index.htm whereas the corresponding offshore atlas http://www.windatlas.dk/Europe/oceanmap.html covers sea. It is seen that the Baltic Sea is not fully covered. Furthermore, information gained since year 1999, in particular, from satellite Earth observation and from atmospheric mesoscale modeling jointly provides a new opportunity to map the wind resource with higher spatial detail.

The main objective is to provide a new wind atlas for the South Baltic Sea using available satellite images and mesoscale modeling. The results will be evaluated to meteorological data.

The satellite Earth observations used in the South Baltic wind atlas include scatterometer wind vectors from the SeaWinds instrument on-board the QuikSCAT satellite collected from 1999 to 2009 by NASA, and Synthetic Aperture Radar (SAR) data from the Advanced SAR (ASAR) on-board the satellite Envisat collected from 2002 to present by the European Space Agency (ESA).

In the South Baltic Sea a new approach to the numerical wind atlas method[2] based on mesoscale modeling is used. The mesoscale model used for the South Baltic is the Weather

Research and Forecasting (WRF) mesoscale model developed jointly by several US agencies. Additional refinement of the results will be with the microscale model Wind Atlas Analysis and Applications Program (WAsP)[3] developed at Risø DTU. The Weibull distribution scale (A) and shape (k) parameters and energy density are some of the outputs, see[1].

The results from satellite and mesoscale modeling are compared, as well as comparison to meteorological masts. The project is on-going. It is approximately mid-term in regard to finalizing the wind atlas, thus the proceedings paper presents work in progress. The investigated area is shown in Fig. 1. The project is related to the South Baltic Offshore Wind Energy Regions (OFF.E.R.) project with partners from Sweden, Germany, Poland, Lithuania and Denmark. The area and team is indicated in Fig. 1.

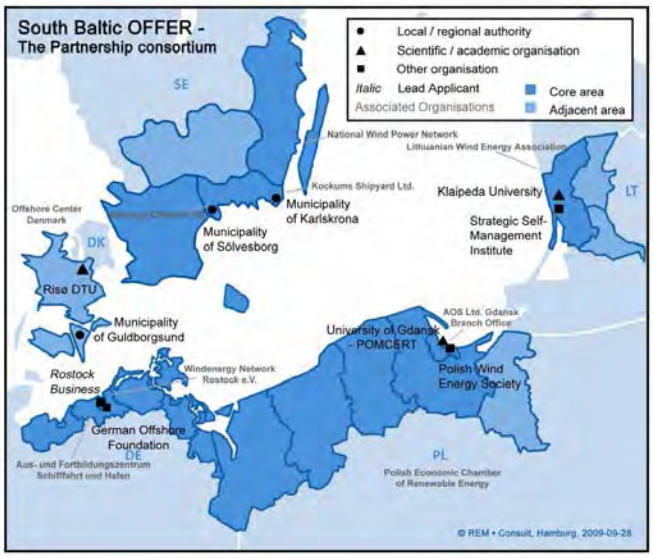

Fig. 1. South Baltic Sea highlighting regions and partners in the South Baltic OFF.E.R. project.

2. Methodology

2.1. Wind profile, meso- and microscale modeling, and satellite remote sensing

The use of satellite remote sensing is motivated by the fact that only satellites provide spatial observations of ocean winds. Meteorological masts observe winds in the local area in which they are located. Meteorological masts are costly to operate. In some cases access to data is restricted. Thus available offshore meteorological mast data in the South Baltic Sea is limited. The advantage of meteorological masts is that observations typically are collected at several heights, and therefore the vertical wind profile can be quantified. It is well known that the wind profile in its simplest form at low heights is logarithmic and that the wind profile in non-neutral atmospheric stratification and at higher heights deviates from the logarithmic profile [4-8]. For wind resource estimation, the most important level is hub-height where the wind turbines harvest the energy.

Satellite ocean winds are mapped at 10 m above sea level. It is clear that wind turbine hub-height is higher, say 80 to 100 m. Thus the satellite-based results have to be extrapolated to higher levels. One option is to use WAsP for the vertical extrapolation. Another option is to use the numerical wind atlas. The latter method is applied in the present context. The advantage of mesoscale modeling is that in such models the advection of air is effectively accounted for through modeling over long distances. In contrast, microscale models account for influences only at shorter distances. In enclosed seas such as the Baltic Sea, the surrounding lands are expected to influence winds over long distances.

2.2. Satellite techniques

The techniques of scatterometer and SAR wind retrievals are presented first. Similarities of the two satellites used – QuikSCAT and Envisat – are that they both map any area at specific local times as both satellites are in sun-synchronous polar orbits. For QuikSCAT the local mapping time is around 6 a.m and 6 p.m. while for Envisat it is around 9 a.m. and 9 p.m. in the South Baltic Sea. Both satellites carry microwave radars, i.e. active instruments sending and receiving microwave signals. Microwave radar works day and night and in all weather conditions. The microwaves penetrate cloud, rain and fog. For QuikSCAT though, rain gives rise to problems in case of heavy rain and therefore rain flags are added to the data such that the user can avoid using rain-affected data.

The physical principle of retrieving oceans winds is similar for scatterometer and SAR. The wind over ocean constantly modulates the sea surface creating capillary and short gravity waves. These very short waves are generated near-instantaneously and decay at the same rate, but appear to be in balance at all times to the mean wind speed as observed at 10 m. The Geophysical Model Function (GMF) that describe the relationship between the backscattered normalized radar cross section is found to be non-linearly proportional to the wind speed, as a function on slant range and relative wind direction in regard to the viewing geometry. For further details on ocean wind mapping see references for scatterometer [9-11] and SAR [12-14]. The nominal accuracy on wind speed is within 2 m s^{-1} for wind speeds between 3 and 25 m s^{-1}.

To highlight major differences between scatterometer and SAR the following may be noted: Scatterometer provides medium spatial resolution, around 25 km by 25 km grid size whereas SAR provides high spatial resolution, around 1 km by 1 km grid size. The resolutions here refer to the final wind results (not the raw sampling which has much higher spatial resolution).

The swath of QuikSCAT was very wide, 1800 km, and this means that most of the globe was mapped twice per day for the 10 years of active observations. This results in roughly 7300 individual ocean wind maps in the South Baltic Sea. The archive is freely available, e.g. from Remote Sensing Systems (http://www.remss.com/qscat/) as so-called level 3 products. This means as gridded geo-coded products of wind speed and wind direction.

In contrast, Envisat ASAR has a swath of 400 km in the so-called wide swath mode (WSM). The sampling in WSM provides a possibility of mapping any location in the South Baltic around 10 times per month. From simple calculation the data could amount to roughly 1000 samples everywhere on the globe. However, Envisat ASAR was and is not always mapping, as the mapping is based 'on demand', typical for science or for commercial activity, and also, the on-board data storage and downlink cannot handle continued operation. The archive at ESA (http://earth.esa.int/EOLi) provide gateway to check the actual data availability. In the present work around 3000 WSM wind maps are used, meaning roughly 400 available samples in each grid cell. For SAR-based wind mapping the raw data are retrieved by Risø DTU and processed into wind maps using the Johns Hopkins University Applied Physics Laboratory software ANSWRS[15].

Finally, an important difference between scatterometer and SAR is that while scatterometer observes the ocean surface from several angles using multiple antennae or rotating antenna (as for QuikSCAT), SAR only views the surface from one direction. This basic difference means that only scatterometer provides both wind speed and direction through the GMF. In order to map wind speed from SAR it is necessary first to estimate the wind direction, and use this *a*

priori information in the GMF. In our case we use the wind direction from the global atmospheric model by the US Navy, the so-called NOGAPS model. Further detail in[12].

2.3. Statistical-dynamical downscaling

The long-term overall statistics based on the NCEP/NCAR re-analysis dataset 1980-2009 will be used in combination with nearly two years of real time simulations using the WRF mesoscale model operated at Risø DTU. The usual procedure at Risø DTU for calculating wind resource with the numerical wind atlas method involves, as a first step, the definition of a set of wind classes. The set of wind classes represent the different wind conditions (wind speed, direction and atmospheric stability) defined from long term, large scale atmospheric reanalysis datasets.

The wind classes are based on geostrophic wind and potential temperature at 0, 1500, 3000, 5500 m above sea level. The wind classes are defined by the distribution of wind speed, direction and stability at one point. For the South Baltic wind atlas the area of interest is large. It is therefore of interest to see how well wind classes defined at one point manages to represent the large scale climate over this large area. There are two issues: 1) do wind classes represent the large scale wind climate well over the entire region of interest; 2) to what extent can a single wind class describe the wind in the region at any given time.

The WRF model is triple nested to the inner domain over Denmark with a 2 km by 2 km grid resolution for the weather forecasts, but the outer grid at an 18 km by 18 km grid covers most of the South Baltic. The weather forecasts plus some additional simulations at higher resolution will be used as basis in the statistical-dynamical downscaling.

3. Results

3.1. Satellite results

Results from the study area using QuikSCAT are shown in Fig. 2. The results are based on all available ocean wind maps from RSS without rain-flag from 10 years, 1999 to 2009. The results are maps of the Weibull A and k parameters. Weibull A is seen to vary from 8.0 to 8.5 m s^{-1} in the South Baltic Sea, and Weibull k is seen to vary from 1.9 to 2.3. Near the coastlines the white area indicates that data are not available.

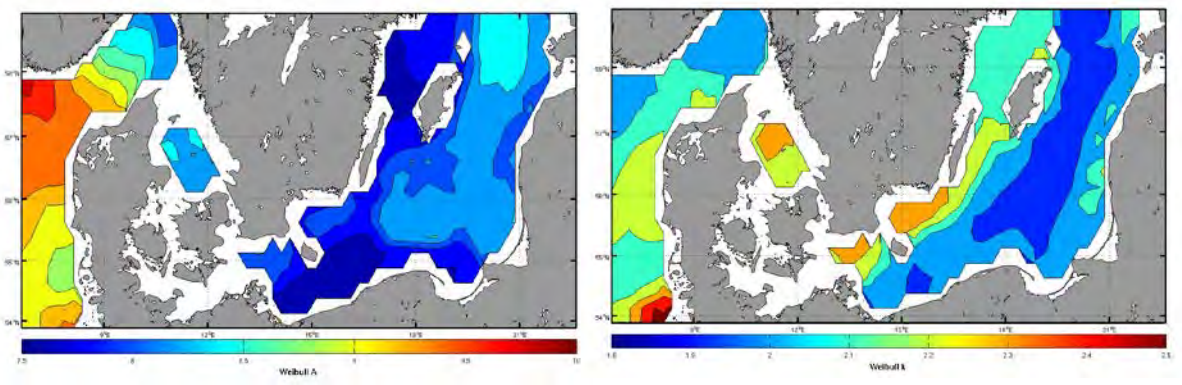

Fig. 2 Weibull A ranging from 7.5 (blue) to 10.0 (red) m $s^{-1}$and Weibull k ranging from 1.8 (blue) to 2.5 (red) in the South Baltic and Danish Seas observed from 10 years of QuikSCAT ocean wind maps. Domain size is 7° to 22° East and 53° to 59° North.

Results from the study area using Envisat ASAR are shown in Fig. 3. The upper panel shows the number of wind maps, the middle panel the mean wind speed, and the lower panel the

energy density. In most of the area there are more than 400 samples. The mean wind speed varies from around 5 m s^{-1} to nearly 11 m s^{-1}. Finally, the energy density varies from 400 to nearly 1200 W m^{-2}. In particular near the coastlines, the energy density is seen to be low. High energy density is found in the open sea.

3.2. Wind class results

Four sets of wind classes were defined, all based on the large scale conditions at 16.25E 56.25N. The sets, named SB1, SB2, SB3, SB4, contain 134, 84, 84, 36 wind classes respectively, see Fig. 4. Sets SB1, SB2, SB4 differ in that a different number of wind classes are allowed for each direction sector (14, 7, 3 respectively) but in each sector the wind speed range of each wind class varies so as to get obtain wind classes with approximately equal frequency of occurrence. Set SB3 uses 7 wind classes per sector, but the wind speed range is fixed and this the frequency of each wind classes varies within each sector.

The first question is, how well do the wind classes represent the large-scale wind climate over the South Baltic. This is answer is: The 134 wind classes of set SB1 capture the wind power in the large scale climate quite accurately with only a small error of less than 3% in the mean of the wind cubed. Whereas the 36 wind classes of set SB4 do more poorly, with an error in the region of 14% in the mean of the wind cubed. Wind classes sets SB2 and SB3 give an error in the region of 5% on the mean of the wind cubed.

The second question concerns to what extent it can be expected that a single wind class, at any given time is influencing the area of interest. The probability of a single wind class acting over a region rapidly drops off when moving away from 16.25E 56.25N. We may conclude that occasions where the same wind class influences large parts of the region of interest happen very rarely. By selecting periods where the wind classes are persistent the probability of locations experiencing the wind class is increased. However, it is not thought that persistency filtering is sufficiently powerful for the South Baltic domain. In conclusion, the variability means that an approach where several wind classes acting more locally, as opposed to acting over the whole domain, will have to be defined and used for the downscaling.

4. Discussion

Satellite wind maps from QuikSCAT provide twice daily 10 year results at 25 km by 25 km resolution. The WRF statistical-dynamical downscaling will provide 30 year results at 5 km by 5 km resolution. Envisat ASAR provides results at 1 km by 1 km resolution. The challenge of using different sources of information is the reliability of each. Comparisons between SAR and three meteorological masts in the North Sea[16] show good agreement, less than 5% error on mean wind speed, Weibull A and k. Comparisons between SAR and meteorological masts in the South Baltic Sea show similar agreement for mean wind speed, but less good agreement for Weibull A and k[17]. Mesoscale model results typically range between 10 to 15% uncertainty. Thus combining satellite wind maps and mesoscale modeling is expected to provide an accurate wind atlas for the South Baltic Sea.

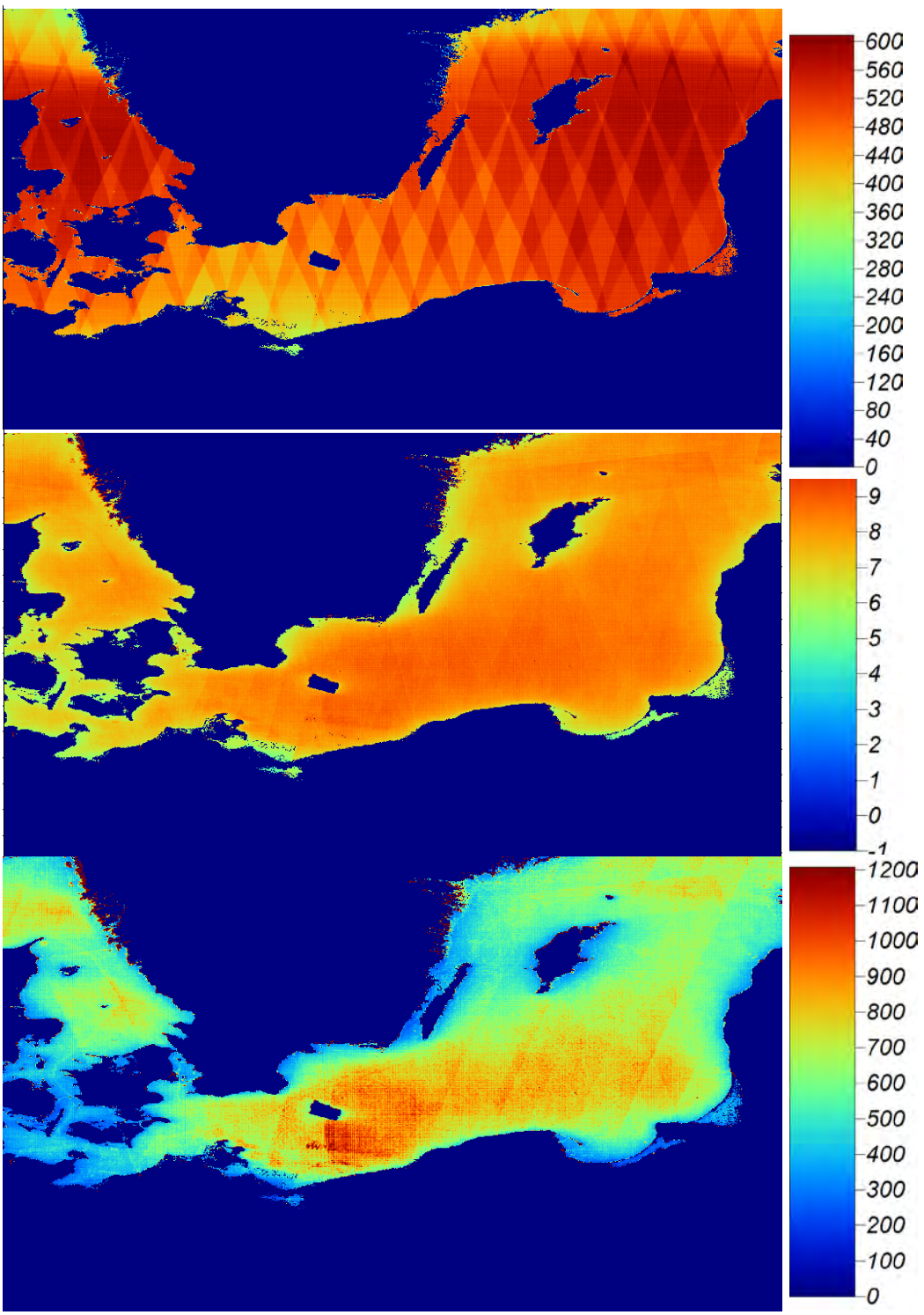

Fig. 3 Envisat ASAR wind maps: (Top) Number of wind speed maps use; (Middle)Mean wind speed in m s^{-1}; (Bottom) Wind energy density in W m^{-2} for the South Baltic Sea. Domain size is 10° to 22° East and 52° to 59° North.

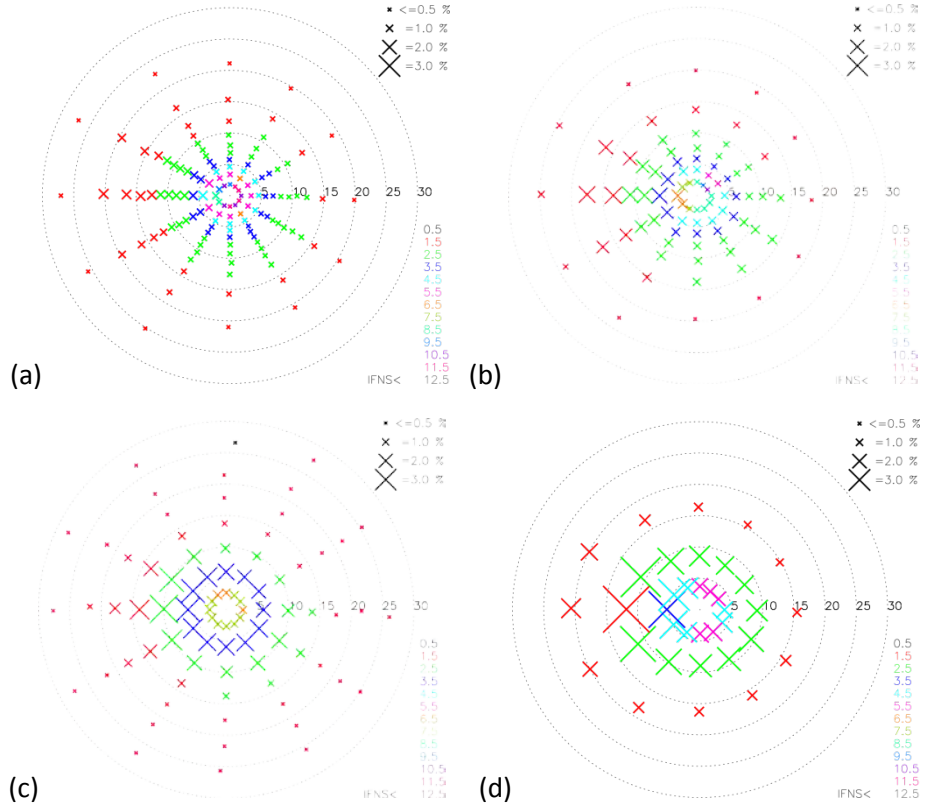

Fig. 4 Four sets of wind classes (a) SB1, (b) SB2, (c) SB3 and (d) SB4. Each cross represents a forcing wind speed (distance from the centre of the diagram) and direction. The speed scale is in m s^{-1}. The colours indicate the inverse Froude number squared (IFNS).

5. Conclusion

The wind atlas for the South Baltic Sea is in progress using satellite remote sensing and mesoscale modeling. The final results will be compared to available meteorological data to estimate the uncertainty of the results. The analysis will be completed in Spring 2011.

Acknowledgements

We acknowledge support from South Baltic OFF.E.R and satellite data from ESA and RSS.

References

[1] I. Troen,; E. L.Petersen, European Wind Atlas; Risø National Laboratory: Roskilde, 1989.

[2] H.Frank; O. Rathmann; N. Mortensen; L. Landberg The Numerical Wind Atlas, the KAMM/WAsP Method;Risø-R-1252(EN); Roskilde, Denmark, 2001.

[3] N. Mortensen; D. N. Heathfield; L. Landberg; O. Rathmann; I. Troen; E.L.Petersen Wind Atlas Analysis and Wind Atlas Analysis and Application program:WAsP 7.0 Help Facility;ISBN 87-550-2667-2; Risø National Laboratory: Roskilde, 2000.

[4] A. Sathe; S.E. Gryning, A. Peña, Comparison of the Atmospheric Stability and Wind Profiles at two Wind Farm Sites over a long marine fetch in the North Sea. Wind Energy **2010,** (in press).

[5] A. Peña; C.B. Hasager, S.E. Gryning; M.Courtney; I. Antoniou; T. Mikkelsen. Offshore wind profiling using light detection and ranging measurements. Wind Energy **2009,** 12, 105-124.

[6] C.B.Hasager; A. Peña; M.B.Christiansen; P.Astrup;M.Nielsen;F.Monaldo;D.Thompson; P.Nielsen.Remote sensing observation used in offshore wind energy. IEEE Journal of Selected Topics in Applied Earth Observations and Remote Sensing **2008,** 1 (1), 67-79.

[7] A.Peña; S.E.Gryning. Charnock's roughness length model and non-dimensional wind profiles over the sea. Boundary-Layer Meteorology **2008,** 128, 191-203.

[8] A.Peña; S.E.Gryning; C.B.Hasager. Measurements and Modelling of the Wind Speed Profile in the Marine Atmospheric Boundary Layer. Boundary-Layer Meteorology **2008,** 129 (3), 479-495.

[9] W.T.Liu;W.Tang Equivalent neutral wind; National Aeronautics and Space Administration, Jet Propulsion Laboratory, California Institute of Technology, National Technical Information Service, distributor: 1996.

[10] H.Hersbach; A.Stoffelen;S.de Haan.An improved C-band scatterometer ocean geophysical model function:CMOD5. J. Geophysical Research **2007,** 112 (C03006).

[11] A.Stoffelen; D.L.T.Anderson. Wind retrieval and ERS-1 scatterometer radar backscatter measurements. Advance Space Research **1993,** 13, 53-60.

[12] M.B.Christiansen;C.B.Hasager;D.R.Thompson;F.Monaldo.Ocean winds from synthetic aperture radar. In Ocean remote Sensing: Recent Techniques and Applications., Niclos, R., Caselles, V., Eds.; Research Singpost Editorial: 2008; pp 31-54.

[13] R.C.Beal; G.S.Young;F. Monaldo; D.R.Thompson; N.S.Winstead; C.A.Schott High resolution wind monitoring with Wide Swath SAR: A user's guide; U.S. Department of Commerce: Washington, DC, 2005.pp. 1-155.

[14] F.Monaldo;D.R.Thompson;N.S.Winstead;W.Pichel;P.Clemente-Colón;M.B.Christiansen. Ocean wind field mapping from synthetic aperture radar and its application to research and applied problems. Johns Hopkins Apl. Tech. Dig. **2005,** 26, 102-113.

[15] F.Monaldo. The Alaska SAR demonstration and near-real-time synthetic aperture radar winds. John Hopkins APL Technical Digest **2000,** 21, 75-79.

[16] M.Badger; J.Badger;M.Nielsen;C.B.Hasager;A.PeñaWind class sampling of satellite SAR imagery for offshore wind resource mapping. J. Applied Meteorology and Climatology **2010,** 49,12,2474-2491.

[17] Hasager, C. B.; Badger, M.; Peña, A.; Larsén, X. G. SAR-Based Wind Resource Statistics in the Baltic Sea. Remote Sensing **2011,** 3,1,117-144.

The wind energy potential in the coasts of Persian Gulf used in design and analysis of a horizontal axis wind turbine

Mehdi Reiszadeh[1], Sadegh Motahar[2,*]

[1]*Islamic Azad University, Shahreza Branch, Shahreza, Iran*
[2] *Department of Mechanical Engineering, Isfahan University of Technology, Isfahan, Iran*
** Corresponding author. Tel: +98 9133219887, Fax: +98 3212239037, E-mail: smotahar@me.iut.ac.ir*

Abstract: There are many wind synoptic stations installed all over Iran. One of these stations in the coasts of Persian Gulf is Bardekhun station in Bushehr province. The goal of this study is to assess the wind energy potential of this region and to design a proper horizontal axis wind turbine for this site. The one-year measured hourly time-series wind speed data are extracted from measurements at a height of 10m, 30m and 40m above the ground level. The Weibull distribution gives the mean wind speed of 4.50 m/s, 5.36 m/s and 5.83 m/s and the power density per year of 125 W/m^2, 196 W/m^2 and 253 W/m^2 respectively for these heights. According to these results, a small wind turbine can be installed in the height of 30m and 40m. A MATLAB code using the blade-element-momentum theory has been developed to design and analyze the three-blade wind turbine rotor. After calculation of geometrical parameters of rotor blade, the rotor power coefficient versus rotor tip speed ratio is evaluated. The energy produced per year by this wind turbine using the Weibull distribution for wind speed will be 155MWh.

Keywords: *Wind potential, Weibull distribution, Wind turbine, produced energy*

1. Introduction

Annual growth in energy consumption and global warming are two important reasons for considering wind as an efficient and clean source of energy. Iran (Persia) is exposed to the continental streams from Asia, Europe, Africa, Indian and Atlantic Pacific. The first vertical axes and drag type windmills on record were built by the Persians in approximately 900 AD [1]. According to the research and studies, it has been estimated that the wind energy potential in Iran is more than 10000 MW for electricity production [2]. There are two wind farm producing electricity in Iran: a 70MW power plant in Manjil and a 28MW power plant in Binalood. Since Iran has many windy regions, utilization of this type of energy would not only be possible but also economically feasible. The Ministry of Energy has serious programs for the evaluation of the wind energy potential in the country. At the first stage, the country's wind energy potential evaluation is performed for a wide range of the country. At the second stage, after the exact investigation on the wind potential, the Iran's wind atlas is prepared. To prepare the wind atlas, 53 wind synoptic stations have been installed all over Iran [3]. These stations record wind data every 10 min. Also, the effects of thunderstorms and turbulences on wind stream are considered in the results.

In the recent years, many researchers have studied the wind energy potential in Iran. Mostafaeipour and Abarghooei [4] investigated the wind energy potential in Manjil area in the north of Iran. They reported it is one of the best locations in the world for installing wind turbine. Mostafaeipour [5] utilized wind speed data over a period of almost 13 years between 1992 and 2005 from 11 stations in Yazd province to assess the wind power potential at these sites. The results showed that most of the stations have annual average wind speed of less than 4.5 m/s which is considered as unacceptable for installation of the wind turbines. Keyhani et al [6] used the statistical data of eleven years wind speed measurements of the capital of Iran, Tehran to find out the wind energy potential. They concluded that the site studied is not suitable for electric wind application in a large-scale and the wind potential of the region can be adequate for non-grid connected electrical and mechanical applications, such as wind

generators for local consumption, battery charging, and water pumping. Mostafaeipour [7] performed an analysis of offshore wind speed in global scale and also studied feasibility of introducing this technology for harnessing wind in Persian Gulf, Caspian Sea, Urmia Lake and Gulf of Oman. He suggested that policy makers to invest and pay more attentions toward harnessing renewable energy sources like offshore wind in Persian Gulf and Gulf of Oman in southern parts of Iran.

This paper presents a study of the wind energy potential in the Bardekhun station. Knowledge of the wind speed distribution is a very important factor to evaluate the wind potential in the windy areas. The Weibull distribution is the best one, with an acceptable accuracy level. A stall-regulated horizontal wind turbine with nominal power of 50kW is designed for this wind station. A MATLAB code was written based on the BEM theory. This code utilizes a generalized rotor design procedure in determining the final blade shape and performance iteratively considering drag, tip losses, and ease of manufacture.

2. Site description and the wind data

This site is located in the vicinity of Deyer port in Bushehr province in the coasts of Persian Gulf. It is situated in the latitude of 27°98' N, the longitude of 51°49' W and the altitude of 4m. Its distance from capital city of Iran, Tehran, is about 1330 km. A well known wind in this region is North Wind which has effect on the architectural and environmental design of buildings. The one-year measured hourly time-series wind speed data, from January 1, 2007 to December 31, 2007 are extracted from Renewable Energy Organization of Iran, SUNA [2].

3. Wind data analysis

3.1. Weibull distribution

Statistical analysis can be used to determine the wind energy potential of a given site and to estimate the wind energy output at this site [1]. This type of analysis relies on the use of the probability density function, *p(U)*, of wind speed. One way to define the probability density function is that the probability of a wind speed occurring between U_a and U_b is given by:

$$p(U_a \le U \le U_b) = \int_{U_a}^{U_b} p(U)dU \tag{1}$$

Where U is wind speed and $\int_0^\infty p(U)dU = 1$.

In general, Rayleigh and Weibull probability density functions are used in wind data analysis. The Rayleigh distribution uses one parameter, the mean wind speed ($\overline{U}$). Determination of the Weibull probability density function requires knowledge of two parameters: k, shape factor and c, scale factor. Both these parameters are a function of wind speed, U, and standard deviation of wind speed, σ_U. The Weibull probability density function is given by:

$$p(U) = \left(\frac{k}{c}\right)\left(\frac{U}{c}\right)^{k-1} \exp\left[-\left(\frac{U}{c}\right)^{k}\right] \tag{2}$$

The cumulative distribution function of the speed U gives us the fraction of time (probability) that the wind speed is equal or lower than U. the cumulative distribution *F (U)* is given by:

$$F(U) = 1 - \exp\left[-\left(\frac{U}{c}\right)^{k}\right] \tag{3}$$

The parameters *c* and *k* are calculated based on the following empirical formulas [1, 8]:

$$k = \left(\frac{\sigma_U}{\overline{U}}\right)^{-1.086}, \frac{c}{\overline{U}} = \frac{k^{2.6674}}{0.184 + 0.816k^{2.73855}} \tag{4}$$

Annual energy produced by a wind turbine with performance curve $P_w(U)$ is [1, 9]:

$$\overline{P_w} = 365 \times 24 \int_0^{\infty} p(U)P_w(U) = 365 \times 24 \times \sum_{i=1}^{N_B} \frac{1}{2}(U_{i+1} - U_i)\left(p(U_{i+1})P_w(U_{i+1}) + p(U_i)P_w(U_i)\right) \tag{5}$$

3.2. Power density

The wind power per unit area, or wind power density, is proportional to the density of the air (for standard conditions sea-level, 15°C, the density of air is 1.225 kg/m^3), the area swept by the rotor (or the rotor diameter squared for a conventional horizontal axis wind machine) and the cube of the wind velocity. The average wind power density is:

$$\frac{\overline{P}}{A} = \frac{1}{2}\rho \int_0^{\infty} U^3 p(U)dU \tag{6}$$

4. Wind turbine aerodynamic design

The primary aerodynamic factors affecting the blade design are: design rated power and rated wind speed, design tip speed ratio, solidity, airfoil, number of blades, rotor power control (stall or variable pitch), rotor orientation (upwind or downwind of the tower) [1]. The analysis here uses momentum theory and blade element theory. Momentum theory refers to a control volume analysis of the forces at the blade based on the conservation of linear and angular momentum. Blade element theory refers to an analysis of forces at a section of the blade, as a function of blade geometry. The results of these approaches can be combined into what is known as strip theory or blade-element- momentum (BEM) theory. This theory can be used to relate blade shape to the rotor's ability to extract power from the wind. The analysis in this paper covers a simple optimum blade design including wake rotation and an infinite number of blades. This blade design can be used as the start for a general blade design analysis. The forces on the blades of a wind turbine can also be expressed as a function of lift and drag coefficients and the angle of attack. In this analysis, the blade is assumed to be divided into *N* sections (or elements) [1, 9].

5. Results and discussions

5.1. Wind energy potential

The data collected for an interval of 10 min have been used to analyze the wind energy potential of this site. All measurements in the wind station are recorded using the cup anemometer at a height of 10m, 30m and 40m above the ground level.

5.1.1. Wind speed distribution

The most critical factor influencing the power developed by a wind energy conversion system is the wind speed. Due to the cubic relationship between speed and power, even a small variation in the wind speed may result in significant change in power.

Results of wind data analysis at three different heights have been summarized in Table 1.The mean wind speed, mean cubic wind speed, standard deviation of wind data and the Weibull distribution parameters for each height are calculated. Maximum wind speed per year and its occurrence time can be used in control and structural analysis of wind turbines. These results obtained for one-year measured data.

Table 1. Results of wind data analysis at different heights

	Height		
	40m	30m	10m
Mean wind speed (m/s)	5.83	5.36	4.50
Mean cubic wind speed (m/s)	7.50	6.96	6.00
Standard deviation	3.313	3.042	4.506
Max. wind speed per year (m/s)	33 (11/4/2007 23:50)	31.1 (11/4/2007 23:50)	28.2 (15/3/2007 11:00)
Weibull distribution constants	k=1.848 c=6.568	k=1.850 c=6.037	k=1.737 c=5.058

The corresponding average wind speeds and best fits to the Weibull distribution at 30m and 40m height in comparison with the distribution of measured data are shown in Fig.1. The Weibull scale and shape factors can be found in Table 1 at each height. As shown in Fig. 1(a), the Weibull distribution function reaches the top point at about 4.00 m/s with a value of about 13.54%, however the Weibull distribution function in Fig. 1(b) reaches the top point at about 4.00 m/s with the value of frequency equal to 12.39%.

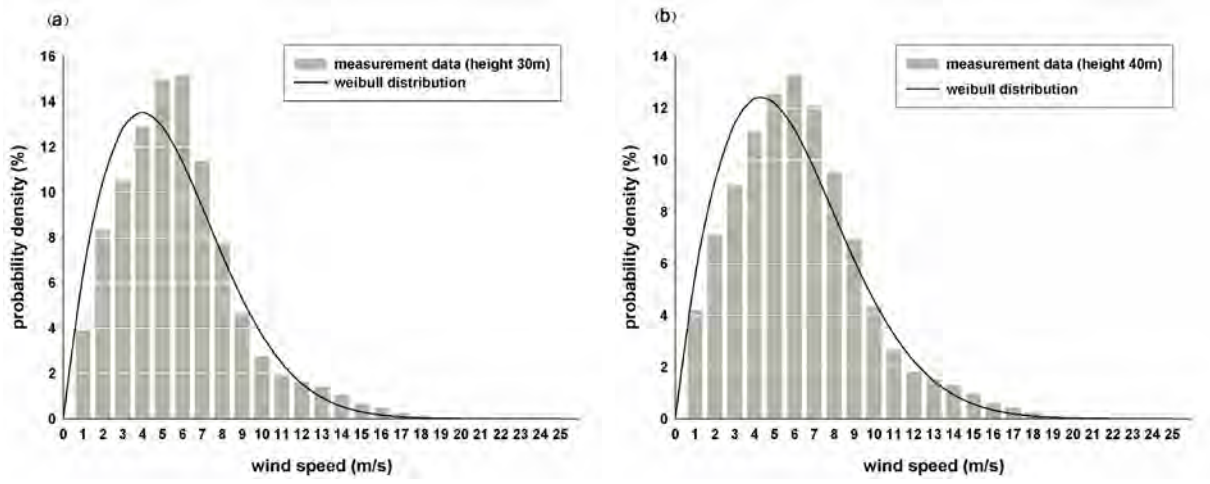

Fig. 1. Weibull probability distribution function at (a) 30m (b) 40m

Fig. 2(a) illustrated the Weibull distribution function at the height of 10m. The distribution of measured data can be seen in this figure. The Weibull distribution reaches to the maximum

frequency of 15.61% at the wind speed around 3.00m/s. The cumulative distribution functions at three given heights are shown in Fig. 2(b). According to this figure, the cumulative density at 40m gets up to 56.50% for mean wind speed of 5.83m/s. This probability is 52.62% and 50.47% for mean wind speed of 5.36m/s and 4.50m/s at 30m and 10m heights, respectively.

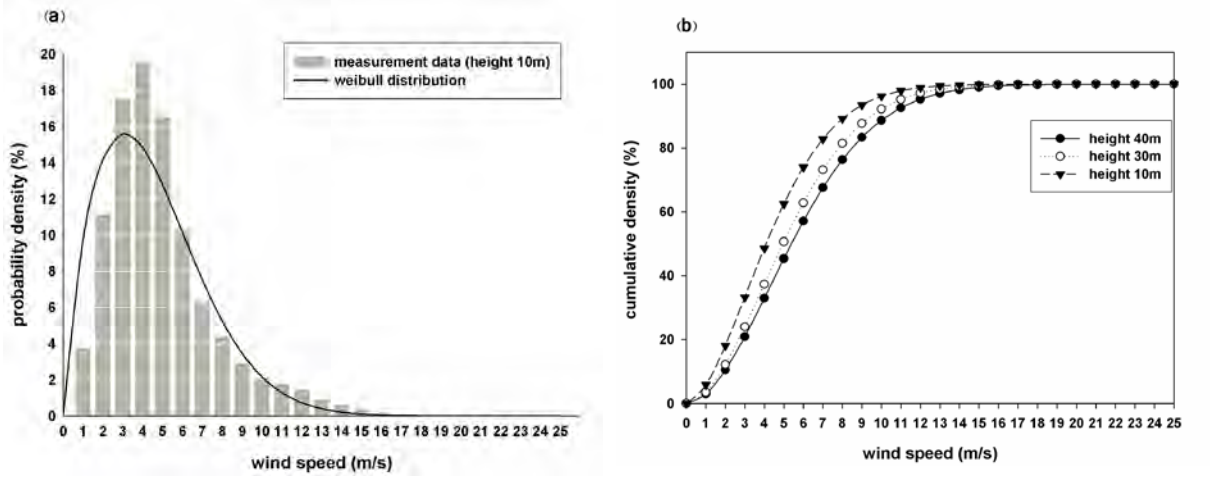

Fig. 2. (a) Weibull probability distribution function at 10m (b) Cumulative function at three heights

5.1.2. Estimation of monthly wind potential

The monthly distribution of the wind speed measured between January 1, 2007 and December 31, 2007 is plotted in Fig. 3(a). It can be seen from this figure, the wind speeds vary between 3.34 and 7.52 m/s. According to these results, the average speed for 10 m is 4.50 m/s. This is below the minimum speed, 5.0 m/s, required for effective wind turbines, but it is enough for water pumping applications. The monthly average wind power density at height of 40m is illustrated in Fig. 3(b). The wind potential of a site, i.e. average power density, which is proper to run a wind turbine, is qualitatively estimated based on the following [1]: $\overline{P}/A$<100 W/m^2 is a poor potential, $\overline{P}/A\approx$400 W/m^2, is a good potential, and $\overline{P}/A$>700 W/m^2 is a great potential. Here, there is a poor potential in October, September and August, because the power density is near to 100 W/m^2 in these months. For the reminders of the year, there is a reasonable potential.

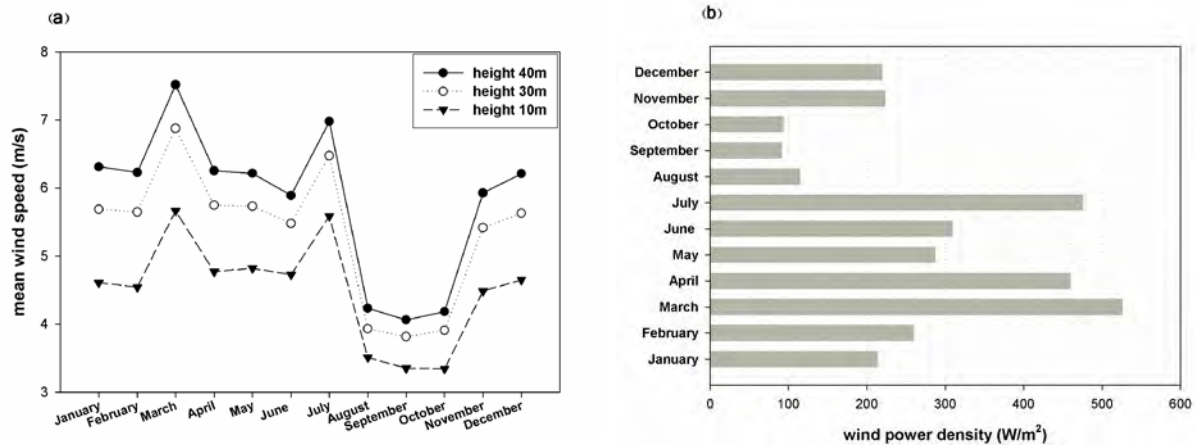

Fig.3. (a) Monthly average wind speed at three heighs (b) Monthly power density at 40m

5.1.3. Wind potential in the site

If annual average wind speeds are known for a certain site, the average wind power density can be found over these regions. Fig. 4 illustrates the power densities per year at three heights. These power densities are drawn for measured data and for the Weibull distribution function. The Weibull distribution function illustrates power density per year a little lower than measured data. The wind power density per year at height of 10m is suitable for water pumping, because it is not actually a good potential. The power density at height of 40m and 30m are more reasonable. A proper wind turbine can be run by the wind at these heights. In the next section, a wind turbine designed and proposed for installation at 40m.

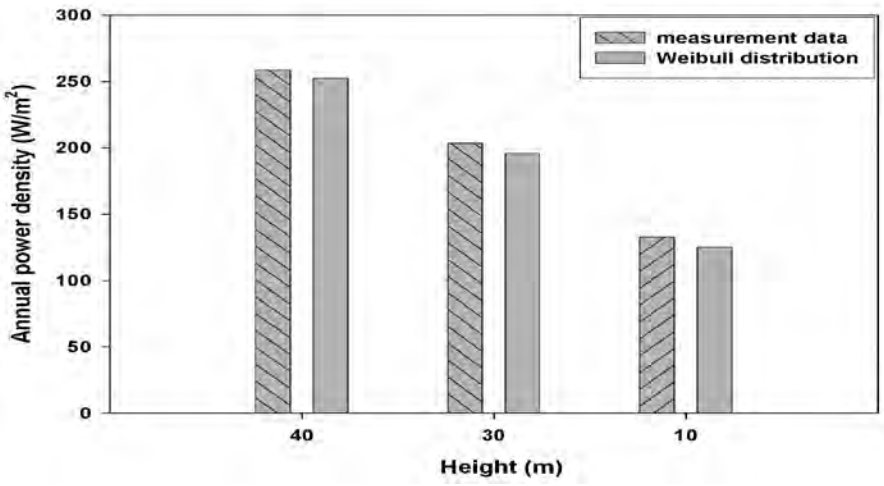

Fig.4. power density per year at three heights

5.2. Wind turbine design and performance results

In order to utilize the wind energy potential for the mentioned site, a power of 50kW is needed at 7.50m/s wind speed (mean cubic wind speed at 40m height). For this purpose, a 3-blade, stall-regulated and upwind horizontal axis wind turbine (HAWT) has been designed based on the BEM theory. The blade has NACA 4415 airfoil and has a tip speed ratio of λ=6.

5.2.1. Blade geometry

To develop the maximum possible power coefficient (C_p) requires suitable blade geometry. The geometrical parameters for blade design are shown in Table 2. Assume the mechanical efficiency and the overall rotor power coefficient are 0.99 and 0.40, respectively. With these assumptions, the radius of rotor will be R=13m. The blade is divided into *N* elements (usually 10-20). The first column, r/R, is fraction of rotor radius. The straight line connecting the leading and trailing edges is the chord line of the airfoil, and the distance from the leading to the trailing edge measured along the chord line is designated as the chord, *c*, of the airfoil (second column in Table 2). The section pitch angle (θ_p) is the angle between the chord line and the plane of rotation. $\theta_{p,0}$ is the blade pitch angle at the tip. The relative wind is the vector sum of the wind velocity at the rotor and the wind velocity due to rotation of the blade. The angle between the chord line and the relative wind is the angle of relative wind ($\varphi = \theta_p + \alpha$).The blade twist angle is the difference between section pitch angle and the blade pitch angle at the tip, i.e. $\theta_T = \theta_p - \theta_{p,0}$. The design aerodynamic condition occurs when C_d/C_L is at a minimum for each blade section. The aerodynamic properties of the airfoil at each section, i.e. C_L-α (lift coefficient vs. angle of attack) and C_d-α (drag coefficient vs. angle of attack) can be obtained from the empirical curves.

Table 2. Blade design of a 26m-diameter Rotor

r/R	Chord (m)	Twist angle (degree)	Angle of relative wind (degree)	Section pitch (degree)
0.0500	2.0091	42.5590	48.8672	42.8672
0.1000	2.6631	33.0493	39.3575	33.3575
0.1500	2.6778	25.7003	32.0085	26.0085
0.2000	2.4742	20.2288	26.5370	20.5370
0.2500	2.2268	16.1518	22.4600	16.4600
0.3000	1.9939	13.0615	19.3696	13.3697
0.3500	1.7907	10.6673	16.9753	10.9756
0.4000	1.6174	8.7717	15.0793	9.0799
0.4500	1.4704	7.2405	13.5474	7.5488
0.5000	1.3453	5.9818	12.2870	6.2900
0.5500	1.2380	4.9307	11.2330	5.2389
0.6000	1.1450	4.0412	10.3374	4.3494
0.6500	1.0634	3.2794	9.5639	3.5876
0.7000	0.9903	2.6201	8.8820	2.9283
0.7500	0.9225	2.0443	8.2625	2.3525
0.8000	0.8558	1.5373	7.6712	1.8455
0.8500	0.7825	1.0876	7.0541	1.3958
0.9000	0.6856	0.6861	6.2952	0.9943
0.9500	0.5029	0.3255	4.9618	0.6338

5.2.2. HAWT performance curves

The Betz limit, $C_{P,max} = 0.59$, is the maximum theoretically possible rotor power coefficient. In practice three effects lead to a decrease in the maximum achievable power coefficient: rotation of the wake behind the rotor, finite number of blades and associated tip losses, and non-zero aerodynamic drag [1]. Although the blade has been designed for optimum operation at a specific design tip speed ratio, the performance of the rotor over all expected tip speed ratios needs to be determined. The results are usually presented as a graph of power coefficient versus tip speed ratio, called a C_P-λ curve, as shown in Fig. 5(a). The maximum value of C_P in C_P-λ curve, Fig. 5(a), is 0.4586 at λ=6. C_P-λ curves can be used in wind turbine design to determine the rotor power for any combination of wind and rotor speed. They provide immediate information on the maximum rotor power coefficient and optimum tip speed ratio.

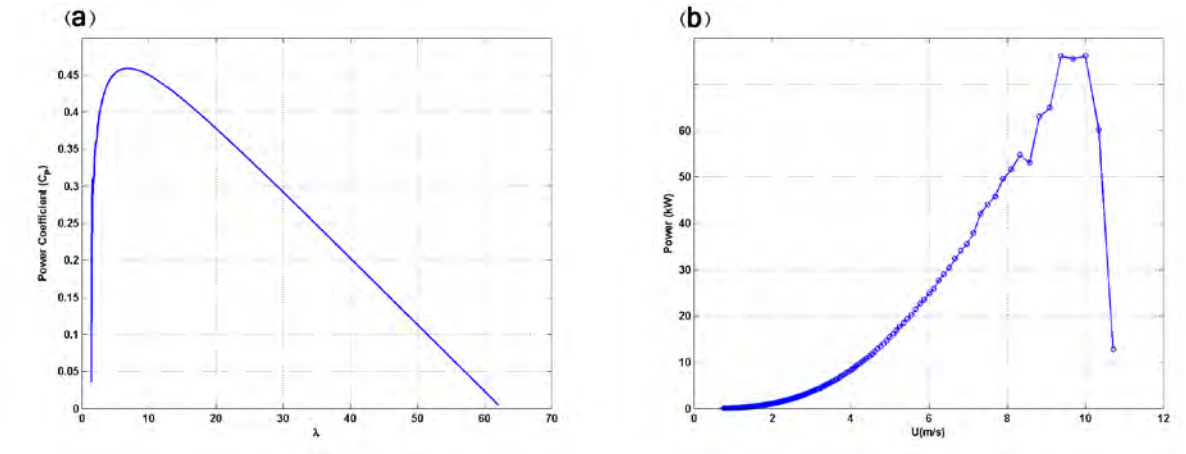

Fig. 5 (a) C_P-λ curve (b) Rotor power vs. wind speed

Fig. 5(b) illustrates the power produced by the wind turbine in various wind speeds. In order to estimate the energy captured per year by this wind turbine, $p(U)$ and $P_w(U)$ are obtained from Fig. 1(b) and Fig. 5(b) respectively and are put in the Eq. (5). So, the energy of the wind turbine per year will be 155 MWh.

6. Conclusions

In this study, a site in the coasts of Persian Gulf was evaluated for wind potential. Statistical analysis of wind data at three heights, 10m, 30m and 40m, showed that there is a promising wind potential for installing wind turbine at height of 30 and 40m. The power density per year at these two heights was 253 and 196 W/m^2, respectively. In the second part of paper, a 50kW horizontal axis wind turbine was designed for installing at 40m. The energy produced per year by this turbine was 155MWh. The wind potential in this coastal region can be utilized for both water pumping and electricity generation by small wind turbine. It might be suitable for the rural parts of Bushehr.

References

[1] J.F. Manwell, J.G. McGowan, A.L. Rogers, Wind Energy Explained: Theory, Design and Application, John Wiley & Sons Ltd, 2002.

[2] Renewable Energy Organization of Iran, http://www.suna.org.ir/ .

[3] M. Ameri, M. Ghadiri and M. Hosseini, Recent Advances in the Implementation of Wind Energy in Iran, The 2nd Joint International Conference on S ustainable Energy and Environment (SEE 2006), Bangkok, Thailand, November 2006.

[4] A. Mostafaeipour and H. Abarghooei, Harnessing wind energy at Manjil area located in north of Iran, Renewable and Sustainable Energy Reviews, 12(6), 2008, pp. 1758-1766.

[5] A. Mostafaeipour, Feasibility study of harnessing wind energy for turbine installation in province of Yazd in Iran, Renewable and Sustainable Energy Reviews, 14, 2010, pp.93-111.

[6] A. Keyhani, M . Ghasemi-Varnamkhastia, M . Khanalia, and R. Abbaszadeh, An assessment of wind energy potential as a power generation source in the capital of Iran, Tehran, Energy, 35(1), 2010, pp. 188-201.

[7] A. Mostafaeipour, Feasibility study of offshore wind turbine installation in Iran compared with the world, Renewable and Sustainable Energy Reviews, 14(7), 2010, pp. 1722-1743.

[8] A. Balouktsis, D. Chassapis and T.D. Karapantsios, A nomogram method for estimating the energy produced by wind turbine generators, Solar Energy, 72(3), 2002, pp. 251-259.

[9] T. Burton, D. Sharpe, N. Jenkins and E. Bossanyi, Wind Energy Handbook, John Wiley & Sons Ltd, 2001.

Measurements of the wind energy resource in the Latvia

P. Shipkovs[1]*, V. Bezrukov[1], V. Pugachev[1], Vl. Bezrukovs[2], V. Silutins[3]

[1] *Institute of Physical Energetics (IPE), Riga, Latvia,*
[2] *Ventspils University College (VUC), Ventspils, Latvia*
[3] *Encom Ltd, Riga,Latvia*
** Corresponding author. Phone/Fax: +37167553537, e-mail: shipkovs@edi.lv*

Abstract: In the Baltic countries interest to the renewable energy is growing. Government support and availability of large unpopulated areas on the coast makes attractive use of these lands for the placement of large wind power plants (WPP). For successful implementation of planned projects reliable information about distribution of the resource of wind energy is needed. Researches in this area are carried out by collaboration IPE with VUC. The paper presents the results of years-long observations on the density fluctuations of wind energy at heights of 10 to 60 *m* in the area in the Baltic Sea coast in the north and the south-west of Latvia. The velocity observations from 2004 till 2010 years have been obtained by measurements complex of the LOGGER 9200 Symphonie type. The results presented in the form of tables, bar charts and graphs. The graphs of seasonal fluctuations of wind speed have been obtained for the heights up to 60 *m* by measurements over the period of 2007 – 2010. The histograms have been composed for the relative frequency of repetition of wind speed. The wind speed distribution on heights up to 60 *m* was analysed and coefficients of approximating functions for the two areas with different terrain types were calculated. Extrapolation results of the distribution curves of wind velocity and density mean values on heights up to 150 *m* were shown.

Keywords: *Wind energy, Measurement of wind speed, Wind speed approximation at 150 m, Wind energy density fluctuation, Acoustic noise level*

1. Introduction

The availability of large unpopulated coastal areas and the developed infrastructure of electric power networks in the Baltic countries make attractive the use of these areas for siting large wind power plants (WPP). In the coastal territories of western Estonia, in the Ida-Virumaa region at the site of the former shale quarries the construction of WPPs is planned whose power will be over 600 *MW*. Further it is also planned to start offshore WPP construction. In Latvia, projects on the construction of 450 *MW* coastal WPPs have been approved; there are also projects as to the construction of a 900 *MW* wind park offshore. In Lithuania, the total power of wind parks in 2010 has made up 200 *MW*, with 1000 *MW* to be reached; after 2020 it is planned to start works in the offshore territories. In Latvia, planned preparation of the infrastructure is going on: construction of thermal power plants and of the transmission line "Kurzeme Arc" (by 2017), which would allow for construction of a ~900 *MW* WPP in the sea near Liepaja (by 2020). The governmental support is confirmed by working out administrative and legislative regulations as well as by creating a favourable tariff policy that would encourage the construction of large WPPs. At the same time, for the territory of the Baltic countries there are no databases of long-term measurements of wind speeds at different heights that can be used to compose an atlas of wind energy resource distribution in this region. The systematic long-term measurements of wind speeds in Latvia since 2007, taking into account the wind speed distribution on several levels, have been carried out in the two sites: on the south-west coast of the Baltic Sea in the Ventspils region and on the north of the country in the Ainaži region in 35 *km* from the shore [1]. The places where the metrological masts are situated are shown on the map of Fig. 1 by black stars. On the same map, by dark grey colour the regions are indicated which, according to the forecasts of meteorological observations and being territorially remote from populated areas, could be promising for siting WPPs.

Fig. 1. The coastal map of Baltic countries with the places of interest for siting WPPs indicated.

2. Research on the cyclic behaviour of wind energy fluctuations

The measurements of wind speed were carried out using certified sensors of wind speed of the NRG #40 type and sensors indicating the direction of the air stream of the NRG #200P type. The sensors are arranged on metallic masts with the height of 53 and 60 *m* above the ground. The periodicity of the information read-out from the sensors at all the height levels was 10 *s*. For storing information an NRG LOGGER Symphonie complex was employed, which has independent supply from batteries and is able to store information from nine sensors in the memory card during a year.

In the observation period a database has been built up containing the wind speed values at heights of 10, 20, 30, 40 , 50 and 60 *m*, wind temperature and direction in two regions in the Latvian territory. At the present time, the database contains more than 3'000'000 records of measurements. To compare the wind energy flow levels on the sea shore in the Ventspils region and in the area remote from the sea in the Ainaži region, in Table 1 average wind speed values, V_a, are given, with standard deviations *SD*, and the wind energy density values, P_d, W/m^2. Dark colour in the table corresponds to a larger value of wind speed or energy density for the month.

The charts of seasonal fluctuations of average wind speed *V* (*m/s*) for the measurement period *T* (*a month*) at the heights 20, 30, 40, 50 *m* in the Ventspils region and 10, 30, 50, 60 *m* in the Ainaži region are shown in Figs. 2 and 3. The results of wind speed measurements taken in the Ventspils and Ainaži regions are systematized and presented in the form of histogram in Figs. 4 and 5. The envelope of the histogram shows the wind speed *V* distribution in the relative frequency of repetition *F*, which corresponds to the relation $F = \frac{T_V}{T} \cdot 100\%$, where T_V is the total duration of wind with the speed *V* in the whole measurement period *T* for the heights 20, 30, 40, 50 *m* in the Ventspils region and 10, 30, 50, 60 *m* in the Ainaži region.

Table 1. Distribution of average wind speed values with standard deviations and corresponding power density values at the height 50 (m) in the observation period.

		Ventspils			Ainaži		
Year	**Month**	V_a, (m/s)	SD, (m/s)	P_d, (W/m^2)	V_a, (m/s)	SD, (m/s)	P_d, (W/m^2)
2009	April	4.27	0.78	76.92	4.48	0.72	85.53
	May	4.82	0.97	93.59	4.58	0.81	93.10
	June	4.80	0.99	95.32	4.56	0.84	97.48
	July	4.28	0.83	77.96	3.87	0.65	57.99
	August	4.37	0.80	73.82	4.14	0.67	64.92
	September	5.04	1.03	113.19	4.61	0.74	83.86
	October	4.78	1.07	151.59	5.00	0.79	139.02
	November	4.97	1.12	103.52	4.73	0.79	84.99
	December	4.23	0.88	81.45	3.98	0.63	66.16
2010	January	3.60	0.67	56.48	3.01	0.43	47.71
	February	3.58	0.74	47.95	3.32	0.48	43.83
	March	4.88	1.08	105.12	4.91	0.81	107.57
	April	3.71	0.80	52.75	4.14	0.71	68.58
	May	4.02	0.88	68.15	4.16	0.77	75.45
	June	4.36	0.91	88.80	4.23	0.79	78.83
	July	4.02	0.76	55.71	3.42	0.61	38.88
	August	4.09	0.81	67.83	3.88	0.68	63.92
	September	4.99	1.02	116.10	4.81	0.70	107.69
	October	4.98	0.99	120.17	5.08	0.78	120.79
	Average:	**4.41**	**0.90**	**86.65**	**4.26**	**0.71**	**80.33**

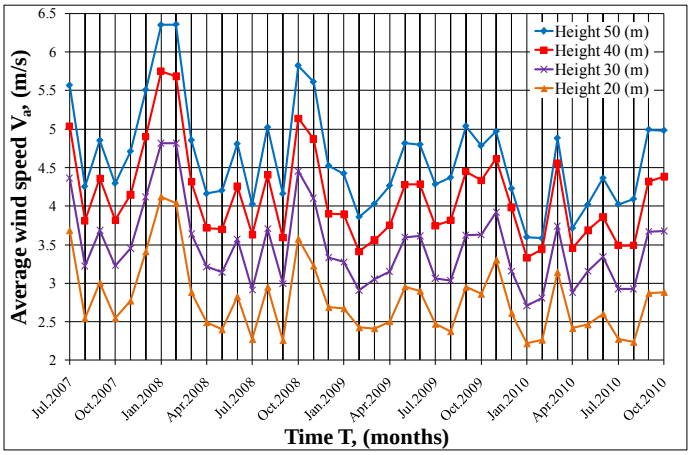

Fig. 2. Average wind speed values V_a in period T (2007/2010) at heights 10, 30, 40 and 50 (m) in the Ventspils region.

The histogram allows determination of the wind energy flow density, which is calculated by the equation:

$$P_d = \rho \frac{V_{a.c.}^3}{2} = \rho \frac{\sum_{n=0}^{n} V_n^3 F_n}{2 \cdot 100}, \qquad (1)$$

where $V_{a.c.}$ – is the average cubic wind speed, *m/s*,

$\rho = 1.23\ kg/m^3$ – is the air density at atmosphere pressure *101.325 kPa* and temperature *15° C*,

V_n – is the wind speed, *m/s*,

F_n – is the relative frequency of repetition, %, corresponding to wind speed V_n and determined by curves on the histograms of Figs. 4.

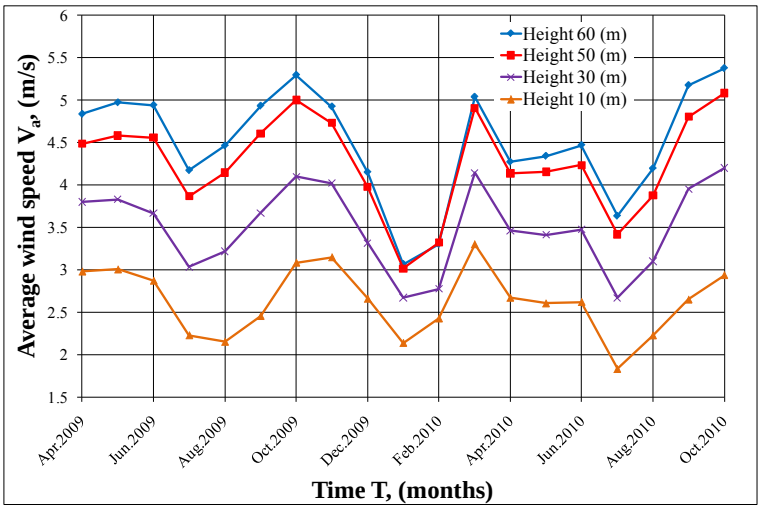

Fig.3. Average wind speed values V_a in period T (2009/2010) at heights 10, 30, 50 and 60 (m) in the Ainaži region.

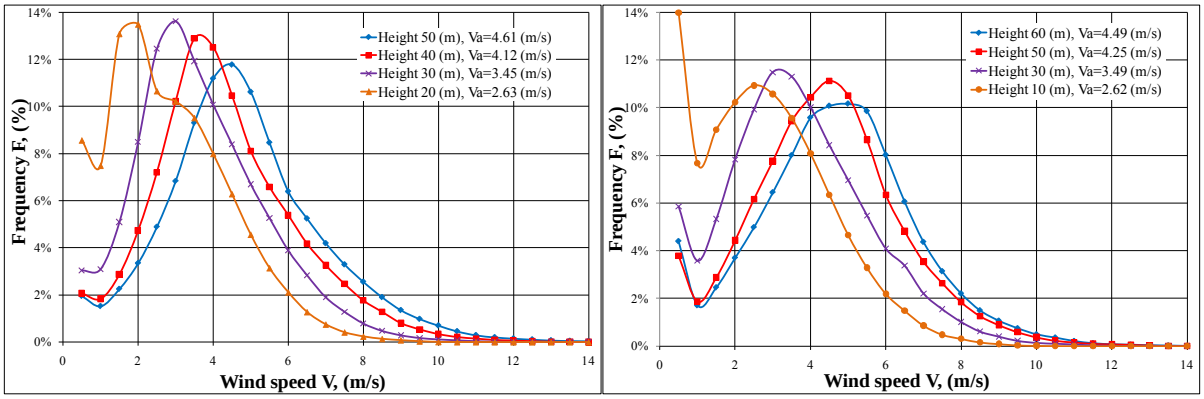

Fig. 4 (left). Distribution of wind speed in relative frequency of repetition F= f(V) at heights 10, 30, 40 and 50 (m) in the Ventspils region and Fig. 4 (right). Distribution of wind speed in relative frequency of repetition F= f(V) at heights 20, 30, 50 and 60 (m) in the Ainaži region.

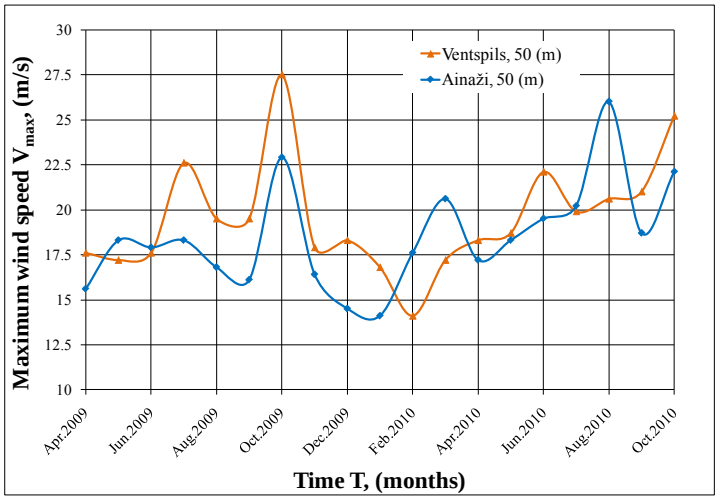

Fig.5. The maximum values of separate wind gusts, V (m/s), with duration 10 (s) in the regions Ventspils and Ainaži, at height 50 (m) above the ground level in the period of 2009/2010.

From analysis of statistical data for 2009/2010 shown in Fig. 5 it follows that in the coastal zone winds are gustier, whereas farther from shore their speeds are more uniform. The maximum value for separate wind gusts lasting not less than 10 *s* in the Ventspils region is not much higher than in Ainaži, with the situation changing in individual months. In January of 2005 the wind gusts in the Ventspils region at a height of 50 *m* reached 34.1 *m/s*.

3. Approximating functions for calculation of the wind speed and wind energy density up to 150 m

The distribution curves of the average wind speed V_a *(m/s)* in height *h (m)* above the ground level in the regions Ventspils and Ainaži obtained based on the data accumulated for a long time are presented in Fig. 6. The measured values of wind speed in the Ventspils region are shown by two curves. Curve 1 corresponds to the average wind speed values in the period of 2007/2010, curve 2 – to the average wind speed values in the period of 2009/2010, and curve *3* – to the distribution of the average wind speed in the Ainaži region in the period of 2009/2010.
Analysis of the distribution curves in Fig.6 obtained for the average wind speed V_a shows that the wind speed distribution in height up to 30 *m* is to a considerable extent determined by the topography of the terrain. In the Ventspils region it is represented by 8 - 10 *m* high tract of forest, whereas in the Ainaži region – an open plain remote from the sea. The points on the curves corresponding to the measured values of wind speed at a height over 30 *m* could be well approximated by the exponential function of the form:

$$V_a = kh^{\alpha}. \qquad (2)$$

For the curves of Fig. 7 the following values for approximating functions have been obtained:

For curve *1* – $V_a = 1.19\ h^{0.37}$, the coefficient of determination $R^2 = 0.9941$;
For curve *2* – $V_a = 1.11\ h^{0.37}$, the coefficient of determination $R^2 = 0.9937$;
For curve *3* – $V_a = 1.02\ h^{0.37}$, the coefficient of determination $R^2 = 0.9977$,

hereafter R^2 – reveals how close is modelled approximation function to actual measured values, most reliable when is at or near 1.

Fig. 7 shows curves *1, 2, 3* for measured values of the average wind speed V_a *(m/s)*, calculated using the corresponding values of approximating functions and extrapolated up to the height *h* of 150 *m*. From analysis of the distribution of the average cubic wind speed depending on the height above the surface $V_{a.c.} = f(h)$ for curves *1, 2, 3* the following coefficients and exponents have been obtained for approximating function in Eq. (2):

For curve *1* – $V_{a.c.} = 1.69\ h^{0.31}$, the coefficient of determination $R^2 = 0.9877$;
For curve *2* – $V_{a.c.} = 1.61\ h^{0.31}$, the coefficient of determination $R^2 = 0.9883$;
For curve *3* – $V_{a.c.} = 1.59\ h^{0.29}$, the coefficient of determination $R^2 = 0.9994$.

With due regard for the relationship in Eq. (1) the distribution curves for the average cubic wind speed values in height $V_{a.c.} = f(h)$ are calculated up to the height of 150 *m* and are presented in Fig. 8 (left). Correspondingly, the distribution curves for the wind energy density $P_d = f(h)$ are presented in Fig. 8 (right). For calculation of the wind energy density in the coastal area and in the regions remote from the coast by 30 - 40 *km* the following functions have been used:

For curve *1* – $P_d = 3.17\ h^{0.93}$ the coefficient of determination $R^2 = 0.9874$;
For curve *2* – $P_d = 2.64\ h^{0.94}$, the coefficient of determination $R^2 = 0.9882$;
For curve *3* – $P_d = 2.57\ h^{0.88}$, the coefficient of determination $R^2 = 0.9995$.

For flat territories typical of the Baltic countries the approximating function Eq. (2) could be reduced to the form more convenient for the use as shown in the Eq. (3) & Eq. (4):

$$V_{a.h} = V_{a.h_1}\left(\frac{h}{h_1}\right)^{\alpha}, \quad (3)$$

$$V_{a.h} = V_{a.h_1}\left(\frac{h - h_0}{h_1 - h_0}\right)^{\alpha} \quad (4)$$

where $V_{a.h}$ – is the calculated value of the average wind speed *(m/s)* at height *h*, *(m)*;

$V_{a.h_1}$– is the measured value of the average wind speed *(m/s)* at height h_1, *(m)* for a flat area;

h_0 – is the height of the surface relief at the installation point of the measuring set,

α – is the approximation coefficient (depending on the remoteness from the sea shore is 0.37 – 0.31).

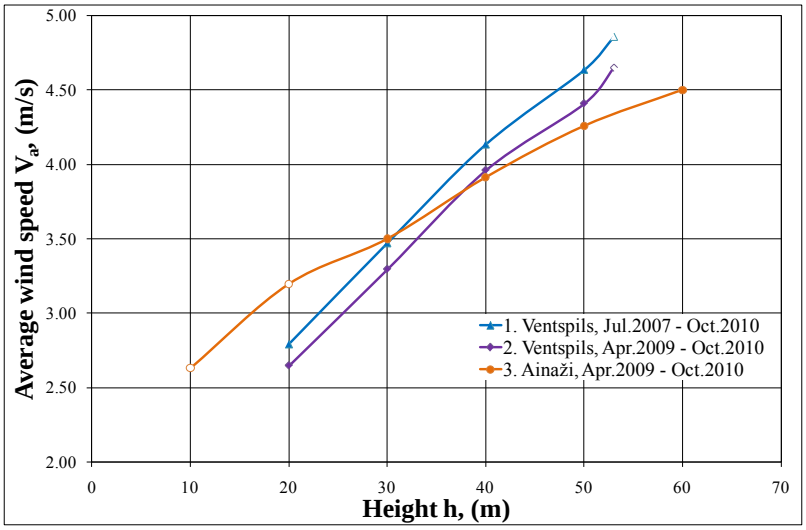

Fig. 6. The curves of the average wind speed vs. height V_a = f(h) in the Ventspils and Ainaži regions obtained by measurements.

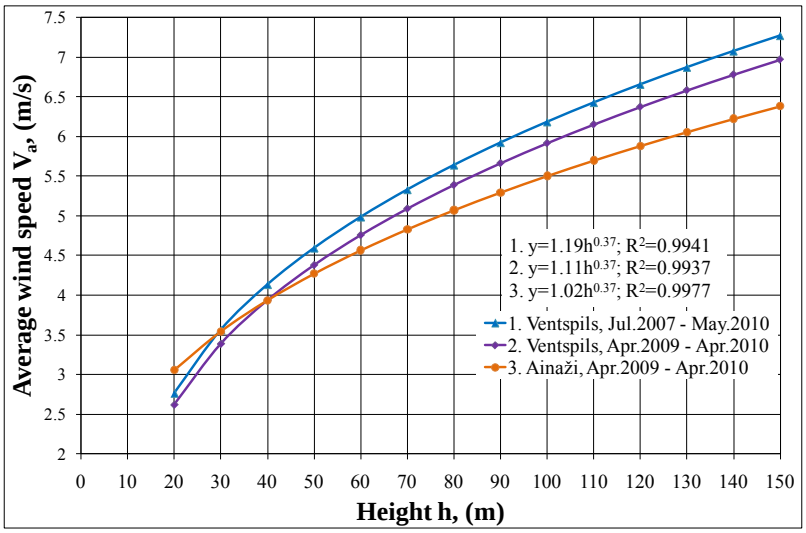

Fig. 7. The curves of the average wind speed vs. height V_a = f(h) in the Ventspils and Ainaži regions extrapolated up to the height of 150 (m).

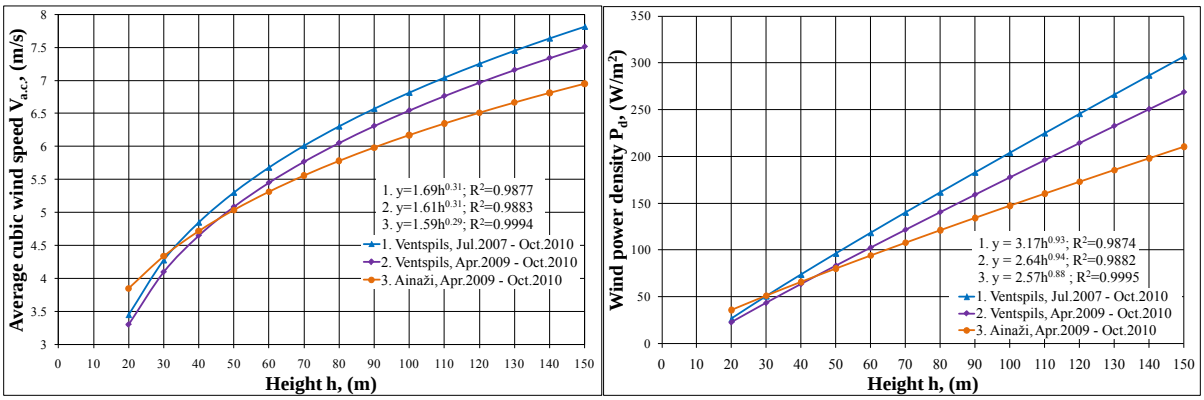

Fig. 8 (left). The curves of the average cubic wind speed vs. height $V_{a.c.}$ = f(h) in the Ventspils and Ainaži regions extrapolated up to the height of 150 (m). Fig. 8 (right). The curves of the wind energy density vs. height P_d = f(h) in the Ventspils and Ainaži regions extrapolated up to the height of 150 (m).

4. Estimation of the acoustic noise level distribution around a WPP

One of the negative aspects of WPP operation is emission of low-frequency noise that acts on humans and disturb comfortable life conditions. Calculations allow to define a zone of noise influence on environment and to determine if the planned projects are in accordance with requirements of the Law of Republic of Latvia, which establishes acceptance standards of noise level in populated areas. In compliance with the sanitary norms in Latvia the noise level accepted at the places of permanent residence of people must not exceed 40 *dB(A).* This means that the construction of WPPs in the proximity of settlements is not allowed.

Fig. 9. The map of noise level distribution around a WPP consisting of 32 generators with the total power of 80.0 (MW) in the territory 8000x5000 (m).

Figure 9 s hows the map of noise level distribution in the territory surrounding a WPP consisting of 32 generators with the total power of 80.0 *MW* in the Ainaži region. The maximum value of the noise level in the WPP territory is 50.14 *dB(A),* the noise level of a generator being 99.0 *dB(A)* [3].

5. Conclusions

1. Availability of large unpopulated areas on the coasts of the Baltic countries, along with the developed infrastructure of electric power networks, makes attractive the use of these lands for siting large wind power plants (WPPs).

2. During long-term observations a statistical database has been accumulated on the distribution of speeds and directions of winds at different heights: 10, 20, 30, 40, 50 and 60 *m* in the Ventspils and Ainaži regions on the Baltic Sea shore.

3. The graphs of seasonal fluctuations of wind speed have been obtained for the heights up to 60 *m* by measurements over the period of 2007 - 2010.

4. The histograms have been composed for the relative frequency of repetition of wind speed over the period of 2007 - 2010.

5. The values of approximating functions have been obtained allowing for the calculations of the wind speed at a height up to 150 *m* above the ground level in coastal zones of the Baltic Sea and in a territory remote from the sea by 35 *km*.

6. The wind speed measurements are noticeably affected by the terrain features, therefore to raise the precision at determination of approximating functions it is worthwhile to dispose the measuring sensors at a height over 30 *m* above the surface level.

7. During the period of observations it has been revealed that in 2009 the average yearly wind speed on the Baltic Sea shore decreased 5% with respect to 2007. To compose the atlas of the wind energy resources it is necessary to investigate the period of cyclic yearly fluctuations of the wind speed.

8. The maximum values obtained for separate wind gusts lasting not less than 10 *s* are not much higher in the Ventspils region than in Ainaži. In January 2005 the wind gusts at a height of 50 *m* in the Ventspils region reached 34.1 *m/s.*

9. In the places of WPP location the level of acoustic noise can be higher than 50.14 *dB(A),* while in compliance with the sanitary norms the noise level allowable for residential areas must not exceed 40 *dB(A).*

References

[1] V. Bezrukov, V. Pugachov, P. Shipkovs, G. Kashkarova, Vl. Bezrukovs „Investigation of the wind energy potential in the Baltic region". SCW2005, ISES Solar World Congress, August 6 – 12, Orlando, US, - 6 pp.

[2] P. Shipkovs, V. Bezrukov, V. Pugachev, Vl. Bezrukovs, V. Silutins, Research of the wind energy resource distribution in the Baltic region, World Renewable Energy Congress XI 23-30 September 2010, Abu Dhabi, UEA, pp.1931 – 1936.

[3] P. Shipkovs, V. Bezrukov, Vl. Pugachov, Vl. Bezrukovs, S. Orlova „Measurements and utilization of wind energy on the Baltic Sea coast". The 10th World Renewable Energy Congress – WREC X, 19-25 July, 2008, Glasgow, Scotland, CD proceedings 2398 – 2403.

Using meteorological wind data to estimate turbine generation output: a sensitivity analysis

M. L. Kubik[1,*], P. J. Coker [2], C. Hunt[3]

[1] *Technologies for Sustainable Built Environments, University of Reading, United Kingdom*
[2] *School of Construction Management and Engineering, University of Reading, United Kingdom*
[3] *AES, Richmond upon Thames, United Kingdom*
** Corresponding author. Tel: +44 (0)118 378 4670, E-mail: m.kubik@pgr.reading.ac.uk*

Abstract: Various studies investigating the future impacts of integrating high levels of renewable energy make use of historical meteorological (met) station data to produce estimates of future generation. Hourly means of 10m horizontal wind are extrapolated to a standard turbine hub height using the wind profile power or log law and used to simulate the hypothetical power output of a turbine at that location; repeating this procedure using many viable locations can produce a picture of future electricity generation. However, the estimate of hub height wind speed is dependent on the choice of the wind shear exponent α or the roughness length z_0, and requires a number of simplifying assumptions. This paper investigates the sensitivity of this estimation on generation output using a case study of a met station in West Freugh, Scotland. The results show that the choice of wind shear exponent is a particularly sensitive parameter which can lead to significant variation of estimated hub height wind speed and hence estimated future generation potential of a region.

Keywords: *Wind shear exponent, Wind profile, Renewable energy, Variability, Intermittency*

Nomenclature

α	*wind shear coefficient*..... *dimless*	k	*von Karman constant*.....*dimless*
u_1	*horizontal velocity component at* z_1 .....ms^{-1}	z_0	*surface roughness factor*.....*m*
u_2	*horizontal velocity component at* z_2 .....ms^{-1}	z_1	*vertical measurement height 1* .....*m*
u_*	*friction velocity*.....ms^{-1}	z_2	*vertical measurement height 2* .....*m*

1. Introduction

Various influential studies investigating the impacts of the variability of renewable resources begin with meteorological (met) station data, as this is often readily available over a wide geographic area [1-3]. Alternative studies instead rely on statistical methods, e.g. [4], have direct access to wind farm generation data, e.g. [5], or take a black box approach and consider the impact of wind at a system level, based upon industry forecasts and policy targets, e.g. [6].

A typical weather station will log hourly mean horizontal wind and gust speeds at a standard height of 10m, which may be extrapolated to estimate the wind speed at a standard wind turbine height. By applying a wind turbine power curve, the wind speed can be converted into a hypothetical generation output, and repeating this process to a greater number of turbines and to a wider geographical area can give insight into how a future involving a high penetration of renewable energy may look.

Two common analytical models are used to map the wind velocity profile with height, and hence allow the calculation of horizontal wind speed at a certain elevation over the earth's surface: the log law and the power law [7]. In reality, the complex and dynamic nature of the atmospheric boundary layer means that one single profile will not provide a consistently reliable extrapolation of wind speed from one height to another. The variables in the log and power laws therefore are particularly important to consider when performing the kind of future resource study suggested above. This paper investigates precisely this sensitivity by

carrying out a resource analysis of hourly mean wind data for a met station in West Freugh, Scotland, in the same manner that other influential resource studies [1-3] have used.

First, the relevant background literature and the methodology used in this research are presented, with particular focus given to the assumptions made in the analysis. The findings of the research are then discussed, the implications identified, and avenues for future research are highlighted.

2. Background literature

There are two main analytical models used to extrapolate wind speeds to greater heights: the log law and the power law. In general, the two models have been shown to perform equivalently in shear extrapolation predictions on average, although at any particular site one model may be better than another [8]. However, for either approach, large errors in the predictions are common and this error is exacerbated further when energy production is estimated. This section introduces the theory and assumptions behind these two approaches, and indicates some of the previous work into better understanding and applying them.

2.1. The Logarithmic Law

The log law's origins lie in boundary layer fluid mechanics and atmospheric research [7]. For determining the horizontal velocity u at a height z is commonly expressed

$$u(z) = \left(\frac{u_*}{k}\right)\ln\left(\frac{z}{z_0}\right) \tag{1}$$

Where u_* is the friction velocity, k is the von Karman constant and z_0 is a measure of surface roughness known as the roughness length; u_* and k are generally determined from a graph of experimental data [9].

There are cases where wind velocity u_1 is known at a reference height z_1, and required at another z_2, in which case it can be derived from equation 1 that

$$u_2 = u_1 \frac{\ln(z_2) - \ln(z_1)}{\ln(z_1) - \ln(z_0)} \tag{2}$$

This is a simpler expression to solve, as it eliminates the need to calculate the friction velocity and von Karman constant, which can be difficult to estimate in the atmosphere. A neutral wind profile is assumed [9], where convection is negligible, the lapse rate (the fall of temperature in the troposphere with height) is nearly adiabatic and stratification is nearly hydrostatically neutral (i.e. there is no *vertical* wind flow in the atmosphere without excitation).

Seasonal variations in local terrain characteristics can have a profound influence the on estimation of z_0 (due to changes in foliation, vegetation, snow cover etc.). Table 1 extracts some guideline roughness lengths for different types of terrain as given in the European Wind Atlas [10].

Table 1- Typical Surface Roughness Lengths z_0

Terrain	z_0 (m)
Water areas (lakes, fjords, open sea)	0.0001
Airport runway areas	0.01
Airport areas with buildings and trees	0.02
Farmland with very few buildings and trees	0.03
Farmland with closed appearance	0.10
City	1.00

2.2. The Power Law

The power law [9] is an empirical equation, expressed

$$u_2 = u_1\left(\frac{z_2}{z_1}\right)^{\alpha} \tag{3}$$

Where α is the wind shear coefficient or power exponent, an empirically derived constant applied over the height range that the power law is applied. Calculating the wind shear coefficient becomes trivial if the wind speeds at two heights are known, as equation 3 may be rearranged in terms of α

$$\alpha = \frac{\ln(u_2) - \ln(u_1)}{\ln(z_2) - \ln(z_1)} \tag{4}$$

The exponent α is a dynamic value that is dependent upon the stability of the atmosphere. The wind shear exponent may be taken as constant for a given height in a given height range, but a different α should be chosen depending on the height range over which the power law is applied [9]. For neutral stability conditions, α is approximately 1/7, or 0.143 (this rule of thumb is known as the "1/7^{ths} power law"), regarded as a reasonable but conservative estimate [11]. However, various site specific studies have found that the coefficient is actually greater, and that this leads to underestimation of the energy resource available [12-14].

2.3. Usage of the two laws

Each method requires knowledge of a wind speed at a reference height, and one further coefficient: a roughness length z_0 in the case of the log law and a wind shear coefficient α in the case of the power law. Both may be calculated using on site measurements, but the power law is common engineering practice [15] favoured by the wind industry and consultants, as the wind shear coefficient is a dynamic value that varies according to a large number of factors including time of day, season, atmospheric stability and regional topography [11]. The log law on the other hand is only valid under certain assumptions regarding atmospheric stability, and actual profiles may deviate from the log law. In the wind industry the two methods are generally checked where possible to ensure that they provide similar results [15].

Unlike wind developers, many researchers do not have the resources to conduct field investigations (for example, by erecting weather masts) to determine the horizontal wind characteristics at likely development sites, and instead rely upon available 10m met station data and shear profile extrapolation for their models, often over a large height range and assuming one constant annual value.

3. Methodology

Meteorological data for this study was obtained from the British Atmospheric Data Centre MIDAS database for a station located at West Freugh airfield, Scotland. A wider number of sites were considered, but this site was chosen because it provided a reliable and continuous data set. Five years (2005-2009) of Hourly Climate Messages (HCM) were chosen over Synoptic (SYNOP) data for analysis, as the latter relies on a 10min wind sample to produce an hourly average. HCM readings sample continuously to produce an hourly average mean wind at a standard height of 10m. The readings were recorded to the nearest knot, but converted to SI units for analysis.

The literature identified that the log and power law extrapolations were each dependent on a single parameter: the surface roughness z_0 and the wind shear coefficient α respectively. Four surface roughness lengths were selected for analysis using Table 1, based upon an understanding of the site topography (i.e. an airfield with building and trees being the best description, and hence the starting point) and similarly, a range of four shear coefficients were also selected, using the $1/7^{th}$ power law as a starting point. Both sets of parameters were selected to represent a realistic spread of values that an analyst might take for the site [15].

A Vestas V80 2MW wind turbine power curve was used for calculation of generation output, with an assumed hub height of 60m. The generation outputs were calculated each year for each of the extrapolated profiles of 10m wind speed, producing an apparent indication of the site's annual capacity factor, energy production, zero generation hours and the proportion of time when a hypothetical turbine would be producing no power output.

4. Results

Annual capacity factors, based upon wind speed extrapolation to 60m, are shown in Figure 1, with all other results summarised in Table 2. A sample week (from June 2005) has been extracted from the analysis and used to illustrate the change in estimated 60m wind speed and generation outputs under each law; this is shown in Figure 2.

Figure 3 maps the profile of wind speed with height from a starting height of z_1=10m, using the log and power law with the variables specified in the methodology. A typical wind speed of u_1=5ms^{-1} was a chosen to illustrate this behaviour. The extrapolated wind speeds at z=60m are emphasised for discussion, as this was the height of interest in this study.

Table 2 - Summary of mean values attained under log and power law

5 year average	power law (α)				log law (z_0)			
	0.100	0.143	0.200	0.300	0.010	0.020	0.030	0.100
Capacity Factor	0.266	0.307	0.364	0.463	0.293	0.306	0.314	0.348
Zero prod hrs	1777	1779	1785	1468	1778	1779	1779	1782
% non gen time	20.4%	20.4%	20.5%	16.9%	20.4%	20.4%	20.4%	20.5%
Total GWh	4.623	5.348	6.344	8.057	5.105	5.320	5.470	6.053

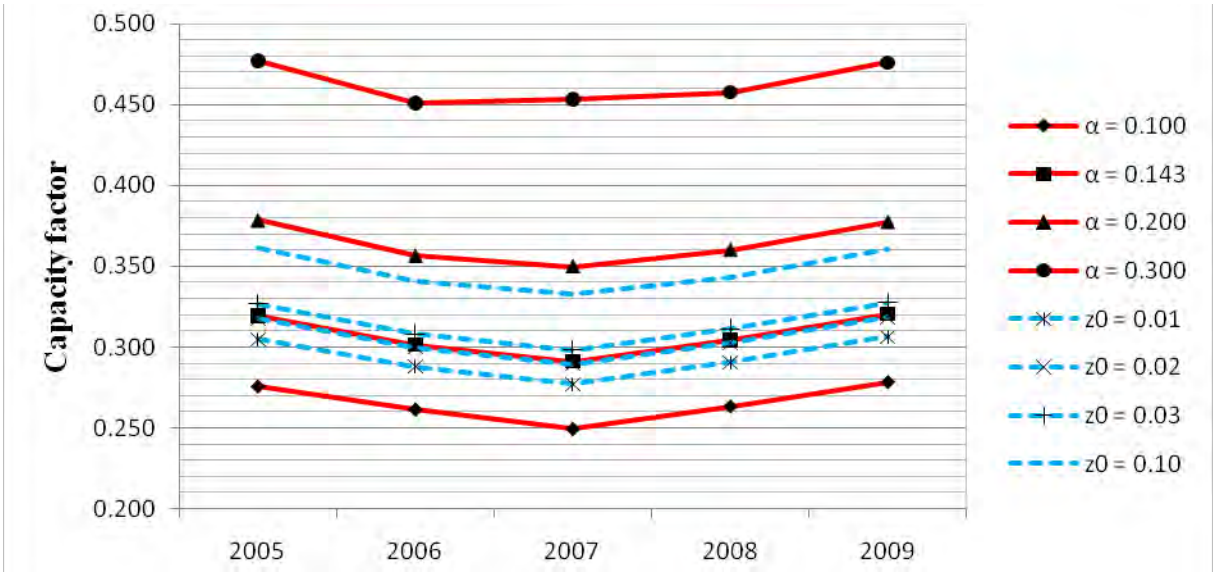

Figure 1 - Graph of extrapolated annual capacity factors

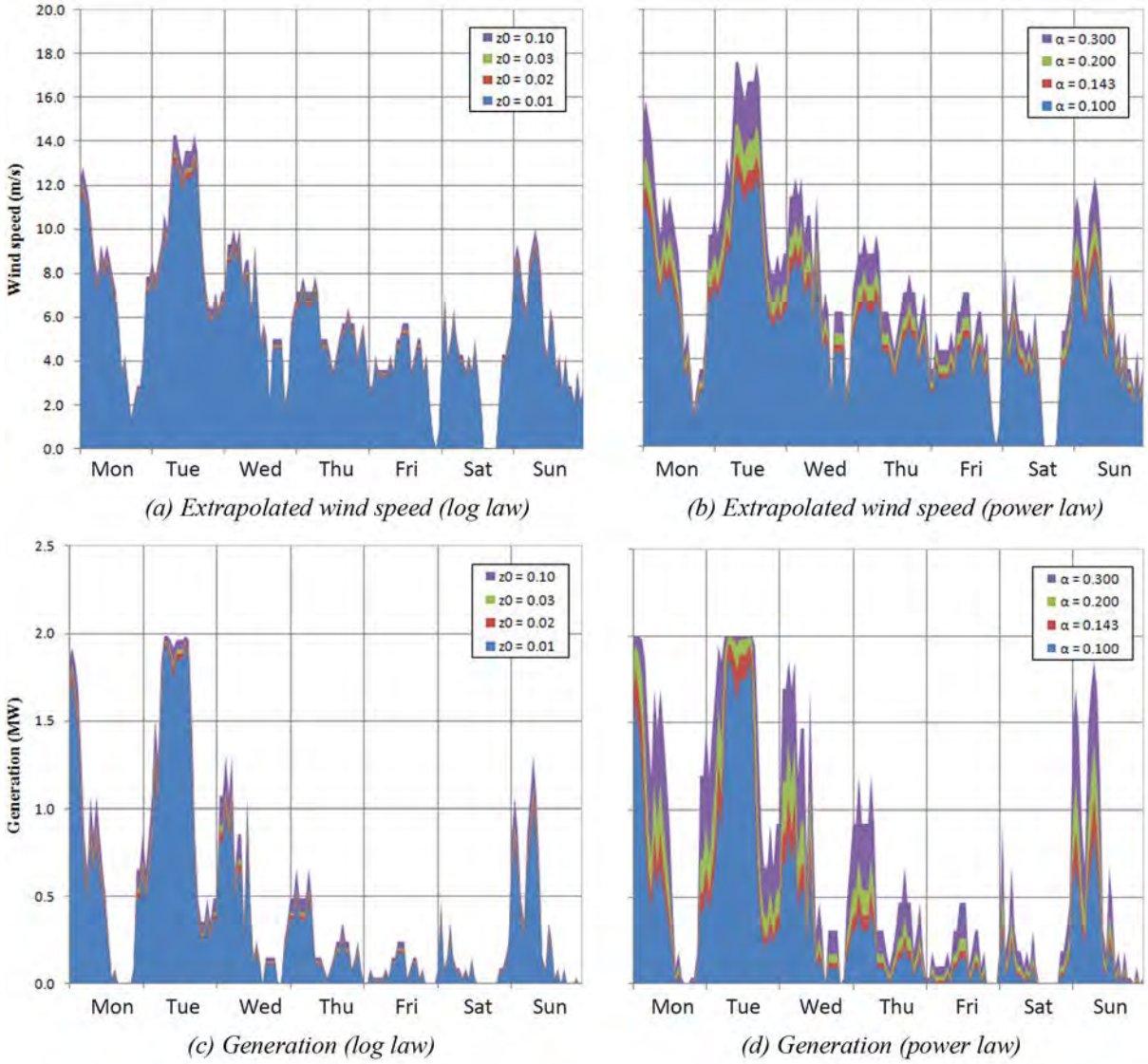

Figure 2 - Sample week of wind extrapolation and estimated generation using the log and power law

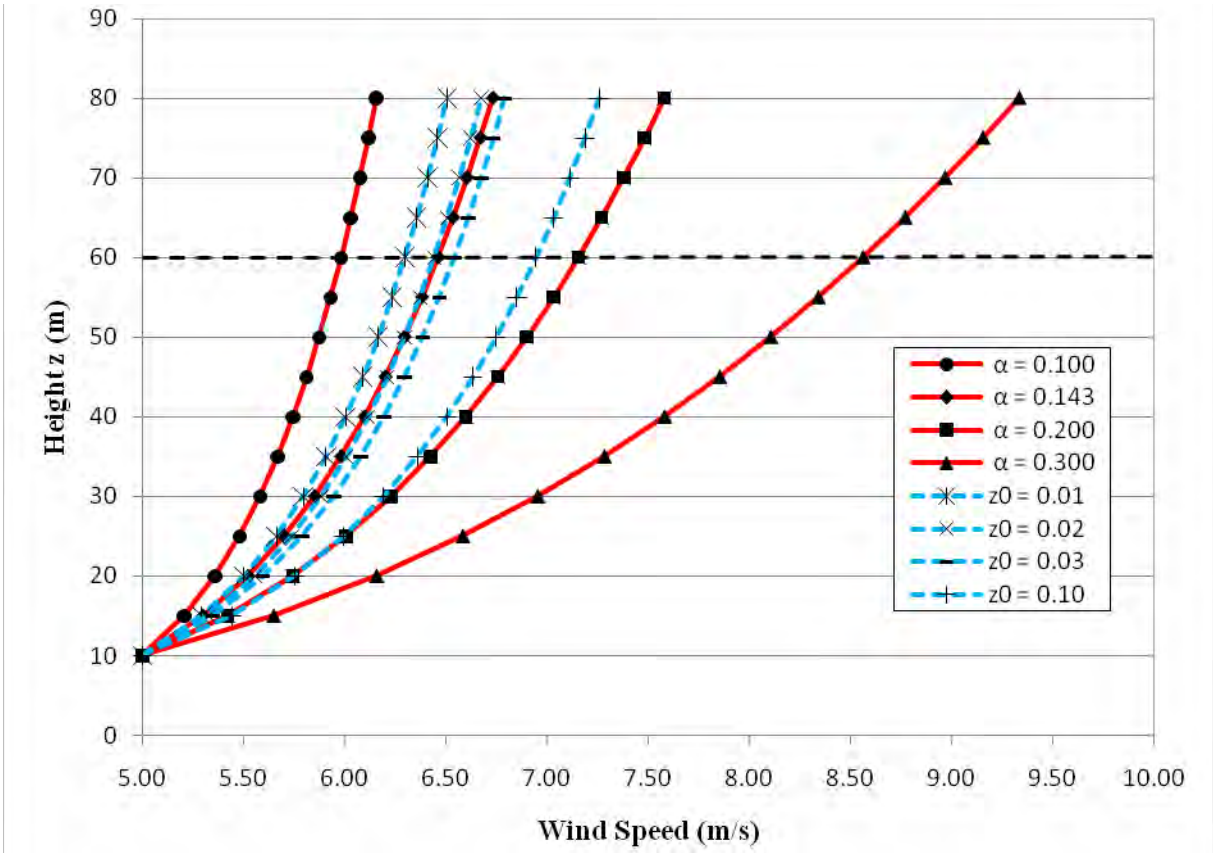

Figure 3- Graph illustrating the wind shear profiles under various log and power law parameters

5. Discussion

It is clear that the base case parameter choices (z_0 = 0.02m and α = 0.143) follow a near identical profile (Figure 3), and hence produce very similar capacity factor estimates and total amounts of energy annually (Table 2). T his is to be expected, as both represent neutral stability conditions. The parameter values in this study were selected to represent the realistic values an analyst might take for the West Freugh site, as discussed earlier in the methodology. Through these choices a wider range of surface roughnesses than shear coefficients were applied (a percentage change of 1000% in z_0 and 300% in α respectively, from the lowest to highest values). Regardless of this disparity, which would be expected to favour a tighter knit set of results for the power law, Figure 3 shows that the range of extrapolated wind speeds at 60m was in fact considerably larger for the power law than the log law (0.65ms^{-1} and 2.58ms^{-1} respectively). This trend is also clearly observed in Figure 2(a) and (b); in the former, the wind speeds for each series are banded close together, in the latter they are considerably more widespread.

Figure 2 also very clearly illustrates the variable nature of the wind resource and the importance that it has on the output of a wind turbine. The sensitivity of the power output is pronounced for different shear coefficients, though relatively similar generation profiles are produced for the range of surface roughnesses, as shown in Figure 2(c) and (d). This is similarly observed in the clustered nature of the log law annual capacity factors in Figure 1, compared to a considerably wider range for the power law.

The reason for the pronounced difference in generation outputs, observed particularly strongly using the power law, is that wind turbine power is related to the cube of wind speed, so a

difference in the wind speed error becomes far more significant in a generation calculation. This is best illustrated with an example; the mean 60m wind speed calculated for West Freugh in 2005, using $\alpha = 0.100$ and $\alpha = 0.200$, together with the limits of one standard deviation, is overlain onto a Vestas V80 power curve in Figure 4. As the cumulative energy generated is calculated by integrating under the area of the curve, it is clearly illustrated how a small change in mean wind speed estimate equates to a significantly larger area under the curve, and hence a large change in total generated energy.

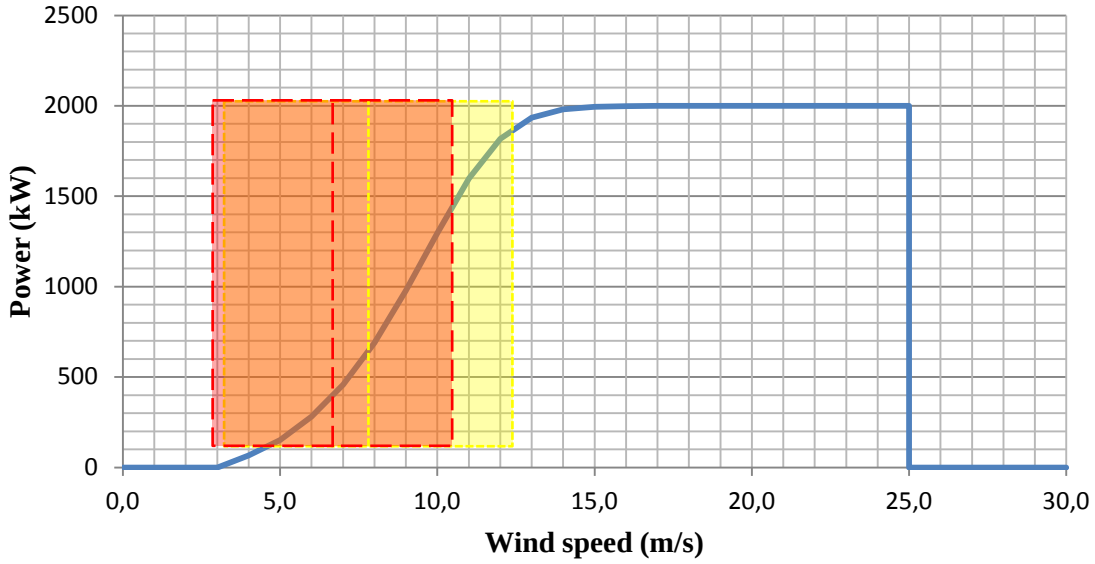

Figure 4- Vestas V80 power curve, annotated. The long red dashes indicate the mean wind and range of one standard deviation for α=0.100, and the short yellow dashes for α=0.200.

6. Conclusions

It is clear from the results that the wind shear coefficient is a more sensitive parameter than surface roughness, and that an equivalent percentage change to each value will impact the wind speed and generation estimates more robustly than when using the log law. However, if properly used, the power law can provide a more accurate idea of the renewable energy output of a particular site or area than the log law, which requires neutral stability conditions to be scientifically exact.

This study is not suggesting that either the power or log laws are intrinsically good or bad, but rather highlights the importance of the quality of information that goes into a model. It is important that there is a good understanding of the site before attempting to apply a single parameter to characterise the system, particularly as in reality the wind shear coefficient is a dynamic value dependant on a large number of parameters.

In order to understand the accuracy of using a single wind shear for the power law model, it is important to compare this theoretical generation data to the output for a real wind farm. Without this information, a critical analysis of this type of approach to future resource estimate cannot be made. Another interesting topic for future research will be to look into how different wind turbine designs, with different power curve characteristics, may change the energy yield of a site. Both of these are aspects of research that the authors intend to investigate in future studies.

Acknowledgements

The authors wish to thank James Cox of Pöyry Energy Consulting for clarifying aspects of the methodology used in their energy models. They also extend their thanks to Lauren Wheatley of AES, and to Thomas Campbell and Richard Mardon of Your Energy Ltd., for their business insight regarding the appraisal of wind sites.

References

[1] Pöyry, *Impact of intermittency: how wind variability could change the shape of the British and Irish electricity markets*. 2009.

[2] G. Sinden, "Characteristics of the UK wind resource: Long-term patterns and relationship to electricity demand," *Energy Policy*, vol. 35, no. 1, pp. 112-127, Jan. 2007.

[3] SKM, "Growth scenarios for UK renewables generation and implications for future developments and operation of electricity networks," BERR Publication URN 08/1021, Jun-2008.

[4] P. Meibom et al., *Final Report for All Island Grid Study Work-stream 2(b): Wind Variability Management Studies*. Roskilde, Denmark: Risø National Laboratory, 2007.

[5] ESB, *The Impact of Wind Power Generation in Ireland*. ESB National Grid, 2004.

[6] B. Klusmann and U. Ziller, *Power supply 2020 - how to reach a modern energy economy*. Bundersverband Erneuerbare Energie, 2009.

[7] J. F. Manwell, J. G. McGowan, and A. L. Rogers, *Wind Energy Explained: Theory, Design and Application*. John Wiley and Sons, 2010.

[8] M. R. Elkinton, A. L. Rogers, and J. G. McGowan, "An Investigation of Wind-shear Models and Experimental Data Trends for Different Terrains," *Wind Engineering*, vol. 30, no. 4, pp. 341-350, May. 2006.

[9] H. Panofsky and J. Dutton, *Atmospheric Turbulence: models and methods for engineering applications*. Pennsylvania State University: John Wiley and Sons, 1984.

[10] WAsP, "WAsP 9 documentation: The roughness of a terrain." [Online]. Available: http://www.wasp.dk. [Accessed: 22-Nov-2010].

[11] P. Gipe, *Wind power: renewable energy for home, farm, and business*. Chelsea Green Publishing, 2004.

[12] M.H. Albadi and E.F. El-Saadany, "The Effects of Wind Profile on Thermal Units Generation Costs," presented at the Power Systems Conference and Exposition, 2009. PSCE '09. IEEE/PES, Seattle, WA, pp. 1-6, 2009.

[13] D. Sisterson, B. Hicks, R. Coulter, and M. Wesely, "Difficulties in using power laws for wind energy assessment," *Solar Energy*, vol. 31, no. 2, pp. 201-204, 1983.

[14] M. W. Tennis, S. Clemmer, and J. Etherington, *Assessing Wind Resources A Guide for Landowners, Project Developers and Power Suppliers*. Union of Concerned Scientists, 1999.

[15] L. Wheatley, T. Campbell, and R. Mardon, "Personal Communication with AES and Your Energy Ltd.," 2010.

Wind speed and power characteristics at different heights for a wind data collection tower in Saudi Arabia

Alam Md. Mahbub[2], Shafiqur Rehman[1,2,*], Josua Meyer[2], Luai M. Al-Hadhrami[1]

[1]*Center for Engineering Research, Research Institute, King Fahd University for Petroleum and Minerals, Dhahran-31261, Saudi Arabia*
[2]*Mechanical and Aeronautical Engineering Department, University of Pretoria, Pretoria, South Africa*
** Corresponding author: Tel: 966 3 8603802, Fax: 966 3 8603996, E-mail: srehman@kfupm.edu.sa*

Abstract: Generating energy with clean and renewable sources of energy has become imperative due to the present days' energy crisis and growing environmental consciousness. The objective of the present study is to assess the wind power, wind shear exponent, air turbulence intensity, energy yield, plant capacity factor and effect of hub height on energy yield and PCF for the site under consideration. To achieve the set objectives, wind speed measurements at different height made during the evaluation period were utilized. The site under consideration was found to be feasible for developing grid connected wind farms in the area with annual energy yield of 11.75GWh with plant capacity factor of 48.8% from one wind turbine of 2.75MW rated power with a hub height of 100m from Vestas.

Keywords: *Wind Energy, Saudi Arabia, Plant Capacity Factor, Wind Speed, Weibull Parameters, Wind Shear, Wind Turbulence*

1. Introduction

The adverse effect of climate change such as tsunami, floods, forest fires, have become common in the recent years due to alarmingly increasing pollution levels and increasing global population and thereof increasing power demands. Each megawatt of electricity generated using fossil fuel adds around half a ton of green house gases equivalent CO_2 in to the atmosphere. The accumulating effect of fast depletion of fossil fuels, alarmingly rising environmental pollution levels, and at the same time gradually emerging awareness of environmental degradation has given rise to the use of renewable sources of energy such as wind, solar, small and large hydro, geothermal, tidal, and bio-energy. Of these clean sources, the rapid development in wind energy conversion technology has made it an alternative to conventional energy systems in recent years. Wind energy is the fastest growing source of energy and is getting worldwide attention due to the technological advances for harnessing the wind power and its competitive cost of production compared to other traditional means. In order to conserve the conventional energy resources and to address the environmental problems, the wind power utilization is the answer to these problems. The worldwide wind power installed capacity is increasing rapidly due to new projects being commissioned in different parts of the world. United States of America (USA) is leading the world with regard to global wind power installed capacity. The other countries contributing towards wind power sectors are Germany, Spain, Denmark, India, China, United Kingdom, Egypt, and others.

Various wind speed and wind power characteristics studies have been reported in and around the Middle East region. Some of these studies include Marafia and Ashour [1] for offshore/onshore wind power project development in Qatar; El-Osta and Kalifa [2] for a proposed 6 MW wind farm in Zwara, Libya; Al-Nassar et. al. [3] showed that the annual mean wind speed in Kuwait lied in the range of 3.7 to 5.5 m/s with mean; Hrashyat [4] reported wind resource assessment of the south western region of Jordan; Elamouri and Amar [5] for Tunisia; Ucar and Balo [6] for Manisa, Turkey; Bagiorgas et. al [7] for Western Greece; Shahta and Hanitsch [8] studied the technical and economic assessment of wind power for Hurghada in Egypt; Toğrul and Kizi [9] for Bishkek, Kyrgyzstan; Jowder [10] reported wind resource assessment for Bahrain; and Himri et. al [11] provided review of

renewable energy in general and the wind in particular for Algeria. Sahin and Bilgili [12] studied the wind characteristics of Belen-Hatay province of Turkey using hourly wind speed records between years 2004 and 2005.

The work on wind resource assessment in Saudi Arabia dates back to 1986, when Ansari et. al [13] used hourly wind speed data to develop a Wind Atlas for Saudi Arabia. In Saudi Arabia, work on wind speed data analysis such as Weibull parameter determination and distribution, wind speed prediction using different methods such as auto-regression and neural network, wind power generation cost determination, and so on has been reported in the literature. Rehman et. al. [14] presented the Weibull parameters for ten anemometer locations in Saudi Arabia and found that the wind speed was well represented by Weibull distribution function. Rehman and Halawani [15] presented the statistical characteristics of wind speed and diurnal variation. The autocorrelation coefficients were found to be matching with the actual diurnal variation of the hourly mean wind speed for most of the locations used in the study. Some of the other studies include Rehman et. al [16], Rehman and Aftab [17] and Rehman et. al [18].

The objective of the present study is to assess the wind power, wind shear exponent, air turbulence intensity, energy yield, plant capacity factor and effect of hub height on energy yield and PCF for the site under consideration.

2. Site, equipment and Data Description

The 40 meter tall tower was installed at Juaymah power plant, a site located in the eastern part of Saudi Arabia. The latitude, longitude and altitude of the measurements site were 26°47' N, 49˚53' E and near sea level, respectively. The data was collected for a period of 33 months stretching from July 01 2006 to April 01, 2009. The area is surrounded by government and private industries and power plants which are connected to the national electric grid. In order to assess the wind potential at the site, an instrumented 40 m tall wind tower, was installed. The meteorological data (wind speeds, wind direction, air temperature, relative humidity, surface station pressure, global solar radiation) were collected for a period of more than two years. The details of the equipment installed at the site are provided in Table 1.

Table 1. Details of the equipment installed at an isolated village.

Item Description	**Technical Information**
Wind speed sensor, NRG#40 Three cup anemometer	AC sine wave, Accuracy: 0.1 m/s, Range: 1-96 m/s Output: 0-125 HZ, Threshold: 0.78 m/s
Wind direction vane, NRG#200P Potentiometer	Accuracy: 1%, Range: 360^o Mechanical, Output: 0-Exc. Voltage, Threshold: 1 m/s, Dead band: Max - 8^o and Typical 4^o
Temperature sensor #110S Integrated circuit	Accuracy: ±1.1 ^{o}C, Range: -40 ^{o}C to 52.5 ^{o}C, Output: 0 – 2.5 volts DC, Operating temperature range: -40 ^{o}C to 52.5 ^{o}C
Barometric pressure sensor BP20	Accuracy: ±15 mb, Range: 150 – 1150 mb, Output: Linear voltage
Relative humidity sensor RH-5 Polymer resistor	Accuracy: ±5%, Range: 0 – 95 % Output: 0 – 5 volts, Operating temperature range: -40 ^{o}C to 54 ^{o}C
Pyranometer Li-Cor #LI-200SA Global solar radiation	Accuracy: 1%, Range: 0 – 3000 W/m^2 , Output: Voltage DC, Operating temperature range: -40 ^{o}C to 65 ^{o}C

3. Results and Discussion

This section provides detailed wind data analysis including calculation of site wind exponent and air turbulent intensity, wind energy yield and cost of energy. Over entire period of data collection the mean wind speeds at 10, 20, 30 and 40 meters AGL were 4.14, 4.84, 5.34 and 5.65 m/s respectively. The climatic parameters like average ambient temperature, relative humidity, barometric pressure, air density, wind shear exponent, roughness, and roughness class were 26.1°C, 17.3%, 1014 mbar, 1.181 kg/m3, 0.228, 0.239, 2.72, respectively.

3.1. Annual, seasonal and diurnal behavior of mean wind speed

The annual mean wind speeds build up a confidence on the amount of energy that could be generated and also provide future trends. In present case, the annual mean wind at 10, 20, 30 and 40 meters above ground level (AGL) were 4.1, 4.8, 5.3 and 5.6m/s, respectively, in the year 2007 and 4.2, 4.9, 5.4 and 5.8m/s, in the year 2008. This shows an increased of about 2% in wind speed in the year 2008 compared to that in 2007. The maximum wind speeds observed during these two years at 10, 20, 30 and 40 meters AGL were 15.9m/s, 17.8m/s, 18.4m/s and 19.5m/s, respectively. The prevailing wind direction was found to be NNW and NW during the data collection period.

Knowledge of monthly variation of wind speed provides confidence on the availability of energy in different months of the year. Monthly changes in wind speed at 10meters AGL, over entire data collection period, are shown in Fig. 2. Highest wind speed was observed in June while lowest in August at all the heights of wind speed measurements. At 40m AGL, the monthly mean wind speed always remained above 5.5m/s except during August to October, which means that a wind turbine with cut-in-speed of 3.5m/s can produce energy during all the months of the year at this site.

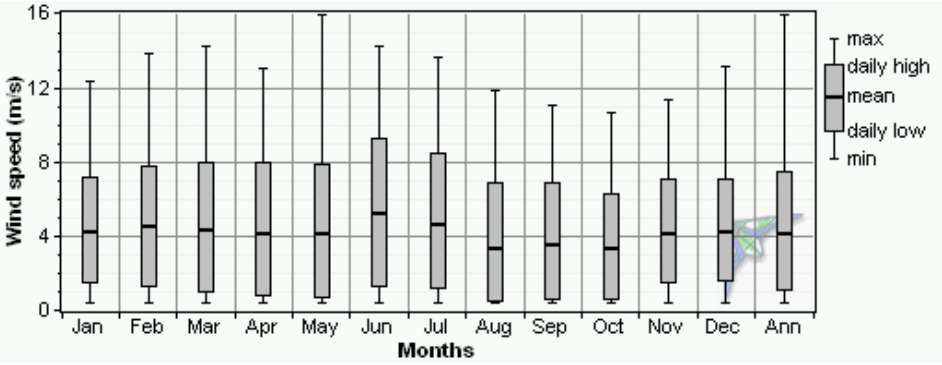

Fig. *1. Seasonal variation of mean wind speed at 10 meters AGL.*

Fig. 3 shows the variation of half hourly mean wind speed at different heights during entire data collection period. It is evident from this figure that as the height of wind measurements increases the wind speed range decreases. At 40m AGL, the half hourly mean wind speed varied from 4.7m/s to 7.0m/s (range=2.3m/s) while at 20m from 3.7m/s to 6.7m/s (range=3.0m/s). At 40m AGL, the wind speed was found above 5.2m/s for most of the time except between 8 P.M. and 12 mid night. This implies that power of the wind can be harnessed during entire day at the measurement site using a wind turbine with cut-in-speed of 3.5m/s and hub height greater than or equal to 40m.

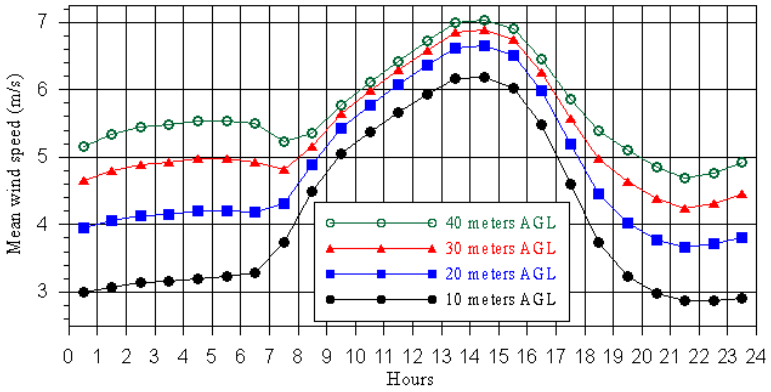

Fig. 2. Diurnal variation of hourly mean wind speed at Juaymah.

3.2. Wiebull parameters and wind frequency analysis

Wiebull distribution function is most widely used function for modeling the wind speed around the globe. The scale factor (c) of the Weibull distribution is related to the average wind speed at different heights and is calculated using the maximum likelihood method. Similarly, the Weibull (k) value is the dimensionless shape factor of the Weibull distribution. This factor reflects the breadth of the distribution. The variation of both scale and shape parameters with measurement heights is shown in Figs. 3 and 4 respectively. Since the wind speed increases with height, hence the scale parameter too follow the trend as can be seen from Fig. 3. The shape parameter also increases with height as shown in Fig. 4. This implies that as height increases, the shape of the distribution tends to be tight which implies less variation in the wind speed. The line of best fit show high values of coefficient of determination (~95%), as given in these figures. The scale parameter increases by about 0.058m/s for each meter increase in measurement height while the shape parameter increases by 0.0157 per meter.

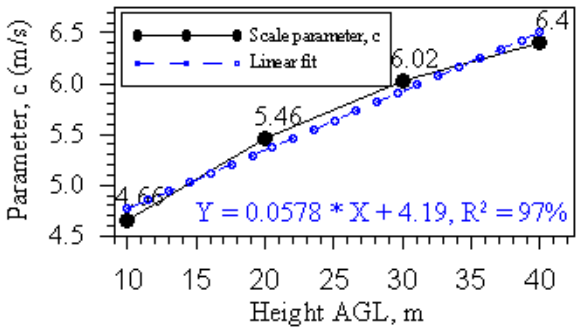

Fig. 3. Variation of scale parameter, c, with measurement height.

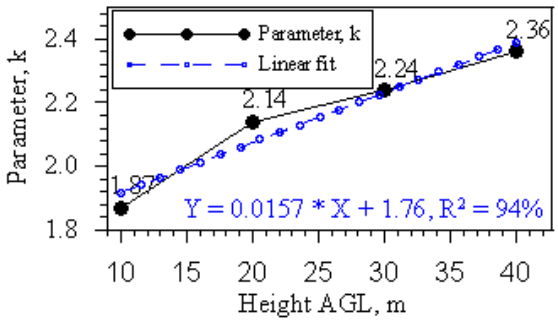

Fig. 4. Variation of shape parameter, k, with measurement height.

Wind speed frequency distribution in different wind speed bins is a very important parameter from energy yield estimation point of view. As the height of wind speed measurement increase, the percent frequency of occurrence of higher winds also increases, as shown in Figures 5(a) and 5(b) at 10 and 40meters AGL. The percent frequencies of 55%, 71%, 78% and 82% at 10, 20, 30 and 40 meters AGL, respectively, were found above 3.5 m/s. An increase of 10 meters in height (from 10 to 20 meters) of the wind speed measurements resulted in an increase of about 16% in the availability of wind speed above 3.5m/s while further increase of 10m in height results only 7% increase in frequency. This analysis confirms that a wind turbine with cut-in-speed of 3.5m/s or more could produce energy for 82% of time at the site of measurements. It is very evident from Figs. 5(a) and 5(b) that as the height increases, the Weibull function fit becomes increasingly better and the wind speed fluctuation also becomes less and less due to decrease in wind turbulence at higher altitudes.

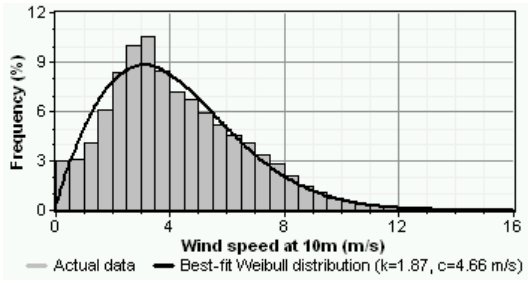

Fig. 5(a). Wiebull fit and frequency distribution of wind speed at 10 meters AGL.

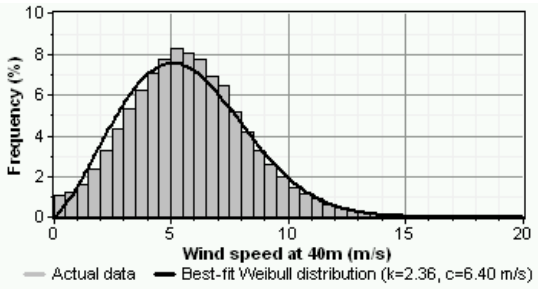

Fig. 5(b). Wiebull fit and frequency distribution of wind speed at 40 meters AGL.

3.3. *Air density and wind power density variation*

In this study, the measured values of air pressure and the temperature were used to calculate the local air density values at Juaymah measurement site. During diurnal cycle, the air density was found to vary between a minimum of 1.159 kg/m^3 during 13:00-14:00 hours and a maximum of 1.201 kg/m^3 during 04:00-05-00 hours. Higher values were noticed during nighttime and lower during day time due to corresponding lower and higher temperatures and air pressure. Around the year, highest mean air density of 1.236 kg/m^3 was obtained in the month of January which characterized by low temperature and relatively high air pressure. On the other hand, lowest air density of 1.136 kg/m3 was recorded in the month of July which is known for high temperature and relatively low air pressure. The mean wind power density values calculated using the local air density and the cube of wind speed during the data collection period at 10, 20, 30 and 40m AGL were 84.7, 119.1, 154.2 and 180.32 W/m^2, respectively. An increase of about 12% was noticed in wind power density in the year 2008 compared to that in 2007 at all measurement heights. The seasonal trends of wind power density values at different heights are depicted in Fig. 6 which indicative of highest values in June and lowest in October.

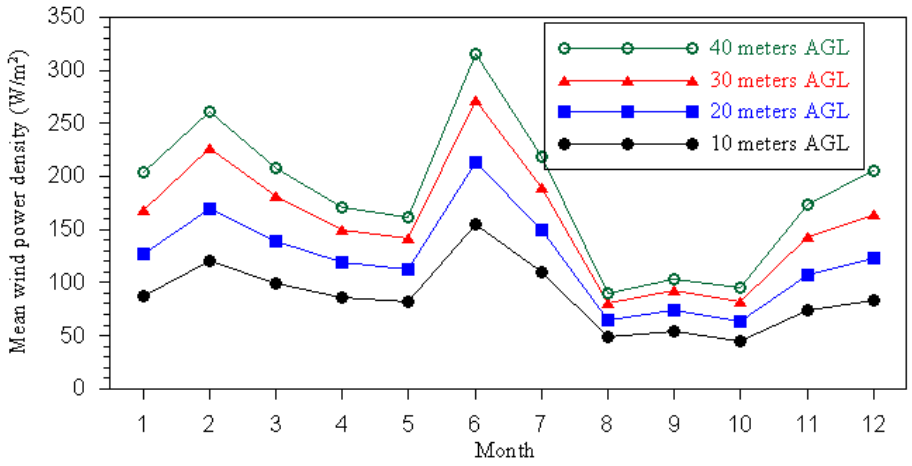

Fig. 6. Seasonal variation of wind power density at different measurement heights.

3.4. Wind shear exponent and turbulence analysis

The power law exponent is a number that characterizes the wind shear, which is the change in wind speed with height above ground. The wind shear exponent (WSE) obtained using all the data values was 0.273 while 0.269 and 0.279 for the data of years 2007 a nd 2008, respectively. Higher values of WSE (~0.285) were observed from October to January and relatively lower (~0.265) during rest of the months with lowest in September. The WSE values are very much dependent on the meteorological changes that take place during 24 hours of day as demonstrated in Fig. 7. It is clear from this figure that higher values of WSE (~0.4) were observed from 7 PM to 7AM and lower (~0.1) from 8:30 AM to 4:30 PM. For precise estimation of wind speed at higher altitudes, different values of WSE during day and

nighttime could be used. The overall surface roughness was estimated as 1.124 m with highest of 1.386 m in October and lowest 0.995 m in June.

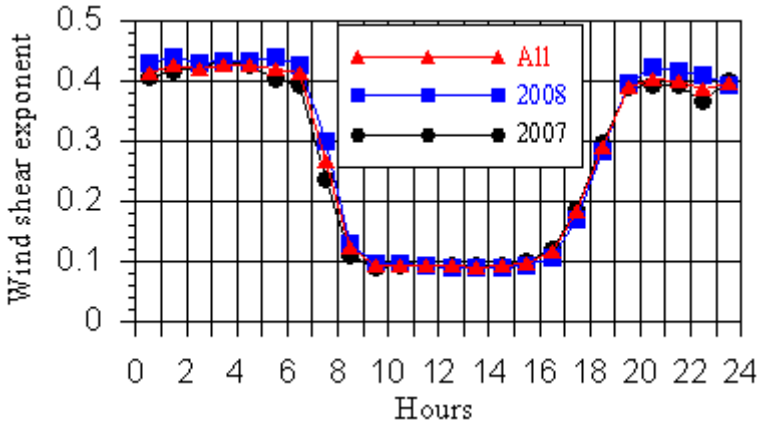

Fig. 7. Diurnal variation of wind shear exponent at Juaymah.

Wind turbulence intensity is critical parameter and dictates the durability or the operational life of the wind turbines. It is highly site dependent and should be well understood before any real time installation. According to International Electrotechnical Commission (IEC, IEC Standard 61400-1) there are standard category A and B values of the turbulence intensities. Any value between these two or below is said to be safe for the normal operation of the wind turbine. The characteristic turbulence intensity, which is another important parameter, is defined as the sum of mean turbulence intensity and the standard deviation of mean turbulence intensity in a wind speed bin. The overall mean turbulence intensity values over entire period of data collection were 0.172, 0.142, 0.127 and 0.122 at 10, 20, 30 and 40m AGL, respectively. The mean turbulence intensity decreases with increasing height AGL as the near ground turbulence effects minimize with height. The mean turbulence intensity along with IEC and characteristic turbulence values is given in Fig. 8. It is evident from this figure that the mean turbulence intensity at the site of measurements is much below even the category C of IEC limits and hence will be safe for normal operating life of the turbines.

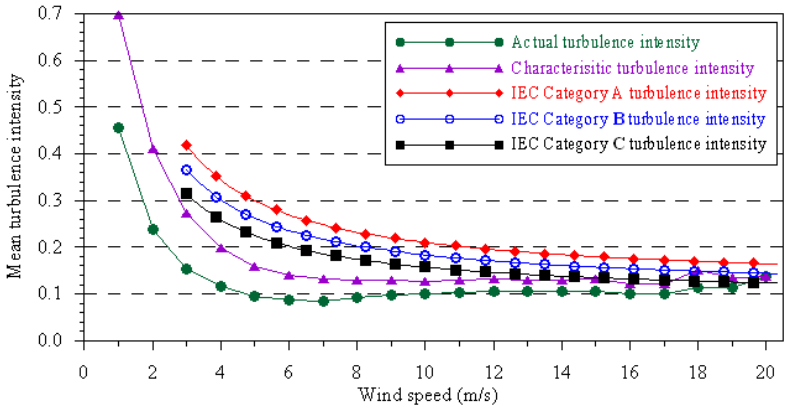

Fig. 8. Varitaion of mean turbulence intensity with wind speed.

3.5. Wind energy yield analysis

For energy yield estimation, a three bladed wind turbine of 2.75MW rated power with rotor diameter of 100m from Vestas was chosen. The net energy yield was calculated by considering the down time, array, soiling and other losses as 4, 5, 1 and 4%, respectively. For energy yield estimation, three hub heights of 60, 80 and 100 meters were considered. The

Annual average wind speed at 60, 80 and 100m AGL was found to be 6.3, 6.8 and 7.2m/s, respectively. The chosen wind turbine could produce average net power of 1,103; 1,239 and 1,341kW corresponding to wind speed at hub heights of 60, 80 and 100m; respectively. Furthermore, the annual net energy equivalent to 9,664; 10,851 and 11,747MWh could be produced with an average plant capacity factor (PCF) of 40.1, 45.0 and 48.8% corresponding to hub heights of 60, 80 and 100m, respectively, from the chosen wind turbine. On an average, the rated power could be produced for only 4% of the time during the year with a hub height of 100m. There will be certain times when the wind turbine will have zero output. It is evident that on annual basis, only 3.6% of the times there will be no power with a hub height of 100m and around 3.9% of the times for 60m hub height. Since wind is an intermittent source of energy, one has to bear with this type of situation.

4. Conclusions

The analysis of the measured data showed that the annual average wind speeds were 4.1, 4.8, 5.3 and 5.7 m/s at 10, 20, 30 and 40m AGL, respectively. The prevailing wind direction was found to be NNW and NW during measurement period. Highest wind speed was observed in June while minimum in August and October at all the heights of wind speed measurements. During entire data collection period, the average wind power density values at 10, 20, 30 and 40m AGL were 85.5, 119.1, 154.2 and 180.3W/m^2, respectively.

The wind shear exponent (WSE) obtained using all the data values was 0.273 while 0.269 and 0.279 for the data of 2007 and 2008, respectively. No definite seasonal trend could be noticed in the values of WSE. The overall mean turbulence intensity values over entire period of data collection were 0.172, 0.142, 0.127 and 0.122 at 10, 20, 30 and 40m AGL, respectively.

The monthly average minimum energy of 526, 600 and 661MWh was generated in August while a maximum of 1,034; 1,127 and 1,192MWh in June corresponding to hub heights of 60, 80 and 100m, respectively. The monthly mean plant capacity factor (PCF) varied between 25.7 and 52.2% for 60m hub height, 29.3 and 57.0% for 60m and between 32.3 and 60.2% for 100m hub height in the months of August and June, respectively.

References

[1] A.H. Marafia, and H.A., Ashour, Economics of off-shore/on-shore Wind Energy Systems in Qatar, Renewable Energy, 28, 2003, pp. 1953-1963.

[2] W. El-Osta, , and Y. Kalifa, Prospects of Wind Power Plants in Libya: A Case Study, Renewable Energy, 28: 2003, pp. 363-371.

[3] W. Al-Nassar, , S. Alhajraf, A. Al-Enizi, L. Al-Awadhi, Potential Wind Power Generation in the State of Kuwait, Renewable Energy, 30, 2005, pp. 2149-2161.

[4] E.S. Hrayshat, Wind Resource Assessment of the Jordanian Southern Region. Renewable Energy, 32, 2007, pp. 1948-1960.

[5] M. Elamouri, and F.B. Amar, Wind Energy Potential in Tunisia, Renewable Energy, 33(4), 2008, pp. 758-768.

[6] A. Ucar and F. Balo, A seasonal analysis of wind turbine characteristics and wind power potential in Manisa, Turkey, International Journal of Green Energy, 5, 2008, pp. 466–479.

[7] H. S. Bagiorgas, G. Mihalakakou, and D. Matthopoulos, A Statistical Analysis of Wind Speed Distributions in the Area of Western Greece, 5(1 & 2), 2008, pp. 120 – 137.

[8] A.S.A. Shahta and R. Hanitsch, Electricity Generation and Wind Potential Assessment at Hurghada, Egypt, Renewable Energy, 33, 2008, pp. 141-148.

[9] İ. T. Toğruland and M.İ. Kizi, Determination of Wind Energy Potential and Wind Speed Data in Bishkek, Kyrgyzstan, International Journal of Green Energy, 5(3), 2008, pp. 157 – 173.

[10] F.A.L. Jowder, Wind Power Analysis and Site Matching of Wind Turbine Generators in Kingdom of Bahrain, Applied Energy, 86, 2009, pp. 538–545.

[11] Y. Himri, A.S. Malik, A.B. Stambouli, S. Himri, and B. Draoui, Review and use of the Algerian Renewable Energy for Sustainable Development, Renewable and Sustainable Energy Reviews, 13, 2009, pp. 1584-1591.

[12] B. Sahin and M. Bilgili, Wind Characteristics and Energy Potential in Belen-Hatay, Turkey, International Jopurnal of Green Energy, 6(2), 2009, pp. 157–172.

[13] J. Ansari, I.K. Madni, and H. Bakhsh, Saudi Arabian Wind Energy Atlas, KACST, Riyadh, Saudi Arabia, 1986, pp. 1-27.

[14] S. Rehman, T.O. Halawani and T. Husain, Weibull Parameters for Wind Speed Distribution in Saudi Arabia, Solar Energy, 53(6), 1994, pp. 473-479.

[15] S. Rehman and T.O. Halawani, Statistical Characteristics of Wind in Saudi Arabia, Renewable Energy, 4(8), 1994, pp. 949-956.

[16] S. Rehman, T.O. Halawani and M. Mohandes, Wind Power Cost Assessment at Twenty Locations in the Kingdom of Saudi Arabia. Renewable Energy, 28, 2003, pp. 573-583.

[17] S. Rehman and A. Aftab, Assessment of Wind Energy Potential for Coastal Locations of the Kingdom of Saudi Arabia, Energy, 29, 2004, pp. 1105-1115.

[18] S. Rehman, I. El-Amin, F. Ahmad, S.M. Shaahid, A.M. Al-Shehri and J.M. Bakhashwain, Wind Power Resource Assessment for Rafha, Saudi Arabia, Renewable and Sustainable Energy Reviews,11, 2007, pp. 937-950.

A wind tunnel method for screening the interaction between wind turbines in planned wind farms

Mats Sandberg[1,*], Hans Wigö[1], Leif Claesson[1], Mathias Cehlin[1]

[1] *University of Gävle, Gävle, Sweden*
** Corresponding author. Tel: +46 26648139, Fax: +46 648181, E-mail: msg@HiG.se*

Abstract: The energy captured by wind farms is reduced if there is an interaction between the individual turbines. In the paper a novel method for studying the interaction between wind turbines is presented. It is based on recording the static pressure on ground in a wind tunnel provided with wind turbine models.
The assumption is that the pressure distribution at ground reflects the pressure distribution at hub height. The pressure distribution at hub height is a result of the flow in the vicinity of the turbine.
The pressure at ground is recorded with a pressure plate provided with 400 pressure taps. The wind turbine model is a porous disk giving a non rotating wake.
At first the pressure response to one wind turbine is recorded. This is the reference case giving the characteristics of a non disturbed wind turbine. Its region of influence can therefore be determined. This provides important information on how to avoid any interaction between turbines. A nearby turbine should not be placed within the region of influence. In the paper we show how the pressure response varies with different distances between two turbines. The agreement between the static pressure on ground and at hub height has been tested by recording the static pressure at hub height with a small Prandtl tube.

Keywords: *Wind farms, Wind tunnel, Pressure distribution on ground, Pressure distribution at hub height, Region of influence*

1. Introduction

To benefit of economies of scale, wind turbines are arranged in wind farms. As wind energy capacity expands, the size of individual wind farms continues to increase requiring tens to hundreds of wind turbines typically arranged in a large array. While organizing wind turbines in wind farms help in reducing the cost of energy production they introduce another problem, aerodynamic interaction. One of the research challenges is to accurately model interactions between the individual turbines to accurately predict power output before wind farm construction. In a wind farm with *N* turbines the wind farm efficiency is defined as

$$\eta_A = \frac{E_{A_i}}{E_T N} \qquad (1)$$

Where E_A is the annual energy captured by the wind farm and E_T is the annual energy captured by one isolated turbine. If there were no aerodynamic interaction the energy captured by the wind farm would be NE_T and the efficiency would subsequently be 100 %. Figure 1 shows a wind turbine with rotor diameter *D*. Array losses can be reduced by optimization of the downwind spacing and the cross wind spacing.

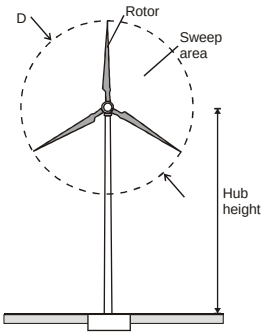

Fig. 1. Definition of some concepts

Behind a wind turbine there is rotating wake with a velocity deficit with respect to the approaching free wind U_∞. If we set the reference pressure (static pressure) in the undisturbed wind to zero there is an under pressure in the wake (compare Figure 5). After a relatively short distance there is pressure recovery. However the velocity deficit goes on for a long distance behind the turbine.

With a too short distance between wind turbines the wind turbines upstream will lower the exposed wind speed of the turbines downstream. Subsequently the power generated by the wind farm will be reduced. This calls for the need of methods for predicting the risk of interaction. Providing such methods in the planning process is the purpose of this research. The importance of accurate design models increases since the turbines gets larger and larger by time. If there is an interaction between wind turbines one can minimize the loss in power generated by suitable control of the wind turbines [1].

It is extremely difficult to predict the power output from wind farms, due to atmospheric turbulence, wind shear, changes in wind directions, wake effect from neighboring turbines etc. In recent times, CFD (Computational Fluid Dynamics) simulations have been performed on wind turbines. Recent wake studies based on CFD using various turbulence models have been presented by e.g. Ivanell [2], Sørensen et al. [3], and Wußow et al.[4]. CFD methods for simulating wake flows and wake interactions need to resolve many different length scales, ranging from the thickness of the blade boundary layer to the distance between the turbines. Hence, there are still limitations in CFD to simulate an entire park, due to computer limitations.

1.1. Basic assumption behind the method

Our approach for studying the aerodynamic interaction between individual wind turbines is based on the assumption that with a plain ground the static pressure distribution on the ground reflects the pressure distribution at hub .Aand the pressure distribution at the hub height reflects the air flow pattern at this height. For natural ventilation the relation between the static pressure in air and on the ground has been explored in [5]. The results were encouraging and are the impetus for this work.

2. Methodology

2.1. Wind tunnel

The experiments were conducted in the atmospheric boundary layer wind tunnel at University of Gävle. The pertinent details of the wind tunnel are shown in Figure 2. Within the empty wind tunnel there is a pressure gradient, see Fig 9. To equalize the pressure within the wind tunnel with the ambient pressure the wind tunnel is provided with a slot of width 6 cm located 255 cm downstream of the centre of the turning table. The slot is running along the whole perimeter of the wind tunnel.

During the tests the wind speed at half height in the test section was about 20 m/s.

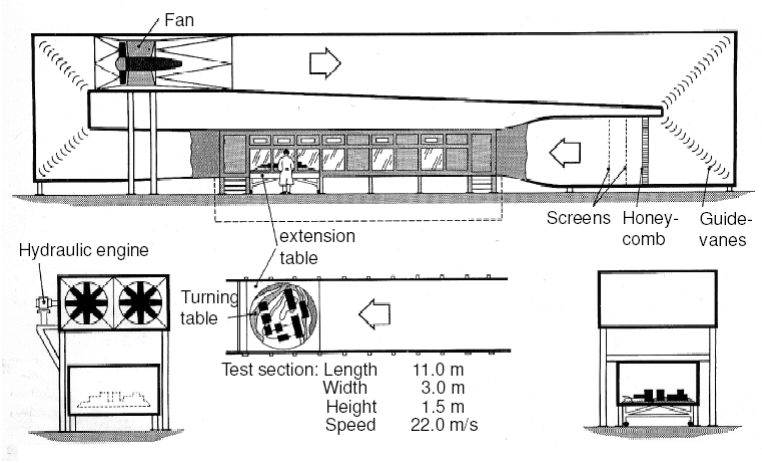

Fig. 2. Atmospheric boundary layer wind tunnel

2.2. Wind turbine model

The wind turbine model used in this study was in scale 1:2000 and had a diameter of 45 mm and the hub height was 45 mm. This corresponds to a wind turbine with 90 meters diameter and a hub height of 90 meters. In the model the rotor where replaced by a porous disc, which was used to simulate the wake behind the wind turbine Medici & Alfredsson [6] .The disc porosity was 42% and the corresponding drag coefficient was 0.85. This value of the drag coefficient is approximately the same as the value obtained for a turbine at high tip speed ratios.

2.3. Technique for measurement of static pressure at hub height and on the ground

The static pressure at hub height (45mm above ground in the wind tunnel) was measured with a Prandtl tube of 3 mm diameter. The static pressure on ground was measured with a pressure plate provided with 400 pressure taps organized in a quadratic pattern with a distance of 37 mm between the centers of the taps, see Figure 3. The pressure was recorded with a pressure transducer connected to a scanner valve. Measuring the pressure in all 400 pressure taps takes about 5 hours

Figure 4 shows the wind tunnel with one wind turbine model placed on the pressure plate. In this picture the wind tunnel was provided with roughness elements and spires to generate a turbulent boundary layer.

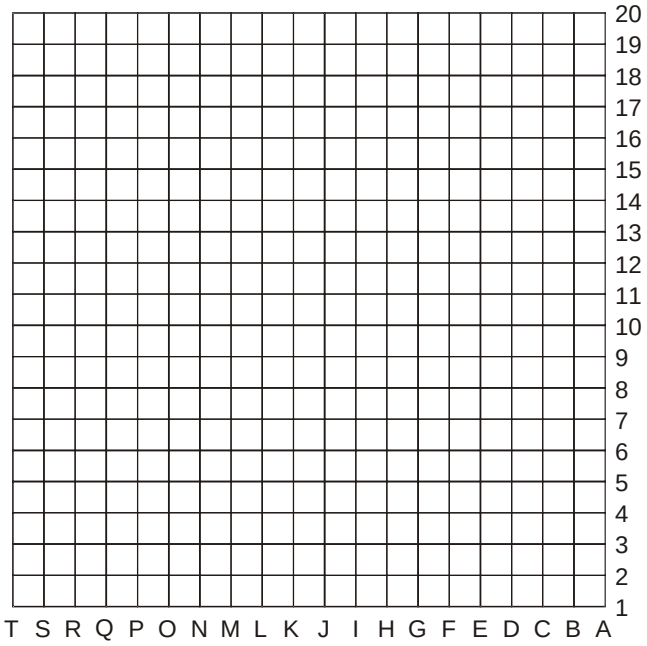

Fig. 3 Notation for the pressure plate

Fig. 4 Wind tunnel with one wind turbine model placed on the pressure plate along line 10 in Fig.3

To eliminate the effect of the pressure gradient along the wind tunnel a measurement was first made with an empty wind tunnel. These data were then subtracted from the pressure readings obtained with a turbine model present.

3. Results

3.1. Pressure response on ground due to one wind turbine

To begin with one wind turbine was placed on the pressure plate along line 10 in Figure 3 and the pressure was recorded. Figure 5 shows the recorded pressure (raw data) quantified as a pressure coefficient.

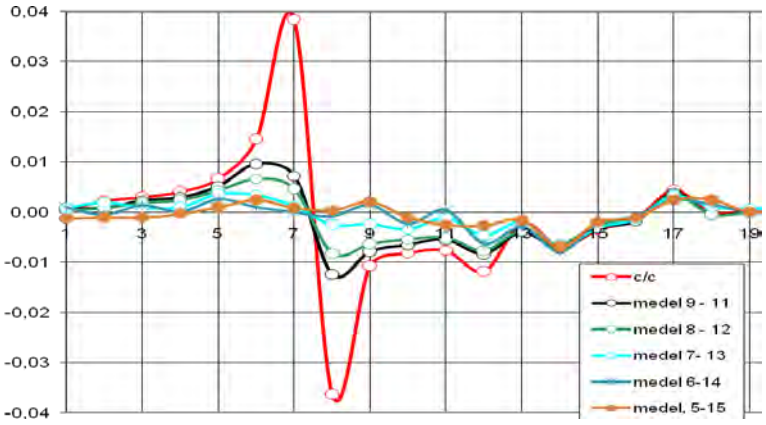

Fig. 5. Recorded pressure coefficients at different positions with one wind turbine on the pressure plate. (medel = average).

The pressure is shown as the pressure distribution along line 10 (center line) in Figure 3.. The pressures in the surroundings are shown as the mean value of the lines 9-11, 8-12, 7-13, 6-14 and 5-15 respectively .

Upwind the pressure reflects the deceleration of the flow when approaching the disk. The highest pressure corresponds to the stagnation pressure on a solid disk. Then there is an acceleration of the flow when passing through the openings of the disk. After reaching the minimum pressure in the wake the static pressure is recovered relatively fast.

3.2. The region of influence of one wind-turbine

The gray area in Figure 6 shows the region of influence, of a wind turbine located on the center line.

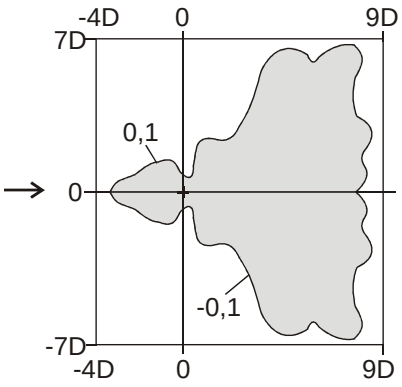

Fig. 6. Region of influence from one wind turbine located at the cross based on static pressure readings on the pressure plate. The pressure has been normalized with the highest pressure..

The region of influence on the upwind side is defined by the line representing 10% of the highest pressure (0.1 line) an on the downwind side by the line representing -10% of the highest pressure (-0.1 line). The pressure has been normalized with the highest pressure which occurs just before the wind turbine.

3.3. An example of interaction between wind turbines

The interaction between two wind turbines was explored by placing two wind turbines with a separation distance of 6.66 D. The wind turbines were located along the center line.
Figure 7 shows the response from one isolated wind turbine which is the reference case.

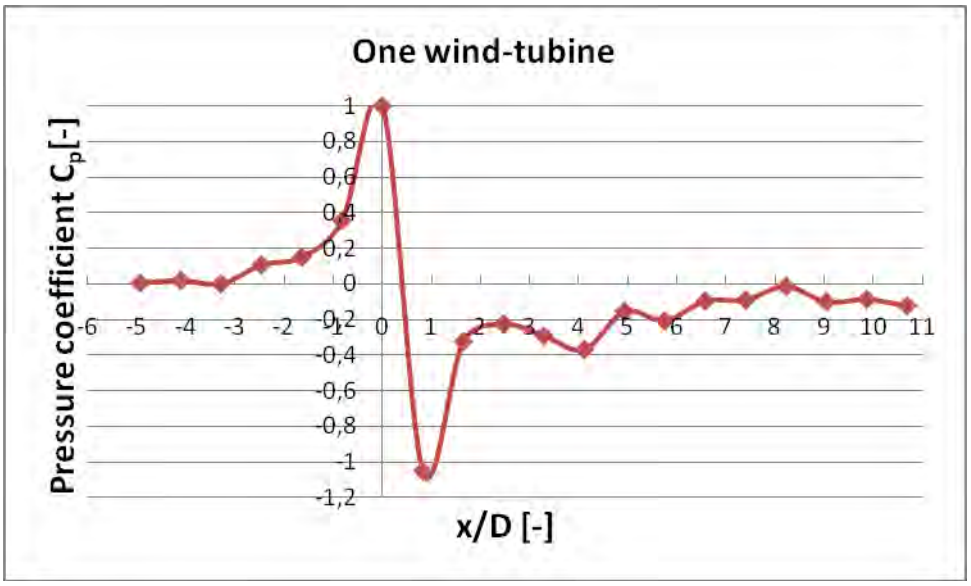

Fig. 7. One undisturbed wind turbine.

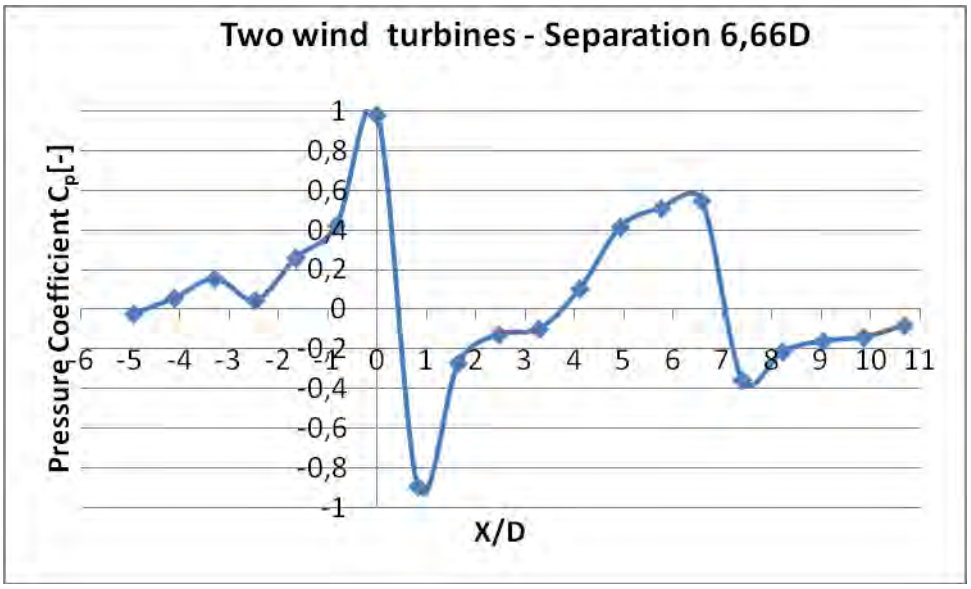

Fig.8 Two wind turbines

By comparing the pressure response of the undisturbed wind turbine in Figure 7 with the pressure response of the wind turbine located downstream in Figure 8 one sees clearly that the wind turbine located downstream is disturbed by the one located upstream.

3.4. Comparison between static pressure at hub height and on the plate

Our method is bases on that that there is a close relationship between the static pressure at hub height and on ground. This has benne tested by measuring the static pressure at hub height with a Prandtl tube. The result is shown in Figure 9.

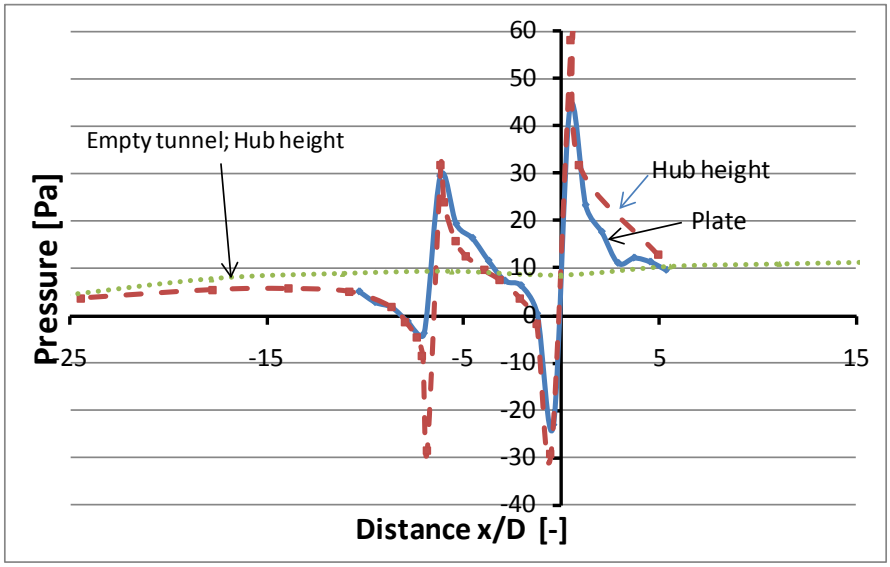

Fig.9 Static pressure at hub height and on ground (pressure plate).

There is a god correspondence between the pressures at the two levels.

4. Discussion

There is a clear response in the static pressure on the pressure plate due the presence of wind turbine models. This makes it possible to quantitatively explore the interaction between wind turbines. There is also a good correspondence between the static pressure on the ground (pressure plate) and the static pressure at hub height recorded with a Prandtl tube. Downstream of a wind turbine there is a relatively fast recovery of the static pressure. Therefore the response in static pressure may underestimate the length of the wake in terms of the velocity recovery. This will be explored by measuring the total pressure at hub height and to in detail investigate the velocity field in the wake region with Particle Image Velocimetry.

5. Conclusions

This is a new method, which is fast and economic, for exploring the interaction qualitatively between wind turbines. The next step is to develop it into a quantitative method that makes prediction of energy production possible.

References

[1] Johnson K. E. and Naveen T (2009). "Wind farm control: addressing the aerodynamic interaction among wind turbines". 2009 American Control Conference, St. Louis,MO,USA, June 10-12.

[2] Ivanell, S. (2009) "Numerical Computations of Wind Turbine Wakes". Doctoral dissertation, KTH, Sweden.

[3] Sørensen, J. N., Mikkelsen, R. & Troldborg, N. (2007) "Simulation and modelling of turbulence in wind farms". In EWEC 2007:Milan, European Wind Energy Association.

[4] Wußow, S., Sitzki, L. & Hahm, T. (2007) "3D simulation of the turbulent wake behind a wind turbine". Journal of physics: Conference series, The science of making torque from wind **75** 012033.

[5] Kobayashi T, Sandberg M, Kotani H, Claesson L, (2010) Experimental investigation and CFD analysis of cross-ventilated flow through single room detached house model *Building and Environment* 45pp. pp. 2723-2734

[6] Medici, D. and Alfredsson, P. H. (2005). Wind turbine near wakes and comparisons to the wake behind a disc. ASME Conference, January 2005, Reno, Nevada. AIAA-2005-0595

Site Matching Of Offshore Wind Turbines - A Case Study

Pravin B Dangar[1]*, Santosh H Kaware[2], Dr.P.K.Katti[3]

Department of Electrical Engineering
Dr Babasaheb Ambedkar Technological University,Lonere,Raigad ,Maharashtra ,India
Corresponding author. Tel : 9867055282 , E-mail: pravindangar@rediffmail.com,

Abstract: The stress on demand and supply gap of electricity has lead the globe to face acute problems. Further use of fossil fuel based energies for improved life and development have lead to adverse environmental effects, like climate change. Offshore wind farms have great potential as sustainable energy source. This accentuates to focus attention on technical issues such as selection, requirements, characteristics and power production from wind turbine. This paper presents a methodology developed for selection of optimum windmill for a specific site based on capacity factor approach by proper analysis of wind data. Offshore wind data for the purpose is obtained from, INCOIS Hyderabad- India for a particular site under proposal in India. The wind data is used to generate mean wind speeds for a typical day in a month by using MATLAB program. The windmill with the highest average capacity factor is the optimum one and to be recommended. The results of said analysis are presented. Such analysis at the planning and development stages of installation will enable the wind power developer or the power utilities to make a judicious choice of potential site and wind turbine generator system from the available potential sites and wind turbine generators respectively.

Keywords: *Offshore wind, Climate change, Capacity factor, Wind data.*

1. Introduction

A Number of potential wind power sites are available all over the world. Of these, not all sites have wind turbine generators installed. The observation with the existing wind farms shows that some of the wind power plants have performed poorly probably due to improper site matching. Hence there arises a n eed for a systematic approach toward the problem of optimum siting of wind turbine generators. [4] The production of electricity by a wind turbine generator at a specific site depends upon many factors. These factors include the mean wind speed of the site and the speed characteristics of the wind turbine itself namely, cut-in, rated, and furling wind speeds including the hub height. Commercially many models of wind turbine generators available, with similar MW and KW ratings. Each of these wind turbines has their own specifications and speed parameters. These speed parameters affect the capacity factor at a given specific site, and subsequently affect the choice of optimum wind turbine generator for the site. In this paper the method to determine capacity factor of different offshore wind turbine under different tower heights, rated wind speeds, is discussed for Mumbai offshore region.

1.1. Capacity Factor

It compares the plant's actual production over a given period of time with mean wind speed the amount of power the plant would have produced if it had run at rated wind speed for the same amount of time and hence can be defined as ;

- The ratio of average power output to the rated power output [1]
- An indicator of how much energy a particular wind turbine makes in a particular place.

$$C.F. = (Pa / Pr) \quad (1)$$

2. Methodology

2.1. Offshore Wind Turbine Site Matching Based On Capacity Factors

The methodology for the selection of the optimum windmill for a specific site is developed the flowchart is shown in Fig 1. The selection is based on the capacity factors (CF) of the available windmills. The long term wind speed data recorded at different hours of the day for many years is used. The particular steps used to determine C F for the mean wind speeds for at different hours of the day are generated with the manufacturer's specifications. The windmill with the highest capacity factor for the specific site is the optimum one and to be recommended.

- Step1: Calculation of Mean Wind Speeds

  The mean wind speed for a typical day of a month need to be generated by averaging all the recorded wind speeds for regular interval of long term data of the wind speeds for the site to be considered.
- Methodology Of Determination Of Capacity Factor

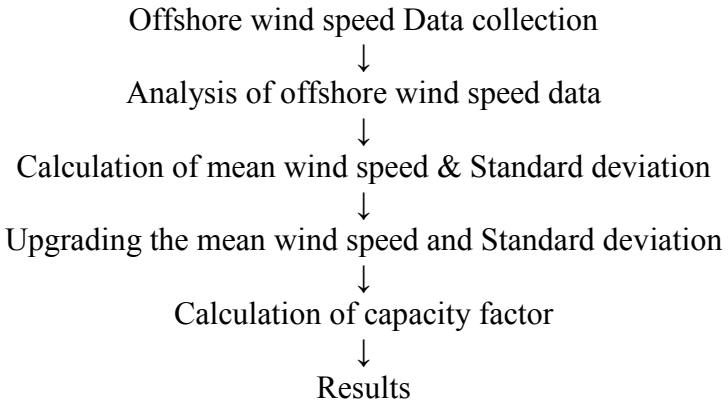

Fig 1 Methodology for determination of capacity factor

The mean wind speed is then calculated using the equation below

$$V_i = \left(\frac{\sum_{j=1}^{N_j} V_j^{\,3}}{N_j} \right)^{1/3} \qquad (2)$$

Where

V_j =observed wind speed
N_j =number of wind speed observations
V_i =mean wind speed

- Step 2 Upgrading the Mean Wind Speed

$$V_z = V_i \left(\frac{Z}{Z_i} \right)^x \qquad (3)$$

Where

V_z= mean wind speed at projected height, Z

V_i= mean wind speed at reference height, Z_i
Z= projected height (or hub height)
x=power law exponent depends upon the roughness of the surface. For open land, x is usually taken as 1/7.

- Step 3 Generation of the Wind Speed Probability Density Functions

$$f(v)=\left(\frac{v}{C_i^{\,2}}\right)\exp\left(-\left(\frac{v}{2C_i^{\,2}}\right)\right) \tag{4}$$

Where

$C_i = v_i/1.253$
v= wind speed
The Weibull probability density function is represented by

$$f(v)=\left(\frac{k}{c}\right)\cdot\left(\frac{v}{c}\right)^{k-1}\exp\left(-\left(\frac{v}{c}\right)^{k}\right) \tag{5}$$

Where;

c=scale factor, unit of speed
k=shape factor, dimensionless
v=wind speed
The Weibull parameters c and k can be found using the following acceptable approximations

$$k=\left(\frac{\sigma}{v}\right)^{-1.086} \qquad 1\le k\le 10$$

$$c=\frac{v}{\Gamma\left(1+\frac{1}{k}\right)}$$

In both the probability density functions, the wind speed v will be the mean wind speed V_Z, calculated at hub height from equation (3)

- Step 4 Calculation of Capacity Factors

The average power output from a wind turbine is the power produced at each wind speed multiplied by fraction of the time that wind speed is, experienced integrated over all possible wind speeds. In integral form the equation is [2,4]

$$P_a=\int_0^{\infty} P_w\cdot f(v)\cdot dv \tag{6}$$

Capacity factor can be defined as the ratio between average power output given by equation (6) and rated power of the wind turbine P_r can be obtained from the manufacturer's details. In equation(6) the power at various wind speeds can obtained from the following equation

$$P_w = \begin{cases} P \cdot \dfrac{v^k - v_c^{\,k}}{v_R^{\,k} - v_c^{\,k}} & for\ v_c \le v \le v_R \\ P & for\ v_R \le v \le v_f \\ 0 & elsewhere \end{cases} \quad (7)$$

Where

P is the rated electrical power,
v_c is the cut in wind speed,
v_R is the rated wind speed
v_f is the cut off wind speed
k is the Weibull shape parameter defined under the equation(5), the relationship betweenpower and wind speed is as under,

$$P = \frac{1}{2} C_p \cdot \rho \cdot A \cdot v^3 \eta$$

For which considering value of air density factor ρ = 3.485 P/T

Where P=101.3 kpa and T=273K the power equation thus can be written as

$P=0.646\ C_p .\ A\ .\ v^3.\eta$ (8)

Thus the capacity factor defined above can be expressed as

$$CF = \frac{1}{P_r} \int P(v) \cdot f(v) \cdot dv \quad (9)$$

- Step 5 Choice of the Optimum Wind Turbine Based on Capacity Factor
  The capacity factors of different turbines are computed from the wind speeds (v_c, v_R, v_f) and rated power data obtained from manufacturer details. Now detailed table for the capacity factor for each turbine is prepared from which it can be clear that certain turbine will have a maximum value of capacity factor. This becomes the candidate which can produce the optimal power for the chosen site and wind data. [4, 5, 6]

3. Computation and Results

3.1. Data Analysis:

The wind speed data that is obtained from Indian National Centre for Ocean Information Services (INCOIS) has been first arranged on the hourly basis. The mean wind speed and standard deviation on the hourly basis and daily basis is computed. The results of computed mean wind speed data has been presented year wise for the year 1998 and 2005 respectively in Figure 2 to 5.

3.2. Computation Of Capacity Factor

The capacity factor of a machine indicates the ability to generate the mechanical energy by utilizing the wind power. This solely depends upon how the wind speed utilized to spin the rotor of turbine. The mean wind speed data that has been obtained from INCOISIS is used to determine the hub height wind speed as per the equation 3 . Further wind turbine data of the

selected machine is used for the computation of capacity factor for each of the machine the details of which are shown in table 1.the computation of capacity factor has been carried out by using MATLAB program.

Table 1. Offshore wind turbine specification

Company Name	Power Rating MW	Cut in wind Speed (m/s)	Rated wind speed (m/s)	Cut out wind speed (m/s)	Rotor diameter in meter	Turbine Height in meter
RE Power	5	3	11.4	25	126	90
GE	3.6	3.5	14	27	111	90
Vestas	3	3.5	15	25	90	90
Vestas	3	3	12	25	112	94

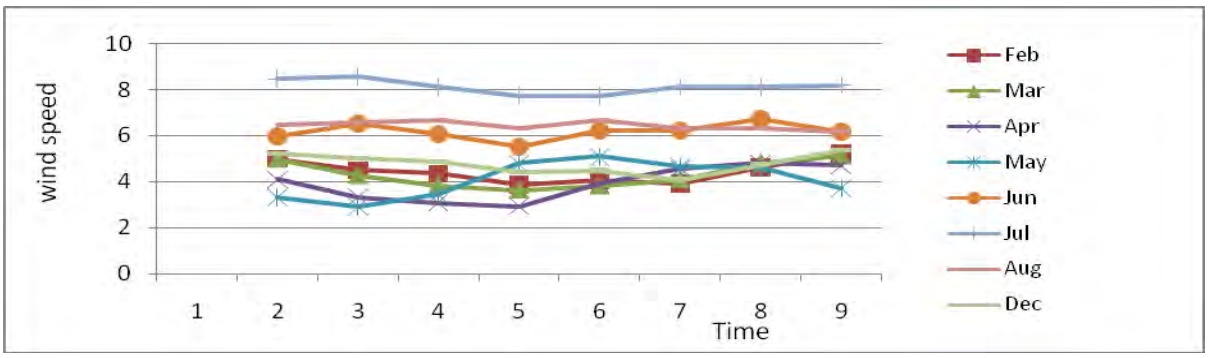

Fig .2 Hourly average mean wind speed of the year 1998

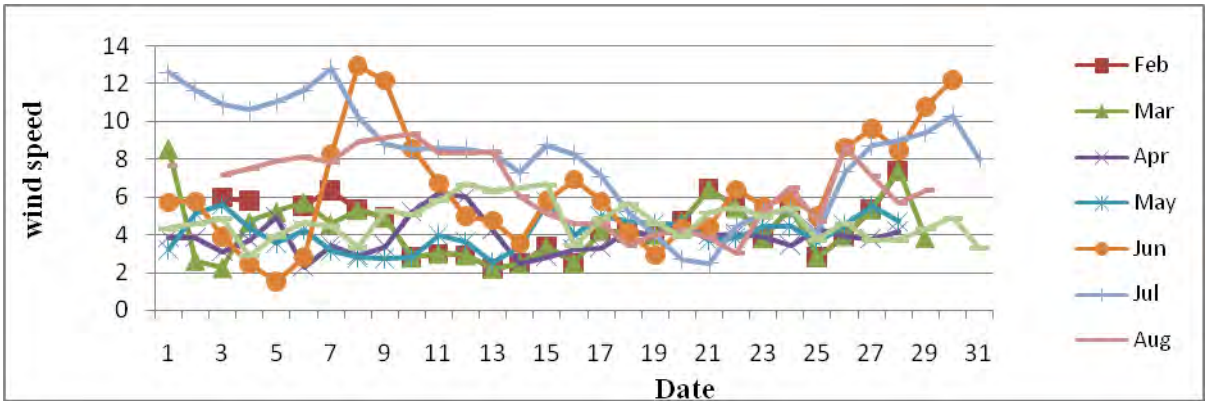

Fig 3 Monthly Average wind speed of the year 1998

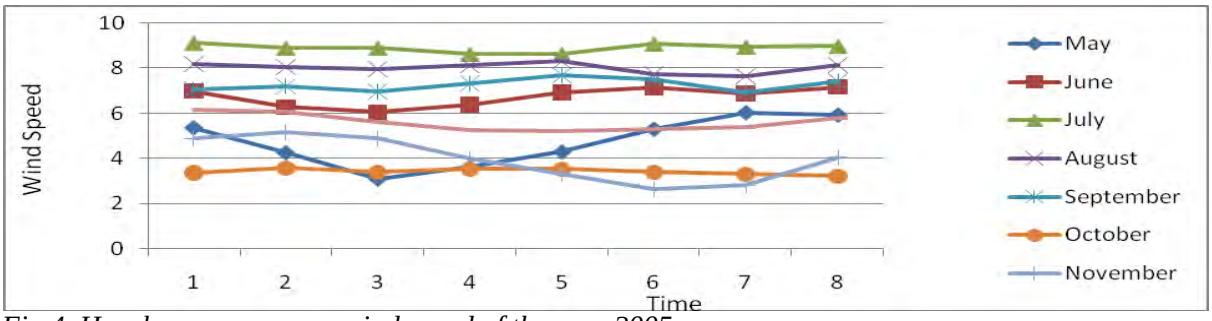

Fig.4. Hourly average mean wind speed of the year 2005

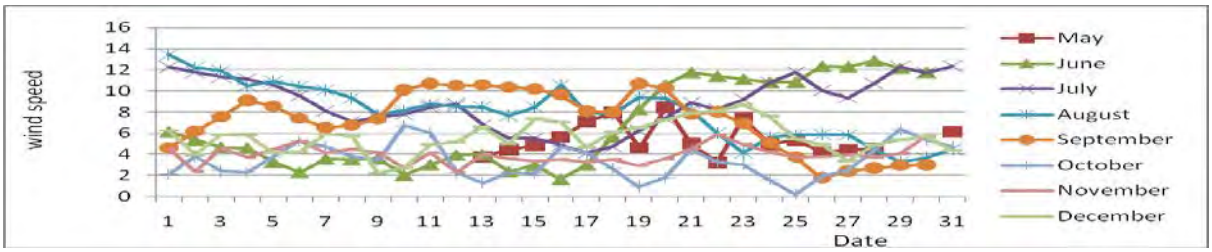

Fig .5. Monthly average wind speed of the year 2005

The graphical representation of monthly capacity factor for the selected machine for the respective years has been presented in Fig 6 and 7. Finally the annual capacity factors for the selected machine have been presented in tabular and graphically in table 2 and Fig.8. From the result available the machine with optimal capacity factor that is RE Power 5 MW and Vestas 112/3.0 MW has been recommended.

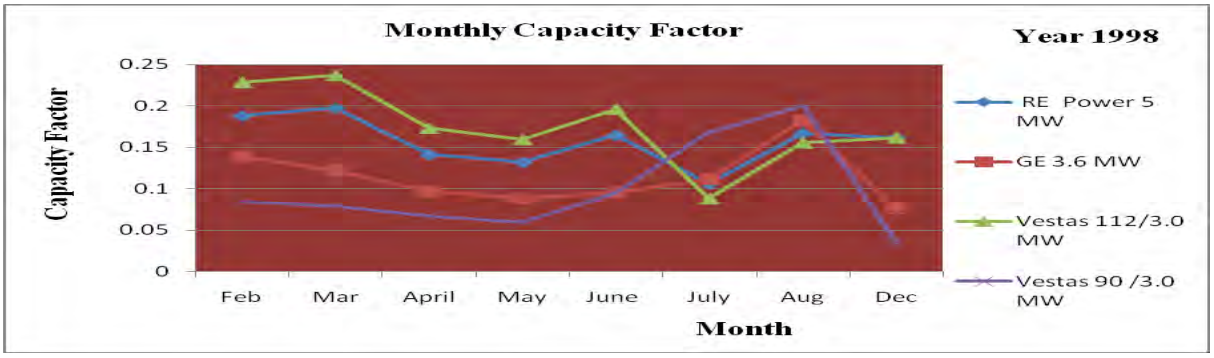

Fig.6. Monthly Capacity factor for the year 1998

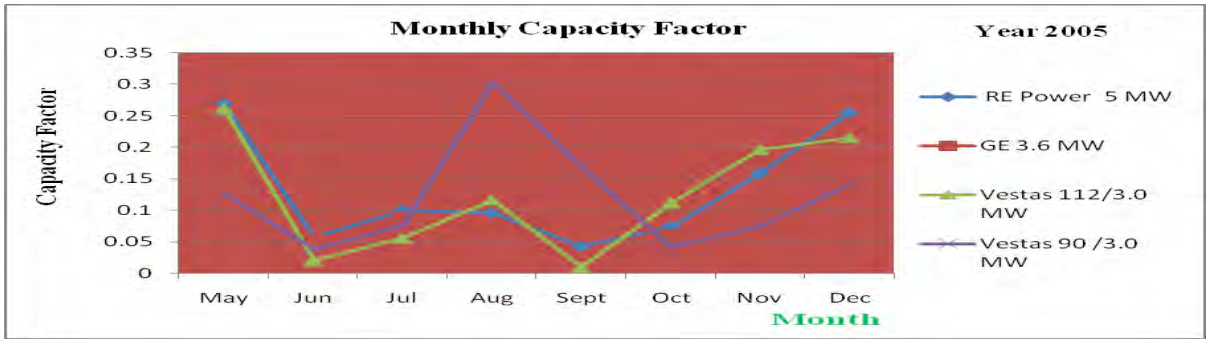

Fig.7. Monthly Capacity Factor for the year 2005

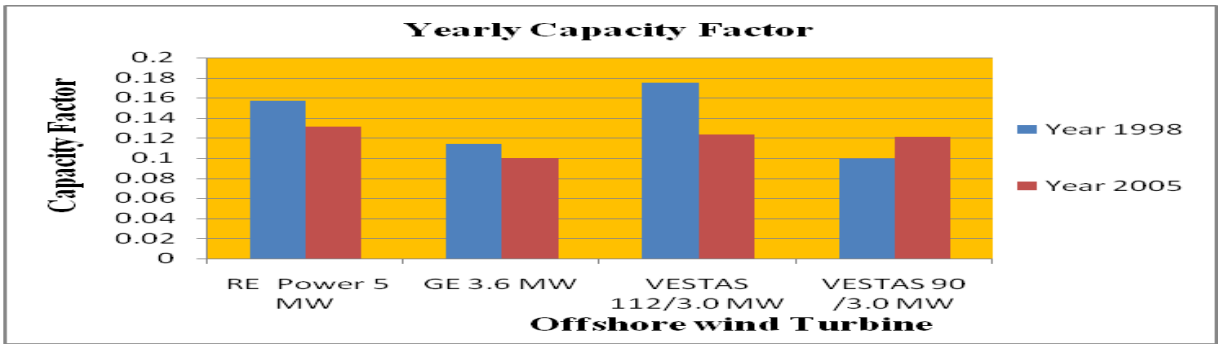

Fig. 8 Average annual capacity factor

Table 2. Yearly average capacity factors

Hub Height		90 m	90 m	94 m	90 m
Buoy ID	Year	RE Power 5 MW	GE 3.6 MW	Vestas 112/3.0 MW	Vestas 90 /3.0 MW
SWO2	1998	0.15727643	0.1142502	0.175344331	0.098867349
SWO2	2005	0.13160839	0.1001096	0.123371867	0.121234018

The typical disposition of the selected wind turbines for the proposed site used in this work as mentioned has been presented in Fig. 9 and 10 respectively for RE power and Vestas machines. This will give an effective feel of how a wind form may appear if installed on an offshore site.

Fig.9. RE Power 5 MW offshore wind turbine layout for 50MW

Fig.10. Vestas 112/3.0 MW offshore wind turbine layout for 50MW

3.3. Conclusions

The paper presents a methodology for assessment of offshore wind data and the capacity factor of wind turbines for their suitability to be used for harnessing offshore wind energy in a better fashion as depicted by the results. This not only helps to choose a better turbine but also to maximize the system performance. Further the illustration presented for a specific site in Konkan region of Maharashtra exemplifies the suitability of method presented.

Acknowledgement

The authors acknowledge thankfully the support extended by Indian National Centre for Ocean Information Services,(INCOIS) Hyderabad for providing necessary offshore wind data for Mumbai (India) offshore area, Department of Electrical Engineering, and Dr. Babasaheb Ambedkar Technological University, Lonere, Dist: Raigad, Maharashtra (India) for their financial support during the work.

References

[1] Jeffrey Logan and Stan Mark Kaplan Wind Power in the United States: Technology, Economic, and Policy Issues June 20, 2008 Specialists in Energy Policy Resources, Science, and Industry Division. pp 1-53

[2] Pradeep.K.Katti, Dr.Mohan K Khedkar, Generation capacity Assessment of Distribute Resources Based on Weather Model for Integrated Operation, International conference CERA -2005, IIT Roorke India . pp1-6

[3] Ziyad M. Salameh lrianto Safari ,Optimum Windmill- Site Matching . IEEE Transactions on Energy Conversion, Vol. 7, No. 4, December 1992. pp 669-676

[4] Suresh H. Jangamshetti, and V. Guruprasada Rau, Optimum Siting Of Wind Turbine Generators , IEEE Transactions on Energy Conversion ,Vol 16, No. 1, March 2001,pp 8-13

[5] Tai-Her Yeh and Li Wang A Study on Generator Capacity for Wind Turbines Under Various Tower Heights and Rated Wind Speeds Using Weibull Distribution , IEEE Transactions on Energy Conversion, Vol. 23, No. 2, June 2008,pp-592-602

[6] Suresh H. Jangamshetti, and Dr. V. Guruprasada Rau, Site matching of wind turbine Generators : A case study, IEEE Transactions on Energy Conversion, Vol. 14, No. 4, December 1999 pp- 1537-1543

[7] Bogdas S.Borowy,Ziyad M Salame Methodology for Optimally Sizing the Combination of a Battery Bank and PV Array in a Wind/PV Hybrid System IEEE Transactions on Energy Conversion, Vol. 11, No. 2, June 1996 pp 367-375

Experimental and Fluid-dynamic Analysis of a Micro Wind Turbine in Urban Area

Marco Milanese[1,*], Arturo de Risi[1], Domenico Laforgia[1]

[1] *Department of Engineering for Innovation – University of Salento, Lecce, Italy*
** Corresponding author. Tel: +39 0832297760, Fax: +39 0832297777, E-mail: marco.milanese@unisalento.it*

Abstract: In urban areas, the evaluation of the energy outcome of a horizontal axis micro wind turbine depends on several factors such as mean wind velocity, location, turbulence, etc. To maximize the micro wind turbine efficiency it is important to define the best location. The present paper focuses on the definition of common rules for micro siting in urban areas.

In this work, the efficiency of a 1 kWp horizontal-axis wind turbine has been evaluated, by means of CFD and experimental data. The numerical results have been compared with the experimental data collected over a period of time of three years, by using a measurement equipment installed on the roof of the Engineering building at the University of Salento. The results have shown that horizontal axis wind turbines suffer from wake effect due to buildings, therefore best sites in urban area have to be identified by a careful fluid dynamic analysis aimed at evaluating all causes that can reduce significantly the performance of the generator.

Keywords: *Micro wind turbine, best location, experimental and fluid-dynamic analysis*

1. Introduction

In the last years, prices of oil have achieved strong variations on international markets. These occurrences have underlined the very important role of energy as fundamental factor for human activity [1,2,3]. In this scenario, small/micro wind generators are gaining an important role due to both the low environmental impact and the possibility to avoid big electrical networks.

Several authors have studied the topic of microgeneration, by taking into account both technical and social aspects [4,5,6]. Kelleher e Ringwood [7] developed software to estimate the economic performance of small/micro solar and wind plants. Watson [8] carried out studies about the microgeneration management techniques considering power supply issues. Besides, in order to estimate micro wind turbine performance several studies have been carried out by using computational fluid dynamic models (CFD), since they can show an exhaustive draft about the wind flow around the micro turbine in any meteorological conditions, allowing saving time and costs [9,10].

For evaluating the economic convenience about the installation of a micro wind turbine in urban area, it is important to calculate positive and negative effects of buildings or other obstacles on the aerogenerator performance. For this reason, the present work focuses on the best siting of small horizontal-axis wind turbines in urban area. Particularly, an aerogenerator has been installed on the roof of the Engineering building at the University of Salento and monitored over a period of time of three years.

During experimental testes it was observed a perpetual transient condition of the microturbine that reduces its performance. Then CFD simulations have been carried out to fully understand the relationship between the aerogenerator performance measured under several meteorological conditions and the shape of the building where the plant is installed. In this way, a useful rule for best placing of horizontal-axis wind turbines in urban areas has been obtained.

2. Experimental setup and numerical model

2.1. Description of the experimental setup

In this work, an experimental apparatus has been developed for monitoring the performance of a horizontal axis micro wind turbine (1 kWp).

Anemometer, PLC, analogic/digital conversion unit, web server, voltage transducers and current transducers composed the measurement apparatus. Table 1 reports the main technical specifications of the experimental setup.

Table 1. Mean technical features of the plant

Elements	Technical features
Aerogenerator	- power: 1 kWp - cut-in velocity: 2.5 m/s - Electric generator: 24 VDC (alternator + rectifier) - n. 4 batteries: Trojan T105, 6VDC - inverter: 24 VDC-220 VAC - fiberglass rotor: D=2.5 m - Pole: 9 m
voltage transducer	R_M 0.47 Ω - Precision T_A=25 °C 0.7%
current transducer	V_{OUT} 0÷10 V - Precision T_A=25 °C 1%
anemometer	optical encoder (precision +0.3m/s up to 3m/s, ±1% over 3m/s)
PLC	8 input-PNP,NPN /8 output-Transistor PNP, interface RS232 COM-Port
analogical/digital conversion unit	8 analogical input 12 bit
Web-server	Ethernet - 10 Mbit/s

The whole system was controlled by a PLC that acquires and processes several signals and monitors all parameters under investigation. Besides the measures were viewable in real time on an Internet web site and stored on a remote hard disk.

2.2. CFD Model

In order to study the wind microturbine performance, a 3D model of the building has been drawn, as Fig. 1 shows. The total height from the ground of the aerogenerator is equal to 20 m.

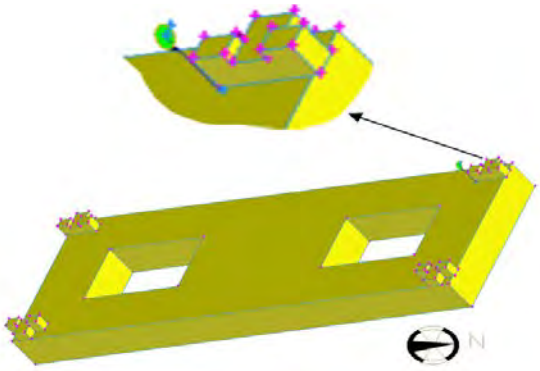

Fig. 1. 3D model of the building where the aerogenerator has been installed.

The fluid dynamic simulation domain has been obtained by subtracting the building volume to a parallelepiped sufficiently large to consider undisturbed fluid-dynamic conditions on the boundary.

For meshing the volume, tetrahedral elements whose size was in the range between 0.2 and 2 m have been used. The computational cell size has been selected to reduce the maximum computational error and to obtain grid-independent solutions.
The mesh sensitivity analysis has been performed by comparing the results from several simulations carried out with different mesh resolutions.

Table 2. Sensitivity analysis results

Cells (n)	Mean wind velocity close to the aerogenerator (m/s)	Variation (%)
579'596	7.93	-
1'084'494	8.16	2.8%
2'552'154	8.26	4.1%

As Table 2 shows, by incrementing the number of cells from 579'596 to 2'552'154 the mean wind velocity close to the aerogenerator changes within 4.1% and this difference outcomes equal to 1.3% switching the number of cells from 1'084'494 to 2'552'154. So it is reasonable to use the denser grid, since further incrementing the number of cells, advantages shouldn't be enough to justify the relative increment of calculation time.

Numerical simulations have been carried out by using FLUENT software and studying eight wind directions with an angular difference equal to 45° and wind velocity within the range 4÷8 m/s. This range has been fixed by taking into account the following considerations:

- Up to 4 m/s, the electric power is lower than 5% of the nominal power and the data statistical dispersion is much large with respect to the measured values: this issue does not allow to do a comparison between experimental and numerical data;
- Over 8 m/s, there are not enough data (less than 2%).

Turbulence has been evaluated using the standard k-ε turbulence model.

3. Discussion of results

3.1. Measured data analysis

The aerogenerator was installed on the roof of the Engineering building at the University of Salento. The following coordinates individuate the exact location: 40°20'03" N, 018°06'51" E and 35 m with respect to the mean sea level.

The wind microturbine has been monitored over a period of three years (2005, 2006 and 2007), measuring several parameters: wind velocity and direction, electric current, voltage and generated power. All parameters have been registered each 10 minutes.
For modeling wind data the Weibull function has been used in accord with following equation.

$$P(v < v_i < v + dv) = P(v > 0)\frac{k}{c}\left(\frac{v_i}{c}\right)^{k-1} \exp\left(-\left(\frac{v_i}{c}\right)^{k}\right)dv \quad (1)$$

Where c is the scale parameter, k is the shape factor, v_i is a generic wind velocity value, dv is the wind velocity increment, $P(v<v_i<v+dv)$ is the probability to register a wind velocity within the range v e $v+dv$ and $P(v>0)$ is the probability to register a wind velocity major to zero.

Weibull function is completely defined if c and k are known: these coefficients have been calculated by using the modified maximum probability method and considering a wind velocity step equal to 0.1 m/s. Table 3 reports the values of c and k for the period under

investigation (2005÷2007), whereas Fig. 2 shows the comparison between experimental data and the Weibull curve.

Table 3. Weibull function parameters for the period under investigation (2005÷2007)

Year	*k*	*c* (m/s)	Most probable velocity (m/s)	Mean velocity (m/s)	Standard deviation (m/s)
2005	1.658	3.457	1.98	3.09	1.91
2006	1.649	3.420	1.94	3.06	1.90
2007	1.669	3.444	1.99	3.08	1.89
Mean values	1.659	3.440	1.97	3.08	1.90

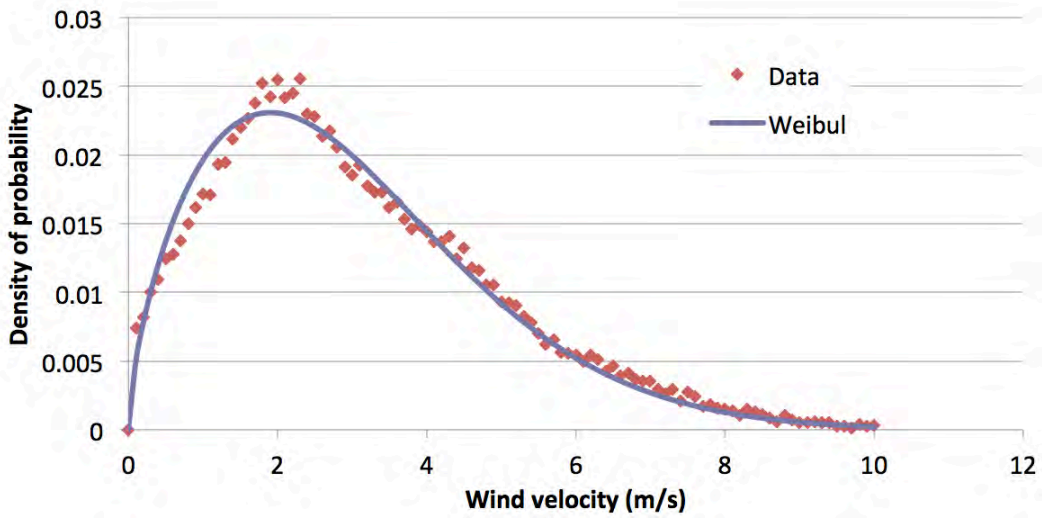

Fig. 2. Comparison between experimental data and the Weibull curve.

The anemometric analysis shows that the mean wind velocity at 20 m from the ground is equal to 3.08 m/s. This value is comparable with the aerogenerator cut-in velocity (2.5 m/s) and so it demonstrates that the site does not have a good wind potential. Nevertheless it is important to remark that at 35 m from the ground the mean wind velocity is equal to 4.9 m/s as the Wind Atlas of Apulia Region [11] shows. In other words, the mean wind velocity has to be halved going from 20 m to 35 m of height from the ground: this issue is common to many sites in urban area and it represents a big problem in order to achieve good performance from micro wind turbines.

Over experimentation time, more parameters have been measured as voltage, current and electric power. These data have been organized and analysed as function of wind direction. In this way it has been possible to study the influence of the shape of the building on the aerogenerator performance.

Fig. 3 shows the measured electric power for wind direction North as a function of wind velocity. Besides it is possible to see the comparison between the mean electric power (best fit of the measures of power - red curve) and the nominal electric power (orange curve). Particularly, for wind velocity up to 3 m/s the mean power curve is higher than nominal one, within 3 and 4 m/s the two curves are about similar and over 4 m/s the mean power curve is lower with respect to the nominal one. Moreover it is possible to observe a noticeable variability of measures due to the irregularity of wind velocity in the site under investigation.

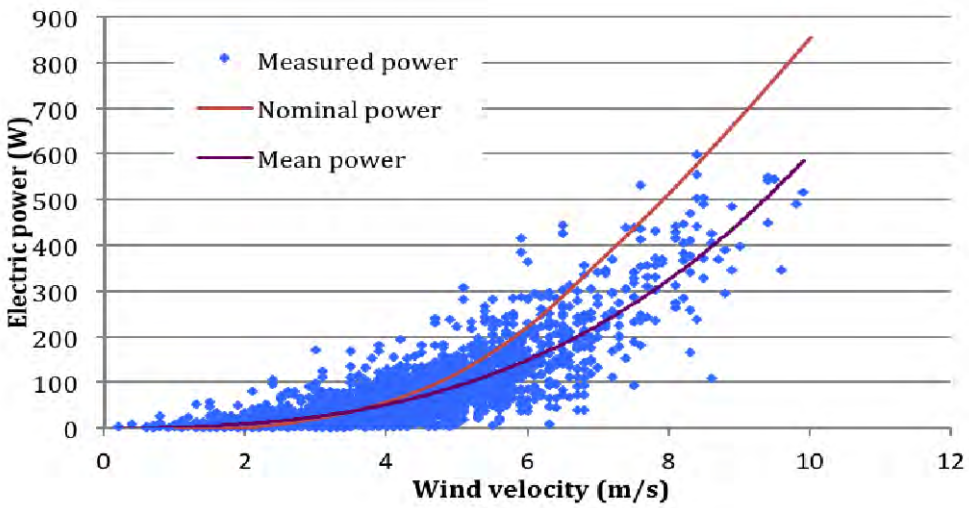

Fig. 3. Electric power output as function of wind velocity (wind direction North). The blue points indicate the measures of power, the red curve indicates the mean power (best fit of the measures) and the orange curve indicates the nominal power.

In order to complete the experimental data analysis, the measured electric power has been examined for each wind direction as Fig. 4 shows.

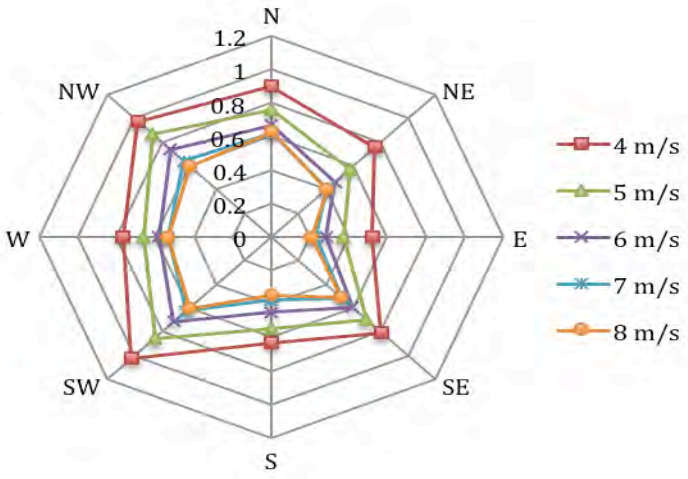

Fig. 4. Ratio between measured electric power and seminal electric power as function of wind direction and intensity

Fig. 4 demonstrates that electric power is very influenced by the wind direction, or in other words, this parameter strictly correlate with the intensity of the wake due to the shape of the building. These effects are more evident by observing the ratio between mean power and nominal power that decreases for high values of wind velocity and for all the considered directions.

3.2. CFD analysis

To fully understand the fluid-dynamic phenomena that influence the wind turbine performance several numerical simulations have been carried out by using the software FLUENT. All results are reported next.

The CFD post-processing analysis was developed taking into account for each wind direction four sections of the calculation domain. Particularly, three sections were positioned

transversely to the wind direction (the first one was placed ten meters forward the building, the second one close to the aerogenerator and the third one ten meter rear the building) and one longitudinal section was placed parallel to the wind direction. This section is very interesting because it shows the flow evolution along the building.

Numerical simulations have been carried out considering the wind velocity within the range 4÷8 m/s like to experimental analysis. Fig. 5 shows the results along the longitudinal sections for wind directions N-S (North is the prevalent wind direction), in the case of wind velocity equal to 6 m/s (mean velocity within the range 4÷8 m/s). It is important to notice that in the other cases under investigation (wind velocity equal to 4, 5, 7 and 8 m/s and other wind directions) the results are qualitatively similar to the case shown next.

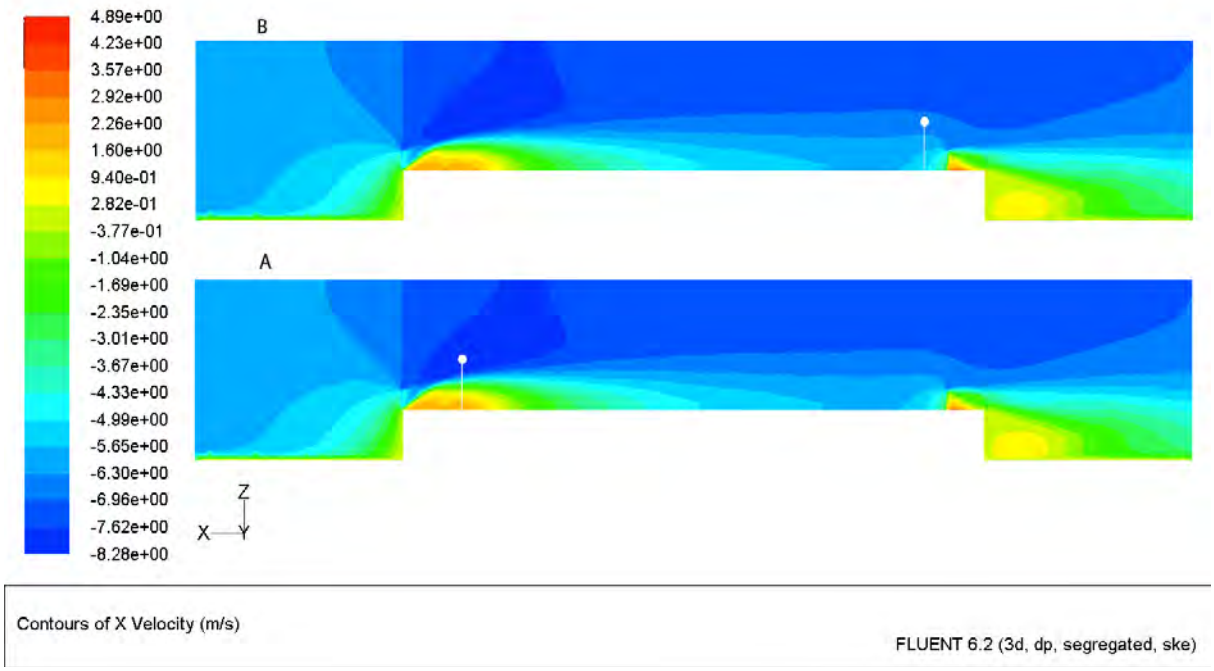

Fig. 5. Contours of X wind velocity: wind intensity on the boundary: 6 m/s; wind direction: North (A) and South (B); the pole is sketched by a line and a white circle

As the contours of X wind velocity demonstrate (Fig. 5), close to the aerogenerator there is a very strong vorticity phenomenon, whereas above this area the wind velocity rise quickly over to 8 m/s, against an inlet wind velocity equal to 6 m/s.

These results allow achieving a possible understanding of the experimental results reported in Fig. 3 and Fig. 4: the building generates an increment both of wind velocity and of vorticity influencing the aerogenerator performance; in fact the electric power results meanly lower than the nominal one, due to the strong vorticity, but in some cases the higher values of wind velocity results in a higher electric power output with respect to the nominal one. For example, under meteorological condition with wind velocity equal to 6 m/s the maximum measure of electric power matches the nominal power curve for a wind intensity equal to 8 m/s, as the analysis of Fig. 3 and Fig. 5 reveals.

Changing wind direction from North to South (Fig. 5B), the wind velocity distributions are similar to the previous case (wind direction North - Fig. 5A), with an opposite relative position of the aerogenerator.

According to experimental results, the longitudinal sections North-South show bigger wind intensity when the direction is North and so also the experimental electric power results bigger than the case South.

Another important consideration can be done taking into account the results shown in Fig. 3. As it is described before, for wind velocity up to 3 m/s the mean power curve is higher than nominal one: in this case the wind intensification effects due to the building are predominant on the vorticity. Instead, when the wind rises over to 4 m/s the vorticity generated by the wake of the building becomes prevalent on t he wind intensification effects, cutting the aerogenerator performance.

To define the best location for the horizontal axis micro wind turbine has to be take into account the turbulence intensity, defined as the ratio of the magnitude of the root mean square turbulent fluctuations to the reference velocity:

$$I = \frac{\sqrt{\frac{2}{3}k_e}}{v_{ref}} \qquad (2)$$

where k_e is the turbulence kinetic energy and v_{ref} is the mean velocity magnitude for the flow. Fig. 6 shows the comparison between the contours of X wind velocity and turbulence intensity. This evaluation allows defining the best location for the horizontal axis micro wind turbine in urban area. In fact, by overlapping areas of higher X velocity with areas of lower turbulence intensity it is possible to individuate an area where the aerogenerator can gives maximum performance.

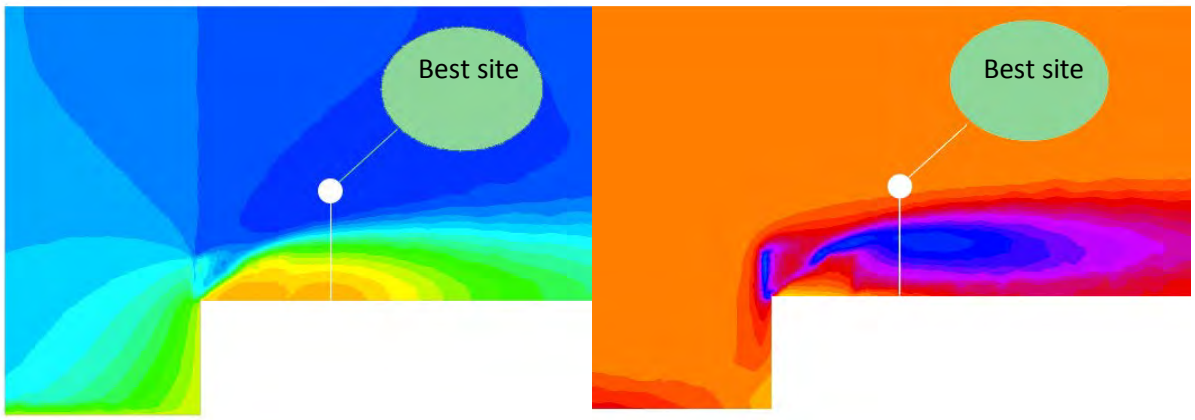

Fig. 6. Comparison between contours of X wind velocity and turbulence intensity. The pole is sketched by a line and a white circle. The best site in sketched by a green ellipse

4. Conclusions

This work focuses on experimental and numerical analysis about the electric power generation from a 1 kW horizontal-axis aerogenerator installed on the roof of the Engineering building at the University of Salento in urban area. Particularly the influence of the building on the micro wind turbine performance has been studied.

Experimental data were collected over a p eriod of time of three years during which it w as observed a perpetual transient condition of the microturbine that reduces its performance. Then to fully understand this occurrence and in order to value the performance of the

horizontal axis wind turbine, several CFD calculations have been carried out, taking into account different meteorological conditions. Numerical simulations calculated wind velocity fields and turbulence intensity above the building due to fluid-dynamic effects.

The experimental and numerical results of this study reveal that the siting of the horizontal-axis micro wind turbine on a building should allow to exploit bigger wind intensity, but often this advantage is neglected from turbulence phenomena; in fact, in the case under investigation, the measured aerogenerator efficiency appears lesser in comparison with the nominal performance curve. But, the best site can be found by crossing the contours of wind velocity with the turbulence intensity fields. In this way it is possible to localize an area (best location) where the aerogenerator can gives maximum performance.

In conclusion, the result presented in the present investigation showed that horizontal axis wind turbines suffer from wake effect due to buildings, therefore best sites in urban area have to be identified by a careful fluid dynamic analysis aimed at evaluating all causes that can reduce significantly the performance of the generator.

References

[1] T. Devezas, D. LePoire, J.C.O. Matias and A.M.P Silva, Energy scenarios: Toward a new energy paradigm, Futures, 40(1), 2008, pp. 1-16.

[2] H. Schiffer, WEC energy policy scenarios to 2050, Energy Policy, 36(7), 2008, pp. 2464-2470.

[3] V.D.Z. Bob and G. Reyen, Climate sensitivity uncertainty and the necessity to transform global energy supply, Energy, 2006, pp. 2571-2587.

[4] G.J. Dalton, D.A. Lockington, T.E. Baldock, Feasibility analysis of stand-alone renewable energy supply options for a large hotel, Renewable Energy, 33(7), 2008, pp. 1475–1490.

[5] R. Sauter, J. Watson, Strategies for the deployment of micro-generation: implications for social acceptance, Energy Policy, 35(5), 2007, pp. 2770–2779.

[6] S.R. Allen, G.P. Hammond, M.C. McManus, Prospects for and barriers to domestic micro-generation: a United Kingdom perspective, Applied Energy, 85(6), 2008, pp. 528–544.

[7] J. Kelleher, J.V. Ringwood, A computational tool for evaluating the economics of solar and wind microgeneration of electricity, Energy, 34, 2009, pp. 401–409.

[8] J. Watson, Co-provision in sustainable energy systems: the case of micro-generation, Energy Policy, 32(17), 2004, pp. 1981–1990.

[9] J. He, C.C.S. Song, Evaluation of pedestrian winds in urban area by numerical approach, Journal of Wind Engineering and Industrial Aerodynamics, 81, 1999, pp. 295-309.

[10] G.T. Johnson, L.J. Hunter, Urban wind flows: wind tunnel and numerical simulations—a preliminary comparison, Environmental Modelling & Software, 13, 1998, pp. 279–286.

[11] L. Tornese, A. de Risi, D. Laforgia, Atlante eolico della Regione Puglia, 2008, Graficazerottanta.

Adjustment of $k-\omega$ SST turbulence model for an improved prediction of stalls on wind turbine blades

Tawit Chitsomboon*, Chalothorn Thamthae

School of Mechanical Engineering, Institute of Engineering,
Suranaree University of Technology, Nakornratchasima, Thailand
** Corresponding author. Tel: +66 044 224414, Fax: +66 044 224413, E-mail: tabon@sut.ac.th*

Abstract: The eddy viscosity in the buffer zones of the turbulent boundary layers was limited to investigate its effects on the points of incipient separation for flows over wind turbine airfoils. The $k-\omega$ SST turbulence model was used as the base model within the framework of a finite volume CFD scheme. Flows over two different wind turbine airfoils were computed and compared with experimental results. Much improvements in the lift and drag coefficients in the stall regions were observed when compared with the results of the original turbulence model.

Keywords: *Turbulence model, $k-\omega$ SST turbulence model, Airfoil stall prediction, Stall in wind turbine*

1. Introduction

Practical flows over wind turbine blades at large angles of attack are very complicated, thus difficult to predict accurately by numerical methods. The difficulties stem from the fact that the boundary layers separate from the blade's suction surfaces due to adverse pressure gradients and its interaction with turbulence. Several investigations have been conducted by various researchers to compute these separated flows; the results have been hitherto only partially successful. Some investigations have over-predicted the lift coefficients [1-3] while some have under-predicted them [4-6]. Moreover, all computations missed the characteristic dips and rises of the lift coefficients in the regions right after the onsets of stalls [1-8]. The reasons for the inaccurate numerical predictions were invariably attributable to the inaccuracies incurred by the turbulence models used in the computations.

Early computations employed the $k-\varepsilon$ turbulence model [9] but later on the $k-\omega$ turbulence model [10] became more acceptable; at present the $k-\omega$ SST model [11-12] seems to be more preferable among wind turbine researchers. This model utilizes both the $k-\varepsilon$ and the $k-\omega$ models under a strategy of a blending function. Like it predecessors this model employs the fully turbulent flow condition as its basic assumption, i.e. the flow devoid of a transition region. The performances of this model in the predictions of separated flows over airfoils were only partially satisfactory since substantial inaccuracies of the lift and drag coefficients predictions were still prevailed in the stall regimes [1-8].

In particular, the $k-\omega$ SST turbulence model had been demonstrated to over-predict the lift coefficients beyond the stall points [1,5,6,8]. It is believed by the authors that these over-predictions were due to the fact that the turbulence levels (hence, turbulent eddy viscosities) in the boundary layers were too high, thus enhancing a momentum transfers to the near wall regions which helped the boundary layer to push through the adverse pressure gradient regions more easily than otherwise. The resulting delayed separation then caused the low pressure on the suction side to spread over more area than normal which thus increased the lift. The turbulence levels that were too high, in turn, were caused by the fully turbulent assumptions that were employed in the turbulence model.

To this end, it should be noted that the buffer zone which bridges the laminar sub-layer and the log-law region in a boundary layer is very important to the physic of turbulence in the boundary layer. This zone is very difficult to model numerically. A small 'model error' in this relatively thin region could induce a large overall error.

The objective of this study was to improve the accuracy of the numerical prediction of separated flows on airfoils by an adjustment of the turbulence intensity in the buffer zones of turbulent boundary layers. The $k-\omega$ SST turbulence model [11,12] will be used as the basis for this investigation.

2. Methodology

In order to limit the eddy viscosities in the regions from the buffer zones to the log-law zone a damping function f_{SST} is proposed. The limited eddy viscosity for the $k-\omega$ SST model thus becomes,

$$\mu_t = f_{SST} \min\left[\frac{\rho k}{\omega}; \frac{a_1 \rho k}{SF_2}\right] \tag{1}$$

The damping function f_{SST} was defined as a function of y^+ (a scaled normal distance from the wall),

$$f_{SST} = f \ (<1.0) \quad ; \quad a \le y^+ \le b \tag{2}$$

$$f_{SST} = 1 \quad ; \quad y^+ < a,\ y^+ > b \tag{3}$$

For simplicity, the damping function was initially defined as a step function as shown in Figure 1 (solid line). Later, it was modified to be a continuous function. The constant a was set in the range 5-30 and the constant b was set in the range 50-300 for a parametric study. The values selected correspond to the edges of the buffer zone and the log law zone of a turbulent boundary layer.

The CFD code used in this study was the FLUENT Code [13]. The computational mesh was an O-type extending approximately to 35 chord lengths away from the airfoil and 250 points were employed along airfoil surfaces. The first cell at any surface point was sized such that $y^+ \le 2$ whereas grids away from it were expanded at a rate less than 20%. This grid system was found to be suitable for a RANS simulation of turbulent boundary layer flows [14,15].

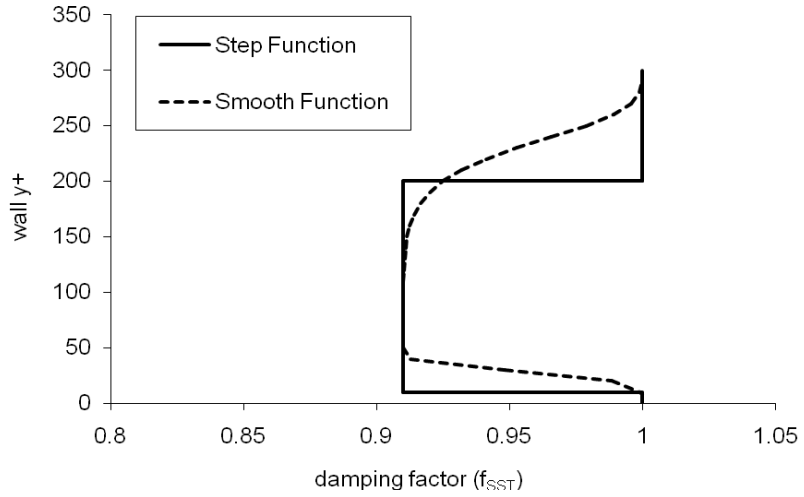

Fig. 1 Example of the step damping function and the hyperbolic (smooth) damping function.

Computations of flows over NREL's S809 airfoil [16] and NACA 63-215 [17] were conducted. An initially parametric study was performed to find out as to how sensitive a boundary layer would respond to changes in the values of a, b and f, using the step function. For this purpose, only some values of angles of attack, namely: 9^o, 11^o, 15^o and 20^o were selected; these are critical points on the lift curve of the S809 airfoil.

3. Results

Figure 2 compares the various computed results with the experimental data at angles of attack 9^o and 11^o. It can be seen that the lifts are quite sensitive to small changes in the values of a, b and f. Actually, several numerical experiments had been performed to weed out the unreasonable ones; only the more meaningful results are demonstrated here.

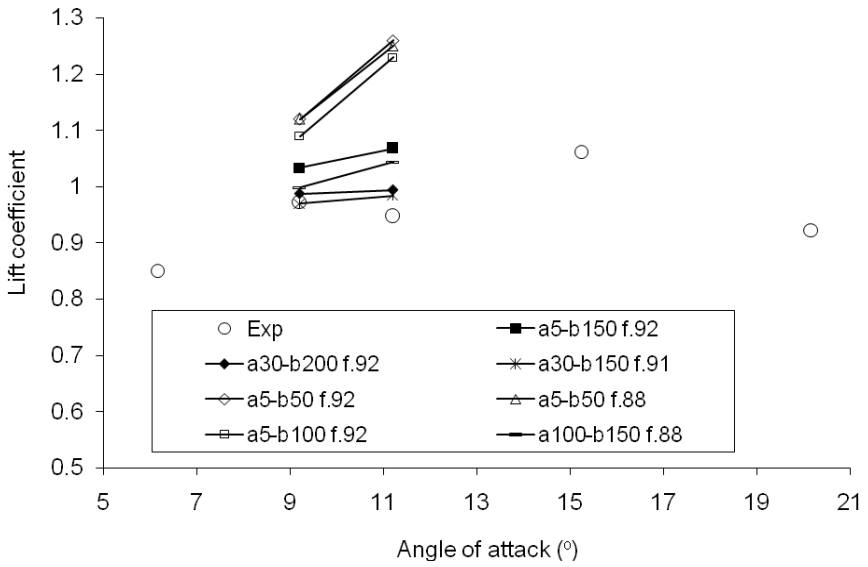

Fig.2 Effects of a, b and f in the step damping function on the lift coefficients.

After getting the feel for the sensitivity of the response, more numerical experiments were performed; the results of which are shown in Fig. 3 wherein it is observed that the characteristic dip and rise of the lift distributions are captured. The value of f a and b in the

ranges 0.90-0.91, 5-10 and 100-200, respectively, were found to be acceptable. Note that the range of acceptable f is very narrow.

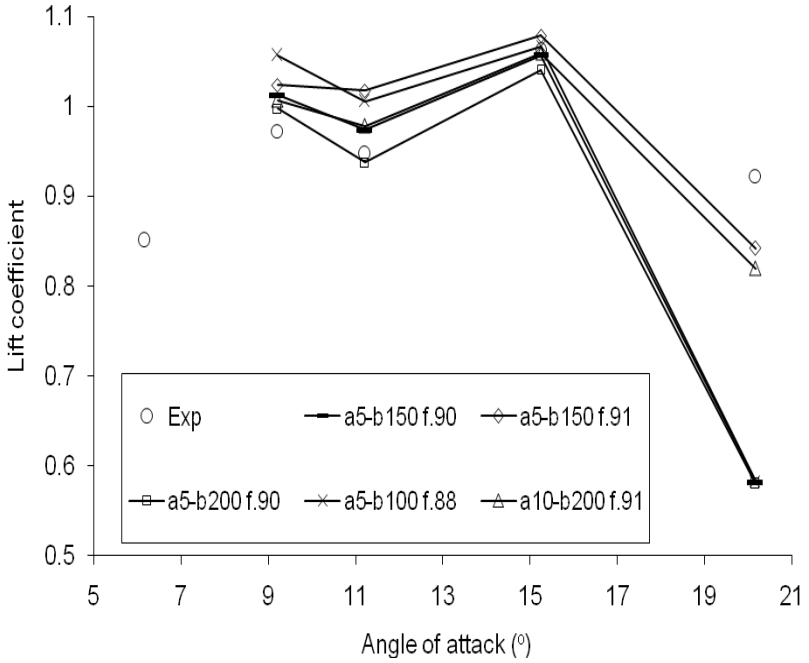

Fig. 3 Effects of a, b and f in the step damping function on lift at high angles of attack.

From the knowledge and experience gained in the parametric study of the step damping function, a continuous function is now proposed as,

$$f_{SST} = 0.1 + \{1 - 0.1\tanh[(0.03y^+)^4]\} \times \{0.9 + 0.1\tanh[(0.005y^+)^8]\} \qquad (4)$$

This damping function is the product of two hyperbolic functions; it was designed (by trial and error) for a rapid rise in the buffer zone and a gradual decrease in the log-law zone, as shown in Fig. 1 (dash line.)

Figure 4 compares the experimental results for lift on the S809 airfoil [16] to three computations, namely: 1) the present model by using the continuous damping function (denoted as SST+), 2) the 2-equation $k-\omega$ SST model (denoted as SST) and 3) the 4-equation $k-\omega$ SST turbulence model with transition [8] (denoted as SST-T.) This last turbulence model is an enhanced version of its 2-equation counterpart wherein a model for transition to turbulence is also incorporated. It is clearly seen that, in the stall region, the SST+ results compare much more favorably to the experiment than those of the other two models. The improvements are not only in a quantitative manner but also in a qualitatively manner, notably the dip and rise of the distribution right after the incipient point of stall at about 10 degree angle of attack. Drag coefficient plot, shown in Fig. 5, also indicates that SST+ results are superior to other models.

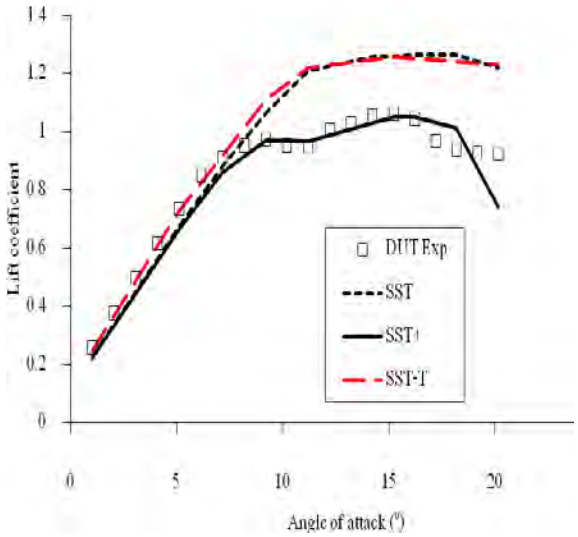

Fig. 4 Lift predictions on S809 airfoil using present and original turbulence models

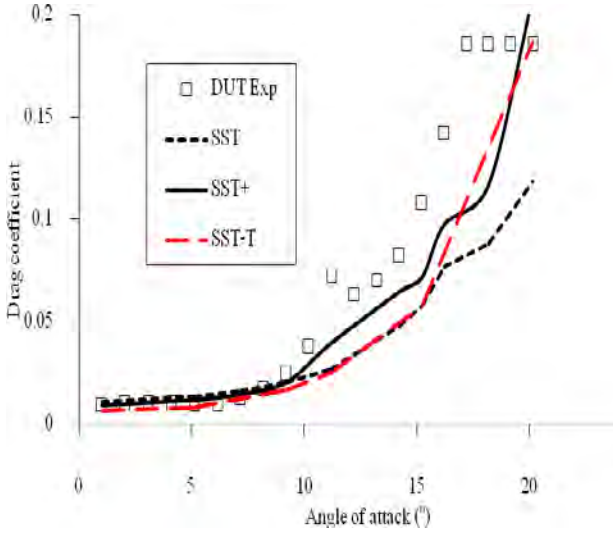

Fig. 5 Drag predictions on S809 airfoil using present and original turbulence models.

It is evident that in the low angle of attack region where the flow is still attached, SST-T gives best results but from the stall point onward SST-T exhibits over-predictions much in the same trend as SST. This perhaps is due to the fact that when flows separate on the suction side there is no transition regions left to give an advantage point to SST-T.

The predicted pressure distributions on the S809 airfoil surfaces at 14^o and 20^o angles of attack are shown in Figs. 6 and 7, respectively. The figures confirm that SST+ gives better overall agreements to the experiment than SST and SST-T. Specifically, the points of separation predicted by SST+ agree better with the experimental results; this is the main reason why it can predict aft-stall lift coefficients more accurately.

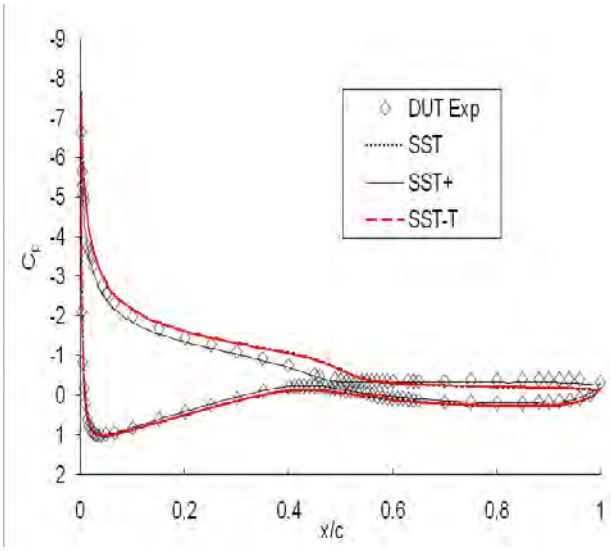

Fig.6 Comparison of pressure distributions on S809 airfoil at 14^o angle of attack

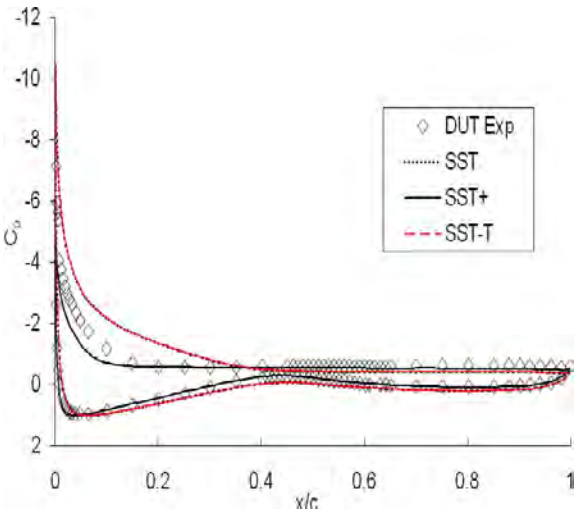

Fig.7 Comparisons of pressure distributions on S809 airfoil at 20^o angle of attack

The incipient of separations can be noticed as the point where the pressure distributions on the suction side are leveled off. Again, SST and SST-T give almost identical results.

To verify that the improved results obtained by the adjustment made to the buffer zone was not specific to an airfoil, flows over another airfoil, the NACA 63-215 [17] were solved under similar conditions. The results are shown in Figs. 8 and 9. Again, SST+ gives much better results than the original models, both quantitatively and qualitatively.

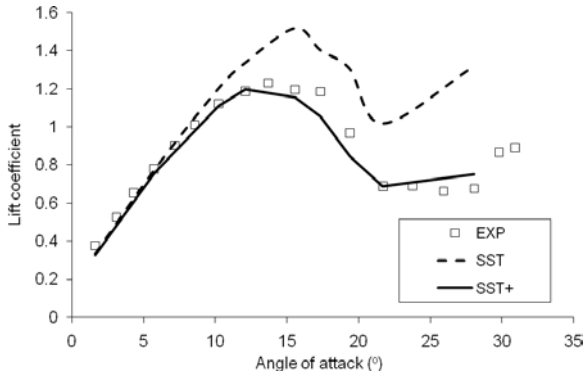

Fig.8 Comparison of lift between modified and original turbulence model.

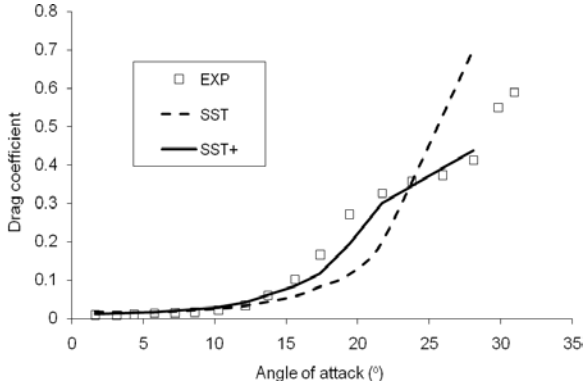

Fig.9 Comparison of drag between modified and original turbulence model.

4. Discussion and Conclusions

It could perhaps be reasoned that the improvements in lift and drag predictions over airfoils after stall were caused by the eddy viscosities in the buffer zones being reduced to about the right levels so as to compensate for the overall collective effects of the transition regions upstream that were neglected by the fully-developed turbulence model. In addition, compensations were also automatically provided for the local phenomena occurring within the buffer zones.

It has been evident that the behavior of a turbulent boundary layer over an airfoil is very sensitive to events in the buffer zone. A small change in the levels of turbulence intensity in the buffer zone could produce a dramatic change in the overall response of the separated flows on airfoils resulting in large changes on lift and drag.

By limiting the turbulence intensities (eddy viscosities) in the narrow buffer zones of turbulent boundary layers by about 10% together with the use of the $k-\omega$ SST turbulence model, this investigation has demonstrated that predictions of lifts and drags (after stall) on two independent airfoils were much improved. The improvements were evidently due to the reductions in the delay of incipient separation points which in turn were caused by the boundary layer being less energetic since the eddy viscosities (hence momentum transfers) were limited.

References

[1] P. Catalano and M. Amato, An evaluation of RANS turbulence modeling for aerodynamics, Aerospace Science and Technology 7, 2003, pp. 493-509.

[2] D.J. Mavriplis, Three-dimensional high-lift analysis using a parallel unstructured multigrid solver. AIAA Paper 98-2619, June 1998.

[3] C.L. Rumsey, T.B. Gatski, Recent turbulence model advances applied to multi element airfoil computations, J Aircraft 38(5), 2001, pp. 904–10

[4] Wolfe, W.P. and Ochs, S.S. "CFD Calculations of S809 Aerodynamic Characteristics," AIAA-97-0973, *Proceeding 35th AIAA Aerospace Sciences Meeting and Exhibit*, Reno 1997

[5] Bertagnolio, F., Sørensen, N.N., and Johansen, J. (2006, December). Status for the Two-Dimensional Navier-Stokes Solver EllipSys2D. Risø-R-1282(EN), Risø National Laboratory

[6] Chow, R. and van Dam, C.P., Computational Investigations of Deploying Load Control Microtabs on a Wind Turbine Airfoil, AIAA-2007-1018

[7] Rumsey, C.L., Ying, S.X., (2002). Prediction of high lift: review of present CFD capability. Progress in Aerospace Sciences 38: pp. 145–180

[8] Langtry, R.B., Gola, J., and Menter, F.R. (2006). Predicting 2D airfoil and 3D wind turbine rotor performance using a transition model for general CFD codes. 44th AIAA Aerospace Sciences Meeting and Exhibit, Reno 2006, AIAA 2006-0395

[9] Jones, W. P., and Launder B. E., The prediction of Laminarization with a Two-Equation Model of Turbulence, International Journal of Heat and Mass Transfer, Vol. 15, 1972, pp. 301-314

[10] Wilcox, D. C., (1993).Turbulence Modeling for CFD. DCW Industries, Inc., 5354 Palm Drive, La Cafiada, Calif.

[11] Menter, F.R. (1993). Zonal two equation $k-\omega$ turbulence models for aerodynamic flows. AIAA Paper 93-2906

[12] Menter, F.R. (1994, Nov). Two-equation eddy viscosity turbulence models for engineering applications. AIAA J 32:1299-1310.

[13] Fluent 6.3 User manual

[14] Franck Bertagnolio, Niels S_rensen and Jeppe Johansen, Status for the Two-Dimensional Navier-Stokes Solver EllipSys2D, Risø–R–1282(EN)

[15] Cummings, R.M., Forsythe, J.R., Morton, S.A., and Squires, K.D., (2003). Computational challenges in high angle of attack flow prediction. Progress in Aerospace Sciences, 39:369–384. doi:10.1016/S0376-0421(03)00041-1

[16] Somers, D.M., (1997). Design and experimental results for the S809 airfoil. Airfoils Inc., State College, PA. NREL/SR-440-6918

[17] Bertagnolio F., Sørensen N N., Johansen J., and Fuglsang P. (2001). Wind Turbine Airfoil Catalog, Risø-R-1280(EN), Risø National Laboratory, August 2001

Acknowledgements

This research was supported by the Royal Golden Jubilee Ph.D. program of the Thailand Research Fund. The authors are thankful to Prof. J.N. Sørensen of the Technological University of Denmark for his collaboration through the RGJ Ph.D. program.

Impact of ambient turbulence on performance of a small wind turbine

William D. Lubitz[1,*]

[1] *University of Guelph, Guelph, Ontario, Canada*
** Corresponding author. Tel: +1 519 824 4120 x54387, Fax: +1 519 836 0227, E-mail: wlubitz@uoguelph.ca*

Abstract: High resolution measurements of wind speed and energy generation from an instrumented Bergey XL.1 small wind turbine were used to investigate the effect of ambient turbulence levels on wind turbine energy production. It was found that ambient turbulent intensity impacts energy production, but that the impact is different at different wind speeds. At low wind speeds, increased turbulence appeared to increase energy production from the turbine. However, at wind speeds near the turbine furling speed, elevated turbulence resulted in decreased energy production, likely to turbulent gusts initiating furling events. Investigation of measurements recorded at 1 Hz showed a time lag of one to two seconds between a change in wind speed and the resulting change in energy production. Transient changes in wind speed of only one second duration did not impact energy production, however, longer duration changes in wind speed were tracked reasonably well by energy production.

Keywords: *Small Wind Turbine, Turbulence, Gusts, Wind Energy*

1. Introduction

Turbulence in the approaching wind can have a significant impact on the power output of wind turbines. This is particularly important for smaller wind turbines, which in practice are often located near buildings, trees and other obstacles. Some small wind turbine installations may experience inflow turbulence intensity many times greater than an open field site.

Current power curve representations do not account for the impact of turbulence on small turbine energy production. For example, curves based on IEC 16400-12-1 are statistical averages of power measurements binned by wind speed, whereby the variance of the data is lost [1]. This approach cannot properly account for site-varying levels of turbulence [2]. IEC 16400-12-1 does not specifically limit turbulence levels of measurements used in power curves, and the resulting power curves provide no guidance on how differing levels of turbulence will affect the power production of the turbine. It can be argued that the effect of site specific turbulence levels in large turbines is manageable, however small turbines may be tested under this or a similar standard while experiencing a wider range of ambient turbulence levels, creating an immediate need to address the impact of site turbulence and provide useful information in the context of the wind turbine power curve.

Ambient turbulence and wind direction variance both have significant impacts on small wind turbines. The smaller masses and length scales of small wind turbines mean that the impacts of turbulence on small turbines will be different from utility scale turbines [3]. Elevated turbulence levels can result in lower wind energy production and greater mechanical stresses on turbine components [4]. The smaller size, gustier operating environment and passive yaw systems associated with small turbines mean they are much more likely to be operating in a yawed state when the turbine cannot align itself to gusting winds [5]. The power output of a horizontal axis wind turbine falls rapidly when the turbine is not aligned to the wind, with a cos^2 dependence on relative wind angle [6]. Elevated turbulence intensity has been found to be the most important factor in reducing turbine structure fatigue life [4], and turbulence intensity impacts furling behaviour [7].

The effect of turbulence on power output is more difficult to generalize, since turbulent gusts impact wind alignment, airfoil performance and furling/power limiting. A small turbine tested in a high turbulence intensity environment was found to temporarily shut down more often due to high gust speeds exceeding limits [8]. Smith [9] used long term small wind turbine performance measurements collected at the National Renewable Energy Laboratory (NREL) to produce power curves and estimate annual energy production (AEP) for seven small wind turbines at varying levels of observed turbulence intensity. The small wind turbines showed a 9% to 32% difference between AEP at the best and worst turbulence levels. Most of the turbines had lower AEP in both the extreme high and low turbulence levels, although one (Skystream) exhibited a trend of increasing AEP with increasing turbulence intensity..

The goal of this study was to determine the impact of varying turbulence conditions on the performance of a representative small wind turbine. High resolution (1 minute and 1 Hz) data from a Bergey XL.1 1 kW capacity horizontal axis wind turbine were analyzed to explore the impact of turbulence on turbine power output.

2. Methodology

A Bergey XL.1 small wind turbine was used in this study. The Bergey XL.1 is an upwind, horizontal axis SWT with a rated capacity of 1.0 kW. It consists of a three blade, 2.5 m diameter fixed-blade rotor directly coupled to a variable speed permanent magnet alternator. This turbine was chosen due to its mechanical and control system simplicity, and because it has been the subject of a wide body of prior studies documenting its performance and operation [10-13].

The Bergey XL.1 was mounted on an 18 m tall, 0.114 m diameter galvanized steel tubular tilt-up tower. An additional 18 m tall, 0.152 m diameter tubular tilt-up tower was installed 13.4 m to the north of the turbine tower to serve as a meteorological mast for obtaining reference measurements of hub-height wind speed.

NRG 40C cup anemometers and one R.M. Young 81000 three-dimensional sonic anemometer were used for this study. The sonic anemometer was mounted on a short arm such that it's sensing volume was 20 cm directly below the rotor disk when the wind was from the prevailing direction of southwest. One NRG 40C and an NRG 200S wind direction sensor were located at the top of the reference mast 1 m above hub-height on separate 1.53 m booms. All NRG 40C anemometers used in this study were manufactured during the initial months of 2009 and calibrated by Otech Engineering (Davis, CA, USA). These calibrations were verified in the University of Guelph wind tunnel before experiment installation.

Power from the turbine was measured by tracking the voltage across a 2180 W, 2.0 Ω dynamic breaking resistor that dissipated the turbine's electrical power output. The 2.0 Ω resistance was selected to mimic the turbine's intended operation as part of a battery charging system under high load, while keeping the parameters needed to characterize electrical performance to a minimum. Additional sensors were installed to measure the yaw angle and rotor speed of the turbine. Ziter [14] gives further details of the experimental equipment.

The turbine and meteorological tower were installed at a representative SWT site on a farm in Oxford County, southwestern Ontario (43°18'N, 80°33'W). The collocated towers were installed in a field (grass, approximately 0.1 m tall) open for several hundred meters to the west and predominantly open to the north and southwest as well. The prevailing wind was from the southwest. Low rise buildings and trees to the east were all more than 100 m distant.

Other potentially significant obstacles included a small cluster of trees located 160 m to the northwest and a barn located almost 200 m to the southwest. Potentially disturbed direction sectors were determined according to IEC 61400-12-1 criteria [1]. Data from disturbed sectors were not used.

3. Results

3.1. One Minute Data

Fig. 1 shows the overall measured XL.1 power curve, based on binning and averaging of 1 minute averaging period, air density-corrected data from undisturbed sectors. The study turbine exhibited a cut-in speed of 4 m/s, and began furling at 9 m/s. Note that because a constant 2.0 Ω load was used, these power curves are not comparable to the manufacturer's or other power curves measured using a grid connection or battery charging controller. The reduced energy generation above 9 m/s for the study turbine is believed to be due to the addition of a nacelle anemometer and solar panel on the tail boom (that were not used in this study), which resulted in earlier furling than would otherwise occur.

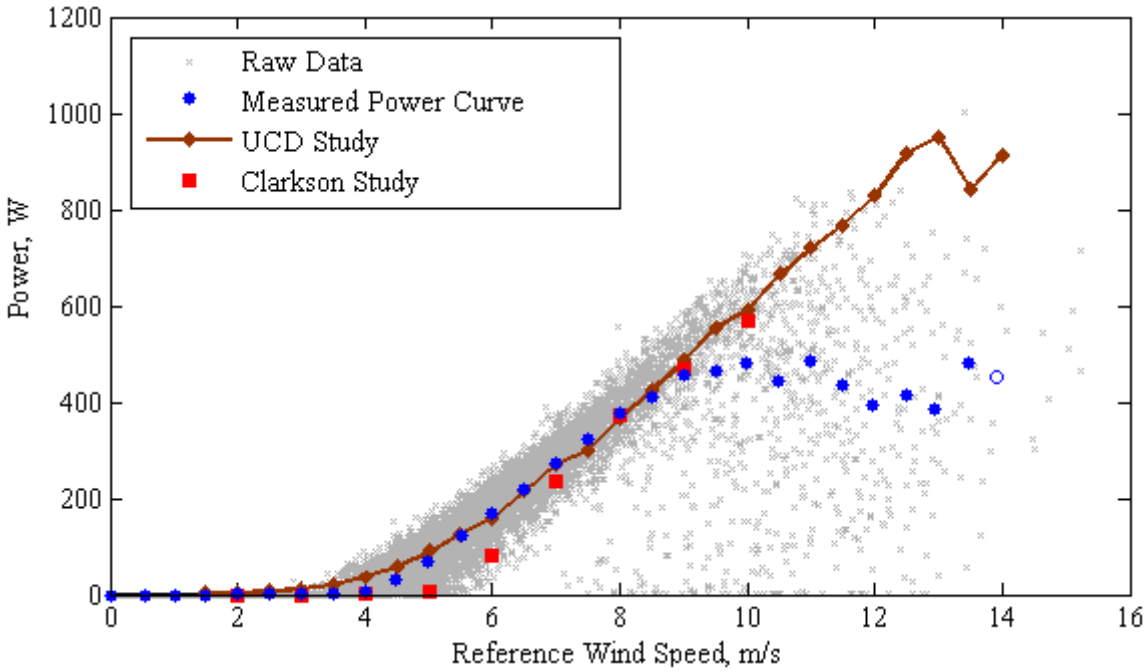

Figure 1. Measured Bergey XL. 1 power curve using a 2 Ω resistive load, with comparisons to UCD [12] and Clarkson [10] XL.1 power curves also measured with a 2.0 Ω load.

Next, the data from the turbine was divided into three categories based on turbulence intensity (which is the standard deviation of the wind speed divided by the mean wind speed during the 1 minute averaging period). The median turbulence intensity for the entire dataset was 0.173. Low turbulence intensity was classified as turbulence intensity less than 0.14. Turbulence intensity greater than 0.18 was considered high. Turbulence intensity between these two values was classified as intermediate. Figure 2 shows the number of observations in each wind speed bin and turbulence category.

Figure 3 shows the percentage difference between the overall power curve and three power curves derived from the categorized data. Low turbulence intensity consistently results in reduced power output (approximately -2%) between 4 m/s and 7 m/s, corresponding roughly to the operating range above cut-in and below the beginning of furling. The results for the

case of high turbulence are less consistent, with the percent increase in power output varying between 0% and +4% in the wind speed bins between 4 m/s and 7 m/s. This variability is likely due to the reduced number of high turbulence intensity observations in individual bins, compared to low turbulence observations. The intermediate differences are almost a mirror image of the low turbulence differences in Figure 3, again supported that these make up most of the observations.

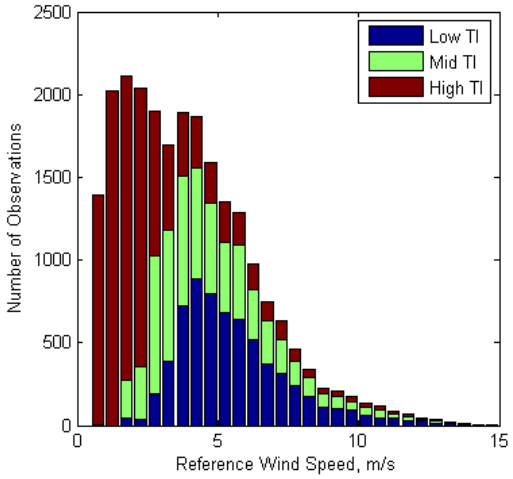

Figure 2. Number of observations by turbulence level and wind speed bin.

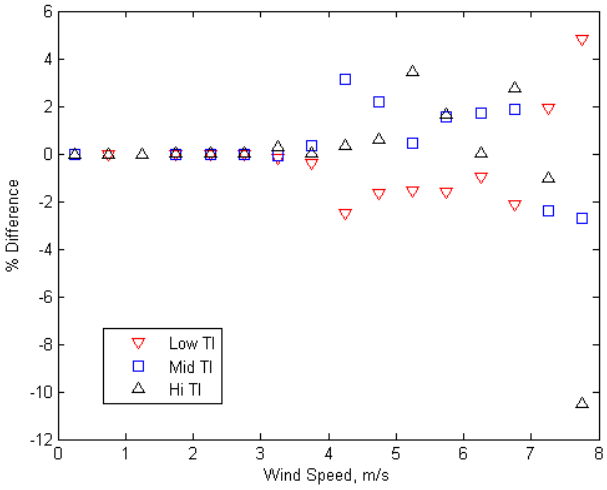

Figure 3. Percent difference between stratified and overall power curves.

The impacts of turbulence on furling were more pronounced. Figure 4 shows the wind percent difference between each of the three stratified turbulence power curves and the overall power curve, over the full range of available data. It is apparent that low turbulence intensity results in increased energy production, likely due to a reduction in intermittent furling and associated hunting. It should be noted that significant variability between bins is likely due to the small number of observations in each bin (Figure 2) at the higher wind speeds.

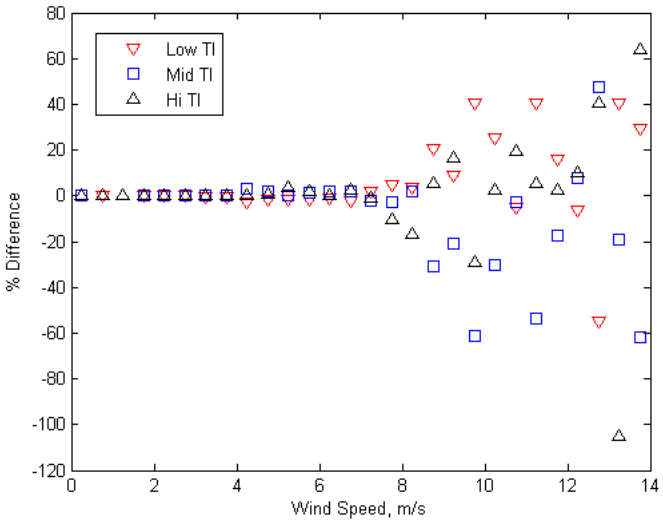

Figure 4. Percent difference between stratified and overall power curves.

Some impact of turbulence was noted at intermediate wind speeds above the cut-in wind speed. The effects of turbulence were found to be most pronounced at wind speeds approaching the furling speed of the turbine, and gusting was observed to cause intermittent

furling and consequently significant hunting and off-axis orientation, reducing power generation.

3.2. One Second Data: Transient Effects

The one second data from the turbine allows direct observation of the turbine response to variations in wind speed. Figure 4 shows 100 seconds of energy production and wind speed. Note that the wind speed shown is that measured by the sonic anemometer immediately below the rotor disk. A prior study [14] found the magnitude of this wind speed to be higher than the reference wind speed, however, turbulence levels were consistent between the two anemometers, and the sonic anemometer is a much closer indication of the wind experienced by the turbine rotor than the reference wind speed, which is over 13 m horizontally distant from the turbine.

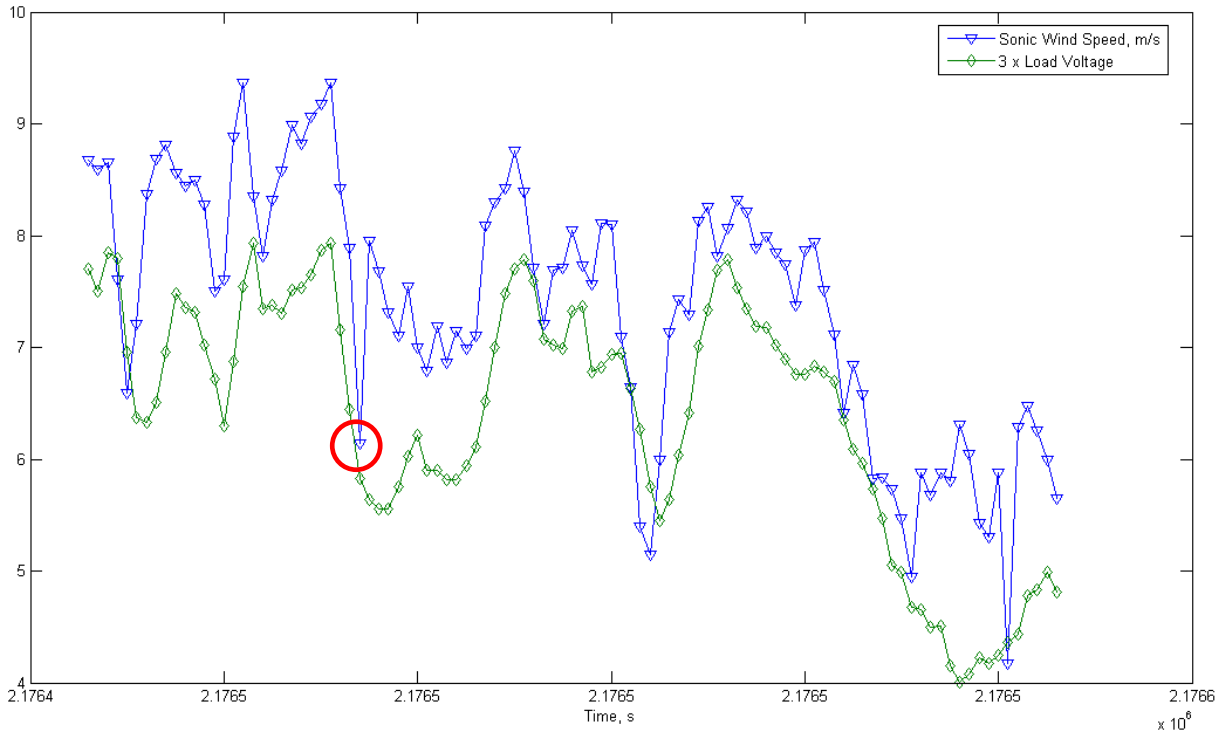

Figure 4. Example of 1 second sonic anemometer wind speed measurements and turbine energy production as measured by voltage across the resistor.

It is apparent that the turbine energy production is approximately one to two seconds delayed relative to the wind at the rotor disk, however, the rate of change and duration of wind speed perturbations appears to influence this. The circle in figure 4 s hows a transient gust of approximately one second duration that is not apparent in turbine energy production. However, changes in wind speed with time constants of many seconds are reasonably well tracked by energy production, factoring in the one to two second delay.

4. Discussion

The UC Davis turbine shown in Figure 1 is mounted on a 9 m mast on the roof of a 3 storey building that contains a penthouse and other roof top infrastructure, on a campus surrounded by other buildings and trees. It would be expected that this turbine would experience higher

ambient turbulence than the Clarkson turbine or the one in this study. With that in mind, it is interesting to note that the UC Davis turbine appears to have a lower cut-in wind speed (at about 3 m/s) than the 4 m/s overall cut-in speed observed for our own turbine, and the 5 m/s cut-in speed of the Clarkson turbine.

Very high turbulence levels resulted in overall decreased performance. It should be noted there are inherent limitations in using a single value of turbulence intensity, which combines all turbulence scales in a single measurement, as the only measure of wind speed variability. It was observed that turbulence impacts depended on the time scale of the turbulence: due to inertia, the turbine had difficulty responding to short time scale turbulence events. This could lead to reduced power output. However longer time period gust events that could be tracked by the turbine would be expected to result in greater overall performance when data was averaged, due to the non-linearity of turbine response to wind speed.

Applying a power curve produced at one level of ambient turbulence to a site with different ambient turbulence is likely to introduce significant errors in site-specific predictions of power output. The results of this study suggest that including additional turbulence information in the performance evaluation of small wind turbines could result in more accurate characterization turbine performance.

5. Conclusions

Measured data from a small wind turbine showed that turbulence has a range of impacts on a small wind turbine. Specifically,

- Turbulence levels had a small but noticeable impact on overall power output at wind speeds between cut-in and furling.
- Low turbulence levels resulted in increased power output at wind speeds associated with furling, likely due delayed onset of furling because of the presence of fewer gusts above the mean wind speed.
- Turbine energy production lagged changes in wind speed by one to two seconds. While changes in wind speed occurring over many seconds were reasonably well tracked by energy production, transient events of approximately one second duration were not tracked by energy production.

The results found here were broadly in agreement with other studies of the impact of turbulence on small wind turbines. The interaction of turbine with turbulent winds is complex and will vary depending on turbine characteristics.

References

[1] International Electrotechnical Commission (IEC), “Wind Turbines – Part 12-1: Power Performance Measurements of Electricity Producing Wind Turbines, Ed. 1.0,” International Standard, IEC 61400-12-1. Geneva Switzerland, Dec. 2005.

[2] Gottschall, J. and Peinke, J., Stochastic Modelling of a Wind Turbine's Power Output with Special Respect to Turbulent Dynamics, J. Physics: Conf. Series, 75 (1), 2007.

[3] Bertenyi, T., Wickens, C., and McIntosh, S., Enhanced Energy Capture Through Gust Tracking in the Urban Wind Environment, *29th ASME Wind Energy Symposium*, Orlando, FL, USA. Jan. 4–7 2010.

[4] V. Riziotis, and Voutsinas, S., Fatigue Loads on Wind Turbines of Different Control Strategies Operating in Complex Terrain, J. Wind Eng. & Ind. Aero. 85, 2000, pp. 211–240.

[5] Larwood, S., Wind Turbine Wake Measurements in the Operating Region of a Tail Vane, 39th AIAA Aerospace Sciences Meeting, Reno, Nevada, USA. Jan. 8–11 2001.

[6] Pedersen, T., On Wind Turbine Power Performance Measurements at Inclined Airflow, Wind Energy, Vol. 7, 2004, pp. 163–176.

[7] Corbus, D. and Prascher, D., Analysis and Comparison of Test Results from the Small Wind Research Turbine Test Project, Tech. Rep. NREL/CP-500-36891, NREL, Nov. 2004.

[8] Van Dam, J., Meadors, M., Link, H., and Migliore, P., Power Performance Test Report for the Southwest Windpower AIR-X Wind Turbine, Tech. Rep. TP-500-34756, NREL, Sept. 2003.

[9] J. Smith, Effects of Turbulence Intensity on the Performance of Small Wind Turbines. Small Wind Conference, Stevens Point, WI, USA. June 14-15, 2010.

[10] Humiston, C., and Viser, K., "Full Scale Aerodynamic Effects of Solidity and Blade Number on Small Horizontal Axis Wind Turbines," Proceedings of World Wind Energy Conference, Cape Town, South Aftrica, 2003.

[11] Klemen, M. A., 2004, "Bergey XL. 1 Power Curve," North Dakota State University [online database], http://www.ndsu.nodak.edu/ndsu/klemen/Bergey_XL.1_Power_Curve.htm [cited 11 November 2009].

[12] Seitzler, M., "The Electrical and Mechanical Performance Evaluation of a Roof-Mounted, One-Kilowatt Wind Turbine," Report CWEC-2009-003. California Wind Energy Collaborative, University of California, Davis. Davis CA, USA. 2009.

[13] Summerville, B. Small Wind Turbine Performance in Western North Carolina, Report. Appalachian State University, Boone, NC, 2005. http://www.wind.appstate.edu/reports/researcharticlesmallwindperformanceBJS.pdf. [cited 5 July 2010.]

[14] Ziter, B., Alternative Methods of Estimating Hub-Height Wind Speed for Small Wind Turbine Performance Evaluation. MASc Thesis, School of Engineering, University of Guelph, ON,Canada. May, 2010.

Feasibility study of 6.6MW wind farm in Greek mainland

George C. Bakos

Democritus University of Thrace, Dept. of Electrical and Computer Engineering, Xanthi, Greece
**Corresponding author. Tel: +30 2541079725, Fax: +30 2541079734, E-mail: bakos@ee.duth.gr*

Abstract: Wind energy has the advantage of being a priority sector of the Greek government. Greece has a considerable potential for electricity generation from wind not only in the island area but also in mainland. This paper deals with the current status of wind energy in Greece and the presentation of technical and economical feasibility of a 6.6MW wind farm applied to a potential wind farm site located in Greek mainland (Rentina-Karditsa). Wind speed, prevailing wind direction and temperature measurements are performed for a period of one (1) year (from 11/5/2009 to 11/5/2010). For economic consideration two different technological scenarios based on capacity factor (CF) are investigated and compared with respect to net present value (NPV), internal rate of return (IRR) and payback period (PBP) criteria. The profitability analysis shows that larger installed capacity with larger rated power wind turbines present higher IRR of the investment. The sensitivity analysis backs up the findings.

Keywords: *Renewable energy, Wind energy, Wind farm techno-economic assessment, RES legislation*

1. Introduction

Recently, there has been a considerable expansion of distributed generation (DG) technologies, thanks to progress in reliability, in competitiveness and operation know-how and incentive policies adopted by many developed countries. The presence of DG facilities brings benefits both to the electric power system and the total energy system. With DGs energy can be generated directly where it is consumed. As a consequence, transmission and distribution networks are less charged; safety operation margins increase, and transmission costs and power losses are reduced. The spread of DG technologies enhances supply safety in the energy field by reducing dependence on fossil fuels [1-4].

Wind power is driving growth in the renewables sector and represents a huge investment potential in Greece. The superb wind resources in Greece are among the most attractive in Europe, with a profile of more than 8 m/s and/or 2,500 wind hours in many parts of the country. Capacity increased by an average of 30% annually between 1990 and 2003 and almost 30% of total capacity was installed in the period of 2003-2004. It is estimated that in addition to the 1200-plus MW operating currently at wind farms, a further 7,500 MW will be installed by 2020. A detailed presentation of current and future wind farm installations on Greek islands is given in Ref. [5].

Electricity from Renewable Energy Sources, High Efficiency Cogeneration of Heat and Power and Other Devices». The main scope of the Law 3468 is to establish an adequate legislative and regulatory framework in order to support investments in renewable energy sources (RES) and High Efficiency cogeneration of heat and power (HE-CHP) energy sectors and eventually increase the penetration of these resources in the energy mix of the country. Aiming at conveying to the Hellenic legislation Directive 2001/77/EC of the European Parliament and of the Council of 27 September 2001 on the «Promotion of Electricity Produced from RES in the Internal Electricity Market», the National target is set to a 20.1% RES contribution on the total electricity production by 2010 while for 2020 the target is 29%. In the internal electricity market, the production of electricity from RES and HE-CHP are promoted in priority over other means of power production with specific regulations and principles. Until 2020, in Greece to achieve the target set by EC, the remaining RES

contribution to total electricity (excluding the large hydro) should be 58,37% wind, 2,73% Small Hydro, 2,73% biomass, 1,94% solar thermal, 22,95% photovoltaic energy (PV) and 11,28% other technologies.

On 4 June 2010, the Hellenic Parliament approved Law 3851 referring to "*Acceleration of RES growing facing climate change and other legislation related to Ministry of Environment, Energy and Climate Change subjects*". Law 3851/10 was published in the Official Gazette of the Hellenic Republic and is in effect since then. The main scope of New Law 3851 is the increased utilisation of the vast renewable energy resource of the country together with complying with the environmental targets of the Kyoto protocol. The attraction of large scale energy investments is also envisaged, in parallel with simplification measures for the necessary licensing procedures.

Wind energy has the advantage of being a priority sector of the Greek government. Greece has a considerable potential for electricity generation from wind not only in the island area but also in mainland. This paper deals with the current status of wind energy in Greece and the presentation of technical and economical feasibility of a 6.6MW wind farm applied to a potential wind farm site located in Greek mainland (Rentina-Karditsa). For economic consideration two different technological scenarios based on CF are investigated and compared with respect to NPV, IRR and PBP criteria. The profitability analysis shows that larger installed capacity with larger rated power wind turbines present higher IRR of the investment. The sensitivity analysis backs up the findings.

2. Case study: 6.6 MW wind farm in Greek mainland

The proposed wind farm site is located in the Prefecture of Thessaly (Karditsa-Rentina) in the heart of Greek mainland. The site, known to local people as “Lepouchi”, covers an area of 200.000 m^2 (Photos 1, 2) and is situated 3km from Rentina village. It is near to Rentina-Fourna national road and therefore quite favorable for wind turbines transportation. However, an improvement of an existing 500m forest road would be required to provide easy access to wind farm site. The proposed site is almost a flat-shrubbery area with presence of rocks, suitable for placement of tower foundations, roadways and crane pads. It is also favorable from the environmental point of view due to absence of wildlife, noise and visual issues. However, an important drawback is its distance (25km) from the nearest electrical substation (situated at Makrakomi-Lamia). The excessive cost associated with electrical issues is considered in economic analysis and affected the economic performance of proposed wind farm installation.

2.1. Analysis of wind power generation input parameters

The data was collected for the period from 11/5/2009 to 11/5/2010 with availability 98,7%. The wind speed data was the major parameter for wind energy generation and utmost care was taken in its collection. Two cup anemometers (one as primary and the other as auxiliary), wind direction vanes, temperature sensor and humidity sensor, certified according to ISO 17025:2005, were installed within the wind farm area (latitude 39º 05’ 02,4’’ and longitude 21º 56’ 46,8’’) placed on the top of a 30m metallic pole. A data recorder STYLITIS 40/41 (SYMMETRON) and a PV 10Wp/12V connected to a lead battery 12V/12Ah were also used.

Wind Speed

Significant variations in seasonal or monthly average wind speed are common over most parts of Greece. In the proposed site, the monthly average wind speed (Table 1) is high during

November-February and reaches a maximum of 7,5m/s because of South-West winds. The annual average wind speed is estimated 6m/s ($\pm 0{,}26$m/s) at wind turbine height of 80m.

Fig 1: Geographic location of wind farm site

Fig 2: Wind farm site

Table 1: Monthly average wind speed

Month	Average Wind Speed (m/s)	Data Availability (%)
January	7,3	96,1
February	7,5	97,0
March	5,3	96,0
April	4,4	100,0
May	4,0	98,0
June	5,0	100,0
July	4,0	95,0
August	2,9	100,0
September	2,9	100,0
October	5,2	95,7
November	5,9	97,1
December	7,4	95,2

Relative Humidity

The relative humidity of air depends on the amount of water vapor in the air, which in turn affects the air density. Moist air is less dense than dry air since water molecules is lighter than either a nitrogen molecule or an oxygen molecule, which are the major constituents of dry air. As the relative humidity increases air density decreases. The air density also depends on temperature and pressure and is given as follows:

$$air density = D\left(\frac{273{,}15}{T}\right)\left[\frac{B - 0{,}3783e}{760}\right] \qquad (1)$$

where D is the density of dry air at standard atmospheric temperature (25 C) and pressure (100kPa) (D=1,168kg/ m^3), T is the absolute temperature in Kelvin, B is the barometric pressure in torr and e is the vapour pressure of the moist air in torr. For the proposed site of wind farm installation, the mean yearly temperature is 10,4C and the monthly variation of relative humidity for the given period is between 50% and 70%.

Generation Hours

The generation hour is the period in which the wind turbine produces electric power from the energy available in the wind:

Generation hour = total number of hours in a year – (low wind hours + wind turbine maintenance hours + turbine breakdown hours + grid maintenance hours + grid breakdown hours)

Wind power generation hour is directly governed by the design of wind turbine, especially the cut-in and cut-out speed of wind turbines. A lesser cut-in speed and higher cut-out speed significantly improves the generation hours. Reduction in stoppage hours of wind turbine due to uncontrollable factors such as grid unavailability and mechanical breakdown improves the wind power generation. Periodic maintenance of turbine and grid are unavoidable and if done during off-seasonal period (when the average wind speed is below the cut-in speed) reduces energy loss and increases the total energy generation of wind turbine.

2.2. Wind farm energy generation

In order to calculate the wind farm energy generation is essential to perform the wind flow calculations. This is carried out using the *MS3D3H/3R* model which is integrated to *WindFarm* code. Then the *WindRose* code was used to estimate the total energy production for different capacity wind turbines. Net energy production is calculated using the energy losses related to wind turbine availability due to technical reasons (such as wind turbine malfunction, stoppage time for maintenance etc), wake and transmission losses. Two different technological scenarios were investigated where different capacity wind turbines were proposed.

Technological Scenario I (TS-I)

Four (4) wind turbines VESTAS V82 – 1,65MW were considered forming a 6.6MW wind farm. Table 2 shows the yearly total energy production per wind turbine, the wind direction and wake losses. Figs. 3-4 show the yearly energy yield (net) and the changes of energy yield due to wake losses per turbine respectively. It was calculated that gross energy production of 12,77GWh/year would be delivered to the grid resulting to 1930 generation hours and CF of 22,1%.

Table 2: Yearly total energy production per wind turbine, the wind direction and wake losses (TS-I)

TOTAL ENERGY YIELD			
Wind Turbine Identifier	Base Yield GWh	Wake Losses % Loss	Total Yield GWh
1	3.63	-1.44%	3.58
2	3.34	-1.76%	3.28
3	3.32	-2.01%	3.25
4	3.23	-1.14%	3.19
Total	13.52	-1.59%	13.30

TOTAL ENERGY YIELD			
Wind Direction	Base Yield GWh	Wake Losses % Loss	Total Yield GWh
0	0.24	-21.17%	0.19
22.5	0.38	-1.99%	0.38
45	0.28	0.00%	0.28
67.5	0.03	0.00%	0.03
90	0.02	0.00%	0.02
112.5	0.03	-4.52%	0.03
135	0.06	-15.74%	0.05
157.5	0.10	-32.59%	0.07
180	0.28	-16.77%	0.23
202.5	1.08	-0.83%	1.07
225	1.74	0.00%	1.74
247.5	2.97	0.00%	2.97
270	5.38	0.00%	5.38
292.5	0.70	-2.09%	0.69
315	0.13	-12.34%	0.11
337.5	0.08	-31.80%	0.06
Total	13.52	-1.59%	13.30

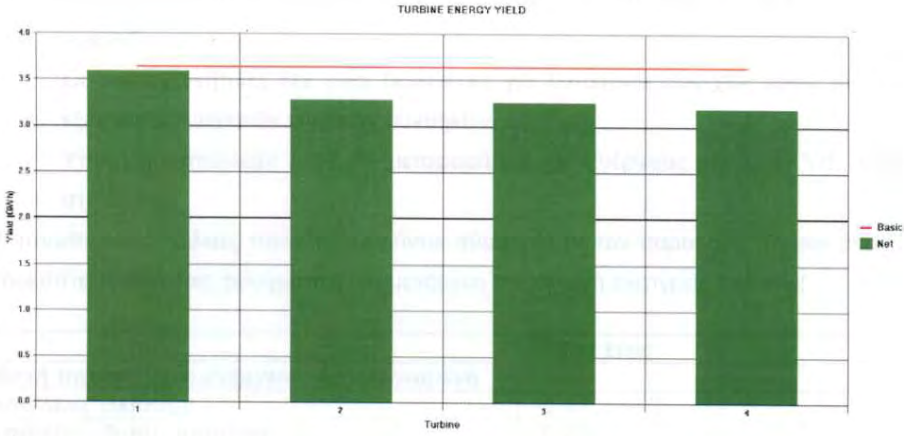

Fig. 3: Yearly net energy yield per turbine (TS-I)

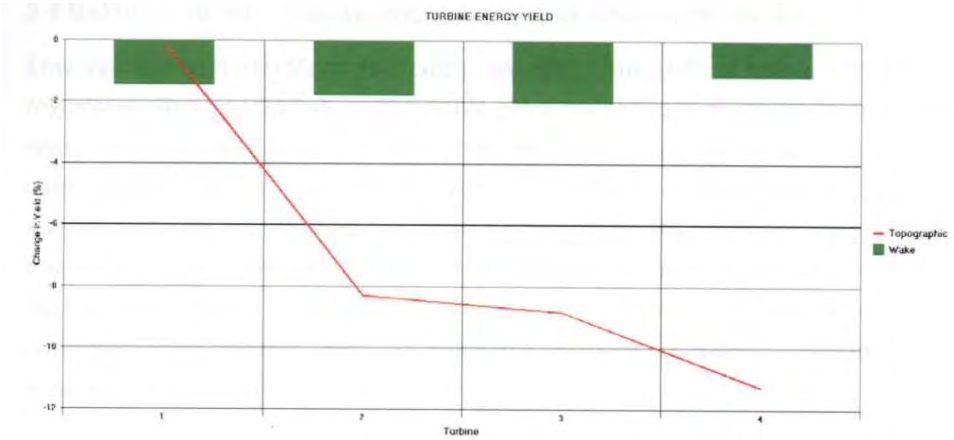

Fig. 4: Wake losses per turbine (TS-I)

Technological Scenario II (TS-II)

Four (4) wind turbines VESTAS V100 – 1,8MW were considered forming a 7.2 MW wind farm. Table 3 shows the yearly total energy production per wind turbine, the wind direction and wake losses. Figs. 5-6 show the yearly energy yield (net) and the changes of energy yield due to wake losses per turbine respectively. It was calculated that gross energy production of

17,30GWh/year would be delivered to the grid corresponding to 2400 generation hours and CF of 27,4%.

Table 3: Yearly total energy production per wind turbine, the wind direction and wake losses (TS-II)

TOTAL ENERGY YIELD

Wind Turbine Identifier	Base Yield GWh	Wake Losses % Loss	Total Yield GWh
1	4.85	-1.88%	4.76
2	4.58	-2.49%	4.47
3	4.55	-2.83%	4.42
4	4.45	-1.54%	4.38
Total	18.43	-2.18%	18.03

TOTAL ENERGY YIELD

Wind Direction	Base Yield GWh	Wake Losses % Loss	Total Yield GWh
0	0.40	-22.71%	0.31
22.5	0.64	-3.26%	0.62
45	0.48	0.00%	0.48
67.5	0.08	0.00%	0.08
90	0.04	0.00%	0.04
112.5	0.06	-4.37%	0.06
135	0.10	-17.22%	0.09
157.5	0.17	-35.90%	0.11
180	0.41	-18.47%	0.33
202.5	1.42	-1.51%	1.40
225	2.18	0.00%	2.18
247.5	3.76	0.00%	3.76
270	7.31	0.00%	7.31
292.5	1.04	-3.17%	1.01
315	0.20	-13.86%	0.17
337.5	0.15	-34.90%	0.10
Total	18.43	-2.19%	18.03

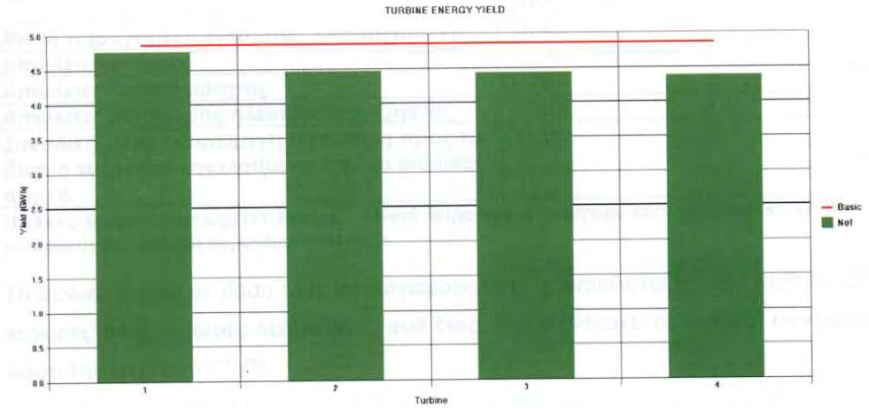

Fig. 5: Yearly net energy yield per turbine (TS-II)

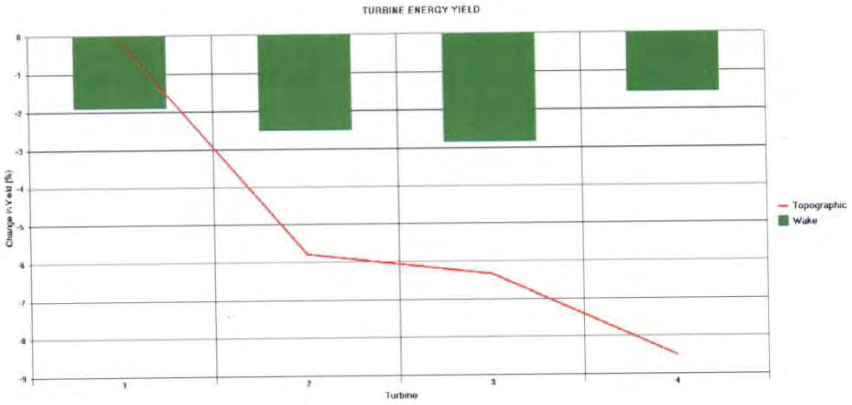

Fig. 6: Wake losses per turbine (TS-II)

2.3 A systematic economic assessment

The analytical technoeconomic general model is the computerized renewable energy technologies (RETs) assessment tool 'RETScreen' [6] which is used for preliminary evaluation of the technical feasibility and financial viability of potential grid-connected wind

installations anywhere in the world. For Greece in particular, it takes into account the prevailing Greek national development and energy laws, the government's subsidy and the prices applicable for buying or selling energy to the PPC by the electric energy producer.

For the technological scenarios TS-I and TS-II, different economic and financial feasibility indices are calculated such as the year-to-positive cash flow, IRR, ROI and NPV. The results of the installed wind power plants are shown in Figs. 6-7 respectively. The initial capital cost for TS-I is 8.500.000€ and for TS-II is 9.500.000€. The owner covers 25% of initial cost and the rest 75% is provided as a loan by private banks (10-year period and interest rate of 6%). The owner also decided to use the extra bonus 20% increase of feed-in tariff provided by Law 3851/2010 (i.e. 105€/MWh).

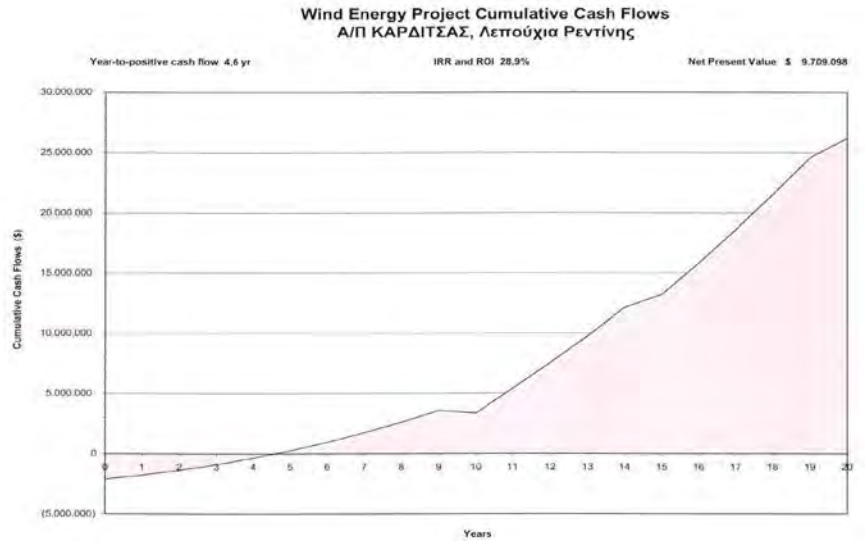

Fig. 6: Wind farm economic analysis (TS-I)

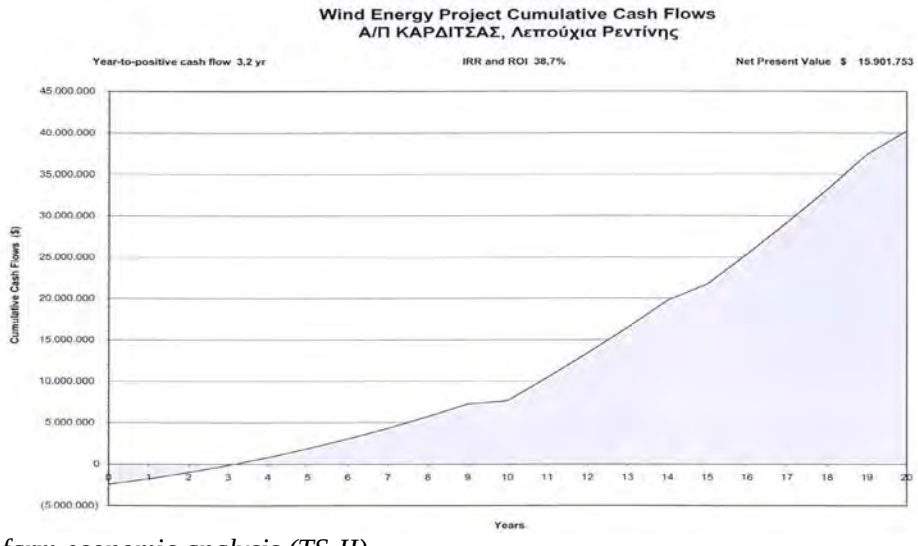

Fig. 7: Wind farm economic analysis (TS-II)

3. Conclusions

Two different technological scenarios were investigated and cash flow economic analysis was performed under the new legislation for RES penetration in Greece. From the results shown in Figs 5-6, it is concluded that Technological Scenario I [four (4) wind turbines VESTAS V82-1.65MW and installed capacity of 6.6MW] constitutes the less profitable investment in comparison to technological Scenario II [larger wind farm of 7.2MW consisted of four (4)

VESTAS V100-1.8MW]. This is due to increased performance of wind turbines in TS-II which compensates for the increased initial cost of the investment. For the particular wind farm installation in the Greek mainland, it was found that larger installed capacity with larger rated power wind turbines presented higher IRR of the investment. Furthermore, the PBP is 7,5 years and 6,2 years for TS-I and TS-II respectively. The results show that the implementation of wind farms in Greek mainland could present a profitable investment despite the fact that the sites are not so favorable compared to the islands. However, the experience of the implementation of wind farms in Greece emphasised the necessity for a simplified licensing procedure and a better coordination through institutions for Environmental Approvals.

The question becomes apparent: where does Greece go from here? According to Greek Ministry of Development, a wind total of 7500MW (including offshore) is planned to be installed until 2020 (while 4000MW of them until 2014). This capacity is limited due to grid stability, due to suggestions from Regulatory Authority for Energy (RAE) for possible excessive charging of consumers and due to public opposition in large scale wind farm installation, particularly in Greek islands. In order to achieve the goal of 7500MW, the Hellenic Parliament approved recently Law 3851 regarding RES electricity. According to this legislation, wind projects can get an extra bonus 20% increase of feed-in tariff, providing that the owner will not apply for a grant to the Greek State. This policy mechanism designed to promote mature wind projects for immediate connection to the grid. Also, the Hellenic State is planning to upgrade the existing grid to overcome grid stability problems and to offer more benefits to local people (such as discounted electricity bills) in order to overcome their opposition.

The main conclusion is that, with respect to electricity supply, wind farm applications will continue to play the most important role in Greece. The country high wind potential through out the year, the increasing environmental sense of Greek population, the elimination of time consuming license procedures, noticed during the implementation of first wind farm installations in Greece, and the improved financial incentives will increase the wind penetration in Greek electricity market.

References

[1] Tsikalakis A.G. and Hatziargyriou N.D. (2007) Environmental benefits of distributed generation with and without emissions trading, Energy Policy 35, pp.3395-3409

[2] Dicorato M. et al (2007) Environmental-constrained energy planning using energy-efficiency and distributed-generation facilities, Renewable Energy (In Press).

[3] Meyer I. Niels (2003) Distributed generation and the problematic deregulation of energy markets in Europe, International Journal of Sustainable Energy Vol. 23, No. 4, pp. 217-221.

[4] Deepak Sharma (2003) The multidimensionality of electricity reform – an Australian perspective, Energy Policy 31, pp. 1093-1102.

[5] Centre of Renewable Energy Sources (CRES), www.cres.gr.

[6] Retscreen Manual (2000), Energy Diversification Research Laboratory (CEDRL), Canada.

Optimal spatial allocating of wind turbines taking externalities into account

Jürgen Meyerhoff[1], Martin Drechsler[2,*]

[1] *Technische Universität Berlin, Berlin,Germany Germany*
[2] *UFZ – Helmholtz Centre for Environmental Research, Leipzig, Germany*
** Corresponding author. Tel: +49 3412351713, Fax: +49 3412351473, E-mail: martin.drechsler@ufz.de*

Abstract: Wind power is one of the most promising options for producing energy in a climate-friendly manner. However, besides its environmental benefits wind power generation causes externalities such as impacts on humans and biodiversity. All studies conducted so far show that these externalities can be substantial. The question is how this knowledge translates into a welfare-optimal spatial allocation of turbines that needs to consider both production and external costs. We present a modeling approach for the determination of the welfare-optimal spatial allocation of wind turbines (WT) and apply it to the planning region West Saxony in Germany. The approach combines choice experiments, a non-market valuation method used to measure externalities of wind power, and spatially explicit ecological-economic modeling within an optimization framework. Optimal is understood here as producing a given amount of wind power at lowest social costs. Social costs comprise (i) externalities measured by the (monetized) impact of WT on biodiversity, the distance of the WT to settlements, the height of the WT and size of wind farms, and (ii) the construction and operating costs associated with the WT. We show that the social costs of wind power production can be reduced substantially if externalities are taking into account.

Keywords: *choice experiment, externality, modeling, spatial allocation, welfare-optimal, wind power.*

1. Introduction

Wind power belongs to the most efficient renewable energy sources and constitutes an important component of the energy mix in many countries. In future, wind power is going to expand further to help meeting ambitious energy and climate policy goals. However, despite its doubtless advantages, wind power generation comes along with considerable negative externalities that lead to conflicts with other important policy goals, including human health and biodiversity conservation. Human health is affected because of the shade and noise effects produced by wind turbines (WT) [1]. Visual impacts of WT on landscapes have been considered by [2,3]. Biodiversity is affected especially through increased mortality and habitat loss for birds and bats [4,5]. External costs of wind power have been quantified, e.g., by [6-8]; see [9] for an overview.

The quality and extent of the monetary and non-monetary externalities of wind power considerably depend on the characteristics of the sites selected for wind power development. One the one hand the unit cost of wind-generated electricity depends on the energy produced per year and this depends on the local wind conditions. On the other hand, WT erected in the vicinity of settlements or bird habitats increase the impact on humans and birds. Different sites available for the installation of a WT will have different pros and cons in terms of wind power production costs and external costs. Since the pros and cons of wind power generation vary in space, they can be balanced and conflicts with other policy goals be mitigated through the appropriate spatial allocation of the WT. In the present article we propose a welfare-economic approach that determines the spatial allocation in a way that the social cost of producing a given amount of wind power is minimized. The mentioned balance of the pros and cons is reflected by the fact that the social cost is calculated as the sum of the production cost (e.g., installation and operating costs) and the external costs. The latter comprise the

monetized impacts on human health, biodiversity, etc. and depend on the preferences of the people, i.e. on how they value these impacts.

Despite their advantages such as their analytical clarity and rootedness in economic theory, welfare-economic approaches have been rarely used to optimize the spatial allocation of land use in general, and WT in particular. An example that goes into this direction is found in [10] which explores trade-offs between wind power production and the conservation of two animal species. However, since the analysis does not include any information about social preferences, it cannot determine the welfare-optimal allocation of WT. The above-mentioned studies [6-9] on the other hand, provide the necessary information about social preferences but do not include any assessment or modeling of how the valued impacts depend on the spatial allocation of the WT. As a consequence, they too cannot determine the welfare-optimal spatial allocation. This lack has recently been criticized [11]. The two approaches, spatially explicit modeling of impacts and the economic valuation of impacts have complementary strengths and weaknesses and combining them allows overcoming the weaknesses. In the present paper we follow this route to determine the welfare-optimal spatial allocation of WT in a study region in Germany. For this region we investigate a number of policy relevant questions: (i) how do society's preferences affect the welfare-optimal allocation of WT, (ii) what is the trade-off between the production and the external costs of wind power production, and (iii) what are the consequences of ignoring external cost in the planning of landscapes for wind power production.

The paper is structured as follows. In section 2 we will outline the modeling approach and present the study region. In section 3 we apply the modeling approach to the study region and present the results in section 4. Section 5 discusses the results and draws conclusions for policy design.

2. Methodology

2.1. The modeling approach

The objective of the analysis is to allocate WT in the study region such that a given level of electricity $E_{\min}$ is produced per year at minimal social cost C. The social cost of wind power supply is composed of the production costs C_p and external costs C_e. To determine external costs we define attributes that capture the relevant externalities as identified through stakeholder interviews (see section 3.1 below). The attributes are quantified through spatially explicit models and valued through choice experiments. In the present case the attributes comprise: the loss rate (L) of important species, the minimum distance of WT to settlements (D), the height of the installed WT (H) and the size of wind parks (S). The attributes D, H and S consider the impact of WT on the landscape and ultimately human inhabitants. The disturbance of humans by the noise of a WT depends, among others, on the height of the WT and its distance to the settlement areas. Attribute H considers that WT technologies with different heights may by installed. Attribute S considers that WT may be allocated in larger or smaller wind parks. The production cost and attribute L depend on the time frame. We consider a time frame of 20 years, which is about the life time of a WT, so C_p measures production costs over 20 years and L measures species decline within 20 years. The analysis is carried out in several steps. First we construct the social cost function

$$C = C_p + C_e(L, D, H, S) \qquad (1)$$

where C_e are the external costs associated with the attributes *L*, *D*, *H* and *S*. They are determined through choice experiments (see section 3.1). We further identify the sites that are physically and legally suitable for the installation of a WT. Given these potential sites, WT allocation strategies are formed as described above, considering that the energy target $E_{\min}$ must be fulfilled. For each allocation strategy we determine the associated attributes C_p, *L*, *D*, *H* and *S* and determine the social cost *C*. For given energy target $E_{\min}$, the welfare-optimal allocation of WT, i.e. the allocation that minimizes *C*, is determined through numerical optimization.

2.2. Application of the modeling approach

The approach is applied to the Planning Region West Saxony in Germany that is a part of the Free State of Saxony. The region has about 500,000 households (2005) and covers an area of around 4,300km². Due to its topography the region is fairly suited for wind power production but at the same time belongs to the core distributional area of the endangered Red Kite (*Milvus milvus*). Red Kites have been frequently observed to be killed by WT. The Red Kite therefore forms the focal bird species in our analysis and *L* measures the rate by which the Red Kite population declines as a consequences of the presence of WT in the region [12]. Below we go through the steps of the modeling approach.

2.2.1. Construction of the external cost function through choice experiments

We consider an external cost function which is the sum of the partial external costs $C_y(y)$ associated with the attributes $y \in \{L,D,H,S\}$:

$$C_e(L,D,H,S) = \sum_{y\in\{L,D,H,S\}} C_y(y) \cdot \sum_{t=1}^{T} (1+r)^{-t} \qquad (2)$$

The partial external cost $C_y(y)$ represents the cost for a single year. Since we are considering a time span of T=20 years, we have to aggregate the costs over these 20 years. We discount the external costs at annual rate *r*. We assume that $C_y(y)$ has the shape $C_y(y)=a_y/(y-b_y)+g_y$ (which can describe concave or convex increases or decreases of C_y with *y*) and carry out choice experiments (CE) [13] to determine the parameters a_y, b_y and g_y for all $y \in \{L,D,H,S\}$. CE are based on the assumption that the utility to consumers of any good (i.e., also public goods such as a landscape) is derived from its attributes or characteristics. Due to this focus CE are particularly useful for valuing multidimensional changes. In a CE, respondents are asked to make comparisons among environmental alternatives characterized by a variety of attributes and the levels of these. Typically, respondents are offered multiple choices during the survey, each presenting alternative designs of the environmental change in question and the option to choose the status quo. The record of choices serves as a basis to estimate the respondents' willingness to pay. Changes in welfare due to a marginal change in a given attribute are calculated using the MWTP. It is defined as the maximum amount of income a person will pay in exchange for an improvement in the level of a given attribute provided and can be identified as the difference in C_y associated with the change in *y*.

In the present study we consider the four different attributes *L*, *D*, *H* and *S* with three levels for each attribute to characterize changes in the environment. They are combined to choice sets using an experimental design that allows determination of the independent influence of the attributes on respondents' choices (details of the CE can be found in [9]). The choices of 353 randomly chosen inhabitants from the study region were considered.

2.2.2. Specifying the decision space and modeling the attributes

We start our analysis by identifying which parts in the landscape are physically and legally qualified for the allocation of WT with the help of a geographical information system (GIS) of the region. Broadly speaking, these are open areas distant enough from infrastructure, settlements and nature conservation areas. The analysis focuses on two WT technologies k=1,2. The k=1 type has a hub height of 78m and rotor diameter of 82m, yielding a nominal power of 2MW, while the k=2 type has a hub height of 105m and a rotor diameter of 90m, yielding a nominal power of 3MW. The suitable parts of the landscape are subsequently filled with a grid of points with each point in the grid representing a potential site for the allocation of a WT, taking technical minimum distances between individual WT into account. The number of potential sites is N=1098. Allocation scenarios are defined by deciding for each potential WT site i=1,…,N whether it should contain a WT of type 1 or type 2 or no WT.

The energy yield E_{ik} for each site i and WT type k is calculated by using the technical parameters of the WT and the relevant frequency distribution of wind speeds observed at the spatial location and altitude of the WT hub (for further details see [12]). The wind speed data were obtained from Eurowind GmbH (Köln, Germany). The total energy E_{tot} produced per year in the region is obtained by summing E_{ik} over all installed WT.

The production cost $C_{p,k}$ (over a time frame of 20 years) associated with a WT of type k comprises the construction and operating costs. The construction costs are composed of selling prices, taken from the companies' price lists, and a 10 percent mark-up to cover on-site construction costs, including grid connection. Annual operating costs are typically estimated at five percent of the construction costs (information provided by interviewed WT operators).

Ecological externalities are partly taken into account by prohibiting the erection of WT in areas protected by nature conservation laws. However, protected areas are by no means sufficient to reach the ambitious goals of biodiversity policy. So the impacts of WT on biodiversity have to be considered even if the WT are installed outside the protected areas. We consider L, the percentage of the regional Red Kite population that is lost due to WT over the modeling time frame of 20 years. We model this loss rate as the sum of "marginal" loss rates l_i over all sites i=1,…,N that contain a WT. We assume that the contribution l_i of site i to L is determined by the probability of an individual of the focal species being found at the site. This depends, e.g., on how close the site is to a nest, whether the site is located within a migratory bird route, etc. In the case of Red Kites we assume that l_i is a declining function of the distances of site i to known nests (i.e., WT close to a nest cause a higher collision risk for the Red Kite with the WT than WT at more distance to a nest).

The modeling of the remaining three attributes is straightforward. Attribute D represents the minimum distance of WT to settlements, considering all settlements and installed WT in the region. Attribute H is modeled as the average over the heights of all installed WT in the region. To determine attribute S we apply the wind park method [14] that clusters all WT into wind parks. S is then the average size of those wind parks.

3. Results

3.1. Construction of the social cost function

The choice experiments yield the following MWTP (in Euros per household per month)[1]: 2.13 for an improvement in the Red Kite loss rate L from 10% to 5% per 20 years; -2.18 for a worsening in L from 10% to 15%; 3.18 for an increase in the settlement distance D from 800m to 1100m; and 3.94 for an increase in D from 800m to 1500m. Changes in the other two attributes, H and S, did not lead to a statistically significant MWTP.

The partial cost functions $C_y(y)$ (eq. 2) are fitted to these measured MWTP to obtain the external cost function $C_e(L,D)$ shown in Fig. 1. One can see that external costs increase with increasing externalities, i.e. with increasing Red Kite loss rate L and decreasing settlement distance D.

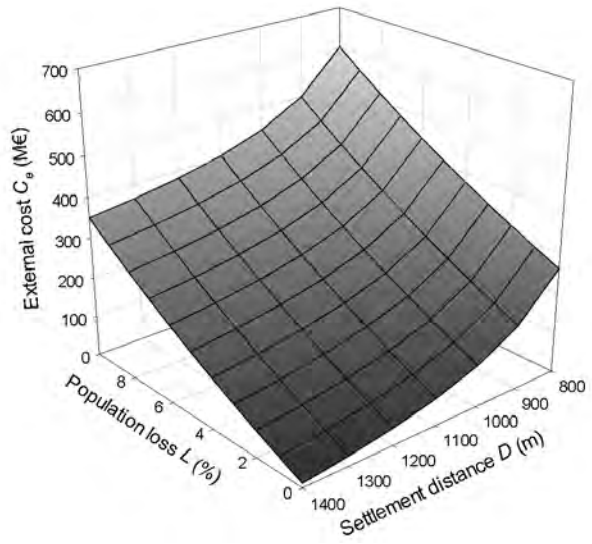

Fig. 1. External cost $C_e=C_L+C_D$ for the study region as a function of Red Kite loss rate L and settlement distance D, considering a time frame of 20 years with annual discount rate r=3%.

3.2. Evaluation of the attributes

Figure 2a shows the production cost C_p (over 20 years, discounted to the present year) for all potential WT sites i in the region. One can see that the production costs are lowest in the south, centre and east, and highest in the north east, which reflects relatively high wind speeds and large energy outputs E_{ik} in the south, centre and east and low wind speeds and energy outputs in the north east.

The external costs are determined by the settlement distance D and the Red Kite loss rate L which is the sum of the impacts l_i associated with each WT site i. The impacts for all potential WT sites are shown in Fig. 2b. We find that the l_i are relatively uncorrelated to the production costs, so there are both "low-conflict" WT sites that have low (high) production costs and low (high) impact on the Red Kite and "high-conflict" sites with low (high) production costs and high (low) impact on the Red Kite.

[1] The conditional logit reveals that only the attributes L and D have a significant influence on respondents' choices among the alternatives presented on the choice sets. Thus, only for these attributes MWTPs are calculated. See [9] for more details on the analysis of the choice experiments.

3.3. The welfare-optimal allocation of WT

The task is to allocate WT to the potential sites i=1,…,N so that the energy target E_{min}=690 GWh per year is achieved at minimal social cost where social cost is given by the sum of production costs (cf. Fig. 2a) and external costs (Fig. 1). The resulting optimal WT allocation scenario is characterized by the following welfare-optimal levels of the attributes: the optimal Red Kite population loss rate is L*=1.2 percent within 20 years, the optimal settlement distance is D*=1,025m and the optimal production cost amounts to C_p*=730 million Euros (sum over 20 years, present value, discounted at 3% per year). Altogether, a number of 122 large WT types but no small WT are installed.

To understand the trade-offs between production and external costs we determined the optimal allocation of WT under the assumption that the MWTP for avoiding externalities are reduced to one tenth of the observed values (cf. section 3.1). By assuming that society places little value to the externalities of the WT (L and D) this scenario considers mainly the production costs, and WT are allocated so that the total production cost (C_p) for reaching the energy target E_{min} are minimized. Consequently, the 690 GWh per year can be produced at a production cost of only C_p*=690 million Euros. While production costs are reduced, the optimal levels of the externalities are increased in this scenario: L* increases to 2.6 percent within 20 years and D* reduces to 800m. That means that the price for reducing the production cost is an increase in the external costs. According to Fig.1, increasing L from 1.2 to 2.6 and reducing D from 1025m to 800m increases the external cost by about 210 million Euros. So altogether, ignoring the externalities saves 40 million Euros of production costs but raises external costs by 210 million Euros and on net raises social cost by 170 million Euros.

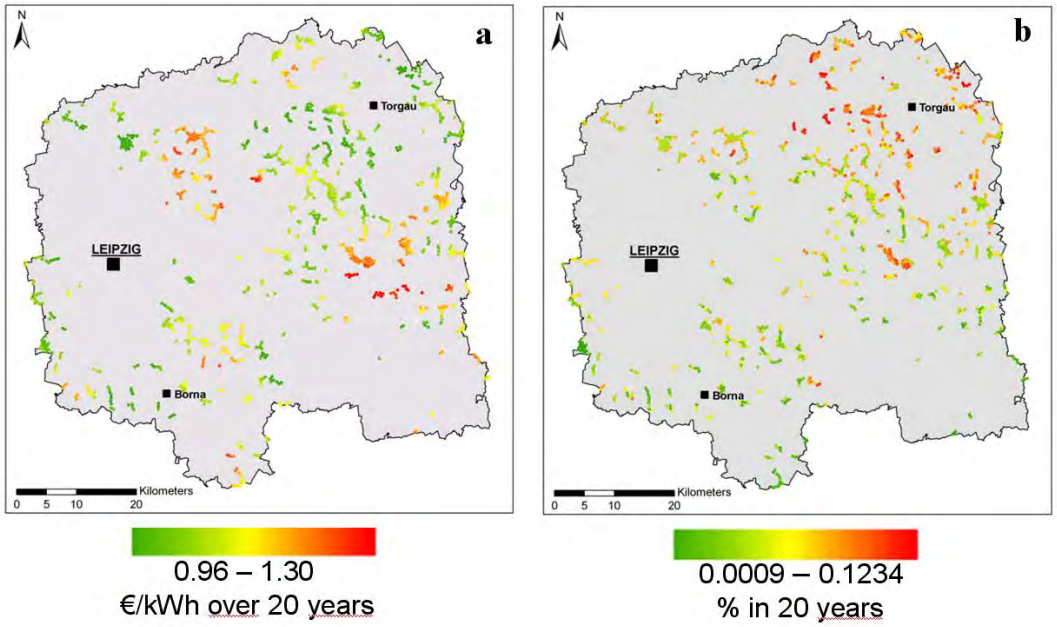

Fig. 2. a: Present value cost of producing 1 kWh over 20 years for each WT site, represented by color scale; b: contribution to Red Kite loss (l_i: see text) of each potential WT site i, represented by color scale. Small WT (k=1) are installed at sites between 750m and 1000m from settlements, large WT (k=2) at larger distances > 1000m.

4. Discussion and Conclusions

Wind power is one of the most promising options for producing energy in a climate-friendly manner. However, it causes negative externalities in terms of adverse impacts on humans and

biodiversity. To alleviate the conflict between the positive impact of wind power on climate policy and its negative externalities, wind turbines (WT) should be allocated so that social costs (i.e., the sum of wind power production costs plus external costs) are minimized with regard to the desired climate-friendly energy target. Determining such an allocation ex ante requires the combination of different methods, including economic modeling of the production costs, modeling of the non-monetary external effects, monetary valuation of these external effects, and numerical optimization.

The goal is to reach a certain energy target in a concrete region ($E_{\min}$) in a welfare-optimal manner, i.e. at lowest social costs. To do this, we explored trade-offs between production costs and externalities by combining choice experiments and spatially explicit modeling. It turned out that in the study region the distance of WT to settlements and the impact on a focal species, the Red Kite, represent significant externalities of wind power supply. On the other hand wind park size and height of the turbines are not. The welfare-optimal allocation balances production costs and externalities and minimizes the sum of production costs and external costs. When determining the welfare-optimal allocation of WT in our study region in Germany it turned out that ignoring the externalities and minimizing only the production costs would reduce the production costs by about five percent from 730 million Euros to 690 million Euros but increase the external cost by 210 million Euros each compared to the welfare optimum. Altogether, ignoring the externalities would increase social cost by 210-(730-690)=170 million Euros.

The magnitude of the chosen energy target reflects the importance of producing energy in a climate friendly manner. The optimal magnitude should be chosen such that the regional social costs of wind power production are outweighed by the benefits accruing from reduced CO2 emission. Determining the "globally" optimal level of the energy target, however, was beyond the scope of this study and is a matter of future research.

The numbers obtained in the analysis depend on several assumptions. In the assessment of the impacts of WT on the Red Kite, e.g., we ignored options of on-site management that make sites unattractive for the Red Kite and would thus reduce the modeled collision risk. Moreover, the search range of Red Kites is not circular. Information on the search behavior of Red Kites, however, is difficult to obtain and requires sophisticated field observations. If this information was at hand it could be easily fed into the model.

In the establishment of the external cost function (C_e, eq. (2)) we assumed that it is separable and can be written as the sum of partial costs. This ignores the possibility of interactions so that the marginal willingness to pay for the reduction of one externality depends on the level of another externality. In the choice experiments we searched for such interactions but did not find any significant ones. If they are significant, interactions can be considered by an appropriate adaptation of the shape of C_e.

With regard to the production costs we ignored the spatial variation of grid connection costs. These very much depend on the distance of a site to the next feed in station, and also on whether a solitary WT or a wind park is connected. Generally connection costs per WT decrease with increasing size of a wind park (economy of scale). Taking these factors into account would require detailed knowledge about the present power grid and even more, assumptions how allocation of WT and expansion of the power grid co-evolve. Since the evolution of power grids and the installation of new smart technologies to make existing

power grids effective for renewable energies are currently a hot topic it may be interesting to further explore this issue in future.

Acknowledgements

The authors thank the German Ministry for Education and Research for funding the research project "Conflicts of interest over wind power" [Nachhaltige Landnutzung im Spannungsfeld umweltpolitisch konfligierender Zielsetzungen am Beispiel der Windenergiegewinnung] (Grant No. 01UN0601A, B) as a part of the fona Programme "Economics for Sustainability [Wirtschaftswissenschaften für Nachhaltigkeit] (WIN)". The views expressed in this paper are the responsibility of the authors alone. In addition we thank the West Saxony Regional Planning Office for the constructive cooperation and commentary.

References

[1] E. Hau, Wind Turbines. Fundamentals, Technology, Application, Economics. Springer, Berlin/Heidelberg, Germany, 2006.

[2] C.L. Krause, Our visual landscape: Managing the landscape under special consideration of visual aspects. Landscape and Urban Planning 54, 2001, pp. 239-254.

[3] B. Möller, Changing wind-power landscapes: regional assessment of visual impact on land use and population in Northern Jutland, Denmark. Applied Energy 83, 2006, pp. 477-494.

[4] H. Hötker, K.M. Thomsen, H. Jeromin, H., Impacts on biodiversity of exploitation of renewable energy sources: the example of birds and bats – facts, gaps in knowledge, demands for further research, and ornithological guidelines for the development of renewable energy exploitation. Michael-Otto-Institut im NABU, Bergenhusen, Germany, 2006 (http://www.batsandwind.org/pdf/impacts%20on%20biodiversity%20of%20renewable%20energy.pdf).

[5] J. Bright, R. Langston, R. Bullman, R., Evans, S. Gardener, J. Pearce-Higgins, Map of bird sensitivities to wind farms in Scotland: A tool to aid planning and conservation, Biological Conservation 141, 2008, pp. 2342-2356.

[6] B. Álvarez-Farizo, N. Hanley, Using conjoint analysis to quantify public preferences over the environmental impacts of wind farms. An example from Spain, Energy Policy 30, 2002, pp. 107-116.

[7] K. Ek, Quantifying the environmental impacts of renewable energy: The case of Swedish wind power, in: D. Pearce D. (Ed.), Environmental Valuation in Developed Countries: Case Studies. Edward Elgar, Cheltenham, 2006, pp. 181-210.

[8] A. Dimitropoulos, A. Kontoleon, Assessing the determinants of local acceptability of wind farm investment: a choice experiment in the Greek Islands. University of Cambridge, UK, Department of Land Economics, Environmental Economy and Policy Research Working Paper No. 35.2008.

[9] J. Meyerhoff, C. Ohl, V. Hartje, Landscape externalities from onshore wind power. Energy Policy 38, 2010, pp. 82-92.

[10] M.J. Punt, R.A. Groeneveld, E.C. van Ierland, J.H. Stel, Spatial planning of offshore wind farms: a windfall to marine environmental protection? Ecological Economics 69, 2009, pp. 93-103.

[11] J. Ladenburg, Onshore and offshore locations for wind power development – what does the public prefer and should it matter? Modern Energy Review 1, 2009, pp. 32-34.

[12] M. Eichhorn, M. Drechsler, Spatial trade-offs between wind power production and bird collision avoidance in agricultural landscapes, Ecology and Society 15, 2010 [online] URL: http://www.ecologyandsociety.org/vol15/iss2/art10/.

[13] J.J. Louviere, D.A. Hensher, J.D. Swait, Stated Choice Methods. Analysis and Application. Cambgridge University Press. Cambridge, 2000.

[14] M. Schmitt, F. Dosch, E. Bergmann, Flächeninanspruchnahme durch Windkraftanlagen. Berichte aus Forschung und Praxis. Raumforschung und Raumordnung 64/5, 2006, pp. 405-412.

Opportunities for co-utilization of infrastructures for wind energy generation

Tarja Ketola[1]

[1] *Industrial Management Unit, University of Vaasa, Finland*
Tel: +358 44 0244 389, E-mail: tarja.ketola@uwasa.fi

Abstract: The co-utilization opportunities of different infrastructures for wind energy generation will be investigated in this paper. Information is derived from previous research and discussions with Finnish wind energy companies as well as with authorities, environmental organizations and local inhabitants in the Ostrobothnia region of Finland. Wind power can be built in areas where there are already other business activities. These co-utilization areas include harbours, industrial sites, roads, railways and existing masts and towers. Moreover, both natural and cultivated environments have vast co-utilization potentials for wind energy offshore, near shore and onshore like in fields, forests and swamps and on hills and islands. The environmental and socio-cultural considerations are of crucial importance when planning co-utilization in natural environments, and very important also in cultivated environments. Industrial areas are the least environmentally and socio-culturally vulnerable, but the potential partners there are businesses that demand substantial financial benefits from co-utilization cooperation, hence making the economic considerations decisive. Co-utilization projects can mitigate or prevent many undesirable environmental, socio-cultural and economic impacts of wind turbines, if they are holistically and carefully planned. Furthermore, wind turbines as structures can serve numerous environmentally, socio-culturally and economically beneficial purposes.

Keywords: *Wind energy, Co-utilization, Infrastructure, Life cycle assessment, Social acceptance*

1. Introduction

Wind turbines can be short, medium-sized and tall, are they can be located off shore, near shore and on shore. They have a variety of environmental, social, cultural and economic impacts, both positive and negative, which depend on the areas they are built in.

Wind turbines can be built in areas where there are already other business activities, and not only in locations where no other human activities take place. These co-utilization areas include e.g. harbours, industrial sites, roads, railways and existing masts and towers. Wind turbines and wind farms can also be built in cultivated environments, i.e. on fields and fallows. In addition, natural environments, such as forests, fields of flowers, arctic hills, swamps, islands and offshore sea areas, are increasingly used as wind farm building sites.

The environmental and socio-cultural considerations of wind turbines are of crucial importance when planning co-utilization in natural environments, and very important also in cultivated environments. Industrial areas are the least environmentally and socio-culturally vulnerable, but the potential partners there are businesses that demand substantial financial benefits from co-utilization cooperation, hence making the economic considerations decisive.

The starting point of this research is the compiling of a sustainability assessment, i.e. an environmental, social, cultural and economic life cycle assessment (LCA) of wind turbines from previous economic and environmental impact and social acceptance studies on wind power and discussions with Finnish wind energy companies and their interest groups. The opportunities for co-utilization will then be mapped in cooperation with Finnish wind energy companies and their interest groups. Wind turbines as structures can serve numerous environmentally, socio-culturally and economically beneficial purposes.

2. Methodology

This is an exploratory study, which derives its information from previous research[1,2,3,4,5,6,7,8] and discussions with wind energy companies, authorities, environmental groups and local inhabitants of Ostrobothnia at a wind energy seminar organized by the Regional Council of Ostrobothnia in Vaasa, Finland, on 30 September 2010, to discuss regional wind power planning. The author of this paper is a member of the CLEEN WIPO research group with 26 Finnish wind energy companies and seven Finnish research institutes. This research group is currently planning a major research project to enhance wind power (WIPO) building and exports. The CLEEN Ltd is the Finnish energy and environment strategic centre for science, technology and innovation with 44 shareholders (major Finland-based companies and national research institutes) established in 2008 to facilitate and coordinate research in the field of energy and environment. This paper analyses current knowledge of wind power impacts and co-utilization, and maps out some research cooperation possibilities for the WIPO project.

3. Results

Table 1 compiles environmental, social, cultural and economic impacts of wind turbines.

Table 1. Environmental, social, cultural and economic impacts of wind turbines.

Environmental impacts	**Social impacts**	**Cultural impacts**	**Economic impacts**
POSITIVE: +Renewable, natural energy production method +Rescue nature from harmful options +Hardly any CO_2 or other emissions +Hardly any hazards to humans or nature +Compensate within 3-6 months the energy used during their whole life-cycle +Nearly all parts of turbines are recyclable	POSITIVE: +Boost local employment: planning, construction & maintenance +Boost entrepreneurship +Boost research & development +Farmers: can lease land, generate small-scale power for their farms and become large-scale wind power producers	POSITIVE: +Traditional; long experience from windmills +Use and upkeep of local knowhow +Could be integrated into contemporary culture, like windmills were: parts of cultural heritage	POSITIVE: +Plenty of business opportunities +Innovation opportunities for many businesses +Major growth opportunities home & abroad +Low maintenance costs +Give nations a great chance to improve their energy self-sufficiency in the most renewable and least harmful way +Help meet CO_2 targets
NEGATIVE: -Wind turbine construction and infrastructure building on natural sites disturb flora and fauna, damage their habitats, and destroy forest, flower field and sea bottom ecosystems, diminishing biodiversity -Propellers and power lines are hazardous to birds, bats and insects -Radar impacts on bats disturb their orienteering - CO_2 & other emissions from parts production and transportation -Noise causes danger (cannot hear predators) and stress to animals	NEGATIVE: -Cause "not in my backyard" (NIMBY) syndrome -Cyclic noise causes stress & stress-related illnesses to humans -Hinder visibility -May spoil visual landscape -Cause light and shadow reflections -May cause accidents to people -May impact real estate values and prices	NEGATIVE: -May upset current cultural landscapes	NEGATIVE: -Local resistance inhibits or slows down investments -Require often many permits and environmental impact assessments (EIAs) with long, exhaustive application procedures -Winds change, challenging even energy supply -Possible radar impacts on military monitoring sensors and air & sea monitoring radars

Table 2 maps co-utilization opportunities of wind turbines in different areas and elaborates on the way they decrease malignant and increase benign environmental, social, cultural and/or economic impacts of wind power.

Table 2. Some co-utilization opportunities of wind turbines.

Co-utilization	**Benefits for environmental, social, cultural and/or economic impacts**
Industrial sites, warehouse areas, harbours	+Infrastructures are already in place; hence there is no need to cause ecological harm by building them. +Usually far away from natural sites and residential areas; hence propeller noise does not disturb nature or humans. +Visual disturbance is minimized by already spoilt scenery and long distance to natural and residential sites. +Require fewer permits & no environmental impact assessments (EIAs). +Wind power generation can be integrated into the site's business operations, thereby giving both energy & financial benefits to companies. +Easy to supply energy to cities and residential areas because of the established grid and power line connections. +Companies on the site can invent multiuse purposes for wind turbines. +The jungle of turbines of wind farms can breed novel business ideas. +Rebuilding power lines underground prevents birds, bats and insects from flying into them.
Roadsides and railway banks	+Propellers' noise is hidden by traffic. +Visual disturbance is lessened by already spoilt asphalt, metal and concrete constructions. +Turbines have tall towers that can be used for traffic control, other surveillance and storage. +Wind energy generation by roads and railways could allow recharging the batteries of electric cars and novel electric trains during the journey. +The jungle of turbine masts can inspire novel means of transportation (e.g. postmodern Tarzans). +Wind farms in public areas will attract extreme sports enthusiasts with their creative inventions. +Building power lines underground prevents birds, bats and insects from flying into them.
Masts and towers	+Radio masts, telecommunication masts and many different kinds of towers can act also as wind turbines. +Possible added negative environmental, social, cultural and economic impacts of attaching propellers to these masts and towers can be easily analyzed and minimized, taking the special characteristics of the location into account. +Both the infrastructure and the turbine trunks are ready-made. +These second-hand wind turbine masts and towers save plenty of steel, fibreglass and metal-plastic composites normally needed to build the turbine trunks. +The trunks could serve also as habitats and nesting places for animals, particularly if they are covered by moss, lichen and other plants. +Building power lines underground prevents birds, bats and insects from flying into them.

Farm fields and fallows	+Little ecological disturbance or damage, as farm fields are typically monocultures with diminished biodiversity. +Farming and wind power generation can be done simultaneously. +Farmers earn either from leasing land and doing turbine maintenance, from generating the energy they need through small-scale wind power, or from becoming large-scale wind power producers and sellers. +Social nuisance is minimized: farmers who benefit do not suffer from the NIMBY syndrome and tolerate the visual harm and noise stress caused by the turbines. +Distance to neighbours is often quite long. +Building power lines underground prevents birds, bats and insects from flying into them.
Swamps	+Swamps that are already in commercial peat energy production are suitable for wind power generation, as they have already been ruined ecologically, socially, culturally and visually, and are plagued by noise from heavy work machinery. +Building power lines underground prevents birds, bats and insects from flying into them. -However, swamps still in their natural state should not be disturbed or damaged by wind power developments, which would destroy their fragile ecosystems and biodiversity once and for all.
Islands	+Wind turbines could be built on the hilly centre of an island with fishermen and/or summer residency, so that they will not disturb the coastal fishermen's houses, summer cottage owners, tourists or nature. +The island's commercial activities (shops, bank, post-office, car battery recharge, etc.) could also be built in the centre. +Building power lines underground prevents birds, bats and insects from flying into them.
Offshore (and near-shore) areas	+The adverse ecological impacts of dredging, building infrastructure and setting up turbines in marine ecosystems can be mitigated by turning the concrete and steel foundations into artificial reefs by erosion protection. +The reefs would attract fish, plants and other marine life, and could develop into holistic ecosystems, thereby preserving biodiversity. +Blocks built from rocks of different sizes can muffle turbine noise that drives fish away. Strong fish populations enhance fishing as a natural livelihood of the area. +Near-shore and offshore wind farms can be built to accommodate research platforms for marine life, weather and tidal energy research. +Shark nets could possibly be attached to the below sea-level turbine constructions of near-shore wind farms. +Building power lines underwater prevents birds from flying into them.

4. Discussion and Conclusions

There are many co-utilization places for wind turbines in which they would not cause much environmental, social or cultural harm and could be made economically profitable.

Industrial sites, warehouse areas, harbours, roadsides and railway banks are environmentally, socially, culturally and economically best places for wind turbines. There they do not damage

nature or disturb humans; their building expenses are low because of the ready-made infrastructures, and profit opportunities are great due to the easy supply of energy to local businesses and residents.

Using existing, i.e. second-hand, masts and towers in these areas would cut down the turbine construction expenses to the minimum and save plenty of unrenewable building material.

Farm fields and fallows are also environmentally, socially, culturally and economically rather benign areas to build wind turbines since they are monocultures, lie often away from residential areas, and wind power generation provides several livelihood opportunities for farmers.

Swamps exploited for peat energy production, are already environmentally, socially and culturally ruined, and therefore, would not suffer much from wind turbines, which would add to the high profits derived from peat energy production. Untouched swamps should be left alone.

Islands are often ecologically valuable areas, but islands with a commercial centre in the middle would not be too much hurt by wind turbines, if they were also built in the centre, which would leave the ecologically fragile and socially important coastal areas untouched.

Offshore wind farm building has several environmentally damaging impacts, but they could be mitigated by turning the concrete and steel foundations into artificial reefs, which would attract fish and other marine life. This could lead also to a beneficial effect on the livelihoods of fishermen. Offshore wind farm platforms could be used by researchers. Near-shore wind farms are more malignant environmentally, socially and culturally, but could possibly be used e.g. for attaching shark nets to.

There are some areas where the malignant environmental, social, cultural and/or economic impacts outweigh the benign ones.

Arctic hills have plenty of space and plenty of wind. In wintertime the colour of wind turbines and snow is synchronized, making a visual match. However, infrastructure building and turbine construction rape virgin land. Moreover, reindeer herders oppose arctic wind farms because they endanger the winter pastures of reindeer. And ultimately, since climate change causes trees to migrate north, plenty of space must be left for the arrival of trees.

Forests of any kind are not suitable or economically profitable places as trees muffle wind. Furthermore, infrastructure building, turbine construction and propeller noise cause such massive disturbance and damage to flora, fauna, soil, rocks, and to the whole forest ecosystem that wind turbines should not be built in forests.

Wind power should not be built in nature protection areas or bird and other animal sanctuaries, on the migration routes of birds, fish and sea mammals, or on environmental or cultural heritage sites. An ample buffer zone between these areas and wind farms should be reserved to prevent any environmental, social or cultural disturbance against these most valuable assets of the humankind.

The findings of this research are based on previous studies of the impacts of wind turbines (which themselves have taken account of hundreds of studies) and on the partially conflicting views of wind energy companies, authorities, environmental organizations and local inhabitants of the Ostrobothnia region of Finland gathered together at a wind power seminar.

This study adds to the knowledge of previous wind turbine impact research through the empirical study. The most important value of this research comes from exploring and mapping out novel empirical findings for a new research area of co-utilization impacts of wind power.

This research has not critically evaluated any of the conflicting views of the seminar participants but listed them all as positive and negative impacts of wind turbines and their co-utilization. The number of participants at the wind power seminar was 63, which is not a representative sample of the population of the city of Vaasa (59,633 inhabitants on 31.10.2010) or the Ostrobothnia region (about 1 million inhabitants during the early 2000s). Those who attended the seminar were more interested in wind power than an average citizen of the city or region, but the participants (wind energy companies, authorities, environmental organizations and local inhabitants) represented the different views and perspectives to wind power development well enough to give a rather balanced account of the positive and negative impacts of wind turbines and their co-utilization.

Similar studies could be conducted at other wind power seminars and at wind farm planning meetings collecting together people with different backgrounds and interests. New issues to address and ideas to solve them would no doubt emerge in such gatherings as wind farms become more widespread and people gain more experience on their impacts.

5. Recommendations

Co-utilization is an effective way of enhancing the social acceptance of wind power. Participation at every stage of the planning process in close cooperation with the wind energy companies tends to make local people, farmers, environmental organizations, authorities and businesses adopt a very positive attitude towards wind power. They appreciate the wind energy companies' respect for their expertise and creativity in mapping out co-utilization possibilities and planning continuous cooperation.

The active involvement in the projects and the resulting structures in turbines that for example, protect nature or collect data, satisfy the needs of most local people, environmental organizations and authorities. Farmers and companies want also business opportunities from co-utilization. The others often shy away from the profit-maximizing limited liability type market economy in co-utilization, but show great interest in socio-culturally beneficial co-op type co-utilization. This poses both an opportunity and challenge for the limited liability type wind energy companies: can they set limits to their short-term profit greed in order to secure long-term survival and success?

These issues are worth contemplating, as wind power is one of the few energy businesses that are strongly supported by environmental organizations. One of the most radical environmental organizations, Greenpeace, estimates that 20 per cent of the world's energy could be produced by wind power by 2030.[6] Such encouragement should be taken advantage of by solving the negative environmental, social, cultural and economic impacts of wind power through co-utilization and other measures.

References

[1] European Environment Agency, Europe's onshore and offshore wind energy potential, An assessment of environmental and economic constraints, EEA Technical Report 6/2009. EEA, 2009.

[2] European Wind Energy Association, Wind at work: wind energy and job creation in the EU, EWEA, 2009.

[3] P. Hokkanen, Kansalaisosallistuminen ympäristövaikutusten arviointimenettelyssä (In Finnish) (Citizen participation in the environmental impact assessment procedure), Acta Universitatis Tamperensis 1285, University of Tampere Press, 2007.

[4] J. Koistinen, Tuulivoimaloiden linnustovaikutukset, Suomen ympäristö 721 (In Finnish), (The bird population impacts of wind power plants, Finland's environment 721), Finland's Ministry of the Environment, 2004.

[5] S. Korpinen, V. Pohjanheimo, K. Auvinen, A. Mäkinen, WWF Suomen kanta tuulivoimasta Suomessa (In Finnish) (WWF Finland's position in wind power in Finland), Worldwide Fund for Nature Finland, 2007.

[6] S. Teske, A. Zervos, C. Lins, J. Muth, Energy (r)evolution: a sustainable world energy outlook, Greenpeace International and European Renewable Energy Council (EREC), 2010.

[7] V. Varho, Calm or storm? Wind power actors' perceptions of Finnish wind power and its future, Environmentalica Fennica 25, Helsinki University Printing House, 2007.

[8] E. Weckman, Tuulivoimalat ja maisema, Suomen ympäristö 5 (In Finnish) (Wind power plants and the landscape, Finland's environment 5), Finland's Ministry of the Environment, 2006.

Optimal Layout for Wind Turbine Farms

Koby Attias[1,*], Shaul P. Ladany[1],

[1]*Ben- Gurion University, Beer-Sheva, Israel*
**Corresponding author. Tel: 972-52-5250815, Fax:972-77-2101037, E-mail:yattias@elta.co.il*

Abstract: A general discrete model was formulated for the expected Net Present Value (NPV) of the profit and for the expected yield of the investment (Internal Rate of Return - IRR) to be derived from rectangular grid shaped wind-turbine farms. The model considers the wind shade in the downwind direction and the effect of the wake behind the turbine, the joint wind-direction wind-velocity probability distribution, as well as the various relevant cost and revenue factors. It was assumed that the wind-turbines are identical and of equal heights, and are spaced equally along the axes of the rectangle, but not necessarily at the same equal distance at both axes. Using the model, the optimal layout that maximizes the expected NPV and/or IRR was derived numerically for a given data set, in stages, determining the optimal number of turbines in a row and the associated optimal distance in-between them, and also the optimal number of turbines in a column and the optimal distance in-between them. Sensitivity analysis has shown that minor changes in the parameters do not affect the selection of the optimal layout.

***Keywords**: wind energy, optimal layout, wind farms*

1. Introduction

The harvesting of wind energy is centuries old as manifested by the middle-age wind mills in Europe. Heier [1] describes how the use of wind energy to generate electricity started in 19th century, but only the oil crisis of October 1973 provided the strong impact. The understanding and use of wind energy has been investigated by Lindley et al.[2], and are summarized by Manwell et al. [3]and Burton et al. [4]. Plans for actions to increase the use of wind energy were introduced by Milborrow et al. [5] , and the success is evidenced by travelers in Denmark and North Western parts of Germany where thousands of wind-turbines have been installed in recent years. The performance of wind farms were evaluated by Haack [6], while the integration of wind power into general power systems is discussed by Ackermann [7]and Heier [1].

Obviously, the erection of multiple wind-turbines in windfarms necessitates the determination of their layout. Bossanyi et al.[8], has dealt with the issue of investigating the efficiency of different layouts and even for designing aerodynamically optimal layouts. However, they did not integrate the economic and financial optimization of windfarms with the aerodynamic aspects. Yet the methods of operational research and operations management determine such optimizations using the maximization of the expected profit as the objective function. For example, see Ladany [9] and [10] in which the optimal layout of urban gasoline-stations was determined.

Hence, the aim of this paper is to develop a model to determine economically optimal layouts for windfarms (i.e. the number of turbines and their setting), which include the aerodynamic interactions between the turbines, the various cost factors and the particular wind regime. Section 2 presents the model; Section 3 considers the aerodynamic interaction between the turbines; Section 4 describes the optimization procedure; Section 5 shows a numerical example; Section 6 offers the conclusions.

Searching through Tables 2 & 3, it is possible to detect solutions that provide the best combination of N_{PV}'s and I_r's, although each is less than its maximum value. For example, for

a layout of I=4, J=6 (24 turbines), with the turbines separated with x=100 m and y=300 m, provides an N_{PV}=$21.5 million, and an I_r=19.7%, which is the authors recommend "optimal solution."

1.1. Aim of this paper

The aim of this paper is to explore and searching a model. By Using the model, we got the optimal layout that maximizes the expected NPV and/or IRR was derived numerically for a given data set, in stages,

2. The model

Consider a rectangular grid layout (see Figure 1) of I x J wind-turbines of equal size and height, 2 adjacent turbines separated by the distance x in one direction and y in the other direction (obviously the minimum of x & y is more than the diameter of the turbine's rotor).

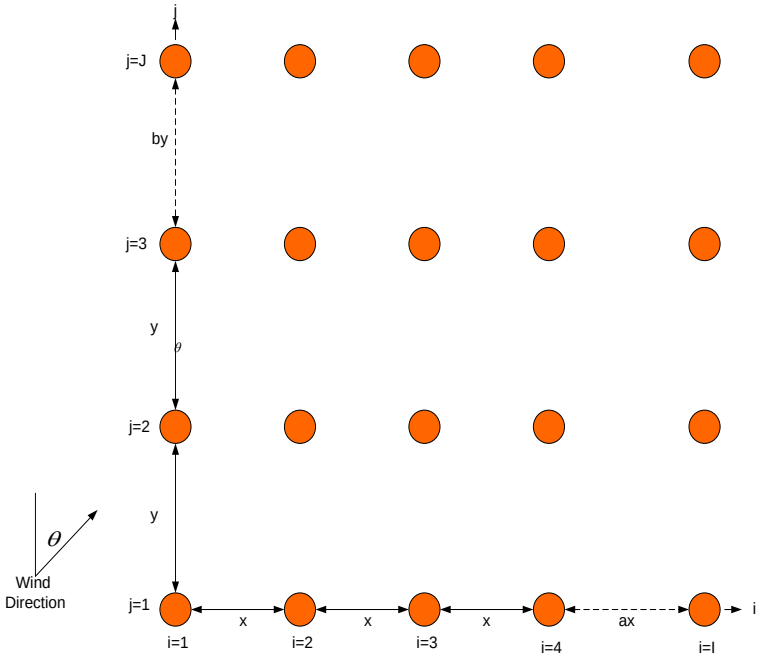

Figure 1: Location of turbine i, j in a rectangular grid layout of I x J turbines

When the wind blows in direction θ with a nominal velocity of V(θ), the effective wind velocity in front of the turbine at position i, j (which takes into account the aerodynamic interaction between the turbines, the wake affect – see the discussion in section 4) is Vij(θ, x, y).

Vij(θ, x, y) is obviously a function of V(θ), and it is developed in section 4. The effective wind velocity incident on 'turbine i, j' is Vij(θ, x, y), so the electrical power generated by the 'turbine i, j' is: eij(θ, x, y) [kwh]:

$$e_{ij}(\theta,x,y) = 0.5\rho V^3_{ij}(\theta,x,y)\cdot BC_pN_m \qquad (1)$$

where ρ is the air density [kg/m3], B is the swept rotor area [m2], Cp is the rotor efficiency coefficient (capacity factor) [%/100], Nm is the efficiency for converting the rotor mechanical power to electricity [%/100].

When the joint probability of the nominal wind velocity and its angle of incidence θ is defined as p (Vθ, θ), the expected annual energy to be generated by turbine i, j is

$$E(e \mid x, y)_{ij} = \sum_{v_\theta, \theta} e_{ij}(\theta, x, y) \cdot p(V_\theta, \theta) \tag{2}$$

while the total expected energy to be generated by the whole farm, T(x, y), is

$$T(x, y) = \sum_{i=1}^{I} \sum_{j=1}^{J} E(e \mid x, y)_{ij} \tag{3}$$

If the lifetime of a turbine is L, then K is the total investment in the windfarm (including the cost of turbines, installations and land cost), F is the net revenue from the selling electricity from the windfarm, r is the appropriate financial interest rate, H is the total operating time per period(for example operating time is: 24 h/d X 328.5 d/y =7884 h/y , and maintenance days are= 365-328.5=36.5d/y), P is the unit sale price of electricity , M is the cost of operation and maintenance of the windfarm per period, the Net Present Value, NPV, of the profit to be derived from the farm is

$$N_{pv}(x, y) = -K + \sum_{k=1}^{L} \frac{H \cdot T(x, y) \cdot P - M}{(1 + r)^{k-1}} = -K + \sum_{k=1}^{L} \frac{F}{(1 + r)^{k-1}} \tag{4}$$

Where $H \cdot T(x, y) \cdot P - M$ =F
The Internal Rate of Return (IRR) on the investment, Ir (x, y) is the value of the interest rate, r, that results in
NPV (x, y) =0.

3. The aerodynamic interaction between the turbines

Since a wind-turbine generates electricity from the energy in the wind, the wind leaving the turbine has less energy content than the wind arriving in front of the turbine. Therefore a wind-turbine will always cast a wind shadow in the downwind direction. This is described as the wake behind the turbine, which is quite turbulent and has an average down-wind speed slower than the wind arriving in front of the turbine.

With effective yawing, we assume the direction of the wind is always perpendicular to the front of the turbine. Hence, the diameter of the turbine is considered always perpendicular to the wind's direction. Nybore [11] has shown that behind the turbine the wind creates a cone-sloped wake which extends 4.5º to the sides, as shown in Figure 2, (i.e. creating a truncated cone with a 9º head-angle.)

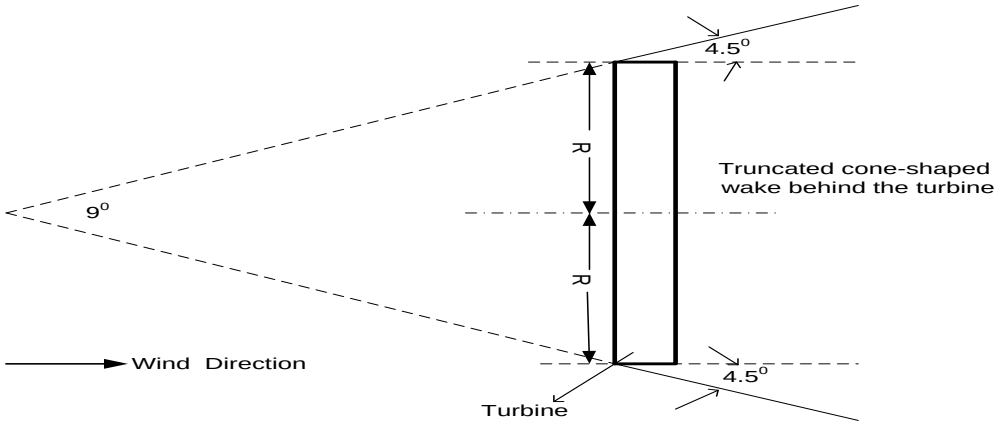

Figure 2: A 2-dimensional representation (top view) of the cone-shaped wake created by the wind behind the turbine

In a windfarm, 'turbine i, j' might or might not be affected by the wake created by another turbine positioned in front of it (in relation to the direction of the wind.) Moreover, the effect might be partial or complete. As a result, we distinguish 4 different states for the wind velocity hitting 'turbine i, j', as shown in Figure 3.

Adapting the findings of Nybore [11] to the notation required for dealing with a grid shaped farm, the wind velocity onto 'turbine i, j', when the general wind velocity in direction θ is V(θ), and the grids are separated by the distances x and y, is:

For state (a) when 'turbine i, j', is not affected by the wake of another turbine m, n ,

$$V_{ij}(\theta, x, y) = V(\theta) \quad (5)$$

Where m, n are the coordinates on the grid of another turbine in front of 'turbine i, j'. m might be less, equal or more than i, and likewise n might be less, equal or more than j, but (m, n) ≠ (i, j).

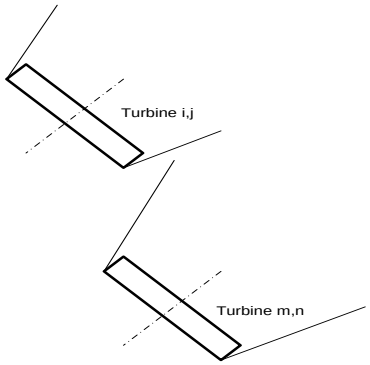

(a) Turbine i, j not affected by the wake of another turbine m, n

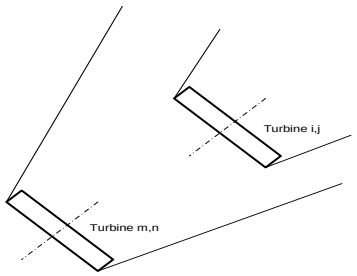

(b) Turbine i, j fully affected by the wake of another turbine m, n

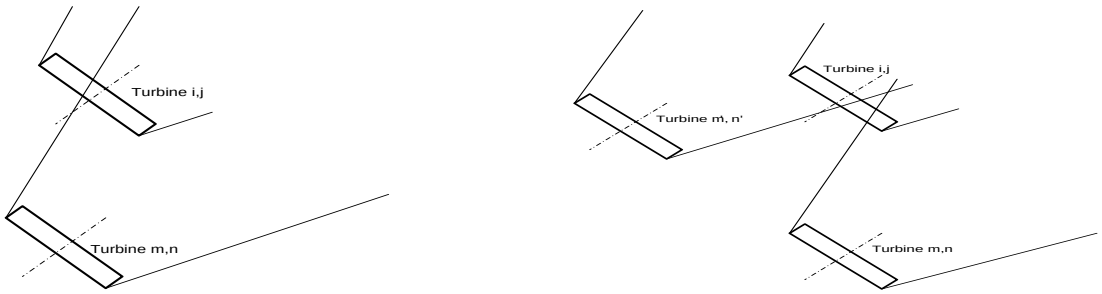

(c) Portion of turbine i, j is affected by the wake of another turbine m, n

(d) Portion of turbine i, j is affected simultaneously by the wake of turbine m, n and of turbine m', n'

Figure 3: Top view of the 4 states in which turbine i, j can be affected by the wake

For state (b) when turbine i, j is fully affected by the wake of turbine m, n,

$$V_{ij}(\theta,x,y) = V(\theta)\cdot\{1-[1-\frac{V_{mn}(\theta,x,y)}{3V(\theta)}]\cdot[\frac{R}{R+0.078d}]^2\} \quad (6)$$

where
R is the radius of the turbine's rotor, and
d is the distance between the centers of turbine i, j and turbine m, n (See fig. 4)
Note: This formula was developed by engineer Niels Otto Jensen from Risoe.

The wind in the wake $V_{ij}(\theta,x,y)$ is related to the surrounding free wind $V(\theta)$, the downwind distance (d meters), the rotor radius (R meters) and the spreading angle of the wind (about 4.5^0) . The factor 0.078 is called the constant of spreading, its corresponds to a spreading angle of about 4.5^0

For state (c) (when a portion (either a major or a minor portion) of turbine i, j is affected by the wake of another turbine m, n), Nybore's [11] equation is adjusted to the prevailing conditions:

$$V_{ij}(\theta,x,y) = V(\theta)\frac{A_{ij}}{\Pi R^2}\cdot\{1-[1-\frac{V_{mn}(\theta,x,y)}{3V(\theta)}]\cdot[\frac{R}{R+0.078d}]^2\} + V(\theta)[\frac{\Pi R^2 - A_{ij}}{\Pi R^2}], \quad (7)$$

where
Aij is the area of intersection between the area of the rotor of turbine i, j and the cross-section (at turbine i, j) of the wake cone affected by turbine m, n.

For state (d) when a portion of turbine i, j is simultaneously affected by the wakes of turbine m, n and also of turbine m', n', Nybore's[11] equation is further adjusted:

$$\begin{aligned} V_{ij}(\theta,x,y) = {} & V(\theta)\frac{A_{ij}}{\Pi R^2}\cdot\{1-[1-\frac{V_{mn}(\theta,x,y)}{3V(\theta)}]\cdot[\frac{R}{R+0.078d}]^2\} \\ & + V(\theta)\frac{A_{i'j'}}{\Pi R^2}\cdot\{1-[1-\frac{V_{m'n'}(\theta,x,y)}{3V(\theta)}]\cdot[\frac{R}{R+0.078d'}]^2\} + V(\theta)[\frac{\Pi R^2 - A_{ij} - A_{i'j'}}{\Pi R^2}], \end{aligned} \quad (8)$$

where
$A_{i'j'}$ is the area of intersection between the area of the rotor of turbine i, j and the cross-section (at turbine i, j) of the wake cone affected by turbine m', n', and
d' is the distance between the centers of turbine i, j and turbine m', n'.
d is the distance between the centers of turbine i, j and turbine m, n.

For states (c) and (d), A_{ij} is depicted in Figure 4.

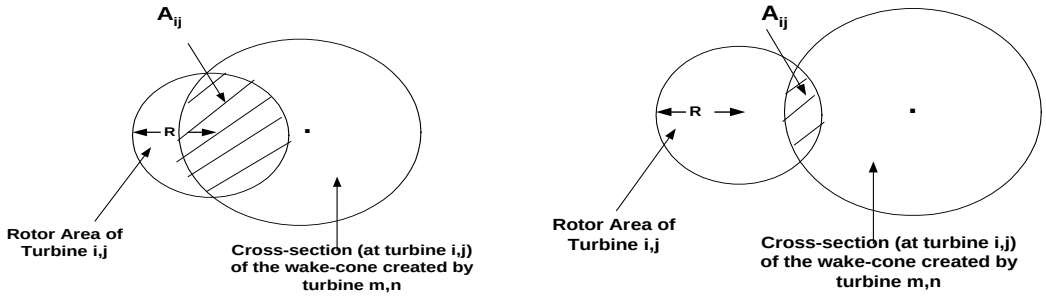

(a) Major portion of turbine i, j is affected (b) Minor part of turbine i, j is affected

Figure 4: Front view of the intersection (shaded) of the rotor area of turbine i, j, and of the cross-section (at turbine i, j) of the wake-cone affected by turbine m, n.

While the occurrence of state (d) in itself is very rare, theoretical situations exist in which in state (d) the cross-section (at turbine i, j) of the wake-cone created by turbine m, n and of turbine m', n' partially overlap while intersecting the rotor area of turbine i, j . Such other states can be dealt with by adjusting Nybore's [11] formula similarly to equation (8).

4. The optimization procedure

The optimization is performed in a sequential manner. An initial minimal sized layout with least possible number of turbines, (J=1, I=1) is selected and its NPV and Ir are calculated. At the second stage the number of turbines is increased, say to J=1, I=2, then numerically the value of x is searched that maximizes NPV, x1, and separately the value of x is searched that maximizes Ir, x2, retaining the resulting maximal NPV and Ir values. At the 3rd step, the number of turbines is further increased, say to J=2, I=2, the combination of values of x and y that maximize N_{PV}, (x_1, y_1), and that maximize IRR, (x_2, y_2), are evaluated, retaining the obtained maximal values of N_{PV} & I_r. The number of turbines is further increased, and the optimal outcomes of x & y for each layout are evaluated, and the corresponding maximal values of N_{PV} & I_r are retained.

5. Numerical example

To demonstrate the use of the model, a realistic set of data was assumed:
L= 20 y, R= 18 m, ρ = 1.225 kg/m^3, H= 7884 h/y (24 h/d X 328.5 d/y =7884 h/y),
P= 0.05 $/kWh, capacity of turbine=600kWh
C_p= 0.4, N_m= 0.95, and r=5% /y.
Total investment in the windfarm $K=I\cdot J\cdot\{C_T+C_I+C_L[(I-1)x\cdot(J-1)y]\}$, (9)
Where (cost in US dollar, $US)
C_T=cost per turbine=450,000$
C_I=cost per turbine installation=100,000$
C_L=cost of land per turbine=10$/m^2
Cost of operation&maintenance of the windfarm per turbine $M=0.015\cdot C_T\cdot I\cdot J$, $/y (10)

The results of the optimization procedure with the objective to maximize N_{pv} are presented in Table 2. The table provides for each combination of values of I x J the maximal achievable N_{pv}, and the values of x and y that generated this N_{pv}. In addition, the value of I_r generated by these values of x and y is also listed. Table 3 lists similar results, providing for each

combination of I x J the maximal achievable I_r, and the values of x and y that generated this I_r. In addition, the value of N_{pv} generated by these values of x and y is also presented .

Table 2: Optimal results of x and y (for any given I x J) for maximal N_{PV}, and I_r

Parameter	**J- Turbines in Column**	**I-Number of Turbines in Row**				
		2	**3**	**4**	**5**	**6**
x (m)	**2**	300	300	300	300	300
y (m)		100	100	100	100	100
N_{PV} (M$)		4.6	6.5	8.5	10.4	12.4
I_r (%)		27.7	25.3	24.4	23.9	23.5
x (m)	**5**	100	100	100	100	100
y (m)		300	300	500	500	500
N_{PV} (M$)		10.6	14.3	18.8	21.9	25.6
I_r (%)		24.1	21.3	17.9	17.2	16.8
x (m)	**6**	100	100	100	100	100
y (m)		300	300	300	500	500
N_{PV} (M$)		12.6	17.1	21.5	25.9	* **30.3**
I_r (%)		23.9	21.0	19.7	16.9	16.4

* Optimal results

Table 3: Optimal results of x and y (for any given I x J) for maximal I_r, and N_{PV}

Parameter	**J- Turbines in Column**	**I-Number of Turbines in Row**				
		2	**3**	**4**	**5**	**6**
x (m)	**2**	300	300	300	300	300
y (m)		100	100	100	100	100
N_{PV} (M$)		4.6	6.5	8.5	10.4	12.4
I_r (%)		* **27.7**	25.3	24.4	23.9	23.5
x (m)	**5**	100	100	100	100	300
y (m)		300	300	300	300	100
N_{PV} (M$)		10.6	14.3	18.0	21.4	24.3
I_r (%)		24.1	21.3	19.9	19.0	18.1
x (m)	**6**	100	100	100	100	100
y (m)		300	300	300	300	300
N_{PV} (M$)		12.6	17.1	21.5	25.6	28.9
I_r (%)		23.9	21.0	19.7	18.8	17.9

From Table 2, it is evident that maximal Net Present Value, N_{PV} of $ 30.3 million can be achieved for I=6 and J=6 (36 turbines), each one separated x=100 m on the x direction, and y=500 m on the y direction. However, this solution provides only an I_r=16.4%. On the other hand, Table 3 shows that a maximal rate of return, I_r of 27.7% is attainable with I=2 and J=2, the turbines being apart, in x=300 m on the x direction, and y=100 m on the y direction. The disadvantage of this high rate of return is that it generates only a Net Present Value of $4.6 million. If the decision would be done by an investment company, they should opt for the largest possible rate of return on their its investments in any given project. However, a power-generating company that is not diversifying its investments in many different types of projects with different level of risks, it would decide on a project that generates a large N_{PV} while satisfying at least a minimal level of I_r. Searching through Tables 2 & 3, it is possible to detect solutions that provide the best combination of N_{PV}'s and I_r's, although each is less than its maximum value. For example, for a layout of I=4, J=6 (24 turbines), with the turbines separated with x=100 m and y=300 m, provides an N_{PV}=$21.5 million, and an I_r=19.7%, which is the authors recommend "optimal solution."

6. Conclusions

The developed model optimizes windfarm layouts on flat ground or over water for both economic and aerodynamic criteria. Although there are other criteria (e.g. visual impact) to consider, the model performance is an advance for economic optimization. The model with its accompanying computer program, can handle different wind-regimes and all the different combinations of cost and technical parameters for rectangular layouts, of which single-line layouts are special cases. Even the seeming dependence of the solution on the initial selection of the directions of the perpendicular axes can be eliminated, by repeating the calculations for different directions of the axes, and by selecting the layout that has the axis given by the "recommended optimal solution" Furthermore, the computer program can be adjusted, for layouts that are not rectangles, but also parallelograms.

References

[1] Heier, Siegfried, Grid Integration of Wind Energy Conversion Systems, 2nd ed., John Wiley & Sons, Inc., New York, N.Y., 2004.

[2] Lindley, D. et al., "The Effect of Terrain and Construction Method on the Flow over Complex Terrain Models in a Simulated Atmospheric Boundary Layer," in Proceedings of the Third B.W.E.A. Wind Energy Conference, edited by Musgrove,P.J., Cranfield, U.K., April 1981, pp.198-199.

[3] Manwell, J.F., Mcgowan, J.G. and Rogers, A.L., Wind Energy Explained, John Wiley & Sons, Inc., New York, N.Y., 2002

[4] Burton, Tony, Sharpe, David, Jenkines, Nick and Bossanyi, Ervin, Wind Energy Handbook, John Wiley & Sons, Inc., New York, N.Y. 2001.

[5] Milborrow, David ,Garrad, Andrew and Madsen, Birger, A Plan for Action in Europe:Wind Energy –The Facts, European Wind Energy Association(EWEA) European Communities, 1999, pp. 133-134.

[6] Haac, Barry N. An Examination of Small Wind Electric Systems in Michigan, Department of Geography, University of Michigan,1977, pp.27.

[7] Ackermann, Tomas, Wind Power in Power Systems, John Wily& Sons, Inc., New York, N.Y.,2004.

[8] Bossani, E.A.et al., "The Efficiency of Wind Turbine Clusters," in Third International Symposium on Wind Energy Systems, edited by Stephens,H.S., and Stapleton, C.A. , Cranfield, U.K., August 1980, pp.403-406.

[9] Ladany, Shaul P., "Optimal Layout for Urban Gasoline Stations ," in Gilad, I.E.& M. '98, Haifa 1998, pp.45-49.

[10] Ladany, Shaul P ., and Li, Jingwen, "Layout Design for Urban Service Facilities," Communications in Dependability and Quality Management, Vol.5, No.2, 2002, pp.16-30.

[11] Nybore, Claus, The WindFarm-Planning Windphysics, The Danish Centre for Renewable Energy, Copenhagen, 1988, pp. 1-29.

What do we really know? A meta-analysis of studies into public responses to wind energy

Ian D. Bishop[1,*]

[1] *University of Melbourne, Melbourne, Australia*
** Corresponding author. Tel: +61 383444180, Fax: +61 393472916, E-mail: i.bishop@unimelb.edu.au*

Abstract: There have now been many studies about the public response to wind energy infrastructure. This includes at least 31 papers already published in 2010. There remains however a large gap between the knowledge required for effective planning and the agreed understanding of visual and other impact levels, and the influence of planning and communication processes There is only limited agreement on some basic impact variables: numbers of turbines, amelioration with distance, role of design and so forth. There is no consensus on what methods should be used to assess acceptability or to design for acceptable outcomes. This means that, in many countries, there is no societal consensus about the acceptability of wide spread deployment of wind energy systems. This paper reviews recent studies in environmental, especially visual, impact and other aspects of the process that shape public response. These deal with issues and measures including both local and regional impacts, willingness-to-pay, validity of visual simulations and the use of virtual environments in design. The response of any individual and, cumulatively, of the community is a combination of affective and cognitive factors. Both are complex in character. Affective response involves primarily aesthetic appreciation but may be influenced by deep-seated philosophical attitudes to renewable energy in the context of global environmental issues. Cognitive responses overlay with the affective response in relation to global issues but also draw heavily on local factors of noise concerns, tourism effects and health issues. Cognitive responses are also dependent on personal circumstance and experiences and perceptions of the reasonableness of the planning process. These different aspects may be applied independently to infrastructure design, planning and evaluation but are often combined inappropriately in multi-factorial studies. A diversity of approaches in the literature are analyzed for their capacity to contribute to effective discrimination of the factors behind public responses to wind farm developments, to agreement on the key elements affecting local responses, and preferred approaches to planning and design. A combination of such meta-analysis and computational innovation in mapping and visualisation may provide the opportunity for integration of these advances in knowledge such that a systematic, objective, comprehensive and acceptable approach to wind energy infrastructure planning and design is feasible and achievable.

Keywords: *Wind energy, Visual impact, Affective response, Cognitive response*

1. Introduction

There has recently been a very rapid expansion of the literature on public responses to wind energy development and the visual landscape effects in particular. Between 2000 and 2006 there were 2-3 papers per year, in 2007 this jumped to 10, in 2009 to 15 and in 2010 over 30 papers were published on the topic. Some of these deal with aesthetic theory, some with impact mapping, some with experiments seeking to determine key impact variables and their relative importance, others deal with specific wind farm developments and the impact mapping, often linked to public consultation, which went with them. Given this surge of interest, provoked by the rapid expansion of the wind energy industry, it is time to ask what have we collectively learned from this research and how it makes for better planning.

While there is a high cross citation rate amongst these papers, there is also a wide diversity of approaches and research questions which means that there are as yet few definitive answers. The first stage of analysis of these contributions must therefore be to determine the research questions being asked and their relationship to each other. Key topics are:

- development of better tools or procedures for public engagement early in the planning process [1-5]

- understanding of relative significance of key design variables such as distance, contrast, colour, movement [6-8], number of turbines [9-11], size of turbines [10, 12] whether on-shore or off-shore [13] and the existing quality of the host landscape [14]
- understanding of non-design variables such as conservation value of location or the planning process [15, 16], broad social attitudes to wind energy [17, 18] or behaviour (e.g. recreation) when exposed to wind energy facilities [19, 20]
- more systematic analysis tools which respect multiple criteria in either site selection [21-25], impact assessment [8, 11, 26-28], historical changes in the landscape [29] or regional or national level impacts [30]
- responses to visual simulations [31]
- use of interactive virtual environments to facilitate interactive design [32]
- changing attitudes as a result of familiarity [16, 33]
- deep convictions about nature, landscapes and seascapes [34] and cultural ecosystem services [35]
- understanding the relationships between stakeholders in environmental conflicts [36]
- willingness-to-pay studies encompassing some of the other variables (such as distance) [13, 37-39]
- project evaluations including environmental externalities [40, 41]
- the NIMBY effect - or not? [18, 42-46]

This review will focus on just a small section of this wide range. That section is the attempt to establish some firm knowledge about how various design and planning variables contribute to expectations and responses to wind farm development. The analysis considers the variables in terms of the provoked affective and cognitive responses [47] since there are clear indications that both are at play in the public response. There is also a distinction to be made between responses to simulated wind energy developments, responses to proposed developments and responses to completed projects [16, 33]. It should also be noted that most studies consider several aspects of impact and response, in the list above and in the Tables below I have tended to focus on my perception of the main findings in each.

2. Findings from the literature

2.1. Affective Response to Wind Energy

As we experience the landscape we form impressions - such as beautiful or inspiring or unpleasant - without be conscious of any thinking behind those impressions. These responses have a high level of commonality within cultures and, in some respects, between cultures. They are largely unaffected by personal experiences, even familiarity with the landscape has been shown to have limited influence [48]. These apparently innate impressions are referred to as affective responses and have been attributed to evolutionary influences by some authors [49]. Because affective responses are relatively consistent across the population, we are in position to built a body of knowledge about typical responses and use these in spatially explicit landscape assessment and impact studies.

In the case of responses to wind energy infrastructure, we can consider our perceptions of the aesthetics of the developments as an affective response. Something we find intrudes on our enjoyment of landscape or something that adds elegance and interest to the view. Some people may have a positive response in certain landscape types and a negative response in a different landscape type, or the response may be influenced by the layout of the wind farm relative to the landscape, the number of turbines, their distance and so forth. However, we can expect similar sets of responses in different populations and similar dominant response types

allowing development of an empirical framework for impact estimation. As mentioned, the key variables have been analyzed in a number of papers [6-13]. Some of the key findings are summarised in Table 1. These are separated into effects of on-shore and offshore installations, as there is limited comparative work. A review of related work [13] concluded that there was less impact from off-shore installation (reflected in greater willingness-to-pay to adopt that option) but the relative impacts of off- and on-shore infrastructure are not yet well defined and the preference for offshore is disputed in at least one recent review [50].

Studies in affective response typically use scenic beauty, visual quality or a similar phrase as a key reported measure - with some examples of willingness-to-pay and choice experiments. Several of the papers studied multiple variables but disentangling these is sometimes difficult. In addition, there are some clear disagreements in findings in several places - including in relation to important considerations like distance and size. Some studies that considered the size of wind farms (numbers of turbines) did so in the context of fixed total power output. In this situation mixed results were reported [12] with some communities preferring more distributed production while other saw benefit in greater concentration. However, this is more of a reasoned factor than a purely aesthetic one and leads us into the next section.

Table 1. Some key finding relating to aesthetic responses to wind energy infrastructure

Variable Increasing	On-Shore Impact	Off-shore Impact
Distance	- linear decline to at least 12 km [6]	- linear decline to ~12 km [7]
	- limited distance effect [14]	- decline with distance [38]
Number of turbines	- increase with number, size and proximity until turbines occupy 15% of view, then constant [8]	no known studies
	- impact proportional to number of windmills [10]	
	- between 2 and 8 turbines best accepted [9]	
Colour/contrast	- increase with contrast [6, 7]	- increase with contrast [7]
	- increase to 1563 CIELAB points then constant [8]	
Size of turbines	-one 5MW turbine has more impact than same from smaller units [10]	no known studies
	- least important attribute [12]	
	- smaller turbines require less compensation [15]	
Movement	no known studies	- less when blades moving especially at low distances [7]
Visual complexity	- fractality introduced by [8], simpler structures preferred	no known studies
Continuity	- bumps in outline envelope not preferred [8]	no known studies
Host landscape	- effect is negative on landscapes of higher scenic quality but a positive on landscapes of lower quality [14]	- greater distance offshore preferred [38]

2.2. Cognitive Response to Wind Energy

It has been argued that the more visceral affective response ('the heart') is indeed conditioned by a rapid evolution driven cognitive response ('the head'). Whatever the truth of this, there are clearly a number of variables in human responses to wind turbines that require more sustained or deeper consideration than the aesthetic, or are dependent on knowledge or experience, and these are generally referred to as the cognitive factors. These may include specifically beliefs about nature, concerns about real estate values and trust in the planning process. Table 2 seeks to summarise findings on issues of this kind. Again, there are studies that were conducted in relation to on-shore installations and others where the focus was offshore, but these are not separated explicitly in this Table. Among the differences is the noise issue (which is in part aesthetic but of more sustained character and believed by some to induce specific negative health impacts hence applied with other cognitive factors here) that applies almost exclusively to on-shore facilities. The second is an argument, recently summarised [50], that off-shore turbines turn quintessentially natural [34] and often sublime sea or ocean views into industrial landscapes. On-shore facilities, on the other hand, are typically in locations long altered by human activities in the form of agricultural and transportation infrastructure.

Studies involving primarily cognitive variables use a range of measures that seem very similar but this similarity could be misleading. Acceptability is not the same as willingness-to-accept compensation, for example. General 'attitude' to wind infrastructure may be different again because of a range of factors reviewed in the environmental economics literature [51].

Table 2. Some key finding relating to cognitive responses to wind energy infrastructure. The variable of column 1 is measured by the measure in column 2. Column 3 indicates the way in which the response measure depends on the variable.

Variable	Response Measure	Findings
protected site [15]	willingness to accept compensation	avoid protected sites
planning with local representatives [15]	willingness to accept compensation	engage locally
prior experience with off-shore wind farms [16]	attitude to visual impacts	experience with more distance farm leads to more positive attitude
local electricity shortages [17]	acceptability	local needs on island suggested as positive contributor
small scale introduction [17]	acceptability	suggested as positive contributor
open-minded, international contacts [17]	acceptability	suggested as positive contributor
the developers, poor local communications [18, 44]	acceptability	suggested as negative contributor
occasional beach use [19]	stated attitude to offshore infrastructure	more positive attitude
regular year-round beach use [19]	stated attitude to offshore infrastructure	more negative attitude
living with wind farm [33]	range of beliefs on benefits, visual qualities, energy security	more awareness of benefits, greater acceptance

3. Discussion and Conclusion

The research methods used in trying to increase our understanding of the many variables introduced in the literature include attitude surveys, observational methods, willingness-to-pay (or be paid) studies, choice experiments and so forth. The entities on which people are asked to comment include real wind farms (post construction), hypothetical wind farms, visually simulated wind farms and abstract concepts in renewable energy. Nearly all the reported results are the outcome of research by professional people and have been peer reviewed.

Despite the breadth and depth of our investigations we do not yet know all the answers. We cannot yet predict what the response to a particular wind farm proposal will be (although many people would be willing to guess), if compensation is a possibility we do not know how to quantify it or spatially distribute it. We don't know what distribution of turbines across the landscape (to meet specific power needs) will have the least visual impact: should we have bigger but fewer turbines? Bigger but fewer farms?

Yet, some points are fairly clear:

- aesthetic impacts are less the further the viewer is from the turbines (although we have no clear idea of the shape of the distance-impact curve)
- contrast with the surroundings and background should be low
- farms should not be located in highly valued landscapes
- the distribution and design of the turbines should have regard for aesthetic factors such as complexity and continuity
- protected sites should be avoided
- less dissent arises through "involvement of the local population in the siting procedure, transparent planning processes, and a high information level" [18].
- familiarity with existing small scale projects is likely to increase later acceptance of further projects

A number of the studies mentioned were multi-factorial and sought to determine the relative significance of a range of contributing variables. If we accept the premise that responses to wind turbines are of two distinct kinds, one largely independent of culture, education, wealth and personal experience (the affective) and one heavily dependent on the circumstances of an affected community, then it is probably unwise to be mixing these together in our research studies. We need to know more about both, but putting both together into a single study can muddy the waters and fail to give a clear answer on either variable type. Once we have deeper knowledge about the aesthetics, for example, then we might combine this with other factors in a more comprehensive study.

In addition, and briefly mentioned above, there have been important attempts to create geographic information system based tools for prediction of visual, and other, impacts [52]. These have a significant potential role to play in relation to initial site selection and design and should complement systems based on wind potential mapping and other engineering factors. Finally, these can be supplemented but interactive collaborative design systems, such as [32], which can help to create the knowledge, participation and sense of involvement which are just as critical to the outcome as the planning and design itself.

References

[1] G. Higgs, R. Berry, D. Kidner and M. Langford, Using IT approaches to promote public participation in renewable energy planning: Prospects and challenges, Land Use Policy, 25, 2008, pp.596-607.

[2] A. Simao, P.J. Densham and M. Haklay, Web-based GIS for collaborative planning and public participation: An application to the strategic planning of wind farm sites, Journal of Environmental Management, 90, 2008, pp.2027-2040.

[3] M. Portman, Involving the public in the impact assessment of offshore renewable energy facilities, Marine Policy, 33, 2009, pp.332.

[4] G. Munda and G. Gamboa, The problem of windfarm location: A social multi-criteria evaluation framework, Energy Policy, 35, 2007, pp.1564-1583.

[5] D. Robb, Thoughtful planning reaps widespread support for New York wind project, Power Engineering, 107, 2003, pp.36-40.

[6] I.D. Bishop, Determination of thresholds of visual impact: the case of wind turbines, Environment and Planning B: Planning and Design, 29, 2002, pp.707-718.

[7] I.D. Bishop and D.R. Miller, Visual assessment of off-shore wind turbines: The influence of distance, contrast, movement and social variables, Renewable Energy, 32, 2007, pp.814-831.

[8] A.D. Torres-Sibille, V.A. Cloquell-Ballester, V.A. Cloquell-Ballester and R. Darton, Development and validation of a multicriteria indicator for the assessment of objective aesthetic impact of wind farms, Renewable & Sustainable Energy Reviews, 13, 2009, pp.40-55.

[9] N. Daugarrd, Acceptability Study of Wind Power in Denmark, Energy Centre Denmark, Copenhagen, 1997.

[10] T. Tsoutsos, A. Tsouchlaraki, M. Tsiropoulos and M. Serpetsidakis, Visual impact evaluation of a wind park in a Greek island, Applied Energy, 86, 2009, pp.546-553.

[11] T. Tsoutsos, A. Tsouchlaraki, M. Tsiropoulos and J. Kaldellis, Visual impact evaluation methods of wind parks: Application for a Greek Island, Wind Engineering, 33, 2009, pp.83-92.

[12] J. Meyerhoff, C. Ohl and V. Hartje, Landscape externalities from onshore wind power, Energy Policy, 38, 2010, pp.82-92.

[13] J. Ladenburg, Stated public preferences for on-land and offshore wind power generation - A review, Wind Energy, 12, 2009, pp.171-181.

[14] A. Lothian, Scenic perceptions of the visual effects of wind farms on South Australian landscapes, Geographical Research, 46, 2008, pp.196-207.

[15] A. Dimitropoulos and A. Kontoleon, Assessing the determinants of local acceptability of wind-farm investment: A choice experiment in the Greek Aegean Islands, Energy Policy, 37, 2009, pp.1842-1854.

[16] J. Ladenburg, Visual impact assessment of offshore wind farms and prior experience, Applied Energy, 86, 2009, pp.380-387.

[17] J.K. Kaldellis, Social attitude towards wind energy applictions in Greece, Energy Policy, 2003, pp.8.

[18] S. Krohn and S. Damborg, On Public Attitudes Towards Wind Power, Renewable Energy, 16, 1999, pp.954-960.

[19] J. Ladenburg, Attitudes towards offshore wind farms-The role of beach visits on attitude and demographic and attitude relations, Energy Policy, 38, 2010, pp.1297-1304.

[20] M.B. Lilley, J. Firestone and W. Kempton, The effect of wind power installations on coastal tourism, Energies, 3, 2010, pp.1-22.

[21] S.M.J. Baban and T. Parry, Developing and applying a GIS-assisted approach to locating wind farms in the UK, Renewable Energy, 24, 2000, pp.59-71.

[22] I.J. Ramirez-Rosado, E. Garcia-Garrido, L.A. Fernancez-Jimenez, P.J. Zorzano-Santamaria, C. Monteiro and V. Miranda, Promotion of new wind farms based on a decision support system, Renewable Energy, 33, 2007, pp.558-566.

[23] P. Lejeune and C. Feltz, Development of a decision support system for setting up a wind energy policy across the Walloon Region (southern Belgium), Renewable Energy, In Press, Corrected Proof, 2010,

[24] M. Petri and S. Lombardo, Renewable energy sources: The case of wind farms analysis, in O. Gervasi and B. Murgante (ed), Computational Science and Its Applications - Iccsa 2008, Pt 1, Proceedings, 2008, pp.111-125

[25] L.I. Tegou, H. Polatidis and D.A. Haralambopoulos, Environmental management framework for wind farm siting: Methodology and case study, Journal of Environmental Management, 91, 2010, pp.2134-2147.

[26] B. Alvarez-Farizo and N. Hanley, Using conjoint analysis to quantify public preferences over the environmental impacts of wind farms. An example from Spain, Energy Policy, 30, 2002, pp.107-116.

[27] J.P. Hurtado, J. Fernandez, J.L. Parrondo and E. Blanco, Spanish method of visual impact evaluation in wind farms, Renewable & Sustainable Energy Reviews, 8, 2004, pp.483-491.

[28] B. Moller, Changing wind-power landscapes: regional assessment of visual impact on land use and population in Northern Jutland, Denmark, Applied Energy, 83, 2006, pp.477-494.

[29] B. Moller, Spatial analyses of emerging and fading wind energy landscapes in Denmark, Land Use Policy, 27, 2010, pp.233-241.

[30] M. Rodrigues, C. Montanes and N. Fueyo, A method for the assessment of the visual impact caused by the large-scale deployment of renewable-energy facilities, Environmental Impact Assessment Review, 30, 2010, pp.240-246.

[31] R. Phadke, Steel forests or smoke stacks: The politics of visualisation in the Cape Wind controversy, Environmental Politics, 19, 2010, pp.1-20.

[32] I.D. Bishop and C. Stock, Using collaborative virtual environments to plan wind energy installations, Renewable Energy, 35, 2010, pp.2348-2355.

[33] D.C. Eltham, G.P. Harrison and S.J. Allen, Change in public attitudes towards a Cornish wind farm: Implications for planning, Energy Policy, 36, 2008, pp.23-33.

[34] K. Gee, Offshore wind power development as affected by seascape values on the German North Sea coast, Land Use Policy, 27, 2010, pp.185-194.

[35] K. Gee and B. Burkhard, Cultural ecosystem services in the context of offshore wind farming: A case study from the west coast of Schleswig-Holstein, Ecological Complexity, 7, 2010, pp.349-358.

[36] M.I. Gonzalez and B. Estevez, Participation, communication and negotiation in environmental conflicts: Offshore wind energy in the Trafalgar Sea area, Arbor-Ciencia Pensamiento Y Cultura, 181, 2005, pp.377-392.

[37] P.A. Groothuis, J.D. Groothuis and J.C. Whitehead, Green vs. green: Measuring the compensation required to site electrical generation windmills in a viewshed, Energy Policy, 36, 2008, pp.1545.

[38] J. Ladenburg and A. Dubgaard, Willingness to pay for reduced visual disamenities from offshore wind farms in Denmark, Energy Policy, 35, 2007, pp.4059-4071.

[39] G. Riddington, D. McArthur, T. Harrison and H. Gibson, Assessing the Economic Impact of Wind Farms on Tourism in Scotland: GIS, Surveys and Policy Outcomes, International Journal of Tourism Research, 12, 2010, pp.237-252.

[40] D. Moran and C. Sherrington, An economic assessment of windfarm power generation in Scotland including externalities, Energy Policy, 35, 2007, pp.2811-2825.

[41] J. Munksgaard and A. Larsen, Socio-economic assessment of wind power-lessons from Denmark, Energy Policy, 26, 1998, pp.85-93.

[42] C.R. Jones and J.R. Eiser, Understanding 'local' opposition to wind development in the UK: How big is a backyard?, Energy Policy, 38, 2010, pp.3106-3117.

[43] W. Roper and N. Campeau, Renewable energy production issues with the Cape Cod offshore wind energy programme, International Journal of Environmental Technology and Management, 6, 2006, pp.405-420.

[44] M. Wolsink, Wind power and the NIMBY-myth: institutional capacity and the limited significance of public support, Renewable Energy, 21, 2000, pp.49-64.

[45] M. Wolsink, Planning of renewables schemes: Deliberative and fair decision-making on landscape issues instead of reproachful accusations of non-cooperation, Energy Policy, 35, 2007, pp.2692-2704.

[46] M. Wolsink, Wind power implementation: The nature of public attitudes: Equity and fairness instead of 'backyard motives', Renewable & Sustainable Energy Reviews, 11, 2007, pp.1188-1207.

[47] S. Kaplan, Aestethics, affect and cognition: Environmental preference from an evolutionary perspective, Environment and Behavior, 19, 1987, pp.3 - 32.

[48] J.D. Wellman and G.J. Buyhoff, Effects of Regional Familiarity on Landscape Preferences, Env. and Behav., 1980, pp.105-110.

[49] J.H. Appleton, The Experience of Landscape, John Wiley, 1975.

[50] C. Haggett, Understanding public responses to offshore wind power, Energy Policy, 2011,

[51] A.M. Freeman, The measurement of environmental and resource values: theory and methods, Resources for the Future, 2nd edition, 2003.

[52] M. Rodrigues, C. Montañés and N. Fueyo, A method for the assessment of the visual impact caused by the large-scale deployment of renewable-energy facilities, Environmental Impact Assessment Review, 30, 2010, pp.240-246.

Economic assessment of wind power uncertainty

Viktoria Gass[1,*], Franziska Strauss[1], Johannes Schmidt[1], Erwin Schmid[1]

[1] *Department of Economics and Social Sciences, University of Natural Resources and Life Sciences, Feistmantelstrasse 4, A-1180 Vienna, Austria*
** Corresponding author. Tel: +43 1476543594, Fax: +43 1476543692, E-mail: v.gass@students.boku.ac.at*

Abstract: Wind energy has been the fastest growing and most promising renewable energy source in terms of profitability in recent years. However, one major drawback of wind energy is the variability in production due to the stochastic nature of wind. The article presents statistical simulation methods to incorporate risks from stochastic wind speeds into profitability calculations. We apply the Measure-Correlate-Predict Method (MCP) within the variance ratio method to generate long-term wind velocity estimates for a potential wind energy site in Austria. The bootstrapping method is applied to generate wind velocities for the economic life-time of a wind turbine. The internal rate of return is used as profitability indicator. We use the Conditional Value at Risk approach (CVaR) to derive probability levels for a certain internal rate of returns, as the CVaR is a reliable risk measure even if return distributions are not normal. In contrast to other scientific publications, our methodology can be generally applied, because we do not rely on estimated distributions for wind speed predictions, but on measured wind speed distributions, which are usually readily available. In addition, the CVaR has not been applied as a measure of risk for wind site evaluation before and it does not rely on any specific function regarding the profitability distribution.

Keywords: *Wind power, Bootstrapping, Measure-Correlate-Predict Method, Conditional Value at Risk, Internal Rate of Return*

1. Introduction

Wind energy was the fastest growing renewable energy resource in the European Union (EU) in the last decade. The annual installed capacity has risen from 814 MW in 1996 to 10,163 MW in 2009 [1]. In 2009, approx. € 13 billion, including € 1.5 billion offshore were invested in wind energy in the EU [1]. In this respect, the wind power capacity shall reach approx. 80 GW by 2010 becoming the renewable energy technology after hydro power with the highest installed capacity in the EU [1]. In 2009, approx. 5.4% of the electricity consumption was produced with wind energy in the EU. It is projected that the contribution of wind energy to total electricity consumption within the EU is increasing to approx. 15.5% in 2020 [2]. The stochastic nature of wind leads to fluctuations in wind energy production. The literature concerning wind speed uncertainty can be divided, for instance, into literature focusing on uncertainty in wind energy output and on economic profitability. With respect to uncertainty in wind energy output, Kwon [3] has elaborated a numerical procedure for evaluating the uncertainty caused by wind variability and power performance using probability models in order to assess the risk of power output deviations. He conducted a case study analysis to show that the standard deviation of the annual energy output normalized by the average value of power output is approx. 11%, which can cause investments to be unprofitable. Tindal et al. [4] have compared the predicted annual power production with the actual power production. Their dataset included 510 wind farms across Europe and the US. They showed that the actual wind power output is 93.3% of predicted wind power output. According to the authors, a major reason for this deviation is the rather poor quality of wind speed measurements which have been conducted before the installation of wind turbines.

A number of articles have statistically analysed wind speed data by assessing the wind energy potential in a certain region (e.g.[5], [6], [7], [8], [9], [10], [11]).The economic potential and profitability have been identified by applying traditional methods of financial analysis such as

the Net Present Value approach, the Internal Rate of Return approach, or the Life Cycle Cost Analysis approach.

Morthorst [12], for example, analysed whether there is a relationship between the expected profitability of a wind turbine and the annual increase in installed capacity in Denmark. He used the net internal rate of return approach (after tax) as a measure for profitability. Kaldellis et al. [13] conducted a sensitivity analysis in order to show the impact of different parameters on the economic viability and attractiveness of a wind energy plant. However, Montes and Martin [14] argue that statistical simulation methods should be used to account for and assess the economic risk resulting from the variability in wind speed.
Some authors analyze the wind energy potential of a specific site by using either Monte Carlo simulations for predicting wind speeds or by using the wind speed measurement data directly if sufficient measurement data are available [15], [3], [16], [9], [17]. However, Monte Carlo simulations require assumptions with respect to the distribution of the wind speeds. Consequently, Carta et al. [18] concluded that not every wind regime can be accurately described with known probability distributions.

The following article presents an approach that accounts for the uncertainty of wind speed in profitability assessments. The approach can easily be applied for any actual and potential wind energy site without specifying the distributions of wind speed. The article is structured as follows: Section 2 presents the methodology. Section 3 presents a case study analysis in which the methodology has been applied to and section 4 discusses the results and draws major conclusions from the methodology and analysis.

2. Methodology

Our approach consists of generating long-term wind speed data for a potential wind energy site (‘target site’) where only short time series of wind measurement data are available using the Measure-Correlate-Predict Algorithm (MCP) with wind speed data from a reference site. A bootstrapping procedure is applied to compute wind speed data for the economic life-time of the wind turbine. The internal rate of return approach is used as profitability index. The bootstrapping procedure allows more accurately reflecting the distribution of the wind regime in the predicted wind speeds than methods currently applied in the scientific literature on wind energy production. Furthermore, the bootstrapping procedure can be applied to any wind regime. As a measure of risk we use the Conditional Value at Risk approach (‘CVaR’). The CVaR can be uniformly applied and is not only appropriate if returns are normally distributed. The CVaR also provides information at which probability level a certain internal rate of return can be expected.

2.1. Assessment of the wind energy potential at a specific site

Wind speed measurement data are usually collected at a specific site (target site) through a period of one year or less. Wind speed frequency distributions are computed from the data in order to estimate a probability density function. Several probability density functions have been used in the literature, but the two-parametric Weibull and the one-parametric Rayleigh distribution, which is a special case of the Weibull distribution, are usually used to predict wind speeds [3], [13], [16], [15]. The two-paramteric Weibull probability density function is given by the following equation [9]:

$$f(V) = \frac{k}{c}\left(\frac{V}{c}\right)^{k-1} exp\left\{-\left(\frac{V}{c}\right)^{k}\right\},\ 0 < V < \infty \qquad (1)$$

where c and k are the scale and shape parameters and V the wind speed. The shape parameter k is usually between 1.5 and 3.0. If the value of the shape parameter is 2.0, the distribution is called Rayleigh distribution. The probability density function of the Rayleigh distribution is shown in Eq. 2 [9]:

$$f(V) = \frac{2V}{c^2} exp\left\{-\left(\frac{V}{c}\right)^k\right\} \quad (2)$$

A review carried out by Carta et al. [18] shows that the two-parametric Weibull distribution has several advantages compared to other probability density functions proposed in the scientific literature. However, not every wind speed regime can be described by a probability distribution. We applied the bootstrapping procedure as it does not require any assumptions on the distribution of the wind speed [18] [19]. However, long-term wind measurement data are needed for the target site. As already indicated, wind measurement data are usually collected through a period of one year or less. We apply the Measure-Correlate-Predict (MCP) algorithm to estimate long-term wind speed data for a target site using wind data from a reference site. We use long-term wind data from a closely located meteorological station at the reference site. According to [21], the MCP algorithm in the form of the Variance Ratio Method gives consistent and reliable estimates of wind speeds. The relationship between the wind speed data at the reference site and the wind speed at the target site can be expressed by the following equation [21]:

$$\widehat{V_t} = \left(\mu_t - \left(\frac{\sigma_t}{\sigma_r}\right)\mu_r\right) + \left(\frac{\sigma_t}{\sigma_r}\right)V_r \ , \quad (3)$$

where $\widehat{V_t}$ is the predicted long-term wind speed at the target site, V_r is the long-term wind speed at the reference site and μ_t, μ_r, σ_t and σ_r are the mean and the standard deviation of the target and the reference site, respectively. If wind measurements have not been conducted at hub height, the measured wind speeds have to be adjusted to hub height. We apply the following equation [10]

$$V_{hub} = V_m \frac{\ln\left(\frac{h_{hub}}{z}\right)}{\ln\left(\frac{h_m}{z}\right)} \quad (4)$$

where V_{hub} defines the wind speed at hub height, V_m the wind speed at measurement height, h_{hub} and h_m are the height of the hub and the measurement facility, and z is the roughness length [22]. The respective surface roughness at a specific site strongly depends on the terrain conditions.

The actual power output $P(V)$ of a wind turbine can be expressed by the following equation [9]:

$$P(V) = \int_{V_{in}}^{V_n} \frac{1}{2}\, cp \cdot \rho \cdot V^3 \cdot \pi \cdot \left(\frac{D}{2}\right)^2 + \int_{v_n}^{V_{out}} P_t \quad (5)$$

where V_n defines the rated wind speed, V_{in} the cut-in wind speed, cp the capacity factor, ρ the air mass density, V the wind speed, D the rotor diameter, V_{out} the cut-out wind speed and $P_t$the rated power output. A wind turbine starts generating power at the cut-in wind speed (V_{in}). From the cut-in wind speed to the rated wind speed (V_n), the power generated continuously increases up to the nominal power of the wind turbine. The turbine produces

constantly electricity at its rated power from the rated wind speed to the cut-out wind speed (V_{out}).

2.2. Profitability Calculations

The economic evaluation of investment projects is usually based on the Discounted Cash Flow (DCF) approach [23]. The approach provides information about the value of a project based on the present value of the cash flows that the project can be expected to generate in the future (cash in- and outflows). In the case of wind energy, cash inflows result from the electricity sold and cash outflows are investment and operating expenses. Operating expenses are mainly maintenance costs, personnel expenses, insurance costs, land lease, etc [24]. Cash in- and outflows are discounted to reflect the time and risk preferences of the decision maker associated with the cash flows. The DCF method comprises the following steps:
- estimating future cash flow for a certain discrete projection period, and
- discounting these cash flows to the present value at a rate of return that considers the relative risk of achieving the cash flows and the time value of money.

The financial attractiveness of wind energy investment projects is usually measured by the NPV and/ or the internal rate of return (IRR) [11], [12], [20], [25]. Investors are usually interested in the maximum NPV for a preferred discount rate of future cash flows. The IRR provides the discount rate at which NPV is equal to zero such that it can also be defined as the return that the project is going to generate considering cash out- and in- flows. A project can be stated to be economically viable, if the IRR is at least above the risk free rate or, if the NPV is equal or greater than zero. Equation 10 defines the IRR [23]:

$$NPV = 0 = CF_o + \frac{CF_1}{(1+IRR)^1} + \frac{CF_2}{(1+IRR)^2} + \cdots + \frac{CF_n}{(1+IRR)^n} = \sum_{t=0}^{n} \frac{CF_t}{(1+IRR)^t}, \quad (8)$$

where CF_t is the cash flow in the corresponding year.

2.3. The Conditional Value at Risk (CVaR)

We apply the CVaR as a measure of risk. Since the Value at Risk (VaR) as well as the variance as risk measures provide only reliable results if the underlying events are normally distributed [26], CVaR does not require a normal distribution of events and considers especially the tails of the underlying distribution [26]. The CVaR and the VaR are closely related, therefore we describe the VaR first. The VaR states that with probability β the expected value will not be lower than a certain threshold α. The CVaR focuses on the tails of the distribution and averages the values which fall short of threshold α depending on the probability level β. Therefore, the CVaR is a more conservative risk measure.

3. Case study analysis

The wind measurement data from a wind turbine site in Styria, which is in operation since 2005, have been used in our case study analysis. The data consist of hourly mean wind speeds as well as of hourly mean power output for the years 2006 to 2008. The hourly mean wind speeds of the year 2007 have been used as target site data. The data from a meteorological station (reference station) includes daily mean wind speeds for the years 1990 to 2009. Therefore, the calculations are based on daily mean wind speeds using the daily average of hourly wind speed measurement data of the target site. We use data from 2007 for the application of the MCP method. The different wind velocities are shown in Fig. 1, where Fig.

1a shows the daily mean wind velocities at the target site for the year 2007 and Fig. 1b shows the daily mean wind velocities at the reference site for the year 2007.

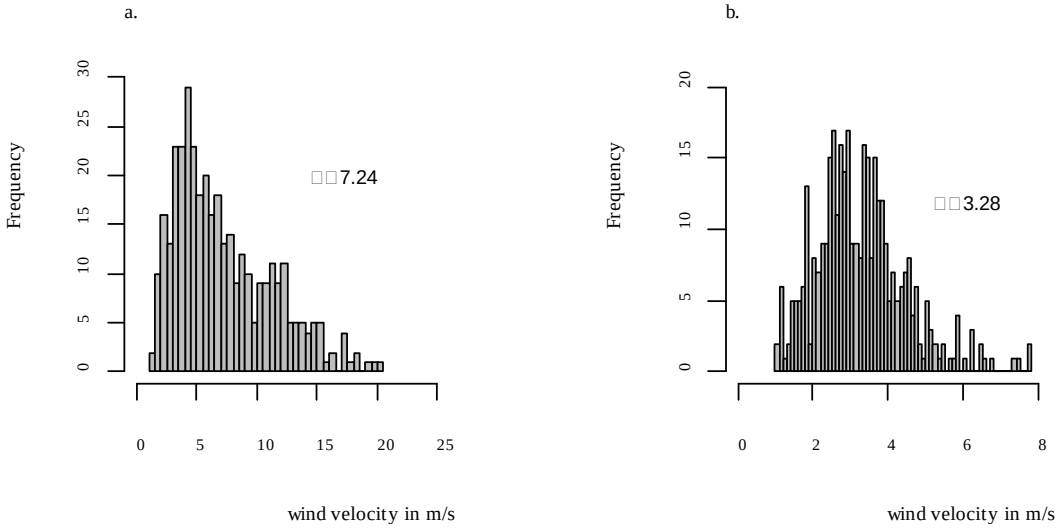

Fig. 1. Histogram of daily mean wind velocities: a. daily mean wind velocities at the target site for the year 2007; b. daily mean wind velocities at the reference site for the year 2007.

The correlation equation of the hourly mean wind velocity at the target site and the hourly mean wind velocity of the reference site derived from Eq. (3) is as follows:

$$\widehat{V_t} = -3.7507 + 3.3065\, V_r \qquad (9)$$

The long term wind velocities at the target site are estimated on the basis of the slope and the intercept of the Eq. (9). However, before applying the MCP method, the wind speed at the reference station has to be extrapolated from the anemometer to hub height using Eq. (4). As the target site is located in mountainous area, the correlation between the target and the reference site is low (0.2120). According to the utility manager (oral communication), the reference station has been used to evaluate the target station before deciding on the construction of the wind park. Therefore, we also use the same reference station in our case study analysis. The daily wind measurement data at the reference site record a period of 20 years such that long-term daily mean wind velocities are computed for this period with the MCP method.

Currently, the feed-in tariffs are guaranteed for a period of 13 years in Austria. Therefore, we assume that a potential investor requires a certain return of investment within the period in which he or she receives a guaranteed electricity price. Our calculations concerning the profitability assessment are based on a 13 year period of predicted daily mean wind velocities. Seasonal differences are reflected in the bootstrapping procedure, which has been repeated 1000 times. Consequently, several trajectories are obtained both for the wind speeds and the power outputs. The trajectories are also used in the statistical evaluations revealing information that are relevant for investment decisions.

The energy power output is derived for a 1.3 MW wind turbine with a turbine diameter (D) of 62 m, a cut-in wind speed (V_{in}) of 4 m/s, a cut-out wind speed (V_{out}) of 25 m/s, and a rated wind speed (V_n) of 13 m/s, respectively. The capacity factor (cp), which is defined as the ratio of the energy generated to nominal energy generation is 0.4. The air mass density (ρ) corresponds to 1.27 kg/m^3. The wind turbine starts producing power at a wind speed of 4

m/s and reaches its rated wind speed at 13 m/s. The daily generated electricity production can be computed by multiplying the computed power output with 24 (hours of a day). The daily generated electricity production is then added up to annual generated electricity production as profitability calculations are conducted on annual time steps.

The histogram of the daily and annual generated electricity in kWh is shown in Fig. 2a and Fig. 2b, which follows a normal distribution according to the central limit theorem. The theorem states that the probabilities of events generated with the sum of independent, identical distributed random variables X approximate to a normal distribution for a sufficiently large number of events. The central limit theorem indicates that the distribution of $\sum X_i$ for an increasing n approaches always the $N(n\mu; \sigma\sqrt{n})$ distribution.

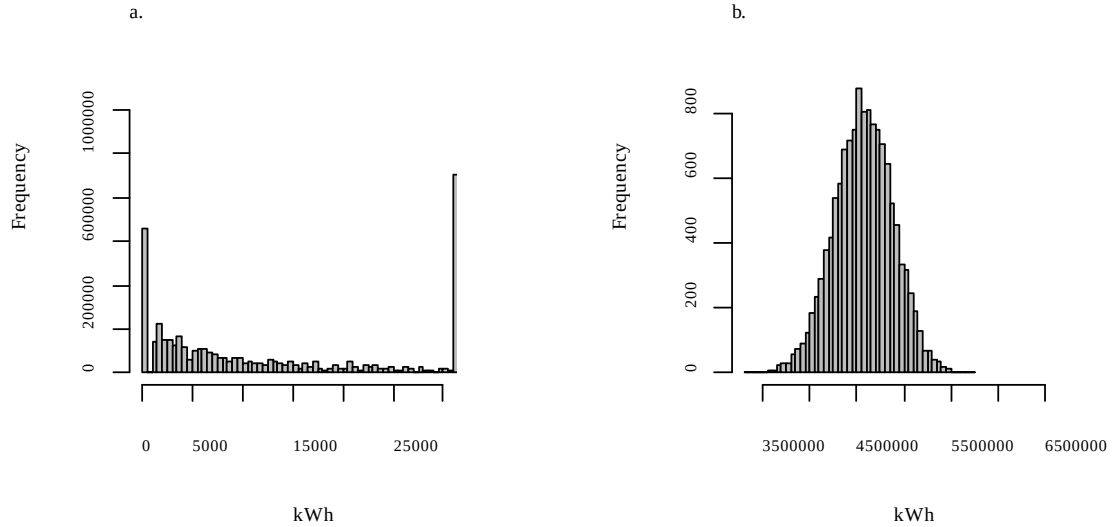

Fig. 2. a. Histogram of the daily generated electricity in kWh; b. Histogram of the annual generated electricity in kWh .

The annual Free Cash Flows (FCF) can be derived from the annual generated electricity. The cash inflows result from the generated electricity, which is sold at the guaranteed feed-in tariff that currently amounts to 0.0753 €/kWh in Austria. The cash outflows are the investment costs for the wind turbine, which are € 1.5 mil. per MW installed according to the provider of the wind measurement data. The operating costs are amounting to 0.020 €/kWh. Further corporate tax payments have to be considered when calculating the FCFs (current corporate tax rate is 25% in Austria). It is assumed that demolition costs at the end of the lifetime equal the revenue which can be generated out of selling the steel from the wind turbine. The internal rate of return has been calculated from the computed annual FCF. A standard criterion for investment decisions is the hurdle rate. It reflects a discounting rate at which the investments provide a positive cash flow. If a negative NPV results out of discounting the FCF with the hurdle rate, the underlying investment will most likely not be approved by the management. Consequently, an investment can be approved if the IRR exceeds the hurdle rate. The resulting probability density functions are shown for different risk aversion levels in Fig. 3. The IRR will be not lower than 7.94% at a probability level of β = 90% according to the probability density function of the IRR shown in Fig. 3 a. If the hurdle rate for an investor is above 7.94% then an investor shall not decide against the investment. However, the investor might realize an IRR above 9.19% with a 10% probability. Fig. 7b shows the resulting IRRs for a 95%- probability level.

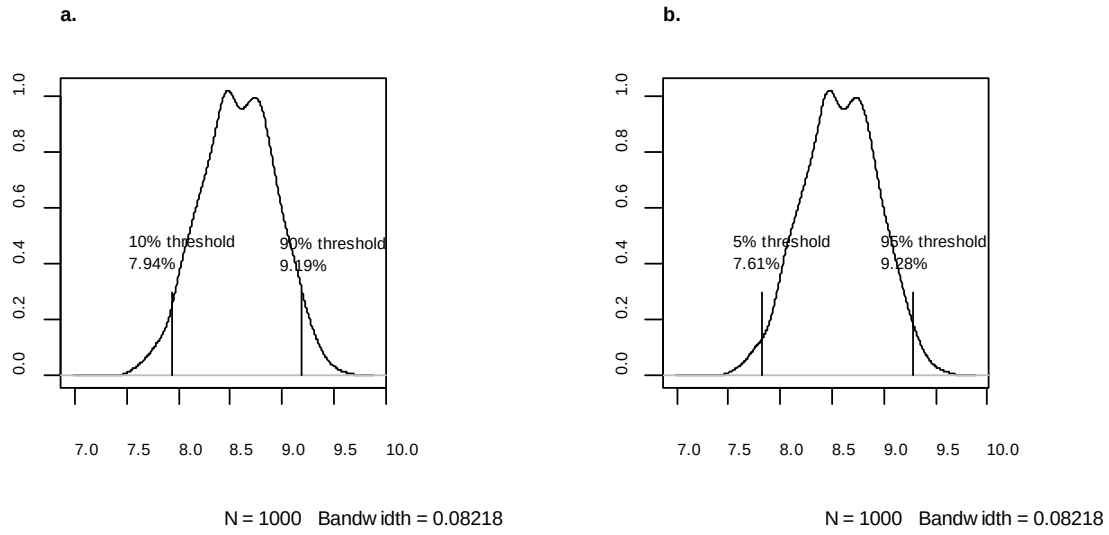

Fig. 3. Probability density functions of the IRR and the CVaR. a. Probability density function of the IRR with the threshold levels of 10% and 90%; b. Probability density function of the IRR with the threshold levels of 5% and 95%.

4. Concluding Remarks

We have developed a methodology to better assess the profitability of a wind energy site in the presence of wind speed uncertainty. Our approach can be applied to any wind regime. We apply statistical simulation methods to close the gap in the scientific literature on wind energy production [14]. Neither the bootstrapping method to predict wind speeds nor the conditional value at risk approach have been applied for investment assessments in combination with wind site evaluations. We have combined and applied these methods for a case study analysis. For a 1.5 MW wind turbine with investment costs of € 1.5 mil. per MW and operating expenses of 0.020 €/kWh, the IRR with a probability of 95% will not be lower than approx. 7.61% for the case study wind energy site. With a 5% probability, however, an investor can achieve an IRR of 9.28%.

References:

[1] EWEA. Wind in power 2009 European statistics. 2010.

[2] EREC European Renewable Energy Council. Renewable Energy Technology Roadmap 20% by 2020. 2008.

[3] Kwon S. Uncertainty analysis of wind energy potential assessment. Applied Energy. 2010;87:856-865.

[4] Tindal A, Harman K, Johnson C, Schwarz A, Garrad A, Hassan G. Validation of GH energy and uncertainty perdictions by comparison to actual production. AWEA Wind Resource and Project Energy Assessment Workshop, Portland2007.

[5] Keyhani A, Ghasemi-Varnamkhasti M, Khanali M, Abbaszadeh R. An assessment of wind energy potential as a power generation source in the capital of Iran, Tehran. Energy. 2010;35:188-201.

[6] Ramachandra T. Wind energy potential assessment in Uttara Kannada district of Karnataka, India. Renewable Energy. 1997;10:585-611.

[7] Ramachandra T, Shruthi B. Wind energy potential mapping in Karnataka, India, using GIS. Energy Conversion and Management. 2005;46:1561-1578.

[8] Rehman S. Wind power cost assessment at twenty locations in the kingdom of Saudi Arabia. Renewable Energy. 2003;28:573-583.

[9] Arslan O. Technoeconomic analysis of electricity generation from wind energy in Kutahya, Turkey. Energy. 2010;35:120-131.

[10] Hoogwijk M. Assessment of the global and regional geographical, technical and economic potential of onshore wind energy. Energy Economics. 2004;26:889-919.

[11] Voivontas D. Evaluation of Renewable Energy potential using a GIS decision support system. Renewable Energy. 1998;13:333-344.

[12] Morthorst P. Capacity development and profitability of wind turbines. Energy Policy. 1999;27:779-787.

[13] Kaldellis JK, Gavras TJ. The economic viability of commercial wind plants in Greece A complete sensitivity analysis. Energy Policy. 2000;28:509-517.

[14] Montes G, Martin E. Profitability of wind energy: Short-term risk factors and possible improvements. Renewable and Sustainable Energy Reviews. 2007;11:2191-2200.

[15] Correia P, Ferreira de Jesus J. Simulation of correlated wind speed and power variates in wind parks. Electric Power Systems Research. 2010;80:592-598.

[16] Friedman PD. Evaluating economic uncertainty of municipal wind turbine projects. Renewable Energy. 2010;35:484-489.

[17] Akdag SA, Güler Ö. Evaluation of wind energy investment interest and electricity generation cost analysis for Turkey. Applied Energy. 2010;87:2574-2580.

[18] Carta J, Ramírez P, Velázquez S. A review of wind speed probability distributions used in wind energy analysis: Case studies in the Canary Islands. Renewable and Sustainable Energy Reviews. 2009;13:933-955.

[19] Efron B. Bootstrap Methods: Another Look at the Jackknife. The Annals of Statistics. 1979;7:1-26.

[20] Burton T, Sharpe D, Jenkins N, Bossanyi E. Handbook of wind energy. Chichester, England: John Wiley & Sons, Ltd.; 2001.

[21] Rogers A, Rogers J, Manwell J. Comparison of the performance of four measure-correlate-predict algorithms. Journal of Wind Engineering and Industrial Aerodynamics. 2005;93:243-264.

[22] Silva J, Ribeiro C, Guedes R. Roughness Length Classification of Corine Land Cover Classes. MEGAJOULE-Consultants; 2007.

[23] Khatib H. Economic evaluation of projects in the electricity supply industry: The Institiution of Engineering and Technology, London, UK; 2003.

[24] Blanco MI. The economics of wind energy. Renewable and Sustainable Energy Reviews. 2009;13:1372-1382.

[25] Talavera D, Nofuentes G, Aguilera J. The internal rate of return of photovoltaic grid-connected systems: A comprehensive sensitivity analysis. Renewable Energy. 2010;35:101-111.

[26] Rockafellar R, Uryasev S. Conditional value-at-risk for general loss distributions. Journal of Banking & Finance. 2002;26:1443-1471.

Economics of DC wind collection grid as affected by cost of key components

Georgios Stamatiou[1,*], Kailash Srivastava[2], Muhamad Reza[2], Pericle Zanchetta[1]

[1] *University of Nottingham, Nottingham, UK*
[2] *ABB Corporate Research, Västerås, Sweden*
** Corresponding author. +30 6976276783, E-mail: geostamatiou@gmail.com*

Abstract: Using High Voltage Direct Current (HVDC) transmission lines to connect offshore wind parks to the onshore power grid has been proven technically advantageous to AC solutions and more cost-effective for relatively long transmission distances (>70km).The concept of applying DC technology can be expanded to the collection grid. DC collection grid offshore wind parks can be developed only if several key components currently nonexistent are available. The technical challenges involved can result in the unpredictability of their costs. This paper investigates the effect the uncertainty of the key components' cost can have on the overall economic performance of DC collection grid offshore wind parks. Results for a wide cost range are presented and corresponding cost boundaries which secure the economic viability of such parks were determined.

Keywords: *DC grid, Offshore Wind park, Techno-economics, DC/DC.*

1. Introduction

In the future the size of offshore wind farms and the distance to shore are expected to increase, thereby leading to higher losses in the AC collection grid and AC transmission. DC technologies can provide lower losses and use cheaper cables than their AC counterparts, thereby compensating for the increased cost of the necessary power electronic devices. HVDC transmission systems have already been proven technically advantageous and cost-effective over AC transmission for distances longer than 60-70 km according to [1], and applying DC technologies not only to the transmission system but also to the collection grid of offshore wind parks could prove additionally effective according to [2].

Key components refer to those components that are not at present available in the market but are needed to realize DC collection grids. According to [3], the following components are identified as key components: DC Circuit Breaker and DC/DC Converter which includes the Medium Frequency Transformer. DC breakers for high power applications have not been constructed and DC/DC converters are not currently available for high power rating beyond 1 or 2 MW [6]. Lundberg in [10] conducts a techno-economic analysis on DC wind parks but omits the cost of DC switchgear and underestimates the cost range of the DC/DC converters, neglecting their challenging nature.

This paper investigates the effect of cost uncertainties of key components on the economic viability of offshore DC wind collection grid. Four different wind park layouts are considered. Initial assumptions on the key components' costs are made and using a cost-benefit programming tool, cost evaluation scenarios take place by altering the cost of the key components. Finally, cost boundaries are defined, beyond which any DC collection grid layout is not economically competitive.

2. Key components

2.1. DC Circuit breaker

Realising DC collection grid for offshore wind farms requires the existence of switching and protection devices specifically designed for DC grids. DC Circuit breakers are a characteristic example. Figure 1 (a) presents a typical DC grid. A capacitor is required to stabilize the

voltage and reduce the voltage ripple at the DC side of the converter. Due to this capacitor, the system can be described by an equivalent constant voltage source V_{Grid} and grid impedance L_{Grid} as in Figure 1 (b). When a short-circuit occurs, all of the grid voltage is applied across the equivalent resistance. As a result, there is a large and constant voltage across the inductance, leading to a constant and steep rate of rise of the current. Therefore, the fault current reaches dangerously high values quite quickly. Decreasing the rate of rise of the current implies the forced application of voltage across the circuit breaker so that the voltage drop across the inductance is decreased. Additionally in contrast to an AC system, a DC system by definition does not have current zero crossings, which could aid for the safe interruption of the fault current.

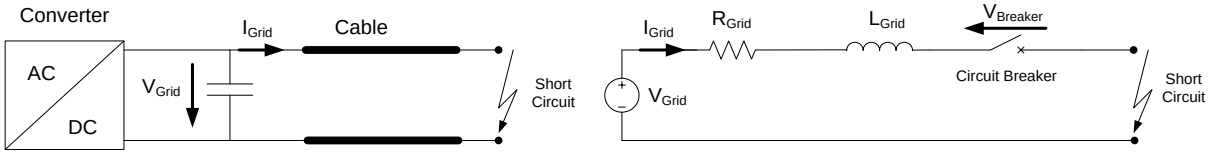

(a) (b)

Figure 1. a) Representation of DC grid under short circuit condition b) Equivalent circuit of a DC grid under short circuit conditions

Therefore a high-power DC breaker must a) be able to act very rapidly to avoid extremely high currents and b) Allow active turn-off.

2.2. DC/DC Converter

The requirement for transforming voltages in a high-power DC grid is one of the major challenges towards the realization of DC power networks including DC collection grid. Different topologies for DC/DC converters have been developed using medium or high-frequency AC link as discussed in [4], based on the general model of Figure 2. A galvanic isolated DC/DC converter consists of an inverter at the input side, an AC link consisting of a transformer and an inverter at the output side to transform back to DC. The voltage at the endpoints of the transformer does not need to be sinusoidal or at 50-60Hz. Hence the frequency of the alternating voltage can be equal to the switching frequency and a rectangular waveform of such frequency can be applied to the transformer. The AC link is based on a medium/high frequency transformer, resulting in galvanic isolation which is important for security reasons in high power applications.

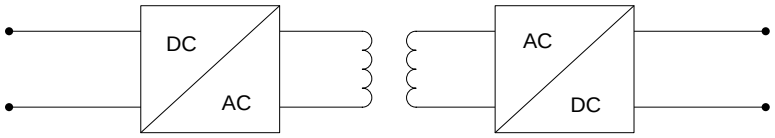

Figure 2. General topology of a galvanic isolated DC/DC converter

The overall dimensions of such a transformer are significantly reduced due to the higher operating frequency, resulting in a compact DC/DC converter. The transformer can be single or three phase. The transformer can be single or three phase with the latter being more advantageous for high-power applications [5].

2.3. Medium Frequency Transformer

As mentioned in section 2.2, the fundamental component of a high power DC/DC converter is the medium frequency transformer, which is also the most challenging to construct for high power applications. The non-sinusoidal excitation of the core and the use of high-frequency components require sophisticated approach methods. The material and the design of the core of the transformer are of utmost importance. Traditional low frequency-high voltage-high power transformers use laminated cores. However, this concept cannot be applied to medium frequency transformers. Increasing the frequency leads to excessive losses and the insulation between the core sheets will lead to a reduced thermal conductivity of the core [3].

3. Methodology

3.1. Layouts

For the scope of this paper, four different offshore wind park layouts where investigated: "Small DC", "Large DC", "Series DC" and "AC/DC". These designs are thoroughly presented in [10] and [7]. All of them have a DC transmission link and DC collection grid with the notable exception of the AC/DC which has an AC collection grid. AC is currently the only technology used in the collection grid of wind parks and therefore, AC/DC layout is used as a benchmark for the rest fully DC wind park designs. It is important to mention that the turbines in all DC collection grids, the turbines consist of a Permanent magnet generator coupled to a rectifier and then to a DC/DC converter while the turbines of the AC/DC park consist of a Doubly Fed Induction Generator (DFIG) connected to a transformer.

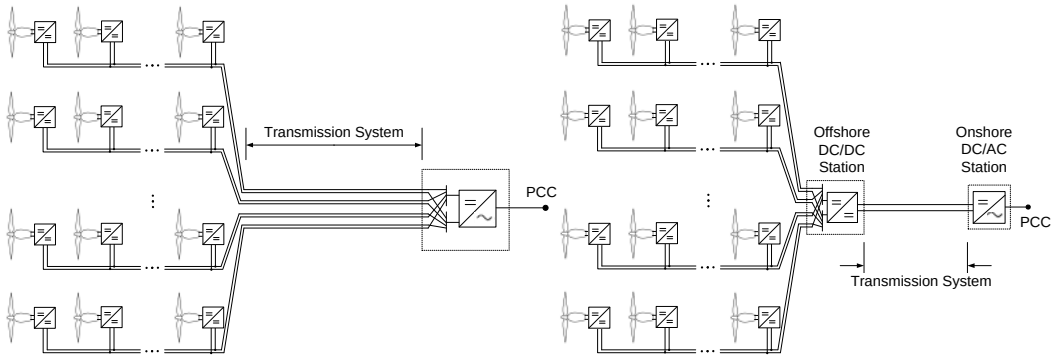

Figure 3. a) Small DC offshore wind park b) Large DC offshore wind park

The small DC layout presented in Figure 3 (a) has DC feeders of Medium Voltage (MV) which are extended to the onshore inverter, located just before the Point of Common Coupling (PCC) to the main grid. Figure 3 (b) presents the Large DC layout which resembles the Small DC but uses a large offshore DC/DC converter on a platform, to achieve High Voltage DC (HVDC) on the transmission system, resulting in decreased transmission losses. The Series DC layout is featured in Figure 4 (a). The turbines have a MV DC output and are connected in series, resulting in HVDC along each feeder and also on the transmission line, without the need of an additional offshore DC/DC converter. The AC/DC layout is depicted in Figure 4 (b), having a conventional AC collection grid and an HVDC transmission system.

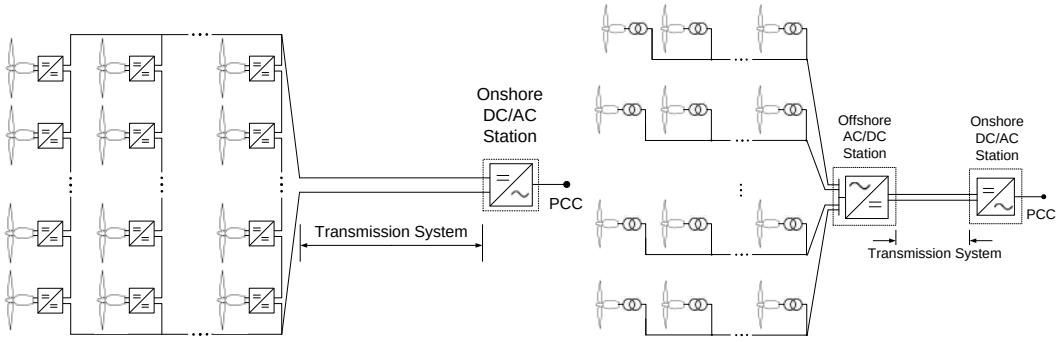

Figure 4. a) Series DC offshore wind park b) AC/DC offshore wind park

3.2. Energy Cost

The minimum cost of energy production for any desired wind farm project is described by the Energy Cost and is given in currency units per kWh delivered to the PCC. Its calculation is given by equation (1):

$$\text{Energy Cost} = \frac{\text{Total capital cost} \cdot \dfrac{\mathrm{r}(1+\mathrm{r})^{N}}{(1+\mathrm{r})^{N}-1} + \text{O\&M}}{\text{Average power production} \cdot \mathrm{T}} \qquad (1)$$

where O&M is the total annual Operation and Maintenance costs, r is the interest rate, N is the lifetime of the wind farm in years and T is the average operational hours per year in the form of T=24·365 hours·0.95, where the last term expresses a park availability of 95% annually. Ideally, a project should have the lowest energy cost possible.

3.3. Cost-Benefit Tool

A Cost-Benefit programming tool was developed in order to calculate the Energy Cost. It consists of sets of function/script in Matlab environment while the management of input and output information is provided by dedicated Microsoft Office Excel files. Every desired offshore wind park is represented by a dedicated Excel file, containing all the important technical and economical parameters that precisely describe its unique configuration. The tool imports this information and after performing a sequence of calculations, determines the Energy Cost according to equation (1).

3.3.1. Energy yield Calculation

The determination of the Energy Cost requires the calculation of the average power production of the wind parks. This is done by considering every wind park as a complex model consisting of interconnected elements. The components which have been modeled are the wind turbines, transformer, DC/DC converter, HVDC station and cables (AC and DC). The modeling details are available in [7]. The power at PCC is calculated for a given instantaneous wind speed and to describe the variations in the wind speed over time, a density function is used and in particular the Weibull distribution $f(w)$ described in [8], were w is the wind speed in m/s, as the ideal representation of real measured wind data. Using the probability density function, the average power can be generally calculated as:

$$P_{average} = \int_0^{\infty} P(w) \cdot f(w) \cdot dw \qquad (2)$$

where P(w) is the power at PCC for wind speed of w m/s.

3.3.2. Capital and maintenance costs

Wind park related cost data was obtained from published sources. A lot of information was available in [9] and [10]. The gathered data is referred in [7] regarded the following: Wind turbine (different for AC and DC grid), foundations, transformer, HVDC stations, cables (AC and DC), cable installation, offshore platform, DC/DC converters (according to type of usage) and switchgear (for AC). No resource was found on DC switchgear and due to the challenging construction, we assumed that setting its cost as double the AC switchgear. Additionally, Lundberg in [10] claims that since a DC/DC converter contains approximately the same amount of semiconductors as an AC/DC converter of the same rating, it is reasonable to have the same cost as the latter, namely 1 SEK/VA. However, regarding the complexities involved in the construction of DC/DC converters, such a cost was not considered adequate. A more careful and trustworthy approach was adopted. The converters on the turbines of the Series DC layout were considered at 3 SEK/VA owing to the high insulation requirements. The high power converters used in the offshore platform of the Large DC were considered at 2 SEK/VA because of the complex construction and the DC/DC converters on the turbines of the Small and Large DC schemes cost 1.5 SEK/VA due to the complexities involved.

In order to calculate the O&M costs, the components which require maintenance were gathered in three sets of related components: "Turbine", "Collection grid" and "Transmission system". According to literature sources, O&M can be taken as a certain percentage of the capital cost. Therefore the corresponding “Turbine O&M”, “Collection grid O&M” and “Transmission system O&M” were defined as 4%, 2% and 0.5% percentages respectively, of the total capital costs of the three initial sets.

3.4. Simulation considerations and assumptions

For each of the four suggested layouts, three different power capacities were considered: a) 160 MW, b) 500 MW and c) 1200 MW. Regarding the design considerations, the collection grid voltage was set at 30kV DC for DC grids and 30kV AC for the AC grids. Additionally the HVDC transmission links were rated at ±150kV for the 160 and 500 MW cases and ±320kV for the 1200 MW. Finally each feeder of the collection grid consisted of 10 turbines in all cases. The design peculiarity of the 1200 MW Series DC requested the need for 32kV DC at the exit of the turbines’ DC/DC converters and 20 turbines per feeder. Finally, every wind park was simulated for transmission distances in the range of 0-200km. Additionally, several assumptions were made as in Table 1.

Table 1. Simulation assumption

Parameter	Assumption
Wake effect	Neglected
Cable inventory	Maximum 4 different cables per model
Turbine's power rating	2MW
Turbine power curve	Same for DFIG (before transformer) and FPCG (before DC/DC converter)
Weibull shape factor	k=2
Converter loss curve	Same for HVDC and DC/DC
Interest rate	7% per annum
Life cycle	25 years
Average wind speed	10 m/s for all cases and all transmission distances

4. Results

4.1. Cost of DC/DC converters

In order to determine how sensitive the economic viability of the DC collection grid is with respect to the DC/DC converter cost, all costs were kept unchanged and the DC/DC converter cost was altered. Assuming that the cost proportion between the 3 different kinds of DC/DC converters as described in 3.3.1 remains always fixed, the following concept is followed: all of these values are multiplied by a common percentage representing the cost fluctuation i.e. a 50% percentage means that the new costs are half the original ones.

Figure 5 presents the results in Energy Cost terms for all layouts of the 160 MW power rating, for percentages of 50%, 100% and 300%. For a specific power capacity, the energy cost curves of the Large DC, Series DC and AC/DC seem to be parallel. This happens because these three layouts share the same transmission lines and increasing the distance will only increase the length of the cables. As a result, all three layouts will experience the same amount of capital and O&M cost increase and therefore energy cost increase. The order of the energy cost curves is defined by the costs with no transmission line involved. This is the energy cost at 0 km of distance. The Small DC differs in a great degree because it features multiple transmission cables and for increasing distance, the huge capital and O&M cost as well as excessive transmission system losses, force the energy cost to increase at a steep rate. As expected, the energy cost curve of the AC/DC layout remains the same in all three scenarios as it contains no DC/DC converters. On the contrary, the energy cost of the Small DC, Large DC and Series DC increase for increasing percentage (more expensive converters). As observed in the figure and also confirmed in [7], the Small DC rarely has the smallest energy cost and when this happens, it is only for distances less than 2-3 km. Additionally, its energy cost increases almost exponentially due to the large number of costly transmission lines and increased losses. Therefore, Small DC is of no interest for offshore development where distances are expected to be in the order of 10s to 100s of km and as a result, it will not be depicted again in the following figures.

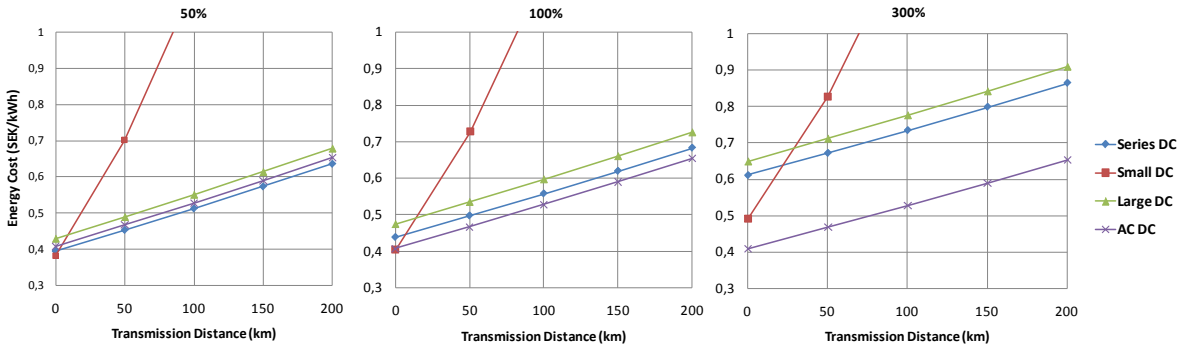

Figure 5. Energy cost curves of 160MW layouts for DC/DC cost percentages of 50%, 100% and 300%

For very small percentages, the Series DC has the smallest energy cost in all distances with the AC/DC following. For increasing percentage, AC/DC remains constant with the Series DC moving upwards until they coincide for a certain percentage. After this, the AC/DC maintains the smallest energy cost for all distances, and effectively all DC collection grid layouts have been ruled out of the competition. In every case, the Large DC has always higher energy cost than both the Series DC and the AC/DC. Therefore, only AC/DC and Series DC are considered as competitive layouts. This break-even percentage is different for each of the three power ratings and the findings are presented in Table 1.

Table 2. Break-even DC/DC cost percentages for each power rating

Wind park Power rating	Break-even percentage
160 MW	67%
500 MW	94%
1200MW	145%

If the results from all layouts and capacities are presented in the same graph as in Figure 6, it can be seen that for the basic scenario of 100% percentage, the AC/DC technology has the lowest energy cost up to a distance of ~100km, with the Series DC having the lowest energy cost for any greater distance. It was observed that by decreasing the DC/DC converter cost, the AC/DC technology was the most cost-benefit solution for smaller distances until it was eventually not competitive at all, with the Series DC being the cheapest for all distances. Reversely, for increasing converter cost the dominance of the Series DC is shifted to higher distances until a certain point when AC/DC has the lowest energy cost for all distances within the range of 0-200km.

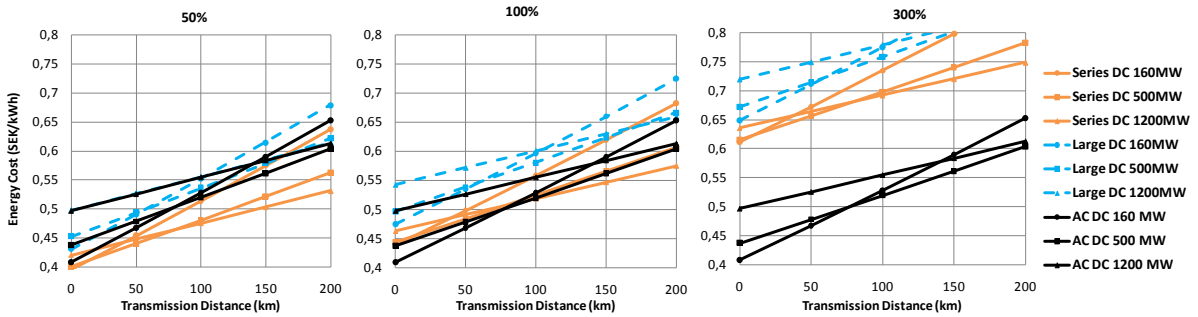

Figure 6. Energy Cost curves of Series DC, Large DC and AC/DC for DC/DC cost percentages of 50%, 100% and 300%.

It was determined that these two percentages are the break-even values for the 160MW and 1200MW as in Table 2. Therefore, for a percentage lower than 67%, the Series DC is the technology with the lowest energy cost for all distances, then AC/DC begins to be the cheapest up to certain distances, and when the percentage exceeds 145%, the AC/DC is the cheapest overall with no DC collection grid layout being competitive any more. The general conclusion is that if DC collection grid is to be regarded as a future solution for offshore wind parks for distances up to 200km, Series DC is the most cost-benefit wise interesting approach and the cost of the DC/DC converters must not exceed 145% of the originally assumed costs described in Table 1. When the cost percentage is less than 67%, Series DC (therefore DC collection grid) is the best solution in all distances.

4.2. DC switchgear cost

The same concept as before was followed in the case of the DC switchgear cost were the uncertainties in the DC breaker cost are involved. The original cost was multiplied by a percentage and break-even costs were determined as in Table 3. It is interesting to notice that no break-even percentage was evaluated for the 160MW case, meaning that AC/DC has always the lowest energy cost for all distances, no matter how cheap the DC switchgear gets.

When all the results are compared, the Series DC remains competitive until the percentage regarding the cost of the DC switchgear exceeds 378% and the AC/DC technology features the lowest energy cost for all 200km. This margin is high due to the smaller contribution of

Table 3. Break-even DC switchgear cost percentages for each power rating

Wind park Power rating	Break-even percentage
160 MW	Nonexistent
500 MW	54%
1200MW	378%

the DC switchgear to the overall capital costs, compared to the DC/DC converters. Even if the percentage drops to 0%, AC/DC will still be the most competitive for distances up to 60km.

5. Conclusions

Under the circumstances where offshore wind farms are growing in the capacity and distance from shore, DC wind collection grid along with DC transmission can be the most cost effective solution. However, any development of such designs depends on the presence of currently unavailable components, namely DC/DC converters and DC circuit breakers, and also on their expected costs. Specifically, the cost of DC/DC converters must be quite close to the suggested values of this paper while there is a lot more margin for the DC circuit breaker's cost. Any future research aiming to materialise the needed key components must be done with respect to the indicated cost boundaries and general findings of this paper.

References

[1] P. Bresesti, W. L. Kling, R. L. Hendriks, and R. Vailati, “HVDC connection of offshore wind farms to the trans-mission system,” IEEE Trans. Energy Conv., vol. 22, no. 1, pp. 37-43, Mar. 2007

[2] Macken, K.J.P.; Driesen, J.L.J.; Belmans, R.J.M., "A DC Bus System for connecting offshore wind turbines with utility system," European Wind Energy Conference 2001, Copenhagen, Denmark, 2-6 July 2001, pp. 1030-1035.

[3] Christoph Meyer, “Key Components for Future Offshore DC Grids” PhD thesis submitted to Electrical Engineering Department, RWTH Aachen.

[4] Ranganathan, V.T., Ziogas, P.D. Stefanovic, V.R., “A regulated DC-DC voltage source converter using high frequency link,” IEEE Transaction on Industry Application (IAS) 18 (1982), No. 3, pp. 279-287.

[5] Jacob, J.H.A.M., “Multi-phase Series Resonant DC/DC Converters,” Aachen Germany, RWTH Aachen University, Aachener Beitrage des ISEA Band 42, PhD Thesis 2006.

[6] Engel, B., Victor, M., Bachman, G., Falk, A., “15kV/16.7 Hz energy Supply System with Medium Frequency Transformer and 6.5 kV IGBTs in Resonant Operation,” European Power Electronics Conference (EPE), Toulouse, France, September 2003.

[7] Georgios Stamatiou, "Techno-Economical Analysis of DC Collection Grid for Offshore Wind Parks", MSc. Thesis, University of Nottingham, 2010, http://hermes.eee.nottingham.ac.uk/mcf/Thesis.pdf

[8] http://www.weibull.com/AccelTestWeb/weibull_distribution.htm

[9] B. Van Eeckhout,” The economic value of VSC HVDC compared to HVAC for offshore wind farms,” Master Thesis submitted to Katholik University of Leuven.

[10] Stefan Lundberg, ”Performance comparison of wind park configurations,” Chalmers University of Technology, 2003.

Study of transient stability for parallel connected inverters in Microgrid system works in stand-alone

F. Andrade[1,*], J. Cusido[2], L. Romeral[1], J. J. Cárdenas[1]

[1] *Universitat Politécnica de Catalunya, Barcelona, Spain*
[2] *CTM Centre Tecnològic, Manresa, Spain*
** Tel: +34937398510, Fax: +34937398016, E-mail: fabio.andrade@mcia.upc.edu*

Abstract: Distributed generators systems and Microgrid are becoming more important to increase the renewable energy penetration in the public utility. This paper presents a mathematical model for connected inverters in Microgrid systems with large range variations in operating conditions. No-lineal tools and computer simulations, phase-plane trajectory analysis, method of Lyapunov and bifurcations analysis for evaluate the limits of the small signal models are used, and conclusion suggested utilizing models that can permit to analysis of the system when subjected to a severe transient disturbance such as loss a large load or loss of generation. The study of transient stability for Microgrid systems in stand-alone of the utility grid is useful to improve the design of Microgrid's architecture.

Keywords: *Microgrid model, Transient Stability, Parallel Inverters, Method of Lyapunov.*

1. Introduction

Distributed generators systems and Microgrid are becoming more important to increase the renewable energy penetration in the public utility [1-2]. Thus, the use of intelligent power interfaces between the electrical photovoltaic generation source and the grid is required. These interfaces have a final stage consisting of dc/ac inverters, which can be classified in current source inverters (CSI) and voltage-source inverters (VSI). In order to inject current to the grid, CSI are commonly used, while in island or autonomous operation, VSI are needed to maintain the voltage stability [3-5].

A Microgrid can be operated either in grid connected mode or in stand-alone mode. In grid connected mode, most of the system level dynamics are established by the public utility, this is due to the relatively small size of local generators. In stand-alone mode, the system dynamics are established by micro generators themselves [6]. This paper presents an analysis of transient stability of power systems for parallel connected inverter in a Microgrid under autonomous operation.

The power inverters do not present the natural relations between frequency and active output power, neither between output voltage and reactive output power. Therefore, in order to reach stable operation, when the inverters are connected in parallel, these inherent operating conditions must be established by the inverter's control system [7].

Previous analysis of stability of stand-alone systems have been done by means of small signal models [5, 8], either assuming an ideal inverter or considering power inverter with a high switching frequency and their closed-loop inner controllers. Simulation and experimental result show that the systems work well when there is a small perturbation, but when the perturbation is bigger, the system could be in unstable operation.

The small signal analysis works with root locus plots Bode diagrams, Nyquist plots, etc., researching the desired dynamic behaviour of the systems. On the contrary, this paper works with no-lineal tools for large signal analysis supported by computer simulations. It is used

phase-plane trajectory analysis and method of Lyapunov to evaluate the limits of the small signal models. It is suggested the utilization of models that allow to analyze the system when it is subjected to a s evere transient disturbance such as loss of large loads or loss of generation.

2. A Microgrid Study

Fig 1 shows the circuit diagram of the Microgrid systems in stand-alone considered in this paper. This system configuration was studied by Duminda, in [8]. It was considered small signal modeling. For simplicity, the system has two inverter connected, but it can be extended for n-number of inverters.

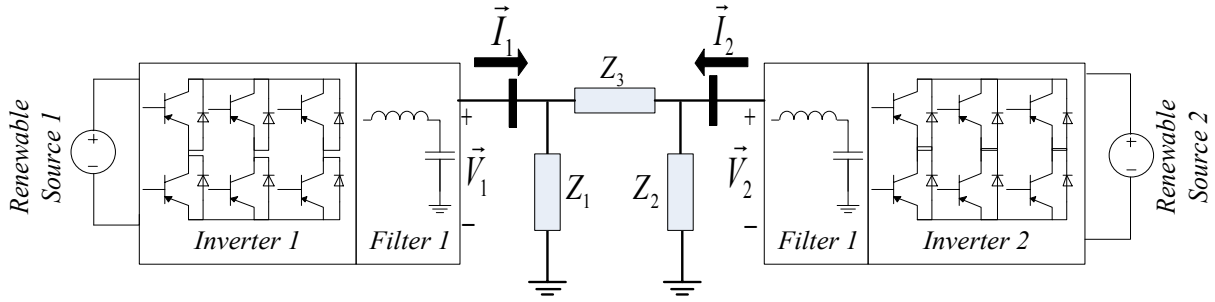

Fig. 1. Parallel connected inverters in Microgrid system works in stand-alone.

The Distributed Generator (DG) considered consists of a power DC renewable source, a three-leg inverter and an output LC filter. By assuming the renewable energy source as an ideal source form, the DC bus dynamics can be neglected. Each DG presents a PWM controller with a current and voltage loop and a PQ controller. The PQ controller must autonomously respond effectively to system changes without communication, only with local variables. Commonly, the PQ controller uses the droop curves (*f vs P* and *V vs Q*) and a filter with a cut-off frequency of approximately a decade smaller than a grid frequency. The task of the PQ controller is to imitate the governor of a synchronous generator. This artificial droop control scheme can be expressed as follows

$$\omega = \omega_0 - k_p P \qquad V = V_0 - k_v Q \tag{1}$$

Where P and Q are filtered with a low pass filter with cut-off frequency ω_f, the equations of these filters in the Laplace domain can be expressed as:

$$P(s) = \frac{\omega_f}{s+\omega_f} P_i(s) \qquad Q(s) = \frac{\omega_f}{s+\omega_f} Q_i(s) \tag{2}$$

P_i and Q_i are instantaneous power and are calculated from the measured output voltage and output current as in

$$P_i(s) = V_d I_d + V_q I_q \qquad Q_i(s) = V_d I_q - V_q I_d \tag{3}$$

2.1. A mathematical model of the each voltage source inverter

Considering (1), (2) and working in the time domain,

$$\dot{\omega} = -\omega_f \omega - k_p \omega_f + P_i \tag{4}$$

$$\dot{V} = -\omega_f V - k_v \omega_f + Q_i \tag{5}$$

The inverters are modeled in a common reference frame (d-q), fig. 2. Each voltage vector has an angle δ_i with respect to the d-axes.

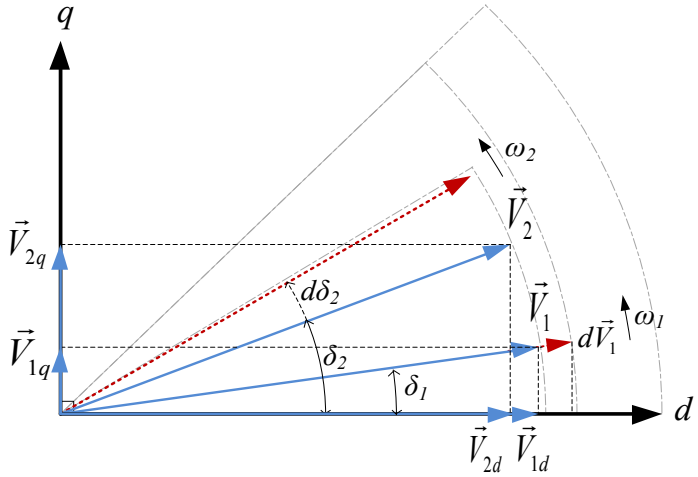

Fig. 2. Voltage vectors in reference d-q frame.

The vector V can be represented as $\vec{V} = V_d + jV_q$ Where

$$V_d = V\cos(\delta) \qquad V_q = V\sin(\delta) \qquad \delta = \arctan\left(\frac{V_q}{V_d}\right) \tag{6}$$

From (4) and fig. 2 it is shown that ω_i changes in response to the real power flow and modifies the angle δ_i. Thus, from (6) it can be expressed

$\omega = \dot{\delta} = \frac{\dot{V}_q V_d - \dot{V}_d V_q}{V_d^{\,2} + V_q^{\,2}}$ Considering $|V| = \sqrt{V_d^{\,2} + V_q^{\,2}}$ and the expressions (4), (5) and (6) it can be obtained the state equation (7) which describe the behavior of each inverter.

$$\begin{cases} \dot{\omega} = \omega_f \omega - k_p \omega_f P \\ \dot{V}_d = -\omega_f V_d - \omega V_q - \dfrac{k_p \omega_f V_d}{|V|} Q \\ \dot{V}_q = \omega V_d - \omega_f V_q - - \dfrac{k_v \omega_f V_q}{|V|} Q \end{cases} \tag{7}$$

2.2. Combined model of all the inverters and network model

In previous section the mathematical model of an individual inverter on a common reference d-q frame was discussed. Let us consider a system with two inverters connected to a network, as shown in fig. 1. The state equation for two inverters is

$$\begin{cases} \dot{\omega}_1 = \omega_{f1}\omega_1 - k_{p1}\omega_{f1}P_1 \\ \dot{V}_{d1} = -\omega_{f1}V_{d1} - \omega_1 V_{q1} - \dfrac{k_{p1}\omega_{f1}V_{d1}}{|V_1|}Q_1 \\ \dot{V}_{q1} = \omega_1 V_{d1} - \omega_{f1}V_{q1} - -\dfrac{k_{v1}\omega_{f1}V_{q1}}{|V_1|}Q_1 \\ \dot{\omega}_2 = \omega_{f2}\omega_2 - k_{p2}\omega_{f2}P_2 \\ \dot{V}_{d2} = -\omega_{f2}V_{d2} - \omega_2 V_{q2} - \dfrac{k_{p2}\omega_{f2}V_{d2}}{|V_2|}Q_2 \\ \dot{V}_{q2} = \omega_2 V_{d2} - \omega_{f2}V_{q2} - -\dfrac{k_{v2}\omega_{f2}V_{q2}}{|V_2|}Q_2 \end{cases} \tag{8}$$

The network in the fig. 1 is described by the nodal admittance matrix equation

$$\begin{bmatrix} \vec{I}_1 \\ \vec{I}_2 \end{bmatrix} = \begin{bmatrix} Y_1 + Y_3 & -Y_3 \\ -Y_3 & Y_2 + Y_3 \end{bmatrix} \begin{bmatrix} \vec{E}_1 \\ \vec{E}_2 \end{bmatrix} \rightarrow \begin{bmatrix} I_{1d} \\ I_{1q} \\ I_{2d} \\ I_{2q} \end{bmatrix} = \begin{bmatrix} G_{11} & -B_{11} & -G_{12} & B_{12} \\ B_{11} & G_{11} & -B_{12} & -G_{12} \\ G_{12} & B_{12} & G_{22} & -B_{22} \\ -B_{12} & -G_{12} & B_{22} & G_{22} \end{bmatrix} \begin{bmatrix} V_{d1} \\ V_{q1} \\ V_{d2} \\ V_{q2} \end{bmatrix} \tag{9}$$

Considering the active and reactive power equations (3) and (9),

$$\begin{bmatrix} P_1 \\ Q_1 \\ P_2 \\ Q_2 \end{bmatrix} = \begin{bmatrix} V_{d1} & V_{q1} & 0 & 0 \\ -V_{q1} & V_{d1} & 0 & 0 \\ 0 & 0 & V_{d2} & V_{q2} \\ 0 & 0 & -V_{q2} & V_{d2} \end{bmatrix} \begin{bmatrix} G_{11} & -B_{11} & -G_{12} & B_{12} \\ B_{11} & G_{11} & -B_{12} & -G_{12} \\ G_{12} & B_{12} & G_{22} & -B_{22} \\ -B_{12} & -G_{12} & B_{22} & G_{22} \end{bmatrix} \begin{bmatrix} V_{d1} \\ V_{q1} \\ V_{d2} \\ V_{q2} \end{bmatrix} \tag{10}$$

Which the above equation, combined with (8), gives the whole system equations

$$\begin{cases} \dot{X}_1 = \alpha_1 X_1 - \alpha_2\sqrt{X_2^2 + X_3^2} - \alpha_3 \dfrac{(X_2X_5 + X_3X_6)}{\sqrt{X_2^2 + X_3^2}} + \alpha_4 \dfrac{(X_3X_5 - X_2X_6)}{\sqrt{X_2^2 + X_3^2}} \\ \dot{X}_2 = \alpha_1 X_2 - X_1X_3 - \alpha_5 X_2\sqrt{X_2^2 + X_3^2} - \alpha_6 X_2 \dfrac{(X_2X_5 + X_3X_6)}{\sqrt{X_2^2 + X_3^2}} + \alpha_7 X_2 \dfrac{(X_3X_5 - X_2X_6)}{\sqrt{X_2^2 + X_3^2}} \\ \dot{X}_3 = \alpha_1 X_3 - X_1X_2 - \alpha_5 X_3\sqrt{X_2^2 + X_3^2} - \alpha_6 X_3 \dfrac{(X_2X_5 + X_3X_6)}{\sqrt{X_2^2 + X_3^2}} + \alpha_7 X_3 \dfrac{(X_3X_5 - X_2X_6)}{\sqrt{X_2^2 + X_3^2}} \\ \dot{X}_4 = \beta_1 X_4 - \beta_2\sqrt{X_5^2 + X_6^2} - \beta_3 \dfrac{(X_2X_5 + X_3X_6)}{\sqrt{X_5^2 + X_6^2}} + \beta_4 \dfrac{(X_3X_5 - X_2X_6)}{\sqrt{X_5^2 + X_6^2}} \\ \dot{X}_5 = \beta_1 X_5 - X_4X_6 - \beta_5 X_5\sqrt{X_5^2 + X_6^2} - \beta_6 X_5 \dfrac{(X_2X_5 + X_3X_6)}{\sqrt{X_5^2 + X_6^2}} + \beta_7 X_5 \dfrac{(X_3X_5 - X_2X_6)}{\sqrt{X_5^2 + X_6^2}} \\ \dot{X}_6 = \beta_1 X_6 - X_4X_5 - \beta_5 X_6\sqrt{X_5^2 + X_6^2} - \beta_6 X_6 \dfrac{(X_2X_5 + X_3X_6)}{\sqrt{X_5^2 + X_6^2}} + \beta_7 X_6 \dfrac{(X_3X_5 - X_2X_6)}{\sqrt{X_5^2 + X_6^2}} \end{cases} \tag{11}$$

Where

$\alpha_1 = -\omega_{f1};\ \alpha_2 = k_{p1}G_{11}\omega_{f1};\ \alpha_3 = k_{p1}G_{12}\omega_{f1};\ \alpha_4 = k_{p1}B_{12}\omega_{f1};\ \alpha_5 = k_{v1}B_{11}\omega_{f1};\ \alpha_6 = k_{v1}B_{12}\omega_{f1};\ \alpha_7 = k_{v1}G_{12}\omega_{f1}$

$\beta_1 = -\omega_{f2};\ \beta_2 = k_{p2}G_{22}\omega_{f2};\ \beta_3 = k_{p2}G_{12}\omega_{f2};\ \beta_4 = k_{p2}B_{12}\omega_{f2};\ \beta_5 = k_{v2}B_{22}\omega_{f2};\ \beta_6 = k_{v2}B_{12}\omega_{f2};\ \beta_7 = k_{v2}G_{12}\omega_{f2}$

3. Study of Stability for the Microgrid

In this section it is constructed a Lyapunov function for the Microgrid system and obtained the respective eigenvalues for the A matrix of lineal system.

3.1. Lyapunov's method

One of the main impediments for the application of Lyapunov's method to physical systems is the lack of formal procedures to construct the Lyapunov function for the differential equations describing the given physical system [10]. A function *V(X)* is called a Lyapunov function of the system *f(X)* where *f(0)=0* if it fulfills the following properties [11]:

i. $V(0) = 0$

ii. $V(X) > 0$ for all X

iii. $\frac{d}{dt}V(X) \le 0$ along all trajectories of the system

Then the point *X=0* is locally stable.

It is proposed to construct the Lyapunov function by using the set of representative variables for each generator. By following this principle, firstly it is chosen the square frequency variables (X1 and X4) divided into the working frequency to obtain "per unit" values and secondly it is used the dq voltage of each generator divided by the module of voltage; this method is repeated for every generator of the Microgrid. Finally, every term of the obtained Lyapunov function are multiplied by a different constant. These constants must be chosen to fulfill the iii property.

$$V(X) = \frac{AX_1^2}{\omega_k} + B\frac{X_2^2 + X_3^2}{\sqrt{X_2^2 + X_3^2}} + \frac{CX_4^2}{\omega_k} + D\frac{X_5^2 + X_6^2}{\sqrt{X_5^2 + X_6^2}} \tag{12}$$

The above equation fulfills (i) and (ii) properties as can be seen by inspection. Condition (iii) can be shown as

$$\frac{\partial V(X)}{\partial X_1}\dot{X}_1 + \frac{\partial V(X)}{\partial X_2}\dot{X}_2 + \frac{\partial V(X)}{\partial X_3}\dot{X}_3 + \frac{\partial V(X)}{\partial X_4}\dot{X}_4 + \frac{\partial V(X)}{\partial X_5} + \dot{X}_5 + \frac{\partial V(X)}{\partial X_6}\dot{X}_6 \le 0 \tag{13}$$

Hence,

$$\begin{aligned} AX_1\dot{X}_1 + B\left(X_2^2 + X_3^2\right)^{1/2} X_2\dot{X}_2 + C\left(X_2^2 + X_3^2\right)^{1/2} + DX_3\dot{X}_3 + CX_4\dot{X}_4 + \\ + E\left(X_5^2 + X_6^2\right)^{1/2} X_5\dot{X}_5 + F\left(X_5^2 + X_6^2\right)^{1/2} X_6\dot{X}_6 \le 0 \end{aligned} \tag{14}$$

Then the Lyapunov function (12) and the mathematical model (11) are simulated in MATLAB/Simulink for reaching the best values of every constant and the region where the Lyapunov function is valid and the system is stable. A first study it is used A=C; B=E and C=F.

3.2. Eigenvalues of lineal system

Considering the system of the figure 1 and the nonlineal model in (11) and applying Taylor's series around the operating point at this model, it can be obtained the state-space equations of the small-signal model. This is acceptable if variations around the operating point are assumed to be small; therefore, the small signal lineal model is $\left[\dot{\tilde{X}}\right]=[A]\left[\tilde{X}\right]$.

Finally the systems with parameters presented on Table I, the initial active and reactive output powers zero, and initial vectors V1 y V2 in phase, the A matrix values are

$$A=\begin{bmatrix} -37.7 & -0.466 & -0.936 & 0 & 0.157 & 0.944 \\ 0 & -36.57 & -0.217 & 0 & -0.94 & 0.157 \\ 154.5 & 0 & 0 & 0 & 0 & 0 \\ 0 & 0.097 & -0.956 & -37.7 & -0.34 & -0.97 \\ 0 & -0.954 & 0.097 & -9.86 & -36.5 & -2.42 \\ 0 & -0.061 & 0.006 & 154.9 & -2.32 & -0.15 \end{bmatrix}$$

And the respective eigenvalues are $\lambda_1=0;\ \lambda_2=-10.8;\ \lambda_3=-26.9;\ \lambda_4=-35.7\ \lambda_5=-37.7;\ \lambda_6=-37.5;$
According to [8] only the nonzero eigenvalues are important for the stability studies. The system has five negative real eigenvalues, and then it is a stable point.

Table I. System parameters.

Variable	Value	unit
Line transmission (Z_3)	0.5+3i	Ω
Local load (Z_1)	13+6i	Ω
Local load (Z_2)	25+13i	Ω
Cut-off freq. of measuring filter (ω_f)	37.7	rd/s
Frequency droop coefficient (k_p)	0.0005	rd/s/W
Frequency droop coefficient (k_v)	0.0005	V/VAR
Nominal frequency	377	rd/s

4. Simulation Results

The methodology used is as follows; firstly of all the Microgrid system is implemented be means of the power electronics toolbox of Matlab/SIMULINK, the system parameters for simulation are shown in table I. Secondly, the simulated values of every state variable in the operating point are used to find the A matrix values and its eigenvalues. This eigenvalues are used to determinate the stability of the system. After that, it is utilized the set of equation (11) to verified the model and then the values of the state variables and its derivatives are used to evaluate the Lyapunov function. Finally it is studied the Lyapunov function and it is determined the region of stability of the system.

The fig 3 shows the PQ power simulation by means of the Power electronic toolbox. This was repeated with a different line inductor values (from 8mH to 0.5mH with step of 0.5mH). For each simulation the values of state variables at the operating point were saved and these were used to study the small signal stability.

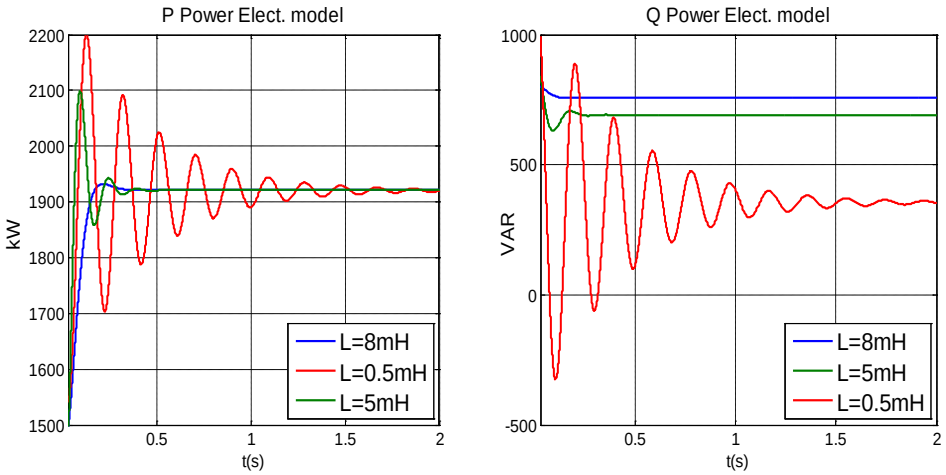

Fig. 3. Simulation results of a DG Microgrid system by means of Power Electronics tools

The fig 4 shows the PQ power simulation by means of nonlineal model of the Microgrid systems obtained in 2.2. It can be seen the same behavior in both transient and steady state values. As explained previously, the line inductance was varied for the nonlineal model. The values of state variables were used to validate the Lyapunov function.

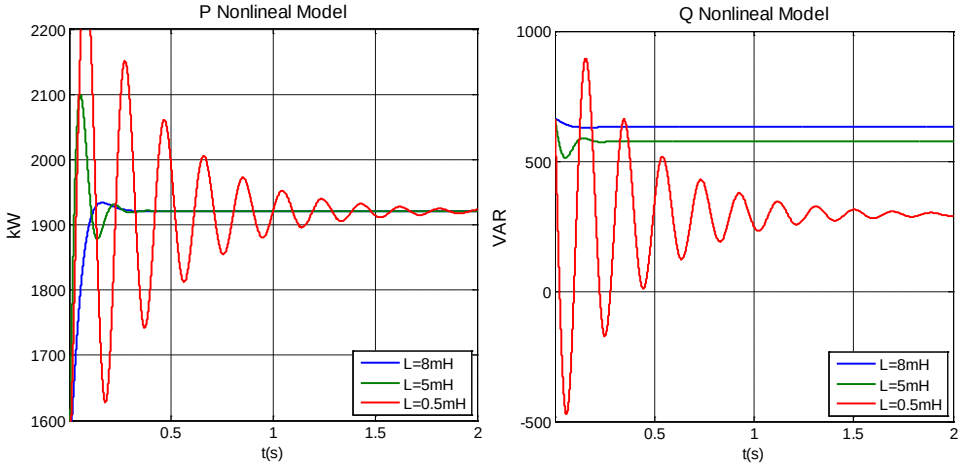

Fig. 4. Simulation results of a DG Microgrid system by means of Nonlineal model.

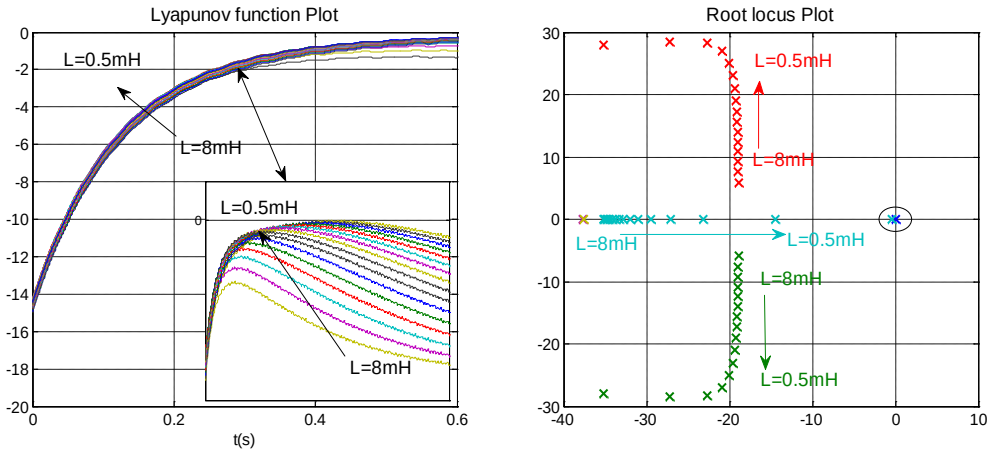

Fig. 5. Study of stability by means of Lyapunov function and root locus plot.

Fig 5 shows the study of stability by using the Lyapunov function and the root locus plot. They can be seen how the stability is affected when the line inductance decrease. The transient stability analysis by a Lyapunov method evaluate all variations starting in around a stable point that converge to it, therefore it can determine the lowest value of V(X) on the surface $\dot{V}(X) = 0$ and by this way the region of asymptotic stability is determined. The small signal stability analysis by a root locus plot shows how the roots are moved when the line inductor decreases, but cannot give an "a priori" region of asymptotic stability.

5. Conclusions

In this paper, a nonlinear state-space model of a Microgrid is presented. The model includes the most important dynamics. This modeling method is able to be extended to n-generators. The model has been analyzed by means of both stability studies Lyapunov function and root locus plot. A general methodology to find a valid Lyapunov function for non linear stability analysis has been presented. Using that Lyapunov function the region of asymptotic stability can be determined. These tools will allow the design of Microgrid systems with loads, generators and storage systems assuring the global stability of the system.

References

[1] A. G. Madureira, Coordinated voltage support in distribution networks with distributed generation and microgrids, IET Renewable Power Generation, 2009, pp. 439 – 454.

[2] P. N. Vovos, Centralized and Distributed Voltage Control: Impact on D istributed Generation Penetration, IEEE Transactions on Power Systems, 2007, pp. 476 – 483.

[3] C. L. Chen, State-space modeling, analysis, and implementation of paralleled inverters for microgrid applications, Applied Power Electronics Conference and Exposition (APEC), 2010, pp. 619 – 626.

[4] A. Arulampalam, Control of power electronic interfaces in distributed generation microgrids, International Journal of Electronics, 2004, pp. 503 – 523.

[5] N. Pogaku, Modeling, Analysis and Testing of Autonomous Operation of an Inverter-Based Microgrid, IEEE Transactions on Power Electronics, 2007, pp. 613 – 625.

[6] N. L. Soultanis, A Stability Algorithm for the Dynamic Analysis of Inverter Dominated Unbalanced LV Microgrids, IEEE Transactions on Power Systems, 2007, pp. 294 – 304.

[7] J. Guerrero, A wireless controller to enhance dynamic performance of parallel inverters in distributed generation system, IEEE Transactions on Power Electronics, 2004.

[8] P. Duminda, Stability Analysis of Microgrids with Constant Power Loads, Sustainable ICSET 2008. IEEE International Conference on Energy Technologies, 2008.

[9] E.A.A. Coelho, Small-Signal Stability for Parallel-Connected Inverters in Stand-Alone AC Supply Systems, IEEE Transactions on Industry Applications, 2002, pp. 533 – 542.

[10] A. Bacciotti, Liapunov Function and Stability in Control Theory, Springer, 2nd edition, 2005, pp. 27 – 80.

[11] H. Khalil, Nonlinear Systems. Prentice Hall, 2nd edition, 1996.

Optimal Design of a Small Permanent Magnet Wind Generator for Rectified Loads

Jawad Faiz[1,*], Nariman Zareh [1]

[1]*Center of Excellence on Applied Electromagnetic Systems, School of Electrical and Computer Engineering, University of Tehran, Tehran, Iran*
** Corresponding author. Tel: +98 61114223, Fax: +98 88533029, E-mail: jfaiz@ut.ac.ir*

Abstract: This paper presents an optimal design procedure for a small permanent magnet wind generator which supplies a full-bridge diode rectified load. The aim is to improve the output voltage waveform of the generator. An electromagnetic-thermal design algorithm is proposed based on an analytical model of a surface-mounted permanent magnet generator. A comprehensive combined model, consisting of design program and simulation of the designed generator under rectified load, is utilized. Design variables are optimized over their appropriate limits using a genetic algorithm. The results indicate the improvement of the output voltage waveform.

Keywords: *Wind Generator, Permanent Magnet Machine, Optimal Design*

Nomenclature

U	*rated wind velocity……..m/s*	D	*air gap diameter……..m*
U_{mean}	*dominant mean velocity of wind..m/s*	$B_{sat\text{-}s}$, $B_{sat\text{-}r}$	*stator, rotor saturated flux density... T*
β	*pitch angle……..rad.*	P	*pole numbers*
R	*blade radius……m*	K_{w1}	*winding factor*
ω_r	*shaft angular speed……rad/s*	C_φ	*flux conical factor*
$C_p(\lambda,\beta)$	*turbine aerodynamic efficiency.… %*	K_c	*carter coefficient*
η_{gen}	*efficiency of generator……%*	p_{rl}	*normalized rotor leakage peamability*
P_{gen}	*rated output electrical power ….....W*	K_s	*stator lamination factor*
n_s	*rotation speed……rpm*	τ_s	*stator slot pitch (πD/S)*
SML_{pk}	*peak specific magnetic loading…..T*	THD_v	*voltage time harmonic distortion*
SEL_{pk}	*specific electric loading……A/m*	K	*shape parameter*
h_{sy},h_{ry}	*stator and rotor yoke height…....m*	$\lambda(\omega_r R/U)$	*tip speed ratio*
w_s	*stator slot width (τ_s-w_t)……..m*	μ_r	*relative permeability*

1. Introduction

Permanent magnet generator (PMG) is a self-excited system and it can be a proper choice to coupling it to wind turbine. The output of the generator can charge the batteries or supply inverter or both [1]. There are different techniques to connect a DC bus (with power electronics devices) to the PMG [2]. Utilization of rectified loads distorts the output voltage waveform of the PMG leading to a low quality power delivered to the load. A proper operation of the generator under such conditions requires a precise design optimization of the PMG. Such design needs an appropriate modeling and comprehensive design algorithm.

Details of PMG design for direct coupling to a wind turbine has been given in [3] in which four configurations including radial-flux, axial-flux, cross-field-flux and claw-pole generators have been compared based on the air gap flux density, copper losses, PM weakening and the system cost. This comparison indicates that a radial-flux, internal-PM is a proper choice for designing a 400 kW generator. Application of different configurations of PMG for wind turbine has been proposed in [4] and 60 configurations has been compared based on the torque density and also cost per developed torque function. It shows a radial-flux PMG using surface-mounted Ferrite PMs has a better performance compared with the internal PM

version. In [5], the axial-flux and radial-flux PMGs, for direct driven wind turbine, have been optimized based on the cost per developed torque objective function. The results indicate that the radial-flux machines have lower cost and torque density. In [6], two types of radial-flux PMG (internal- and surface-mounted PM) with inner rotor structures for direct coupling to wind turbine are analyzed and compared. The electromagnetic behavior of generators and optimal shape of the PMs have been estimated by finite element method (FEM). The results indicate lower torque ripples in the surface-mounted PMG. Design and performance analysis of an ironless axial-flux PMG have been proposed in [7] and [8]. The particular ironless machine configuration leads to a longer effective air gap of the machine. Also a multi-variable optimization algorithm based on the design parameters for improvement of the PMG performance of the machine has been introduced. Finally, a prototype 3.5 kW machine has been built and tested in which noise, cogging torque and copper losses have been reduced in expense of heavier machine. In [9], a small radial- and axial-flux wind generators have been optimally designed using an optimization algorithm based on population growth which tries to maximize annual energy gaining from variable speed wind turbine-generator. However, thermal analysis of the PMG has been neglected.

In recent years application of power electronics components in variable speed drives and controlling output of generators has been increased. Therefore, a reliable, economical design and satisfactory operation of these machines are crucial. This paper considers the electromechanical conversion of wind energy. Electromagnetic design procedure of a surface-mounted radial-flux PMG and its thermal model are proposed. A comprehensive combined model consisting of the generator design routine and simultaneous simulation of the typical design in the presence of a rectified load is introduced and impact of this type of load upon the distortion of the output voltage waveform of the generator is studied. Finally, the design optimization procedure is proposed to achieve a near sinusoidal output voltage waveform.

2. Electromechanical Conversion of Wind Energy

Wind speed is modeled as a continuous stochastic variable. The probability of the occurrence of a define wind velocity can be expressed by a probability density function. Comparisons of the measured wind speeds show that if the time interval is long enough, the Weibull distribution function is suitable to describe the wind velocity [10, 11]:

$$f(U) = \frac{k}{c}\left(\frac{U}{c}\right)^{k-1} e^{-\left(\frac{U}{c}\right)^{k}} \tag{1}$$

where k=2 and c is the magnification parameter ($2U_{mean}/\sqrt{\pi}$). *A portion of the wind energy transmitted* to the shaft is converted into mechanical energy by blades of the turbine and its efficiency depends on the blades profile, and air density. Wind energy converted into mechanical energy (P_{shaft}) is:

$$P_{shaft} = 0.5\rho_{air}\pi R^2 U^3 \left(0.51\left(\frac{116}{\lambda_1} - 0.4\beta - 5\right)e^{-\frac{21}{\lambda_1}} + 0.006\lambda\right) \tag{2}$$

Nowadays most horizontal three-blade turbines are designed as such that their operating point are placed in the range of 5 to 7 m/s. In this case, turbine operates with maximum $C_p(\lambda,\beta)$ between 0.35 and 0.45 [9]. R and ω_r can be determined as follows:

$$R = \sqrt{\frac{P_{gen}}{\frac{1}{2}\rho_{air}\pi U^3 C_P \eta_{gen}}}$$

$$\omega_r = \sqrt{\frac{\frac{1}{2}\rho_{air}\pi\lambda^2 U^5 C_P \eta_{gen}}{P_{gen}}} \tag{3}$$

(4)

Eqns. (3) and (4) can be used as a guide for estimation of *R* and *U* in the design process of the small wind generator.

3. Design of PMG

Low-Carbon soft-steel is used in the rotor and silicon-steel laminations in the stator of PMG. The slot has semi-closed shape. The PM (NdFeB) pieces are mounted on the external surface of the rotor. The apparent power of the air gap of a radial-flux generator (S_g) versus the main dimensions of the machine is as follows [12]:

$$S_g = \frac{1}{2}\pi^2 . K_{w1} . D^2 L . n_s . SML_{pk} . SEL_{pk} \tag{5}$$

Product D^2L determines the capability of the energy absorbed by the turbine:

$$D^2 L = \frac{\varepsilon P_{gen}}{0.5\pi^2 . K_{W1} . n_s . SML_{pk} . SEL_{pk} . \cos\varphi} \tag{6}$$

where $\varepsilon = E_f / V_a$. Ratio $K_L = L/D$ is chosen in the range of 0.14 and 0.50 based on the main design and available backgrounds [12-14]. Therefore, diameter and stack length are evaluated using this ratio. In choosing *D* a particular attention must be paid to the required *P* and a proper pole pitch. On the other hand, in order to reduce the overhang copper losses and its additional expense, *D* must be limited as possible.

3.1. Magnetic Design

The generator pole numbers, PM dimensions, stator and rotor dimensions are determined in this stage.

Air gap Flux Density: The air gap flux density is limited by saturation level of the stator teeth. An appropriate value for SML_{pk} is 0.9 T. This can hold a relative balance between the magnetic circuit saturation and power absorption capability of PMG [15, 16].
Generator Poles Number: Frequency range of small PMGs is between 10 and 70 Hz or 30 and 80 Hz [9]. Therefore, the rated frequency of the generator can be chosen in the range of 45-65 Hz and P is then calculated. Conventional PM machines have normally low P and the pole pitch is considerably larger than the PM pitch; therefore, the pole arc to PM arc ratio (α) is not so crucial. However, in wind PMG, P is high and pole pitch and PM pitch are comparable and suggested range is between 0.67 and 0.77 [14].
PM Dimensions: Operating point of the magnetic circuit can be determined by intersection of the PM demagnetization curve and load line of the magnetic circuit. The slope of the load line shows the resistance of the PM against demagnetizing. A security margin in a surface-mounted PMG is guaranteed by choosing PC≥6. The PM length is estimated as follows [13]:

$$l_m = (PC - p_{rl}\mu_r) . C_\phi K_c l_g \tag{7}$$

p_{rl} is typically between 0.05 and 0.2 [15]. As seen, the required length of PM for providing the excitation flux depends on the air gap length. The air gap length in this design is taken to be about 0.01*D*.
Dimensions of Stator and Rotor: To prevent the saturation of the PMG yoke, a special attention must be paid to the dimensions and cross-section of the yoke. Assume a define stack length for PMG; the height of the yoke is evaluated as follows [17]:

$$h_{sy} > \frac{\alpha \pi D}{4pK_s} \cdot \frac{B_g}{B_{sat-s}} \tag{8}$$

$$h_{ry} > \frac{\alpha \pi (D - 2l_{m)}}{4p} \cdot \frac{B_g}{B_{sat-r}} \tag{9}$$

In order to be ensuring about non-saturated teeth of the stator, the following constraint must be held [17]:

$$w_t > \frac{\tau_s}{K_s} \cdot \frac{B_g}{B_{sat-s}} \tag{10}$$

In most electrical machines w_s is taken to be almost equal to the tooth width as such that $0.5<w_s/\tau_s<0.6$ [18]. However, if $w_s=w_t=0.5\tau_s$, the product of the electric and magnet loading approaches its peak value, and this maximizes the power absorption capability of PMG. Therefore, in a PMG with equal slot and tooth width, the non-saturation condition is as follows:

$$B_g < \frac{1}{2} . K_s . B_{sat-s} \tag{11}$$

3.2. Electrical Design

SEL_{pk} of a PMG is limited by the slot filling factor, slot height and stator conductors current density. The typical range of SEL_{pk} for a PMG is 1000 to 4000 A/m [9]. For low-voltage PMGs, the slot filling factor is in the range of 0.3 and 0.5 and current density of the stator conductors is between 3 and 8 A/mm^2. Of course, for higher current density up to 10 A/mm^2, class F insulation for windings and a proper cooling system are suggested [16]. For given SEL_{pk}, filling factor and conductor current density in a radial PMG with elliptic slots, the slot height is as follows [9]:

$$h_s = \frac{SEL_{pk}}{\sqrt{2} . J . K_{sf} . (1 - w_t / \tau_s)} \tag{12}$$

3.3. Thermal Modeling of PMG

Thermal analysis of any electrical machine is a crucial stage of the design process. Different models, depending on the required precision and complexity, have been so far proposed for thermal analysis of the PM machines. Here, an equivalent thermal-resistance network is used [18] to estimate the temperature distribution over 8 different points of PMG. To use the model, the corresponding losses of any node are calculated and by applying the losses to the resistance network, the temperature rise of the above-mentioned points are evaluated. A particular attention must be paid to the temperature rise of the PM and winding in PMG. Conducting resistance between any two-node is used to complete the 8 points in the equivalent thermal model of the motor as seen in Fig. 1. Computation procedure for the resistances is complicated and it is necessary to take into account the precise heat flow, heat convection, internal heat generation sources, different materials and dimensions of the PMG. To simplify the model, heat transfer between the PMG and cooling environment is considered assuming a mean temperature for the cooling material (15 degrees).

Two nodes have been assigned to the stator, one node to the yoke and one node to the tooth. In the full-load PMG, windings are the main source of the generated heat. Two nodes are considered in the model, one for the conductors in the slots and one for the end windings. Prediction of the PMs temperature rise is important in the thermal modeling of the PMG,

therefore one node is assigned to the PMs. Estimation of the temperature rise of PMG by n+1 thermal networks need to solve n related equations. These equations are extracted from $\theta = G^{-1}P_d$ [18], where P_d is the dissipated losses vector corresponding to any node and θ is the temperature rise vector. Thermal resistances model for forming the thermal conduction matrix G is as follows:

$$G = \begin{bmatrix} \sum_{i=1}^{n} \frac{1}{R_{1,i}} & -\frac{1}{R_{1,2}} & \cdots & -\frac{1}{R_{1,n}} \\ -\frac{1}{R_{2,1}} & \sum_{i=1}^{n} \frac{1}{R_{2,i}} & & -\frac{1}{R_{2,n}} \\ \vdots & \vdots & \ddots & \vdots \\ -\frac{1}{R_{n,1}} & -\frac{1}{R_{n,2}} & \cdots & \sum_{i=1}^{n} \frac{1}{R_{n,i}} \end{bmatrix} \quad (13)$$

This model is used in the final stage of the electromagnetic design of PMG temperature constraints are maximum permissible temperature of winding=120°C, and PM=100°C. If these constraints are satisfied, the design will be completed; otherwise the design process returns to the initial stage of the design routine and necessary modifications for the current density and magnetic flux density are made in order to decrease the heat and thus losses.

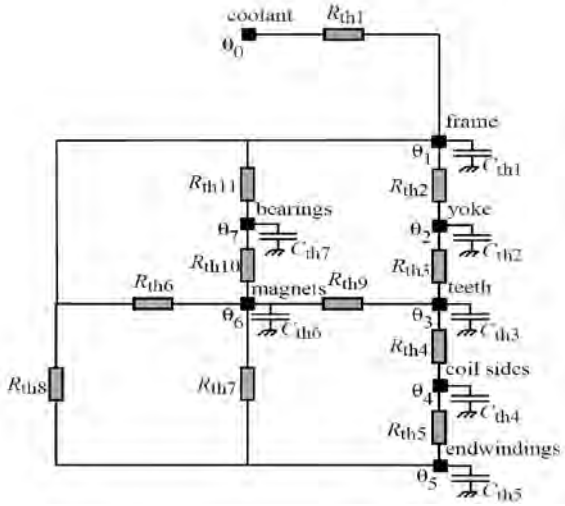

Fig. 1. Equivalent circuit of thermal model of PMG [18]

3.4. Cost Estimation for PMG Manufacturing

The cost of manufacturing a machine in an industrial plant is under influence of many factors such as identical built machines every year, technology and automation level used, organizing the product process, expense of the skilled labor, and quality of materials used. Since, here it is not possible to take into account all the above-mentioned factors in a mathematical model for cost estimation, a logical procedure is followed and the active materials of the machine are considered to evaluate the cost index and express it as a function of the dimensions of the PMG. The active materials of a PMG consist of PM, copper and iron used in the rotor and stator. Therefore, the cost index of a PMG is approximated as follows:

$$C_{total} = C_{PM}.\rho_{PM}.V_{PM} + C_{cu}.\rho_{cu}.V_{cu} + C_{fe}.\rho_{fe}.V_{fe} \quad (14)$$

where ρ is the density, V is the volume and C is the unit weight cost of the materials. The cost of each material includes: Iron 1.65 €, PM 50 € and Copper 3.1 €.

3.5. Synthetic Simulation Model

To study the impact of a rectified load upon the PMG operation, a synthetic comprehensive system consisting of simultaneous generator design routine and simulation has been proposed and applied. In this system, first the design routine calculates characteristics of the generator based on the proposed voltage, power, power factor and frequency; then turbine-generator-rectifier set included in Simulink receives the required data such as flux-linkage under each pole, resistance, inductance and poles number. At the end of simulation process, voltage waveform and performance characteristics of generator are determined. In this system, generator design algorithm is programmed. At the end of design routine, system model consisting of turbine, generator and rectifier system are implemented.

A 3 kW, 220 V, 50 Hz optimally designed PMG based on efficiency [9] is re-designed here in the presence of a nominal rectified load. The generator voltage waveform has been presented in Fig. 2. The results show that the harmonic distortion index of the voltage waveform is 15.5% which indicates the low quality output power of the PMG.

3.6. Optimization

As shown in Fig. 2, rectified load distorts the output voltage waveform and a genetic algorithm is implemented to improve the output voltage waveform. For this a fitness function based on the THD_v reduction is defined as follows:

$$Fitness\ Function = \frac{1}{THD_v} \tag{15}$$

Test designs on the wind PMG are obtained and the corresponding fitness functions are evaluated, then new design is generated by combining the best previous results. The PM residual flux density, ratio between the stack length and air gap diameter, PM arc, number of slot per pole per phase, magnetic permeance coefficient, specific electrical loading and current density are taken as design variables.

Also the range of variables values has been restricted to reasonable limits as shown in Table 1. Fig. 3 shows the obtained voltage waveforms based on the objective function of (15). Table 2 summarizes the design details of two generators. Referring to the obtained results in the design with optimal voltage, THD of voltage improves 9%. The induced voltage is Ldi/dt, and THD can be reduced by decreasing the number of winding turns.

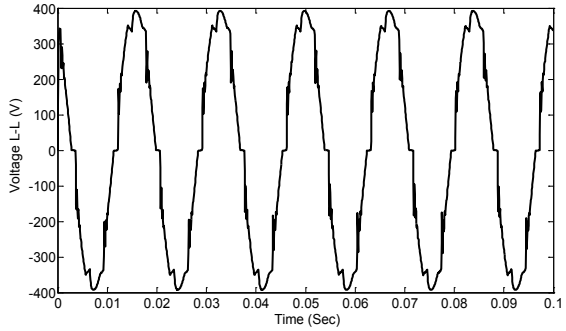

Fig. 2. Non-optimal induced line voltage of a generator under rectified load

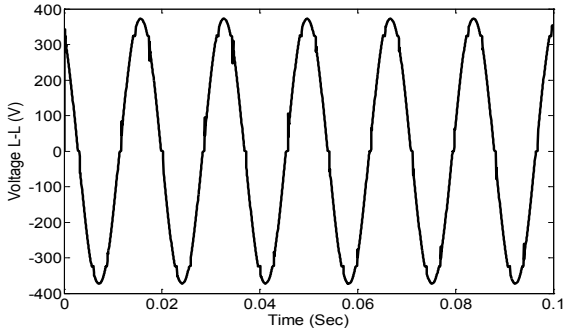

Fig. 3. Optimal induced line voltage of generator under rectified load

Also contribution of the PM arc in the pole of PMG rises in order to compensate the back-emf. Following these improvements, voltage distortion is reduced, but considering the increase *SEL* and *SML*, the magnetic loading is decreased to provide the required power. Consequents of these changes are: rising the iron losses due to the increase of the air gap flux

density, increasing the cost due to increase of PM volume, decreasing copper losses due to lower number of winding turns and resistance. Since the losses distribution in the optimal design of the PMG is subject to the change of the temperature rise of the six above-mentioned points, the PMG are in the permissible ranges

Table 1. Constraints of variables in optimization routine.

Parameter	Symbol	Value
PM residual density (T)	B_r	1-1.4
PM arc (ºElec)	A	90-170
Current density (A/mm^2)	J	3-8
Specific electrical loading (kA/m)	SEL	10-40
Air gap width to diameter ratio	k_L	0.2-1
Slot No./pole/phase	Q	1-2
Magnetic permeance coefficient	PC	5-16

Table 2. Comparison of design and performance of a 3 kW, 220 V and 60 Hz PMG with optimal efficiency and voltage in presence of rectified load (U=12 m/s).

Parameter	Symbol	Optimal Efficiency	Optimal Voltage
Shaft speed (rpm)	N_m	440/66	440/66
Generator stack length (m)	L	0.1437	0.164
Air gap diameter (m)	D	0.1437	0.232
PM arc (elec. Deg.)	A	144	157.5
PM height (m)	l_m	0.01	0.0183
PM residual flux density (T)	B_s	1.2	1.25
Phase winding no. of turns	N_{ph}	N_{ph}	176
No. of slots/phase/pole	q	1	2
Air gap length (m)	l_g	0.0011	0.0012
Winding diameter (m)	D_{cond}	0.0011	0.0013
Copper losses/Iron losses (W)	P_{cu}/P_{fe}	95.9/80.8	56.5/136.6
Power factor	Pf	91	93
Efficiency (%)	η	94.18	93.1
Air gap flux density (T)	B_g	0.72	0.79
Specific electric loading (kA/m)	SEL	30	10
Winding current density (A/mm^2)	J	5	3.64
THDv (%)	-----	15.5	5.7
Materials cost (€)	Cost	249.9	776.4
Stator winding resistance (Ω)	R_s	2.55	1.27
Stator winding leakage inductance (H)	L_l	0.003	0.00064
Stator winding mutual inductance (H)	L_m	0.005	0.0011

4. Conclusion

In this paper a comprehensive electromagnetic-thermal design algorithm for a wind PMG was presented. A combined model consisting of simultaneous generator design program and simulation in the presence of a rectified load was used to study the impact of this type of load upon the induced voltage distortion. Base on the presented model and genetic algorithm optimization routine, specifications of an optimal generator for improvement of the induced output voltage waveform of the PMG were obtained which leads to 9% decrease of the harmonic distortion index.

References

[1] L. Hansen, F. Blaabjerg, Conceptual survey of Generators and Power Electronics for Wind Turbines, Riso National Laboratory Report, December 2001.

[2] .Baroudi, V.Dinavahi, A.Knight, A Review of Power Converter topologies for Wind Generators, IEEE Conference on Renewable Energies, Canada, Sep. 2005.

[3] E. Spooner, A.C. Williamson, Direct-coupled, Permanent-magnet Generators for Wind Turbine Applications, IEE Proc. B, Electr. Power Appl., Vol. 143, pp. 1-8, Jan. 1996.

[4] M.R. Dubois, H. Polinder, J.A. Ferreira, Comparison of Generator Topologies for Direct-drive Wind Turbines, ICEM 92, pp. 761-765, Manchester, UK, 1992.

[5] M.R. Dubois, H. Polinder, J.A. Ferreira, Axial and Radial-Flux Permanent Magnet Generators for Direct-Drive Wind Turbines, EWEC, Copenhagen, Denmark, 2001.

[6] S. A. Papathanassiou, A. G. Kladas, M. P. Papadopoulos, Direct-Coupled Permanent Magnet Wind Turbine Design Considerations, European Wind Energy Conference (EWEC'99), Nice, France, 1999.

[7] N.F. Lombard, Design and Evaluation of an Ironless Stator Axial Flux PM Machine, M. Eng. Thesis, University of Stellenbosch, Matieland, South Africa, 1997.

[8] N. F. Lombard, M. J. Kamper, Analysis and Performance of an Ironless Stator Axial Flux PM Machine, IEEE Trans. Energy Conversion, Vol. 14, pp.1051-1056, Dec. 1999.

[9] M.A.Khan, Contributions to Permanent Magnet Wind Generator Design Including the Application of Soft Magnetic Composites, PhD. Thesis, University of Cape Town, 2006.

[10] M. R. Patel, Wind and Solar Power Systems, CRC Press,1999.

[11] Andreas Petersson, Analysis, Modeling and Control of Doubly-Fed Induction Generators for Wind Turbines, Ph.D. Dissertation, Chalmers University of Technology, 2005.

[12] M.A.Khan, P.Pillay, Design of a PM Wind, Optimized for Energy Capture over a Wide Operating Range, IEEE Conference on Electrical Machines and Drives, Spain, 2005.

[13] P. Lampola, J. Perho, Electromagnetic Analysis of a Low-Speed Permanent-Magnet Wind Generator, IEE Opportunity and Advances in International Power Generation Conf., pp. 55-58, 1996.

[14] N. Bianchi and A. Lorenzoni, Permanent Magnet Generators for Wind Power Industry: An Overall Comparison with Traditional Generators, IEE Opportunity and Advances in International Power Generation Conf., pp.49-54, 1996.

[15] T. J. E. Miller, Brushless Permanent-Magnet and Reluctance Motor Drives, New York: Oxford University Press, 1989.

[16] G. R. Slemon, Design of Permanent Magnet AC Motors for Variable Speed Drives, Tutorial Course of IEEE-IAS Annual Meeting,, Michigan: IEEE, 1991.

[17] S. Huang, J. Luo, F. Leonardi, and T. A. Lipo, A General Approach to Sizing and Power Density Equations for Comparison of Electrical Machines, IEEE Trans. Ind. Applications, vol. 34, pp. 92-97, Jan. / Feb. 1998.

[18] J. Lindstrom, Thermal Model of a P ermanent-Magnet Motor for a Hybrid Electric Vehicle, Ph.D. Thesis, Dept. of Electric Power Engineering, Chalmers University of Technology, Sweden, 1999.

Storage of Renewable Electricity through Hydrogen Production

Christoph Stiller[1], Patrick Schmidt[1], Jan Michalski[1,*]

[1] *Ludwig-Bölkow-Systemtechnik GmbH, Daimlerstr. 15, 85521 Munich/Ottobrunn, Germany*
** Corresponding author. Tel: +49 8960811041, E-mail:christoph.stiller@LBST.de*

Abstract: With more than 20 GW of installed wind power capacity installed in Northern Germany and more to come when offshore wind power expands, there are periods when the available wind power exceeds the grid capacity or even the electricity demand in reach. This excess wind power could be utilised for the electrolytic production of hydrogen, which can be stored and used as a transportation fuel, feedstock for the chemical industry, for re-electrification or for natural gas (NG) pipeline injection.
Based on the potential availability of excess wind power for hydrogen production and in view of the expected build-out, the paper drafts and discusses the economic framework and modalities of hydrogen production. Potential usages are discussed in general and specially for Northern Germany, where a hydrogen demand of 320 mill. Nm^3 was identified by 2020 for industry and transportation.
With some initial incentives, electrolytic hydrogen production can be made competitive by 2020. It is concluded that Northern Germany is an ideal region for the production of hydrogen from renewables due to the its high wind power density, its geologic conditions allowing for cavern storage, its industrial demand for hydrogen and also its pioneering role in hydrogen fuelled road transportation.

Keywords: *Hydrogen, Storage, Electrolysis.*

1. Introduction

With the increasing renewable power capacity, especially wind power, installed in many countries, there will be periods when the available power exceeds the capacity of the grid or even the demand in reach. This excess electricity may be eliminated by cutting down renewable power feed-in or, more advantageously, by adding additional temporal demand through electricity storage devices. In countries without excessive potential for pumped hydro storage, the storage technology with the highest energetic potential is offered by hydrogen. Hydrogen can be produced from electricity by water electrolysis and stored inexpensively in underground salt caverns where geologic conditions are suitable, or at higher costs in aboveground pressure vessels or liquid dewars. The hydrogen can be used for power generation when renewable generation is low, but also as a transportation fuel, as a feedstock for the chemical industry or other purposes. Therewith, hydrogen not only makes renewable electricity storable over long periods but also creates cross-links to other energy-intensive sectors.

This paper presents the main results of a recent study on the potentials of hydrogen production from wind power in Northern Germany [1], where more than 20 GW of wind power capacity are installed today and there will be tremendous increases in the coming years due to the expansion of offshore wind power. It will first review the current framework of the German electricity generation. Then, based on the expected electricity generation and demand, the amount of excess power available for hydrogen production will be estimated. This will be followed by a discussion of operation models for hydrogen electrolysis, rounded off by a discussion of required storage demand and possible uses and costs of the hydrogen.

2. General framework of the German electricity generation

Since 1990, electricity production in Germany has only increased by about 0.8% p.a. on average, and almost the entire surplus has been covered by renewable electricity [2].

Due to the age structure of the power plant park and in view of the previously planned nuclear phase-out, currently a large number of new fossil power plant projects (especially hard coal) are in the planning phase; yet, it needs to be mentioned that the realization of many projects is becoming ever more uncertain, partly due to the postponement of the nuclear phase-out but also due to decreasing public acceptance for infrastructure projects [3].

The share of renewables for electricity production in Germany has increased from 10 to 15% in only three years (2005-2008), and for 2011 the Transmission System Operators (TSOs) expect a total of 112 TWh renewable electricity, representing almost 20% of overall production [4]. Highest shares are being achieved in the North (e.g., in Schleswig-Holstein, renewable energy generation, mainly wind power, exceeds 40% of the electricity demand). Specifically in regions with high intermittent renewable capacities installed, already today grid capacity issues occur and wind turbine power need to be cut off temporarily in order not to cause grid breakdown (regulated in the renewable energy law as "feed-in management") [5]. Further extensive renewable potentials lie within repowering of onshore wind farms and the build-out of offshore wind energy use in the North and Baltic Sea.

By 2020, according to the "Lead scenario 2009" [6], 33 GW from onshore and 9 GW from offshore wind power are expected to be fed into the German grid. The offshore feed-in is expected to grow to 24 GW by 2030. Since all offshore capacity is landed in Northern Germany (mainly in Schleswig-Holstein and Lower Saxony) where also the density of onshore generation is high, this will at times cause massive excess power production. This implies grid reinforcement and extension to transmit the power to neighboring regions; however, even Germany-wide power production may exceed the demand and export capacities at times of low load and high wind.

Possible remedies are the temporal shift of loads by demand-side management and battery electric vehicles; however, potentials are limited both with respect to quantities and time periods over which the loads can be bridged [7]. Therefore, large-scale electricity storage will be urgently required in order to more easily integrate the further increase in intermittent renewable electricity generation into the grid.

3. Availability of excess power for hydrogen production

In order to analyse the potentials of hydrogen production from excess renewable electricity, the quantities of power surplus have to be estimated. In this sense "excess power/electricity" will be defined as the portion of power/electricity which cannot be utilised in times of high generation (renewable+fossil+nuclear) and low demand as well as export capacities of a region. In such cases the renewable generation will have to be cut off in order to assure grid stability. The quantity of excess power production depends mainly on the following four factors:

- Installed capacity of intermittent renewables, especially wind power. The feed-in of photovoltaics is less relevant in this context as it provides electricity during daytime where demand is comparatively high.
- Installed capacity of conventional power plants, especially base load plants. In particular, lignite and nuclear power plants are operated at high load also in times of high winds increasing the excess power. For example, during the night of October 4th, 2009, high wind volume and low electricity demand resulted in the negative spot market price of 0.50 €/kWh. Since at this time German nuclear power plants still operated at an average load of 77%, lignite at 65%, hard coal at 12% and natural gas at

9% [8] we assume this capacity utilization as the minimum practical part load of conventional plants during situations with excess electricity.

- Electricity demand and demand profile of the region. In general, the excess electricity can be reduced either by demand-side management or by an increased demand for a given level of power supply.
- Export capacity to neighbour regions. This is not only limited by the available transfer capacities, but also by the fact that adjacent regions are meteorologically linked. In this sense, excess wind power generation may occur not only in Northern Germany but also in other regions with own wind parks. In consequence, extension of grid capacity alone is not always effective to reduce excess power.

For the calculation of the excess power, specific assumptions regarding the capacity of energy generation per type and demand curves had to be made. The minimum generation of dispatchable power plants was derived from the estimated available capacity and the minimum part load numbers mentioned above. Onshore wind power curves were based on scaled Germany-wide production curves of the reference year 2008. Wind speed data from FINO platforms in the North and Baltic Sea were used in order to calculate the offshore power curves based on the characteristics of a 5 MW turbine. To estimate the electricity demand, hourly data from 2008 provided by UCTE / ENTSOE [9] were scaled to the respective future demand. Due to metrological linkages between adjacent regions, electricity export to neighbour countries was not considered as a way to use excess electricity. From the comparison of resulting generation and demand, the excess power generation could be estimated as shown in Figure 1.

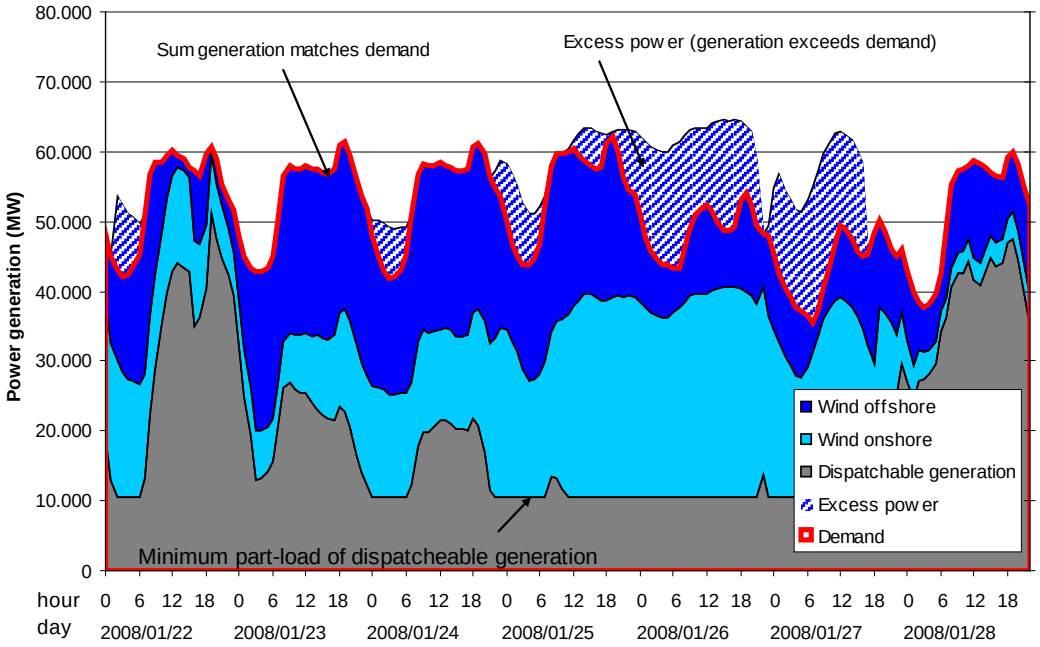

Fig. 1. Methodology to determine excess power (1 week displayed)

With this methodology, the excess electricity was estimated for different scenarios based on the generation and demand projections of the "Lead scenario 2009" [6]. Two variations from the lead scenario were considered: a scenario where 15 GW nuclear generation capacity would remain online (compensated by lower capacities of hard coal and natural gas), and an extreme scenario where the 2008 values for fossil and nuclear generation capacity and demand were frozen and the onshore and offshore generation capacity ramped up as in the

Lead scenario (33 GW onshore + 9 GW offshore by 2020, and 36 GW onshore + 24 GW offshore by 2030). Figure 2 shows the resulting excess power generation per year in Germany until 2030. In the lead scenario, only up to 9 TWh of excess electricity accrue until 2030 due to the consequent phase-out of fossil power plants. Retaining nuclear capacities will strongly increase excess electricity, and assuming that the power plant park of 2008 is retained while ramping up renewables, huge amounts of excess electricity will accrue until 2030. According to this estimation, by 2020 between 1.1 and 13 TWh of electricity (corresponding to 1.1-13% of overall wind power generation) cannot be used when they accrue and will therefore be available for energy storage in the form of hydrogen. For comparison, other authors with similar approaches have concluded that for whole Europe, 16 to 260 TWh excess power would accrue by 2020 [10]. Wietschel et al. [11] found that for Germany, 9 TWh excess power would accrue with 38.3 GW wind power installed, increasing to 28 TWh with 48.3 GW wind power installed.

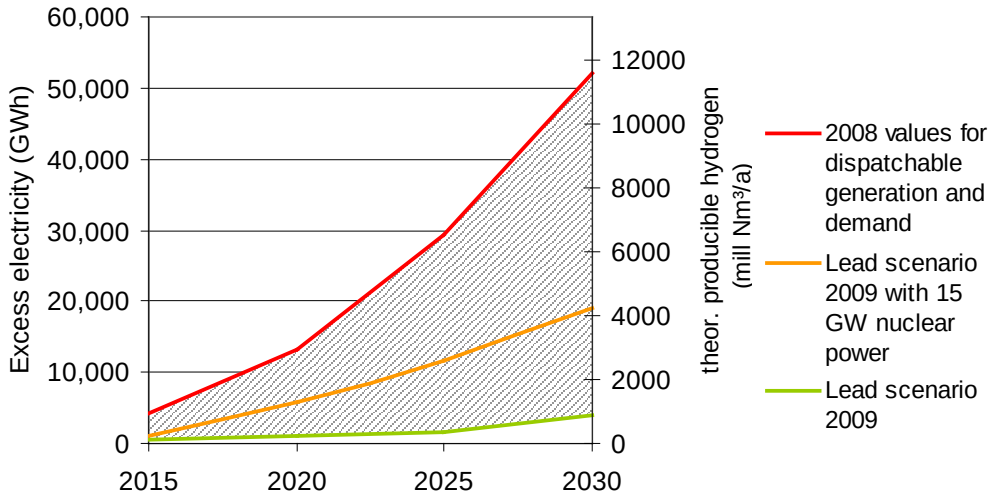

Fig. 2. Resulting excess power generation in Germany through 2030

4. Operation model for hydrogen production

Northern Germany is generally an ideal location for hydrogen production from renewables and large-scale storage due to the high concentration of wind power capacity and the geologic conditions facilitating the construction of underground salt caverns suitable for hydrogen storage. With the aim to develop a sound operation strategy for hydrogen production based on the use of excess electricity while at the same time unstraining the grid in the most economic way, the location of electrolysers as well as the economics of purchasing electricity (i.e. the connection to the electricity market) are the main criteria to be addressed.

In general there are three major options for the allocation of electrolysers: directly at the larger on- and offshore wind farms, at the end user location (e.g., an industrial sites or a hydrogen refuelling station) or at grid hubs of the high or ultra-high voltage grid in the areas with the highest wind loads and the heaviest loads on the grid (e.g., along the west coast of Schleswig-Holstein). Placement directly at the wind farms helps to unstrain the electric grid regionally and super-regionally, but hydrogen production is dispersed and the distribution to the consumers is comparatively complex, especially from offshore locations. Placement directly at the consumer site omits the transportation of hydrogen, but does not unstrain the electric grid between the wind farm and the consumer. Furthermore, access to large-scale storage caverns for longer-term storage of hydrogen cannot be provided easily in either of the distributed placement strategies. Therefore we assume that placing larger electrolysis plants at

grid hubs in areas with high wind power capacity is most beneficial, since this concept effectively unstrains the electric grid and allows for access to large-scale storage and efficient distribution of the produced hydrogen. The maximum electrolysis capacity installed at the grid hubs should be limited to a certain share of the upstream wind power. Figure 3 shows the scheme of a large-scale hydrogen storage plant (re-electrification by either CCGT or fuel cell is optional).

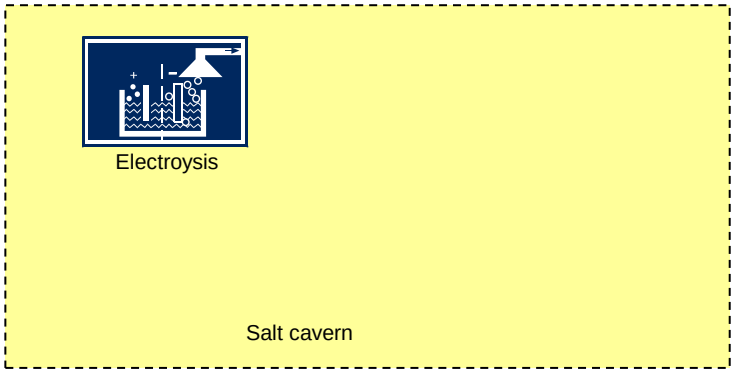

Fig. 3. Scheme of a hydrogen storage plant with optional re-electrification

As a price basis for the required electricity, either the feed-in tariffs for renewable electricity, or the day-ahead spot market hourly price curve of the European Energy Exchange (EEX) are reasonable. The latter can be interpreted either as purchasing the power at the EEX or directly from the wind farm operators, who otherwise would trade at EEX. Today, most wind power is fed in according to the fixed feed-in tariffs regulated by the German Renewable Energy Law. However, it can be expected that by 2020 the fixed feed-in tariffs will have been changed into market premiums, and most wind power will be directly traded at the spot market. Moreover, the spot market price represents the balance between electricity demand and supply: in times of low demand and high renewable energy generation the spot market price will be low, and vice versa. Hence, taking the spot market price as a base for electricity purchases ensures the operation of electrolysers in a way which indirectly unstrains the grid by using the excess electricity at low costs. As a simple operation strategy, electrolysers may be operated at full load during hours when the price is below a certain threshold, and may be kept in warm stand-by mode when the price is above the threshold. The number of operation hours per year and the average electricity price paid then depend on the price threshold set.

Further revenues for hydrogen producers can result from control reserve, since electrolysers represent a controllable load within the power grid. An electrolyser can be turned off or switched on upon request in order to provide positive or negative control reserve. The provision of the so-called “minute reserve” is tendered jointly by the transmission system operators (TSO) in Germany in 4-hour blocks for the following day. It is important to mention that the pure provision of control power (without actually being called) is already compensated by a per-MW rate. While tendering for control reserve brings additional revenues to the hydrogen production, it also increases the administration effort; since the control reserve is awarded at 10:00 AM for the next day, and the day-ahead spot market auction is at noon, the operator has to rely on a forecast of the spot market price in order to

decide whether the electrolyser should be operated during every 4 hour block (i.e. tender positive control reserve), or not (i.e. tender negative control reserve). Once control reserve has been awarded, the electrolyser must be operated according to the plan, even if electricity prices differ from the forecast. Therefore and due to the implication to operate in 4-hour blocks, the average electricity price levels will be somewhat higher if control reserve is to be provided.

A further benefit for the hydrogen producers can be achieved by directly utilising stranded wind power from turbines which otherwise would need to be temporarily cut down due to local grid restrictions (so-called "feed-in management"), provided that there are no grid restrictions between the wind turbines and the electrolysers. However, the TSOs are obliged to reinforce the power grid in order to avoid such events; hence, the potential benefits from this strategy are limited and uncertain.

5. Required storage demand, options for usage of the hydrogen, and costs

A strategy as described above will lead to a variable electrolyser utilisation with a tendency to higher production in the winter time with high wind power feed-in. In order to optimally level out the seasonal variations in production and facilitate a constant delivery of hydrogen to the end customers we found that a hydrogen storage capacity of approximately 700 full load hours is needed. If the hydrogen consumption can be adapted to the availability (higher consumption in winter than in summer), the storage capacity can be lower; on the other hand, if the hydrogen consumption is inflexible and peaks in summer, the storage capacity will need to be higher. Generally, the economic optimum of design storage capacity will be a trade-off between storage costs and timely flexibility of electrolysis operation (leading to savings in electricity costs). In the case of large-scale storage in salt caverns, the storage only contributes a minor part to the overall costs; however, if storage in e.g. aboveground pressure vessels or liquid hydrogen dewars is chosen, then the costs will be a multiple of the electrolysis costs.

A viable use of the renewable hydrogen is the partial or complete substitution of hydrogen generated from natural gas for uses in chemical and process industry. Besides saving fossil primary energy for hydrogen production by reforming, this has the potential to reduce the greenhouse gas emissions of the industries, improving their carbon footprint and avoiding costs of CO_2 certificates. Furthermore, hydrogen-powered road transportation will be an emerging market in the mid term. Offering renewable hydrogen at the refuelling stations to be erected is an interesting option, especially when considering the fact that the consumers might prefer "green hydrogen" and could also be forced by legislation (California has already implemented a law that 33% of all hydrogen for transportation will need to be renewable).

By screening the hydrogen consuming industry and using estimates on the hydrogen demand for road transportation, we have identified a demand potential of about 320 mill. Nm^3 hydrogen from wind power in the federal states Hamburg and Schleswig-Holstein by 2020 [1]. Based on lower heating value, this represents an energy of 960 GWh, which equals about 4.5% of the overall industrial final energy use in this region today. For the production and distribution of the hydrogen, about 1.55 TWh of electricity would be needed per year that could be predominantly supplied from excess electricity. The use of the this amount of renewable hydrogen in industry and transportation in Hamburg and Schleswig-Holstein instead of fossil hydrogen would save about 320.000 tons of CO_2-equivalent emissions. Beyond this, there might be potential to export renewable hydrogen, e.g. as a transportation fuel to other regions in Europe.

Based on current technology, the specific costs of hydrogen production from wind energy in Schleswig-Holstein including distribution will, depending on quantity and location of the consumption, amount to 0.42-0.75 €/Nm³ by 2020 (0.14-0.25 €/kWh of lower heating value). This is about 0.12-0.32 €/Nm³ more than the cheapest supply from fossil energy sources today. However, in the case of an incentive-supported early implementation of electrolytic hydrogen production, hydrogen from wind energy can become competitive by 2020, mainly through the rise of fossil energy prices and the cost reduction potentials of electrolysis.

A further use of the hydrogen could be used for power generation (so-called re-electrification) in combined cycle gas turbines or fuel cells. Re-electrification is a way to stabilise the electric grid by not only taking away power in times of excess renewable electricity but also providing backup power to compensate lack of renewable generation, e.g. in times of low wind. Co-firing gas turbines with natural gas at flexible shares is technically feasible. Also, the injection of hydrogen into the natural gas grid to substitute a certain part of the natural gas is possible. Almost all NG end users can tolerate hydrogen fractions up to 5% by volume (representing 1.6% by energy) without modifications. From the NG grid perspective, mainly the process gas chromatographs will have to be modified in order to detect hydrogen. In a future scenario, also up to 20% by volume hydrogen could be admixed to natural gas [12].

6. Conclusion

The paper showed that due to the ongoing build-out of intermittent renewable generation capacity and limited part-load ability of dispatchable power plants, significant amounts of excess electricity will accrue in the German electricity system in the future. This excess energy may be used to generate hydrogen, which can then be economically stored in large-scale salt caverns and utilized in industry and transportation sector or for electricity generation at times of low feed-in of renewables. An operation model based on central electrolysis plants at grid hubs, the spot market as a price basis for electricity purchases and a threshold-price strategy can yield minimum overall hydrogen production costs and at the same time facilitate effective unstraining of the grid.

Northern Germany is an ideal region for the production of hydrogen from renewables due to the its high wind power density, its geologic conditions allowing for cavern storage, its industrial demand for hydrogen and also its pioneering role in hydrogen fuelled road transportation (Berlin, Hamburg). Hydrogen storage is the only technology that can provide sufficient storage potential (multi-TWh) in Germany for a fully renewable electricity system. With some initial incentives, electrolytic hydrogen production can be made competitive within some years after the start of its deployment.

References

[1] C. Stiller, P. Schmidt, J. Michalski, R. Wurster, U. Albrecht, U. Bünger, M. Altmann, Potenziale der Wind-Wasserstoff-Technologie in der Freien und Hansestadt Hamburg und in Schleswig-Holstein. A study commissioned by Wasserstoffgesellschaft Hamburg e.V., Free and Hanseatic city of Hamburg (represented by the Administration of Urban Development and Environment), and the federal state of Schleswig-Holstein (represented by the Ministry of Science, Economics and Transport). Ludwig-Bölkow-Systemtechnik, March 2010. Available at: http://www.h2hamburg.de/index.php?page=download.

[2] M. Reichmuth, G. Schröder, R. Pohl, A. Scheuermann, A. Schiffler, A. Weber, Jahresprognose 2011 zur deutschlandweiten Stromerzeugung aus regenerativen

Kraftwerken. Available at: http://www.eeg-kwk.net/cps/rde/xbcr/eeg_kwk/2010-10-12-IE-EEG-Jahresprognose2011.pdf

[3] Hamburger Abendblatt, 11 December 2009: Climate protectors cheer: No power plant in Lubmin (in German: "Klimaschützer jubeln: Kein Kraftwerk in Lubmin"). http://www.abendblatt.de/wirtschaft/article1304949/Klimaschuetzer-jubeln-Kein-Kraftwerk-in-Lubmin.html

[4] Arbeitsgemeinschaft Energiebilanzen e.V.: Electricity generation by energy carriers 1990 to 2008 (in TWh) Germany, Status 27 May 2009; http://www.ag-energiebilanzen.de/viewpage.php?idpage=65

[5] Act Revising the Legislation on Renewable Energy Sources in the Electricity Sector and Amending Related Provisions – Renewable Energy Sources Act (EEG 2009) –official document, Federal Law Gazette (Bundesanzeiger) 2008 I No. 49, Bonn, 31 October 2008, p. 2074.

[6] German Federal Ministry for the Environment, Nature Conservation and Nuclear Safety: Lead scenario 2009. http://www.bmu.de/files/pdfs/allgemein/application/pdf/leitszenario2009.pdf

[7] M. Klobasa, Nachfrageseitige Regelungsmöglichkeiten im Energiesystem; in: EnInnov 08, 10. Symposium Energieinnovation. Energiewende: 13.-15. Februar 2008; TU Graz: Verlag der TU Graz, 2008; ISBN: 978-3-902465-94-8, pp. 89-90

[8] EEX Transparency data, power plant information (visited October 2009); available at: http://www.eex.com/en/Transparency/Power%20plant%20information

[9] European Network of Transmission System Operators for Electricity: Hourly load values of a specific country for a specific month; available at: http://www.entsoe.eu/index.php?id=92, visited October 2009

[10] C. Hoffmann, M. Greiner, L. Von Bremen, K. Knorr, S. Bofinger, M. Speckmann, K. Rohrig, Design of transport and storage capacities for a future European power supply system with a high share of renewable energies. IRES Conference 2008, Berlin, 24-25 November 2008.

[11] M. Wietschel, U. Hasenauer, N. Juncà Vicens, M. Klobasa, P. Seydel, Ein Vergleich unterschiedlicher Speichermedien für überschüssigen Windstrom. Zeitschrift für Energiewirtschaft 30 (2006) 2, pp. 103-114.

[12] J. Hüttenrauch, G. Müller-Syring, Zumischung von Wasserstoff zum Erdgas. Energie-Wasser-Praxis 10/2010, pp. 68-71; available at: http://www.gat-dvgw.de/fileadmin/gat/newsletter/pdf/pdf_2010/03_2010/internet_68-71_Huettenrauch.pdf

Combined cycle plants as support for wind power

N. Afonso Moreira[1*], A. Borges[1], A. Machado[2]

[1] *CITAB – Universidade de Trás-os-Montes e Alto Douro, Vila Real, Portugal*
[2] *Sonorgás – Departamento de I&D, Vila Real, Portugal*
** Tel: +351 932 505 044, E-mail: nam@utad.pt*

Abstract: The growing interest in diversifying the energy sources used, the major environmental objectives established, and the need to reduce the current European energy dependence, have been causing a growing and significant increase in betting on renewable energy sources. Thus recent years have witnessed a continuous increase of installed power from sources like solar, biomass, photovoltaic, wind, Biofuels, biogas among other.
The integration of renewable energy is mainly in the production of electrical power, in which has already a significant contribution. In the group of renewable energy sources used for the production of electrical power wind is the source that has registered further progress, and is also expected, that represents in the future, large part of the electric energy produced by renewable energy sources.

Although the wind helps to meet many of the problems, it's also presents some disadvantages, or constraints. Among the best-known disadvantages associated with wind, as noise and visual impact, stands out as the major technical problems the flashing of its production. The inability to predict the production of wind, leads to problems in securing demand, as well as in network integrity.

In this scenario the Combined Cycle Gas Turbine (CCGT) stands out as a great complement to wind power. Their ability to quickly put into operation, as well as the advantages that technology and fuel used presents, makes it the optimal solution to integrate with the wind energy.

Keywords: *Combined cycle plants, wind power,*

1. Introduction

In the last decade it has been attended an increasing interest on renewable energy sources. This trend is mainly in response to the increased consumption of fossil fuels, to the problem of security of supply and still to tackle the environmental problems caused by such consumption. Alternative power plants, as the solar, biomass and wind energy are the great trends. However in the majority of the cases the alternative energies are incapable to support, alone, the existing demand, forcing then, a combination with other fossil fuels like natural gas, oil, etc.

Natural gas emerged as the best fuel to be used in partnership with renewable. Its combustion gives low emission levels of pollutants, ash free, the content of carbon monoxide (the most responsible for acid rain) is practically zero and the levels of NO_x formed are well below the values of any other fossil fuel. Additional in its combustion, CO_2 emissions (responsible for the greenhouse effect) are much lower than other fuels, may even make the comparison between the products of combustion and respiration of the human (CO_2 and H_2O). For this reasons natural gas is the best option to use in support to renewable energy.

Since 1990 gross electricity generation from renewable energy sources (RES) in Europe grew significantly. Among new renewable (excluding large hydropower), wind power has the largest addition to renewable energy capacity. One of the main disadvantages of wind power is that wind is very unpredictable. Strength can vary from none to storm force. Therefore, wind turbines are unable to produce a continuous amount of electricity during the time, creating problems with network stability, and uncertainty regarding the availability of energy.

The combination of natural gas combined cycle plants and wind power is a good answer to grid stability problems and makes the whole system more secure. Gas is used as a back-up to overcome the intermittency of wind power.

2. Renewable energy policies in Europe

In the last decade, the number of countries that exploit renewable energy production has increased exponentially, and wind energy has been highlighted as a promising and attractive option among the other renewable energy sources.

Renewable have a long history of European policies and associated measures. Since 1986 the European Commission has listed among its objectives the promotion of community renewable energy [1]. In 1997 set the goal of achieving a target of 12% renewable energy by 2010. Most recent measurements, as the document "AN ENERGY POLICY FOR EUROPE" [2], published in 2007, amends the targets for 20% integration of renewable energy by 2020 and 10% integration of renewable energy in the transport.

2.1. European policies for wind power

The 20% target means that more than one-third of the EU's electricity will come from renewable sources in 2020 – up from 16% in 2006. By 2020, wind energy is expected to have overtaken hydropower as the EU's largest source of renewable electricity (Table 1).

Table 1. Renewable contribute to EU electricity consumption in 2020 [3].

Type of energy	2005	2020 - Targets	
	TWh	TWh	%
Wind	70,5	477	34,8
Hydro	346,9	384	28
Photovoltaic	1,5	180	13,1
Biomass	80	250	18,3
Geothermal	5,4	31	2,3
Solar thermal elect.	---	43	3,1
Ocean	---	5	0,4

To achieve this objective, the EU adopted a new Renewable Directive in April 2009, which set individual targets for each member state. In response to the Directive 2009/28/EC [4] member countries in 2010 presented its National Action Plan for Renewable Energy [5]. This plan sets national targets for 2020 relating to the share of energy from renewable sources consumed in transport, power generation and heating and cooling (Figure 1).

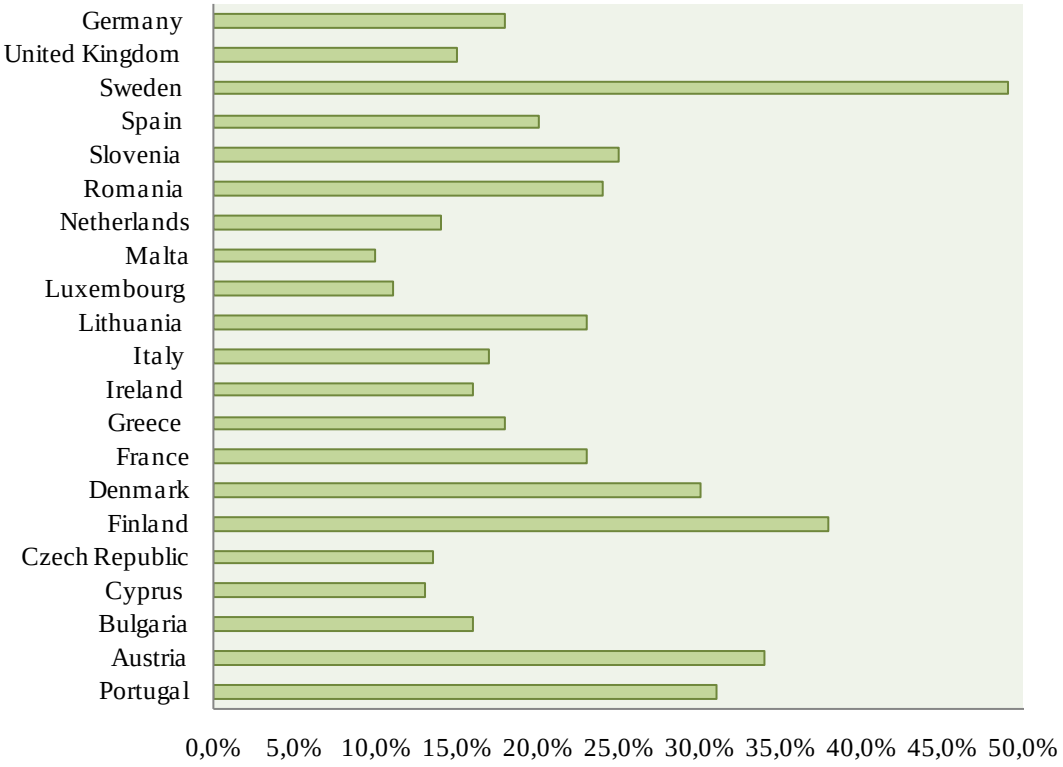

Fig. 1. Targets for Renewable Energy inclusion in final energy consumption in 2020.

With few exceptions, the field of electric energy production is the sector which foresees a greater share of energy produced by renewable energy sources. Wind energy stands out as a renewable energy source with greater participation (figure 2), and on average, excluding countries like the Czech Republic and Finland that does not estimates wind power production, the average of European countries to integrate wind power in 2020, as estimated targets, is approximately 42.3%.

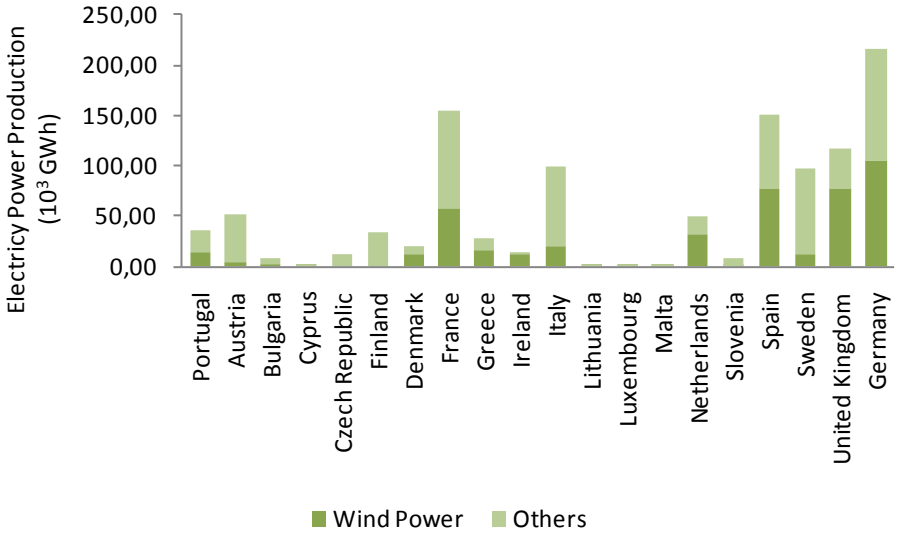

Fig. 2. Targets for Wind Power and others in electricity power production.

2.2. European wind energy tariffs

In most EU member states electricity utilities now buy electricity generated from renewable sources produced by individuals and companies. Prices paid for 'self-produced' electricity is called a feed-in tariff.

Table 2. Fee-in tariffs on member state in 2010 (€/kWh) [6].

Member state	Windpower 'On-shore'	Wind power 'Off-shore'	Solar PV	Biomass	Hydro
Austria	0.073	0.073	0.29 - 0.46	0.06 -0.16	n/a
Belgium	n/a	n/a	n/a	n/a	n/a
Bulgaria	0.07 - 0.09	0.07 - 0.09	0.34 - 0.38	0.08 - 0.10	0.045
Cyprus	0.166	0.166	0.34	0.135	n/a
Czech Republic	0.108	0.108	0.455	0.077 - 0.103	0.081
Denmark	0.078	0.078	n/a	0.039	n/a
Estonia	0.051	0.051	0.051	0.051	0.051
Finland	n/a	n/a	n/a	n/a	n/a
France	0.082	0.31 - 0.58	n/a	0.125	0.06
Germany	0.05 - 0.09	0.13 - 0.15	0.29 - 0.55	0.08 - 0.12	0.04 - 0.13
Greece	0.073	0.073	0.29 - 0.46	0.06 -0.16	n/a
Hungary	n/a	n/a	n/a	n/a	n/a
Ireland	0.07 - 0.09	0.07 - 0.09	0.34 - 0.38	0.08 - 0.10	0.045
Italy	0.166	0.166	0.34	0.135	n/a
Latvia	0.108	0.108	0.455	0.077 - 0.103	0.081
Lithuania	0.078	0.078	n/a	0.039	n/a
Luxembourg	0.051	0.051	0.051	0.051	0.051
Malta	n/a	n/a	n/a	n/a	n/a

The rates of remuneration for wind energy are generally among the lowest rates of pay for electric energy produced by renewable sources in EU countries. The exceptions are Estonia, Latvia and Lithuania who practice the same tariffs for electricity produced by renewable energy sources, and Denmark, where the remuneration of the energy produced by wind is greater than the produced from biomass.

3. Development of installed capacity and production of wind and combined cycle plants power

During 2009, 10,526 MW of wind power was installed across Europe, of which 10,163 MW in EU countries. This represents growth in the EU of approximately 15, 5% compared with the values of installed power in 2008 (figure 3).

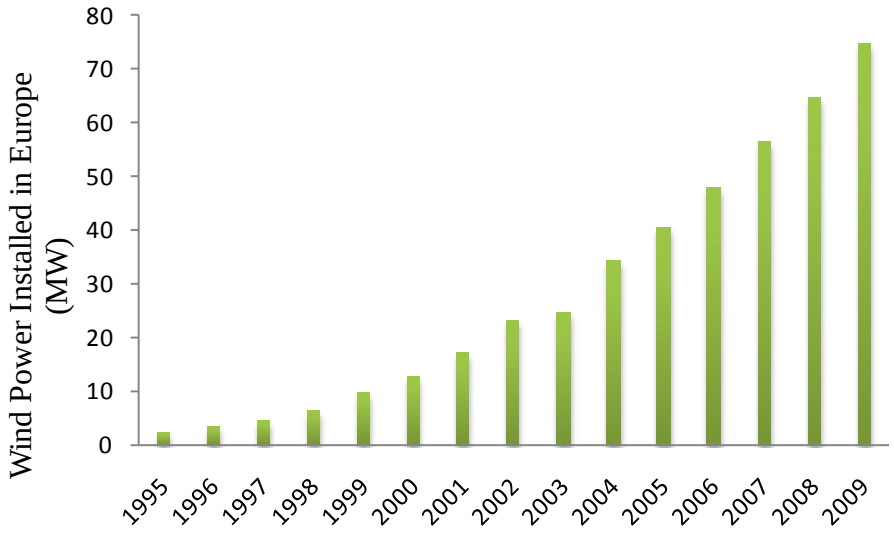

Fig. 3. Wind Power Installed in Europe [7].

The facilities in Europe are characterized by a continuous development in mature markets like Spain and Germany, along with countries like Italy, France and the UK. In 2007, production of electrical power through the wind reached a value of 104.3 GWh in the European Union [8].

Spain is the second EU country with the highest installed capacity of wind power. In 2009 it had an installed capacity of 18 GW, double the number counted in 2005 (figure 4).

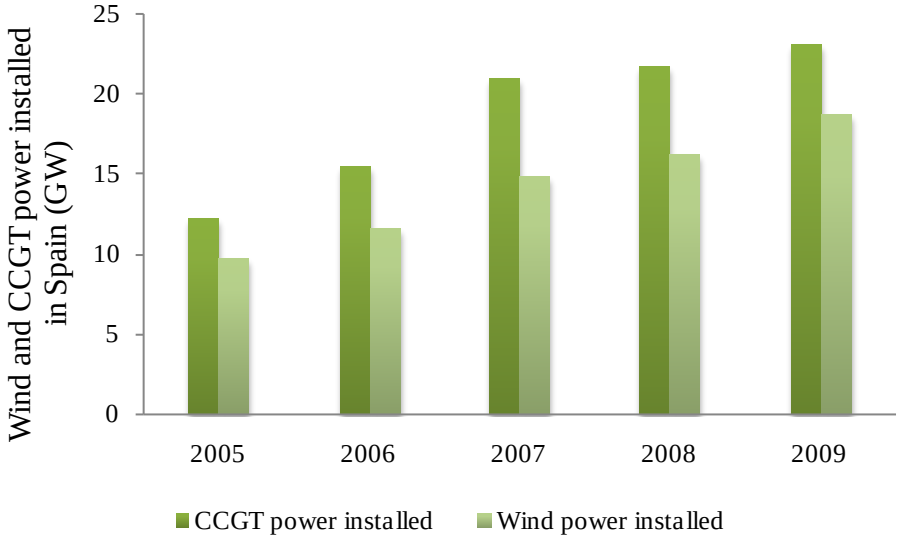

Fig. 4. CCGT and Wind Power Installed in Spain [10].

Many of the world`s electric utilities and independent power producers are turning to gas turbine combined-cycle power technology for new capacity. The major reasons for the predominance of this technology are high efficiency, moderate capital cost, low environmental impact, favorable natural gas prices and short construction schedules. Recent advances in gas turbine technology allow for a combined-cycle efficiency of almost 60 percent. The turbines used in Combined Cycle Plants are commonly fuelled with natural gas, which is found in abundant reserves in several countries. Natural gas is becoming the fuel of

choice for private investors and consumers because it is more versatile than coal or oil and can be used in 90% of energy applications.

In the last decade, most countries concentrated their power generation investments in gas-fired power plants, especially combined-cycle gas turbines (CCGT). The document "European Energy and Transport - Trends to 2030" [9], indicates that the CCGT plants accounted for about 51% of total investment in power plants combined, between 2005 and 2010. Also according to the estimates presented in this document, in 2030 the CCGT plants will reach a total installed capacity of 145 GW in Europe.

A country that reflects the growing interest and increasing investment in CCGT plants is Spain. In 2005 Spain had a total installed capacity of 12 GW of CCGT, in 2009 reached 23 GW, which represents an increase of 88% (figure 4).

4. Correlation Analysis

Although wind energy has many advantages, like being a renewable source of energy, not emissions of greenhouse gases, among other well-known advantages, also has considerable disadvantages. The disadvantages more marked are the related to visual and noise pollution caused by the same; however to technical level the biggest disadvantage of wind power is the intermittency of production. That is, wind does not present a continues production, as it is not possible to predict in advance with will be its real production.

For this reason, it is necessary to resort to so-called support system. The support system is a complementary system to the wind power, than is able to put into operation that is, to produce electrical power, in case of failure of electric power generation by wind energy, ensuring availability to demand.

The most common support systems used to support wind power plants are Combined Cycle Gas Turbine. This choice is justified by the use of a fuel that although is a fossil fuel, has great advantages when compared to the other, as well as the highly effective technology applied.

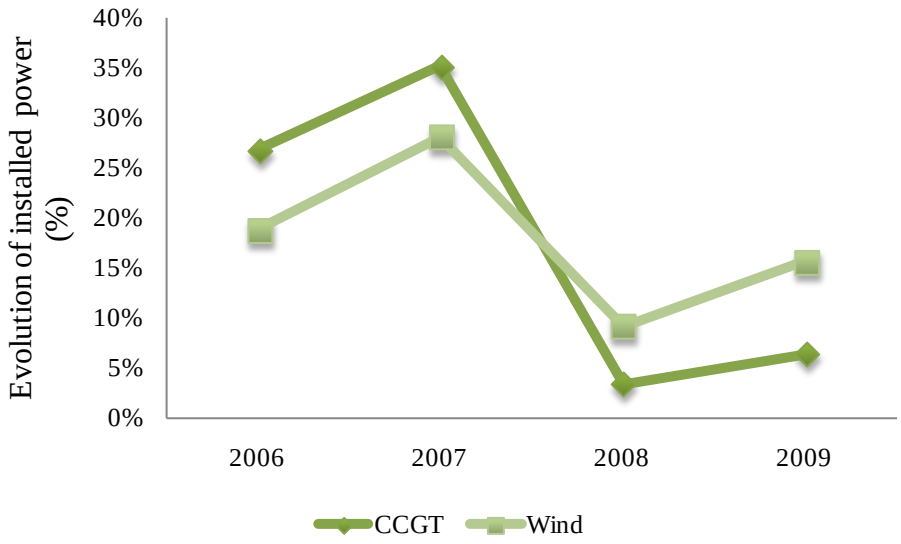

Fig. 5. CCGT and Wind evolution of installed power in Spain [10].

As we can see by the analysis of figure 5, the evolution of installed power to CCGT and wind power is very similar. Both forms of energy have a significant increase of installed power to the scheduled between 2006/07 and 2008/09, and both show a decrease in the growth of installed capacity in 2008.

In the year 2007, which corresponded to the years where there was a greater increase of installed power, CCGT reached a total installed capacity of 20 GW, corresponding to an increase of 5.5 GW compared to the previous period, and the energy wind power grew by 3.2 GW, reaching a total of 14.8 GW.

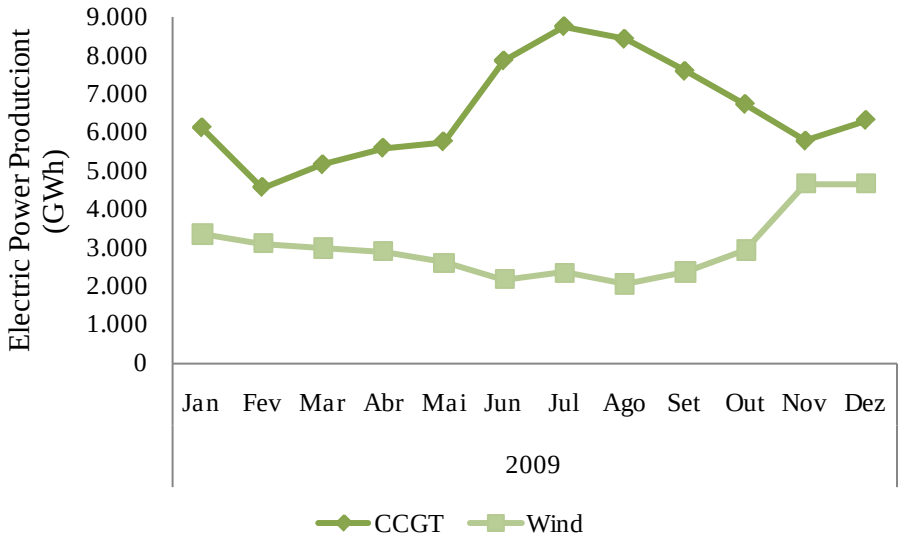

Fig. 6. CCGT and Wind electric power production in Spain [11].

As we can see by the analysis of the previous figure (Fig. 6) the electricity produce by CCGT follows the production of electric power by wind. That is, whenever there is a decrease in wind generation, the CCGT start working to remedy this breach. With the increase of electricity generation by wind, CCGT production decreases.

Thus the intermittency of electricity generation by wind does not because failures in the availability of energy and do not create problems in the network integrity.

5. Development Perspectives

According to estimates the installed capacity of wind power will tend to continue to increase. The figures for Europe are that the production of electricity by wind power to reach 477 TWH in 2020.

Assuming that the trends are maintained, the increase in installed capacity of CCGT will also maintain its growth trend, and is also expected that due to the development of technology associated with CCGT this increase will be even higher than expected. With current technology, the CCGT are already the best option to serve to support the production of other renewable energy sources, specifically through the production of wind energy.

References

[1] Official Journal C 241, 09/25/1986 p. 0001 - 0003;

[2] COM (2007) 1 final; 2007;

[3] European Renewable Technology Roadmap 2008;

[4] Directive 2009/28/EC of the European Parliament and the Council of 23 April 2009

[5] http://ec.europa.eu/energy/renewables/transparency_platform/action_plan_en.htm

[6] Price for Renewable Energies in Europe; Report 2009; European Renewable Energies Federation.

[7] Wind in power - 2009 European statistics; The European Wind Energy Association; February 2010

[8] European Environment Agency; 2008

[9] European Energy and Transport - Trends to 2030; European Commission; Directorate-General for Energy and Transport; 2007.

[10] El sistema eléctrico espanõl; RED ELÉCTRICA DE ESPANÃ; 2010

[11] Boletin Mensual; RED ELÉCTRICA DE ESPANÃ; 2010

Learning a wind farm power curve with a data-driven approach

Antonino Marvuglia[1,*], Antonio Messineo[2]

[1] *CRP Henri Tudor/CRTE, 66 rue de Luxembourg, L-4002 Esch/Alzette, Luxembourg*
[2] *Faculty of Engineering & Architecture, Kore University of Enna, Italy*
**Corresponding author. Tel: +352 425991652, Fax: +352 425991555, E-mail: antonino.marvuglia@tudor.lu*

Abstract: Improving the performance of prediction algorithms is one of the priorities in the wind energy research agenda of the scientific community. In a very simplistic approach, short-term predictions of wind power production at a given site could be generated by passing forecasts of meteorological variables (namely wind speed) through the so-called wind farm power curve, which links the wind speed to the power that is produced by the whole wind farm. However, the estimation of this conversion function is indeed a challenging task, because it is nonlinear and bounded, in addition to being non-stationary due for example to changes in the site environment and seasonality. Even for a single wind turbine the measured power at different wind speeds is generally different to the rated power, since the operating conditions on site are generally different to the conditions under which the turbine was calibrated (the wind speed on site is not uniform horizontally across the face of the turbine; the vertical wind profile and the air density are different than during the calibration; the wind data available on site are not always measured at the height of the turbine's hub).

The recent developments in data mining and evolutionary computation (EC) offer promising approaches to modelling the power curves of turbines. In this paper we use a self-supervised neural network called GMR (Generalized Mapping Regressor) to learn the relationship between the wind speed and the generated power in a whole wind farm. GMR is an incremental self-supervised neural network which can approximate every multidimensional function or relation presenting any kind of discontinuity. The approach used is a data driven one, in the sense that the relationship is learned directly from the data, without using any explicit physical or mathematical relationship between input and output space. The model is potentially applicable to any site, provided that a statistically consistent amount of wind and power data is available. The methodology allows the creation of a non-parametric model of the power curve that can be used as a reference profile for on-line monitoring of the power generation process, as well as for power forecasts.

The results obtained with the proposed approach are compared with another state-of-the-art data mining algorithm (namely, a feedforward Multi Layer Perceptron) showing that the algorithm provides fair performances if a suitable pre-processing of the input data is accomplished.

Keywords: *Wind farm, Power curve, Data-driven, Neural network, Machine learning*

1. Introduction

An interesting aspect of current research on wind power generation is the definition and implementation of accurate models to predict the energy output of a whole wind farm, rather than single wind turbines. In power systems a traditional generator is usually described as 'dispatchable', whereas wind generation is often referred to as 'non dispatchable'. Even though wind power generation has reached maturity in power systems, it is often still considered as a negative load because it is less predictable than thermal generation [1; 2].
Accurate wind power forecasting and prediction reduces the risk of uncertainty and allows for better grid planning and integration of wind into power systems.

There has been much debate and discussion in relation to the costs associated with wind power integration. A common conclusion is that as the levels of wind power penetration increase additional system balancing is required. Wind power forecasting and prediction tools are therefore invaluable because they enable better dispatch, scheduling and unit commitment of thermal generators, hydro plant and energy storage plant and more competitive market trading as wind power ramps up and down. Overall they reduce the financial and technical risk of uncertainty of wind power production for all electricity market participants.

Researchers have applied different methodologies in studying wind farms. In [3] the author built a model to predict the power produced by a wind farm using the data from the weather prediction model (HIRLAM) and the local weather model (WASP). In [4] a regression and a neural network (NN) model are compared in order to estimate a turbine's power curve. A novel approach for the analysis and modelling of wind vector fields was introduced by Goh et al. [5] and developed by Mandic et al. [6]. In these papers the wind vector is represented as a complex-valued quantity and wind speed and direction are modelled simultaneously. In [7] a new algorithm based on fuzzy logic was applied to estimate wind turbine power curve. In [8] a variety of different approaches have been used to build prediction models and characterize power curves of a wind farm by a nonlinear parametric model. In [9] parametric and non-parametric models have been applied for the same task and results have been compared. An extensive review of the existing wind speed and related generated power forecasting approaches can be found in [10].

The key issue addressed in this paper is the estimation of the relationship between the wind speed and a wind farm power output. This relationship is expressed as a power curve, which has a logistic function shape. However, as discussed in [8], the experimental power curve of a wind turbine (and of an entire wind farm as well) is not an ideal logistic function. All regions outside of the logistic curve represent either power losses or power gains. The presence of outliers and abnormal values might be due to several reasons: the presence of values of wind speed close to the cut-in or the cut-out speed of the installed wind turbines; environmental issues (blades affected by dirt, bugs and ice); shut-down due to maintenance or energy curtailment; control system issues; sensors malfunctions; pitch control malfunctions; unsuitable blade pitch angle setting; blade damage [8; 11]. Finally, the measured powers at different wind speeds are generally different than the rated power also because the operating conditions on site are generally different than the conditions under which the turbine was calibrated (the wind speed on site is not uniform horizontally across the face of the turbine; the vertical wind profile and the air density are different during the operation phase than during the calibration; the wind data on site are not always measured at the height of the turbine's hub). Moreover, due to the nonlinearity of the wind farm power curve, the uncertainty in its estimation dramatically amplifies the uncertainty contained in the wind speed forecasts. If the model of a power curve reflecting a normal status was available, the abnormal status of a turbine could be monitored and detected by this model.

The main motivation of this paper lies in the detection of the abnormalities of the wind turbines (and as a consequence also wind farms as a whole) power curve. The recent developments in data mining and evolutionary computation (EC) offer promising approaches to modelling turbines power curves. In this paper we use a self-supervised neural network called GMR (Generalized Mapping Regressor) [12; 13] to learn the relationship between the wind speed and the power generated in a wind farm. GMR is an incremental self-supervised neural network which can approximate every multidimensional function or relation presenting any kind of discontinuity. The approach used is a data driven approach, in the sense that the relationship is learned directly from the data, without using any explicit physical or mathematical relationship between input and output space. The methodology allows the creation of a non-parametric model of the power curve that can be used as a reference profile for on-line monitoring of the power generation process, as well as for power forecasts.

2. Methodology

GMR is an incremental self-organizing neural network with chains (second layer weights) among neurons. The basic idea of GMR is to transform the function approximation problem

into a pattern recognition problem under an unsupervised framework. Hence, a coarse-to-fine covering strategy of the mapping is used. Suppose we want to model the mapping relationship between a set of inputs **x** and a set of outputs **y**. GMR algorithm works transforming the data mapping problem *f*: $\mathbf{x} \rightarrow \mathbf{y}$ into a pattern recognition problem in the augmented space *Z* represented by vectors $\mathbf{z} = [\mathbf{x}^T \ \mathbf{y}^T]^T$, which are the inputs of GMR. In this space, the branches of the mapping become clusters which have to be identified.
The algorithm comprises four phases (training, linking, merging, and recalling) which are schematized in Fig. 1.

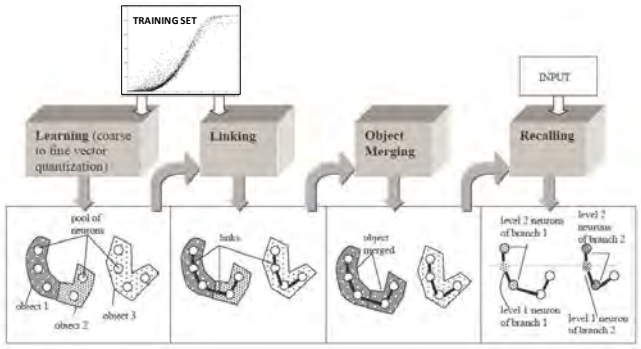

Fig. 1. The four phases of the GMR algorithm.

The ***training phase*** concerns the *vector quantization* of the *Z* space. The aim of vector quantization is, in practice, the reduction of the original data set to a small representative set of prototype vectors that are easier to manage [14]. During training, the augmented space is recovered by either creating neurons or adapting their weights according to the novelty of the input data. At the presentation of each input belonging to the training data set (TS), there are two possibilities: either creation of a new neuron (whose weight vector is equal to the input vector) or adaptation of the weight vector of the closest neuron (in input/weight space). Given a threshold ρ (*vigilance threshold*), a new neuron is created if the hyperspheres of radius ρ, centered in the already created weight vectors, do not contain the input. The parameter ρ is very important: it determines the resolution of training. Learning can be divided into two sub-phases: *coarse quantization* and *fine quantization*. The vigilance threshold used in the coarse quantization phase (ρ_1) is higher than the one used in the fine quantization, ρ_2. In general, the first epoch (i.e. presentation of the entire TS) defines the number of neurons needed for mapping and the others adapt their weights for a better approximation. The neurons thus obtained identify the *objects*, which are compact sets of data in *Z*. The resulting neurons are called *object neurons*. In the second sub-phase, at first a pre-processing is required for labelling each neuron with the list of the input data which had the neuron as winner (i.e. whose weight vector is the closest to the input vector); it can be accomplished by presenting all data (*production phase*) to GMR and recording the corresponding winning neurons. At the end, for each neuron a list of the inputs for which it won is stored. This list represents the *domain* of the object neuron. Every list is considered as the TS for a subsequent training which takes place separately (and in parallel) for each object domain. At the end, the neural network is made up of the neurons generated by the secondary learning phases (*final neurons*), labelled as belonging to an object by the corresponding object neuron.

The next phase is the ***linking phase***. Neurons' linking is accomplished by computing the second layer weights, which are discrete and equal to zero in the absence of a link. A link is computed at the presentation of each piece of data from the TS. The technique used in this paper to perform the linking phase exploits the direction of the principal component of the domain data (i.e. the direction corresponding to the highest eigenvalue of the autocorrelation matrix of the domain data) [12]. This direction is here referred to as domain *principal*

direction (PD). For each data point, the weights are sorted according to the Euclidean distance from it, and the winning neuron is determined. It is then linked to another neuron chosen in a subset of neurons (*candidate neurons*). The subset was here determined by defining in advance a number *k* of nearest neighbours of the input. Then, for each candidate, the absolute value of the scalar product between its PD and the winner's PD is evaluated. The winner is linked to the candidate yielding the maximum scalar product (i.e., the candidate whose PD is closest in direction to the winner's PD). This approach is justified by the fact that clusters with similar shapes have to be connected.

In the ***merging phase***, GMR checks whether different objects are linked. If they are, the objects are merged. The ***recalling phase*** replaces the neurons in the reduced manifold with Gaussians representing the domain. Their parameters are estimated by the maximum likelihood (ML) technique. This phase is essentially a process of Gaussian labelling followed, if required, by an interpolation step. A more detailed description of GMR is contained in [12].

3. Results

The data used for the case study refer to a wind farm (whose location is not disclosed for confidentiality reasons) and the available data set comprises a wind speed time series (one whole year) measured by an anemometer located at 50 m above the ground level (a.g.l.), as well as the power produced by each of the wind turbines, collected by a SCADA (Supervisory Control and Data Acquisition) systems at the wind farm. Since the aim of the study was modelling the power curve of the wind farm as a whole, the sum of the power produced by all the turbines was used for the application of the proposed algorithm. A training and a test set containing respectively 90% and 10% of the entire time series available (randomly selected across the whole data set) were created. In order to speed up the training, a sampling of one datum out of three was then made on the training set (TS), so to select a smaller subset (that was used as the actual TS). Before starting the training phase, the data which had been clearly recorded erroneously, due to a malfunctioning of the SCADA system, were filtered out (namely, data with an abscissa greater than the cut-in speed of the wind turbines and with a null ordinate). The remaining data were normalized in the interval [–1; +1] and denoised using the Kernel Principal Component Analysis (KPCA) technique with a bandwidth of the Gaussian kernel $\sigma = 0.4$. KPCA is a *generically nonlinear* signal processing technique; it is often used for denoising in image applications [15]. The denoised TS used to train GMR contains 2828 observations. A test data set containing 876 observations has been used in the recalling phase. Figure 2 shows the data before (a) and after (b) the normalization and denoising procedure. The data showed in Fig. 2(a) have been previously rescaled, only for visualization purposes, in order to protect data confidentiality.

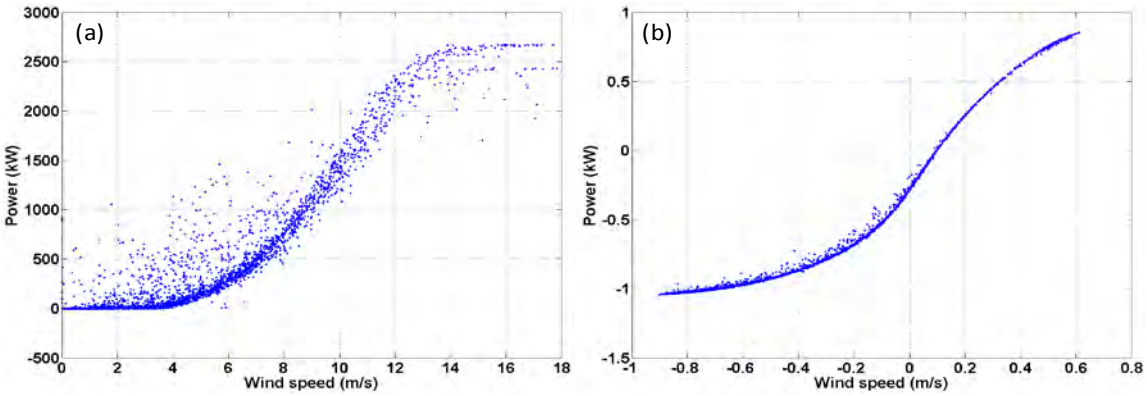

Fig. 2. Training set data before (a) and after (b) normalization and denoising.

A number of nearest neighbours k=4 was used during the linking phase. In the rough phase the vigilance threshold was set to $\rho_1 = 0.5$ and in the fine tuning phase $\rho_2 = 0.025$ was used. The number of final neurons is 101 and the number of object neurons is 26. During the recalling phase, GMR was used both without interpolation and with Gaussian interpolation. Figure 3 shows the results of the linking and merging phases of GMR. A zoom of the part of the curve contained in the dashed box is showed in the upper left and lower right corners of Fig. 3(b). In the lower right corner different objects are represented with different symbols to improve readability.

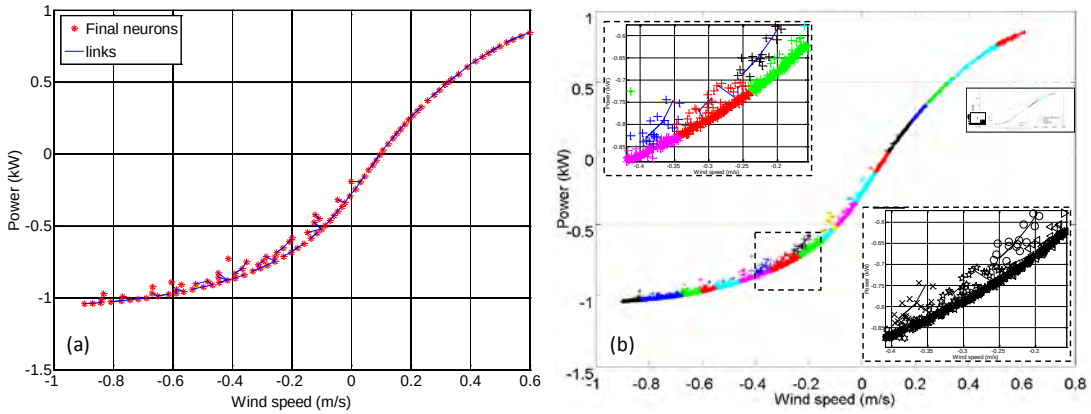

Fig. 3. Results of the linking (a) and merging (b) phases of GMR.

The same TS used for the GMR model was also used to train a feedforward Multi Layer Perceptron (MLP). The learning algorithm used is backpropagation with momentum [16]. The network has two layers of neurons, the hidden layer with 10 and the output layer with 1 neuron (since the output is mono-dimensional). A logistic sigmoid function and a linear function were respectively used as the activation function of the first and the second layer.
Figure 4 shows the results of the modelling obtained both on the TS and test set data, with the two models, while Table 1 summarizes their prediction accuracy.

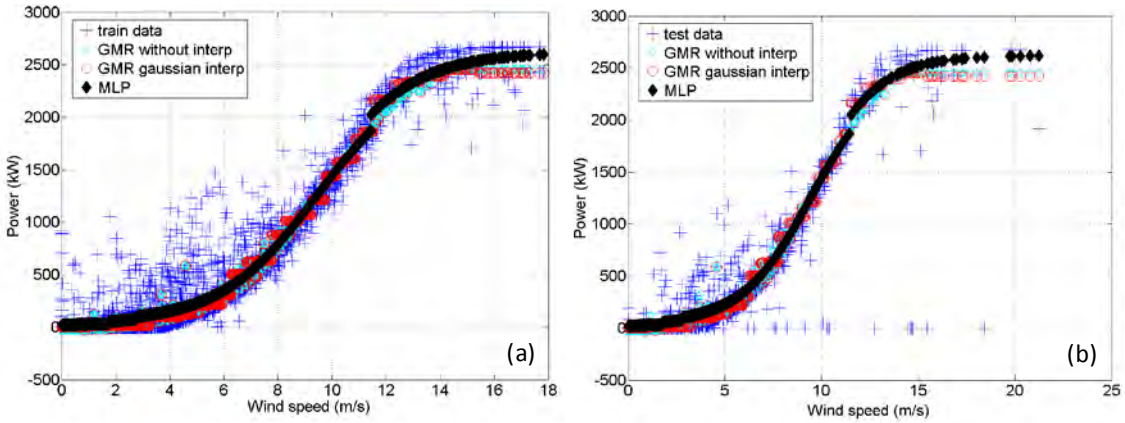

Fig. 4. Results of the GMR and MLP predictions on the training set (a) and the test set (b).

Their performances have been assessed computing the mean absolute error (MAE) and the symmetric mean absolute percentage error (sMAPE), using the test set data. The respective standard deviations (Std dev, in Table 1) have also been computed.
The sMAPE measure computes the absolute error in percent between the absolute value of the actual observation y_t and the absolute value of the forecast $\hat{y}_t$ across all observations t of the test set of size n [17]:

$$sMAPE = \frac{1}{n}\sum_{t=1}^{n}\frac{|y_t - \hat{y}_t|}{(|y_t| + |\hat{y}_t|)/2} * 100 \quad (1)$$

The MAE of MLP is worse than the one of the two GMR models, because GMR recognizes that the "thickness" of the data cloud around the average logistic sigmoid trend actually contains some information content and it is not just due to noise (see the links in Fig. 3(a)), whereas the MLP follows the average trend of the data, thus finding a smooth curve profile.

Table 1. Prediction accuracy of the models applied (GMR and MLP).

	MLP	GMR gaussian interp	GMR without interp
MAE (kW)	1990.60	436.11	458.63
Std dev of AE (kW)	2515.40	918.34	906.40
sMAPE (%)	68.03	64.19	68.35
Std dev of sMAPE (%)	76.25	73.73	76.40
minimum AE	71.79	1.02	0.47
maximum AE	9159.40	8585.10	8585.10

3.1. On-line monitoring by residual approach and control charts

Once the two non-parametric models mentioned above have been trained, they can be used to characterize the wind farm power in normal conditions, and therefore they can serve as an on-line wind farm power generation profile. The residual control chart techniques (statistical quality control) [18] are used to analyze residuals between model predicted power and observed power. The control chart approach allows the residuals and their variations to be monitored, thus detecting abnormal conditions of a turbine.

The means of the residuals obtained on the TS (μ_{Train}) and the test set (μ_{Test}), as well as their standard deviations (σ_{Train}; σ_{Test}) were computed. Once μ_{Train} and σ_{Train} are known, the upper and lower control limits of the control chart can be computed and used to detect the anomalies. Control limits for the control chart can then be derived using Eq. (2) [18]:

$$UCL_1 = \mu_{Train} + \eta\frac{\sigma_{Train}}{\sqrt{N_{Test}}}; \quad LCL_1 = \mu_{Train} - \eta\frac{\sigma_{Train}}{\sqrt{N_{Test}}} \quad (2)$$

N_{Test} is the number of points in the test data set, but it can be adjusted to make the control chart less sensitive to the data variability and thus reduce the risk of false alarms. The parameters in Eq. (2) could be adjusted dynamically, based on ope rations of individual turbines. In the application described in this paper, N_{Test} was set equal to 10, while η was set to the widely used value $\eta = 3$ [9]. If μ_{Test} is above UCL_1 or below LCL_1, the power generation process at the generic sampling time $y_{TestSet} = [y(i), \hat{y}(i)]$ is considered to be deficient (or "out-of-control"), otherwise it is not considered abnormal, i.e. it is considered "in-control". Similarly, the control limits for σ^2_{Test} can also be calculated to detect out-of-control points, using control limits defined as a function of the variance of σ^2_{Train} [8; 9; 18].
Figure 5 shows the out-of-control points detected in the TS by GMR and the MLP on the basis of the limits defined by Eq. (2). Out of the 876 points of the test set, GMR detected 183 out-of-control points, while the MLP network detected 136 of them. It is possible to notice that GMR in this case is more conservative in the part of the curve closer to the cut-off wind speed. This is due to the choice of the parameters η and N_{Test}, but also to the fact that the MLP model tends to find a smooth solution, passing between the two data clouds in the last part of

the curve, whereas GMR remains closer to a constant value of the output power for wind speeds equal to or higher than the cut off speed, as it should be in case of ideal functioning of the turbines. It is also possible to notice that GMR detects some of the points above the left tail of the curve as "in-control" points, while MLP labels them as "out-of-control". This is due to the fact that GMR finds some links and, as a consequence, some branches of the mapping, also in this zone of the space (see Fig. 3). This is reasonable and in line with the results found in [9] using a parametric model and a non-parametric model based on the k-nearest neighbour (k-NN) algorithm. In fact, one of the main advantages of GMR, compared with feedforward neural networks, lays into the fact that, while for many functional (i.e. single-valued) approximation problems feedforward network can work well by minimizing a sum-of-squares error function, they can actually give rise to high imprecision in presence of multi-valued mappings, or mappings whose structure varies for different regions of the input space. The prominent feature of GMR is its capability to output all the solutions and their corresponding mapping branches.

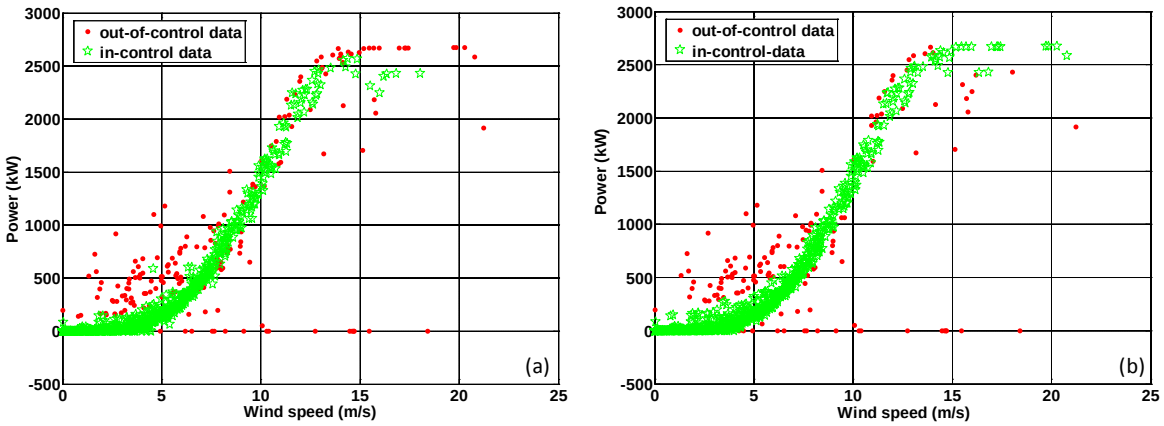

Fig. 5. Data (within the test set) detected as "in-control" and "out-of-control" according to the limits defined in Eq. (2), using GMR with Gaussian interpolation (a) and MLP (b).

4. Conclusions

The paper presents an application of a data-driven technique for mapping the power curve of a whole wind farm and shows its utilization for the creation of quality control charts. The results obtained with the proposed methodology are compared with those obtained with a "traditional" non-parametric method: a MLP neural network. A few other applications have already been presented in the literature, dealing with the same topic. The originality of this paper is twofold: on one hand, its application to the modelling of the power curve of an entire wind farm, instead of a single wind turbine; on the other hand, the utilization of GMR, which is an incremental self-organizing competitive neural network with adaptive linking among neurons, able to approximate every kind of mapping (function or relation) in both senses, i.e. $M(x,y): x \in \Re^m \leftrightarrow y \in \Re^n$. The models can be used as the reference power curve (on-line profile) for monitoring the performances of a w ind farm as a whole. In a real, on-line application, the models will be updated using the most current operational data.

The case study here presented demonstrated that the control chart approach produces satisfactory results in monitoring power curves. In future research, other data mining algorithms will be assessed for enhancing accuracy of non-parametric models. In particular, the application of Bayesian networks will be considered to identify links between anomalies and the specific reasons causing them, which is not possible simply using control charts.

References

[1] R.M.G. Castro, A.F.M. Ferreira, A comparison between chronological and probabilistic methods to estimate wind power capacity credit, IEEE Trans Pow Syst 16(4), 2001, pp. 904-909.

[2] P. Børre Eriksen, T. Ackermann, H. Abildgaard, P. Smith, W. Winter, J. Rogríguez García, System operation with high wind penetration, IEEE Pow Energ Magazine, November/December 2005.

[3] L. Landberg, Short-term prediction of the power production from wind farms, Journal of Wind Engineering and Industrial Aerodynamics 80(1-2), 1998, pp. 207–220.

[4] S. Li, D.C. Wunsch, E. O'Hair, M.G. Giesselmann, Comparative analysis of regression and artificial neural network models for wind turbine power curve estimation, J Solar Energ Engineering 123(4), 2001, 327–332.

[5] S.L. Goh, M. Chen, D.H. Popović, K. Aihara, D. Obradovic, D.P. Mandic, Complex-valued estimation of wind profile, Renew Energ 31, 2006, pp. 1733–1750.

[6] D.P. Mandic, S. Javidi, S.L. Goh, A. Kuhc, K. Aihara, Complex-valued prediction of wind profile using augmented complex statistics, Renew Energ 34, 2009, 196–201.

[7] T. Üstütaş, A.D Şahin, Wind turbine power curve estimation based on cluster center fuzzy logic modelling, Journal of Wind Engineering and Industrial Aerodynamics 96, 2008, pp. 611–620.

[8] A. Kusiak, H. Zheng, Z. Song. Models for monitoring wind farm power, Renew Energ 34, 2009, pp. 583–590.

[9] A. Kusiak, H. Zheng, Z. Song, On-line monitoring of power curves, Renew Energ 34, 2009, pp. 1487–1493.

[10] M. Lei, L. Shiyan, J. Chuanwen, L. Hongling, Z. Yan, A Review on the Forecasting of Wind Speed and Generated Power, Renew Sust Energ Rev 13(4), 2009, pp. 915-920.

[11] B. Bell, Individual wind turbine and overall power plant performance verification, San Diego, CA, 2008.

[12] Cirrincione G, Cirrincione M, Lu C, Van Huffel S. A novel neural approach to inverse problems with discontinuities (the GMR neural network), Proceedings of 2003 Int. J Conf Neural Networks (IJCNN'03), Portland, Oregon, pp. 3106–3111.

[13] C. Lu, The Generalised Mapping Regressor (GMR) neural network for inverse discontinuous problems, MSc Thesis, 2000, Katholieke Universiteit Leuven (Belgium).

[14] R.M. Gray, Vector quantization, IEEE ASSP Magazine 4(2), 1984, pp. 4–29.

[15] A.R. Teixeira, A.M. Tomé, K. Stadlthanner, E.W. Lang. KPCA denoising and the pre-image problem revisited, Digit Signal Process 18, 2008, pp. 568–580.

[16] M.T. Hagan, H.B. Demuth, M.H. Beale, Neural network design, PWS Publishing, 1996.

[17] S. Haykin, Neural Networks – A Comprehensive Foundation, Prenctice Hall, Upper Saddle River, 1999.

[18] D.C. Montgomery, Introduction to statistical quality control, John Wiley & Sons, New York, 5th ed. 2005.

Dynamic stall for a Vertical Axis Wind Turbine in a two-dimensional study

R. Nobile[1,*], M. Vahdati[1], J. Barlow[1], A. Mewburn-Crook[2]

[1] *University of Reading, Reading, UK*
[2] *Wind Dam Renewables Ltd, Swansea, UK*
***** *Corresponding author. Tel: +44 1183784666, E-mail: r.nobile@reading.ac.uk*

Abstract: The last few years have proved that Vertical Axis Wind Turbines (VAWTs) are more suitable for urban areas than Horizontal Axis Wind Turbines (HAWTs). To date, very little has been published in this area to assess good performance and lifetime of VAWTs either in open or urban areas. At low tip speed ratios (TSRs<5), VAWTs are subjected to a phenomenon called 'dynamic stall'. This can really affect the fatigue life of a VAWT if it is not well understood. The purpose of this paper is to investigate how CFD is able to simulate the dynamic stall for 2-D flow around VAWT blades. During the numerical simulations different turbulence models were used and compared with the data available on the subject. In this numerical analysis the Shear Stress Transport (SST) turbulence model seems to predict the dynamic stall better than the other turbulence models available. The limitations of the study are that the simulations are based on a 2-D case with constant wind and rotational speeds instead of considering a 3-D case with variable wind speeds. This approach was necessary for having a numerical analysis at low computational cost and time. Consequently, in the future it is strongly suggested to develop a more sophisticated model that is a more realistic simulation of a dynamic stall in a three-dimensional VAWT.

Keywords: *Vertical Axis Wind Turbine (VAWT), Urban Area, Computational Fluid Dynamics (CFD), Dynamic Stall, Turbulence Model*

Nomenclature

N	*number of rotor blades*	λ	*tip speed ratio* $(\Omega R/ U_\infty)$
c	*airfoil/blade chord* ..... *mm*	θ	*azimuth angle* ..... *deg*
t	*thickness of the blade* ..... *mm*	α	*angle of attack* ..... *deg*
s	*span of the blade* ..... *mm*	V	*relative wind speed* ..... *m/s*
R_r	*radius of rotor* ..... *mm*	ω	*rotational speed* ..... *rad/s*
R_m	*radius of central mast* ..... *mm*	*PIV*	*Particle Image Velocimetry* .....
U_∞	*undisturbed velocity* ..... *m/s*	Ω	*rotation frequency/vorticity* ..... *rad/s*

1. Introduction

In the last few decades, the production of electricity from wind turbines has seen a rapid growth in many countries around the world. The major drivers are the recent need to reduce CO_2 emissions into the atmosphere and meet the growing demand for electricity [1]. One promising alternative for the future generation of electricity is the installation and integration of wind turbines in the built environment combined with other alternative sustainable systems [2], [3]. The benefits are mainly generation of electricity on the site where it is needed with reduction in transmission losses and cable costs [3].

In the late 1970s and early 1980s, very little research was conducted on V AWTs on understanding the aerodynamics and flow interaction between blades during the operation of a wind turbine [4]. Recently, the progress of small wind turbines in the built environment has been mainly focused on Horizontal Axis Wind Turbines (HAWTs) rather than Vertical Axis Wind Turbines (VAWTs). But several studies have shown that VAWTs are more suitable for urban areas than HAWTs [3], [5], [6], [7]. The advantages are mainly: omni-directional without a yaw control, better aesthetics to integrate into buildings, more efficient in turbulent environments and lower sound emissions [8]. In addition there is some research speculating

that VAWTs are appropriate for large scale of 10 MW or more, as VAWTs can operate mechanically better than HAWTs [9], [10]. They can withstand high winds due to their aerodynamic stall behaviour [5]. Generally, the aerodynamic analysis of a VAWT is very complicated, as the blades are called on to operate in unsteady flow, pitching relative to the mean flow and cutting the stream tube twice [5]. One important aspect to consider during the operation of a VAWT at low wind speeds is the generation of a phenomenon called dynamic stall. The phenomenon is mainly characterised by the development of vortices that will interact with the airfoil of the blades and have a substantial impact on the design and power generation of the wind turbine [11].

The main purpose of this work is to understand how ANSYS CFX 12.0 is able to approach the development of dynamic stall around the blades of a VAWT. Also, the final objective of the numerical study is to make a contribution in the field of dynamic stall as many straight-bladed VAWTs are called to operate. In this paper a number of simulations are explored to understand static and dynamic stall around the rotor of a 3 straight-bladed VAWT. To reduce time and memory costs a 2 -D case is explored for all numerical simulations. The Computational Fluid Dynamics (CFD) Software used was ANSYS CFX 12.0. Here, the three turbulence models analysed were the k-ε model, the standard k-ω model and the SST (Shear Stress Transport) model. The numerical simulations were studied for different tip speed ratios and compared with the small amount of experimental data available in literature.

2. Methodology

In order to understand the physics involved during dynamic stall of a straight-bladed vertical Darrieus wind turbine, a 2-D rotor is proposed and analysed. This 2-D approach is adopted for reducing time and computational costs. The airfoil analysed, for the VAWT, is a NACA 0018 and its characteristics are listed in Table 1. The rotor is composed of 3 blades and a central mast. The solid model of the rotor was generated with ProEngineer 4.0 and imported into ANSYS CFX 12.0.

Table 1: Properties of the rotor

NACA0018					
Cord c (mm)	Thickness t (mm)	Span s (mm)	Rotor Radius R_r (mm)	Number Blades N	Mast Radius R_m (mm)
490	88.2	50	3000	3	75

The mesh, as shown in Figure 1, is mainly composed of three sub-domains: one fixed sub-domain outside the rotor, one dynamic sub-domain around the blades of the rotor and one fixed sub-domain for the remaining part of the rotor. The mesh was generated by adopting a Sweep Method with one element deep and the total number of elements is 4.58×10^5, as listed in Table 2.

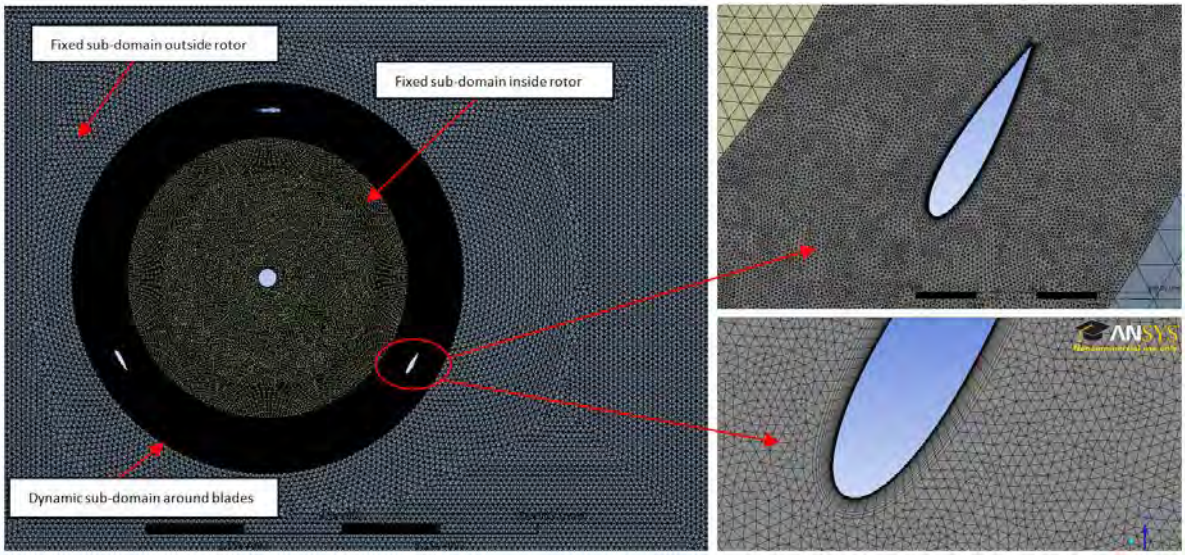

Fig. 1. Mesh for the 2-D rotor

Table 2. Sub-domain properties

Sub-domain	Number of elements
1) Fixed sub-domain outside rotor	$20*10^3$
2) Dynamic sub-domain around blades	$42*10^4$
3) Fixed sub-domain inside rotor	$18*10^3$
Total number of elements	$4.58*10^5$

All sub-domains were meshing by using only triangle elements, as they are more appropriate for simulations involved fluids [12]. The mesh around the blades of the rotor, which is a wake development region, was refined through the use of the facing sizing and inflation options available in ANSYS 12.0. In this region, the use of prism elements is able to capture boundary layer effects more effectively and efficiently. The three different meshes were linked together with the use of domain interfaces. Symmetrical boundaries were used for the top and bottom parts of the 2-D model with no-slip boundary conditions at the two sides. An opening boundary was chosen for the output and a constant wind speed of 6 m/s, with a turbulence intensity of 5%, was defined for the inlet. The two wall sides were placed at 4c from the diameter of the blades respectively. The outlet and inlet were placed 4c and 10c away respectively. Table 3 gives a summary of the parameters employed in the four different cases where different time steps and tip speed ratios (TSRs) were defined. For all transient simulations a total time was defined to give enough time for the flow to develop around the blades of the rotor. Finally, the residual target, in the convergence criteria, was set to be 10^{-4}.

Table 3. Input data for the four cases analysed

Simulation Case	Tip speed ratio	Angular speed (rad/s)	Time for one rotation (s)	Angle of attack (deg.)	Time Step Simulation (s)
Case 1	$\lambda_1=2.3$	$\omega_1=4.7$	$t_1=1.33$	$-30\leq\alpha_1\leq30$	0.0037
Case 2	$\lambda_2=3.0$	$\omega_2=6.0$	$t_2=1.05$	$-21\leq\alpha_1\leq21$	0.0029
Case 3	$\lambda_3=4.0$	$\omega_3=8.0$	$t_3=0.78$	$-15\leq\alpha_1\leq15$	0.0022
Case 4	$\lambda_4=5.0$	$\omega_4=10$	$t_4=0.63$	$-12\leq\alpha_1\leq12$	0.0017

The effect of different TSRs are presented and discussed in the conclusions section of this paper.

2.1. Dynamic Stall

Although VAWTs have several advantages over HAWTs, the aerodynamics around the blades is very complicated [11]. VAWTs, during their operation, are called to work under both static and dynamic stall conditions. Consequently, the blades are subjected to cyclic forces due to the variation of incidence angle of the blade relative to the wind direction [13]. Although the presence of dynamic stall at low TSRs can have a positive impact on the power generation of a wind turbine, the formation of vortices can generate other problems such as vibrations, noise and reduction of fatigue life of the blades due to unsteady forces [13]. Larsen et al. [14] show that dynamic stall is mainly characterised by flow separations at the suction side of the airfoil. This can be summarised in four crucial stages: 1) Leading edge separation starts, 2) Vortex build-up at the leading edge, 3) Detachment of the vortex from leading edge and build-up of trailing edge vortex, 4) Detachment of trailing edge vortex and breakdown of leading edge vortex. The sequence of these four flow events will generate unsteady lift, drag and pitching moment coefficients with a large range of flow hysteresis dependent on the angle of attack [15]. The expression of the angle of attack α adopted for the simulation, without induction factor, is given by Eq. (1):

$$\alpha = \arctan\left(\frac{\sin\theta}{\lambda - \cos\theta}\right) \tag{1}$$

where θ is the azimuth angle and λ the TSR. In this study, as shown in Table 3, four different cases are analysed with different parameters that are highly dependent on the TSRs.

2.2. Turbulence Models

Wang et al. [16] show that the most popular turbulence models, adopted in the CFD community, are mainly Direct Numerical Simulation (DNS), Large Eddy Simulation (LES) and Reynolds-Averaged Navier-Stokes (RANS). The DNS method today requires a large amount of computing resources and time. The LES method is more appropriate for 3-D simulations. Therefore, the only method adopted for this 2-D numerical study was the RANS method. The three RANS turbulence methods analysed, due to low computational costs, are: the standard k-ω model, the standard k-ε model and the SST model. A more detailed description about the turbulence methods can be found in the book by Wilcox [17].

3. Results

In this section of the paper a number of numerical simulations are analysed for different TSRs. The numerical simulations obtained during the present study are mainly compared with the study carried out by Wang et al. [16], as this previous numerical study showed a good agreement with experimental data. However, it should be point out few differences between the two numerical studies. The main differences are summarised and listed in Table 4.

In this numerical study, a number of cycles of the rotor were calculated at different TSRs until a periodic solution was achieved. The total time was set to be 4s to give enough time for the rotor to reach a period state in all four cases.

Table 4. Main differences between the two numerical methods

Present Study	Wang et al. Study
ANSYS CFX	FLUENT
Rotor with 3 blades and central mast	Single pitching blade
Free-stream turbulence intensity 5%	Free-stream turbulence intensity 0.25%
Variable time step with angular velocity	Constant time step
Triangle elements	Quadrilateral elements
$\alpha=\arctan(\sin\theta/\lambda-\cos\theta)$	$\alpha=10^0+15^0\sin(\omega t)$
Wake interactions	No wake interaction
No converged steady state	Initial input from converged steady state

In Fig. 2 and Fig. 3, the left side, show graphically the results obtained for this numerical analysis, while the right side compare the CFD results of Wang et al. with experimental data by Lee and Gerontakos [18]. Furthermore, Fig. 2 and 3 show how the lift and the drag coefficients, C_l and C_d, are affected by different angles of attack and TSRs. The curve shapes are in good agreement with the experimental data obtained by Lee and Gerontakos. Here, the final results are more realistic and less fluctuating than the CFD simulation conducted by Wang et al [16]. Also, a strong instability at high angles of attack is observed and is thought to be due to the deep dynamic stall that is typical for low TSRs. However, the few exceptions are the absence of a second peak on the curves due to the presence of a trailing edge vortex and the lack of intersection points between upstroke and downstroke paths that are seen in the experimental graphs on the right.

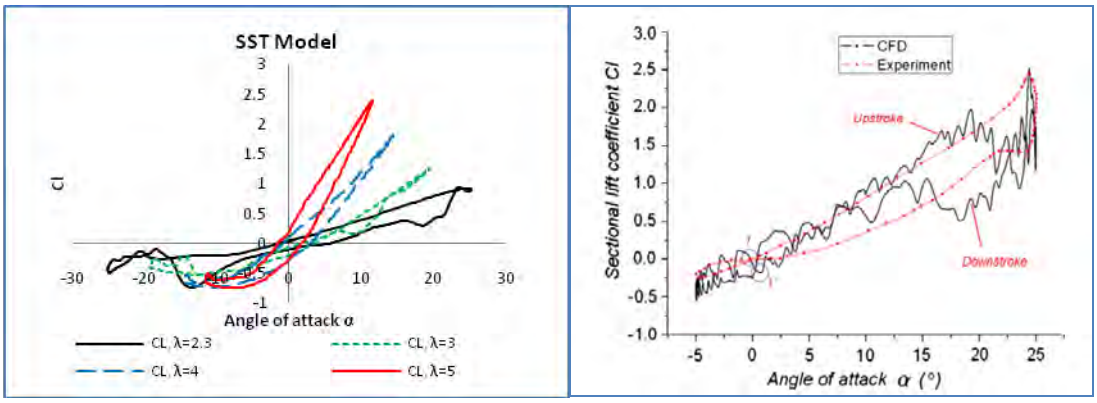

Fig. 2. Lift coefficient C_L for the two numerical studies and experimental data

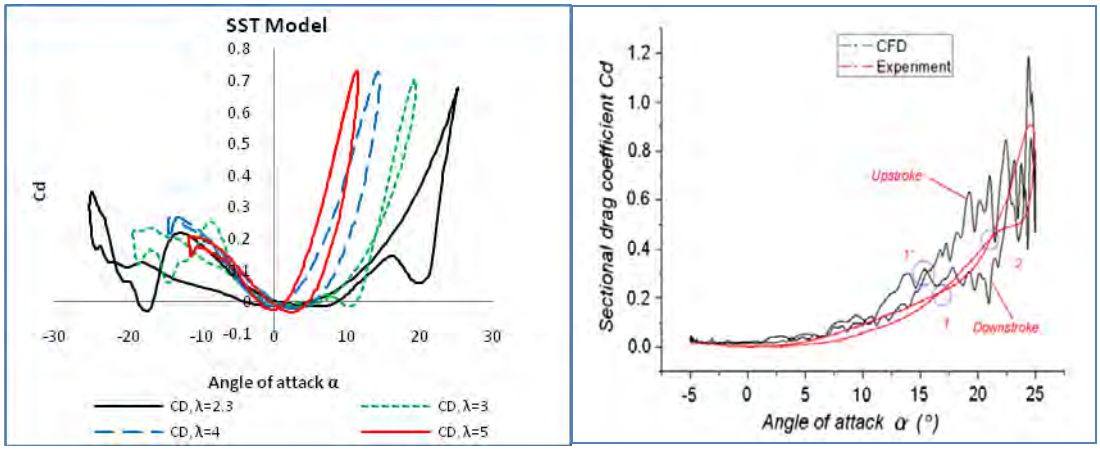

Fig. 3. Drag coefficient C_D for the two numerical studies and experimental data

However, the development of several peaks, especially for negative angle of attacks and low TSRs can be associated with the development of upstream wakes that will interact with the downstream blades. Also the presence of a central mast will generate several wakes that will affect the flow downstream. The different hysteresis loops in Fig. 2 and 3, show clearly the development of two phenomena called dynamic and static stall. Dynamic stall typically will develop at high angle of attacks for $\lambda<4$ and is characterised by its fluctuating nature, while static stall will take place at low angle of attacks for $\lambda \geq 4$ with smoother curves and less intersection points. One important consideration is that the range of angle of attack is different from the experimental data obtained by Lee and Gerontatos. This is mainly due to the use of Eq. (1) instead of using $\alpha=10^0+15^0\sin(\omega t)$ that is typically adopted for the case of a pitching motion single blade.

Finally, the numerical results are analysed by comparing the evolution of the shed vorticity with the experimental data available in the field of dynamic stall. Fig. 4 shows the vorticity field at $\theta=120^0$ for the three turbulence methods adopted in this numerical study. The SST method shows a good agreement with the experimental data obtained by Ferreira et al. [19] and Wang et al. [16] than the k-ω and k-ε methods that are more dissipative. This turbulence method is able to show the generation of specific vortices at the leading and trailing edges respectively. A more detailed explanation will be given in the next section for the SST method, as the results best agreeing with experiments

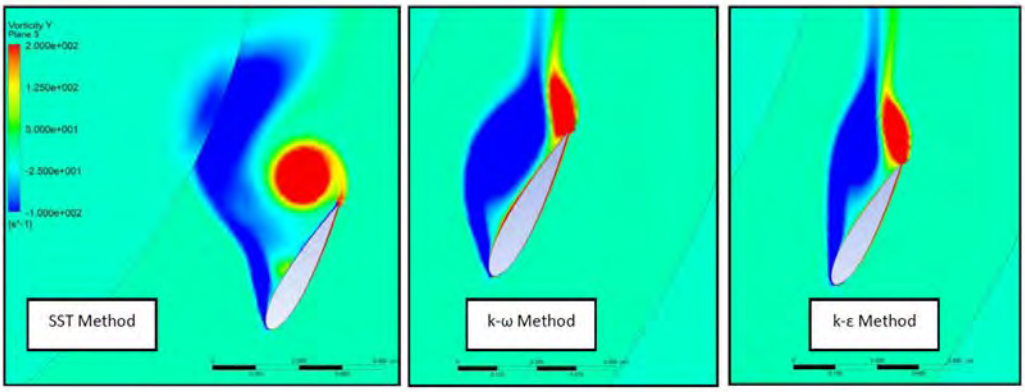

Fig. 4. Vorticity field for θ=120º for the three different turbulence methods

3.1. SST Results

In this section only the SST method is analysed in its several stages during a complete revolution of the rotor when a periodic solution is achieved. Fig. 5 clearly shows the several stages involved through dynamic stall for a TSR of 2.3 at different azimuth angles θ. This specific TSR was chosen because it corresponds to the case with deep stall. Fig.5 shows that for an azimuth angle θ between 180^0 and 240^0 the flow is almost attached to the blade. Then at an angle of $\theta=260^0$ a leading edge vortex will start to develop and expand until 280^0. Also, in this stage there is the generation of a trailing edge vortex that will detach at approximately 300^0. Afterwards, there is a progressive reattachment of the flow to the blade with leading and trailing edge vortices moving downstream. At $\theta=360^0$ there is again the presence of a second small leading and trailing edge vortices that will disappear between 20^0 and 40^0. Then the development of a third leading edge vortex will take place at 60^0 followed by a trailing edge vortex at 80^0. Finally, the flow will start to become laminar and to reattach to the blade until the same dynamics will start again from the beginning stage. From the final results it can be stated that the SST model shows a good agreement with the four stages related to dynamic

stall mentioned above. Furthermore, this 2-D study has the advantages of showing how the two kinds of vortices will move down and eventually affect the physics of the blades that are called to work downstream.

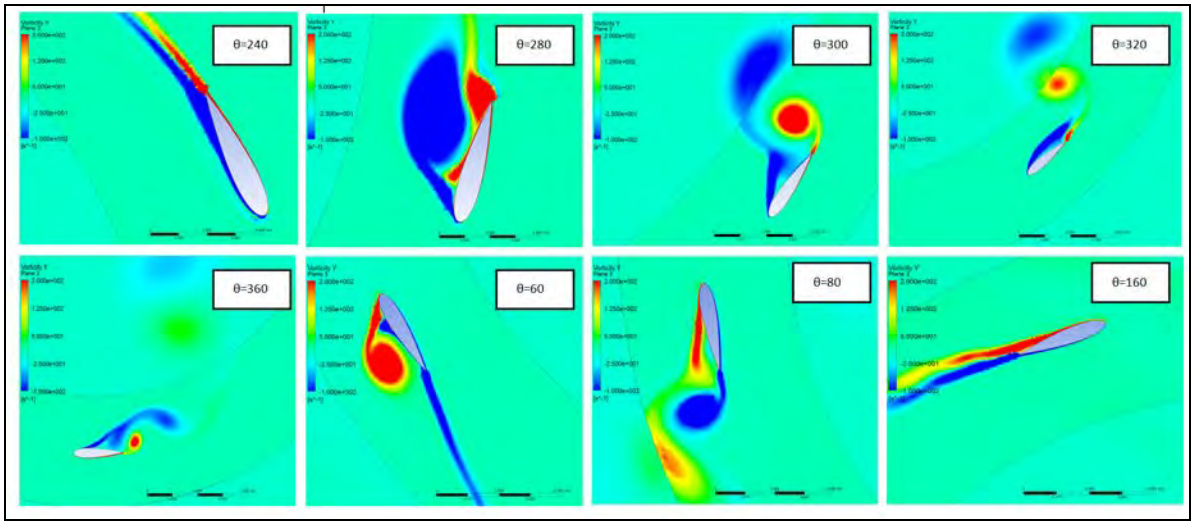

Fig. 5: Vorticity field at different azimuthal angles θ for the SST model at λ=2.3

4. Conclusions

A numerical analysis of the physics involved during dynamic stall of a rotor of a straight-bladed VAWT, composed of 3 bl ades with profile NACA0018, was conducted at four different TSRs. In this study three RANS turbulence models have been explored for the four cases analysed. The lift and drag coefficients are in good agreement with the study carried by Wang et al, but a number of differences have been found between the two studies. The most relevant are the absence of a second peak on the curves due to the development of the trailing edge vortex and the lack of intersection points at high TSRs. But at low TSRs there is an increase in the number of intersection points especially for negative angles of attacks that can be related to deep dynamic stall. This instability is mainly associated with the development of upstream wakes from upstream blades and mast that interact with the downstream blades. In this numerical study, the analysis has proved the presence of two different phenomena called dynamic and static stall that are highly depended on the TSRs adopted. In here the SST model is examined in terms of vorticity distributions around the blades. In general the method shows more reasonable accuracy with some existing wind tunnel experiments than the k-ε and k-ω turbulence methods that seem to be more dissipative. Also, the method is able to show the main four phases involved during dynamic stall. But one important observation for the SST method is the presence of single-vortices instead of having several small vortices that are typically found around the airfoil for PIV dynamic stall tests. A better improvement can be achieved in the future investigation of a 3-D case where the LES and the DES methods are strongly recommended. The two methods will take into consideration the 3-D nature of the vortices developed during dynamic stall. In general this paper gives a substantial contribution to the aerodynamics involved at different TSRs and angles of attack for a 2-D rotor with central mast. This is necessary because the development of dynamic stall in VAWTs can have a substantial impact on both the design and power generation of a wind turbine.

References

[1] K. Pope et al., Effects of stator vanes on power coefficients of a zephyr vertical axis wind

turbine, Renewable Energy, 2009, pp. 1-9.

[2] J. Knight, Urban wind power: Breezing into town, Nature, vol. 430, no. 6995, 2004, pp. 12-13.

[3] S. Mertens, Wind energy in the built environment: concentrator effects of buildings. TU Delft, 2006, pp. 3-14.

[4] R. Howell, N. Qin, J. Edwards, and N. Durrani, Wind tunnel and numerical study of a small vertical axis wind turbine, Renewable Energy, vol. 35, 2010, no.2, pp. 412-422.

[5] A. Mewburn-Crook, The Design and development of an augmented vertical wind turbine, School of Mechanical, Aeronatical and Production Engineering, 1990, pp. 1-59

[6] S. Stankovic, N. Campbell, and A. Harries, Urban Wind Energy. Earthscan, 2009.

[7] C. J. Ferreira, G. van Bussel, and G. van Kuik, 2D CFD simulation of dynamic stall on a Vertical Axis Wind Turbine: verification and validation with PIV measurements, presented at the 45th AIAA Aerospace Sciences Meeting and Exhibit, 2007, pp. 1-11.

[8] C. Hofemann, C. J. Simao Ferreira, G. J. Van Bussel, G. A. Van Kuik, F. Scarano, and K. R. Dixon, 3D Stereo PIV study of tip vortex evolution on a VAWT, 2008, pp. 1-8.

[9] G. Marsh and S. Peace, Tilting at windmills: Utility-scale VAWTs: towards 10MW and beyond? , Refocus, vol. 6, no. 5, 2005, pp. 37-42.

[10] G. Marsh, Wind turbines: How big can they get? , Refocus, vol. 6, no. 2, 2005. , pp. 22-28.

[11] C. J. Simão Ferreira, A. van Zuijlen, H. Bijl, G. van Bussel, and G. van Kuik, Simulating dynamic stall in a two-dimensional vertical-axis wind turbine: verification and validation with particle image velocimetry data, Wind Energy, vol. 13, no. 1, 2010, pp. 1-17.

[12] ANSYS Meshing: Application Introduction, ANSYS, 2009.

[13] N. Fujisawa and S. Shibuya, "Observations of dynamic stall on Darrieus wind turbine blades," Journal of Wind Engineering and Industrial Aerodynamics, vol. 89, no. 2, 2001, pp. 201-214.

[14] J. Larsen, S. Nielsen, and S. Krenk, Dynamic stall model for wind turbine airfoils, Journal of Fluids and Structures, vol. 23, no. 7, 2007, pp. 959-982.

[15] J. A. Ekaterinaris and M. F. Platzer, Computational prediction of airfoil dynamic stall, Progress in Aerospace Sciences, vol. 33, no. 11, 1998, pp. 759-846.

[16] S. Wang, D. B. Ingham, L. Ma, M. Pourkashanian, and Z. Tao, Numerical investigations on dynamic stall of low Reynolds number flow around oscillating airfoils, Computers & Fluids, vol. 39, no. 9, 2010, pp. 1529-1541.

[17] D. C. Wilcox, Turbulence Modeling for CFD. DCW industries La Canada, 2006.

[18] T. Lee and P. Gerontakos, Investigation of flow over an oscillating airfoil, Journal of Fluid Mechanics, vol. 512, 2004, pp. 313-341.

[19] C. J. Simão Ferreira, A. van Zuijlen, H. Bijl, G. van Bussel, and G. van Kuik, Simulating dynamic stall in a two-dimensional vertical-axis wind turbine: verification and validation with particle image velocimetry data, Wind Energy, vol. 13, no. 1, 2010, pp. 1-17.

Simulation and technical comparison of different wind turbine power control systems

Mojtaba Tahani[1], Iman Rahbari [2,*], Samira Memarian[2], Saeedeh Mirmahdian[3]

[1] *Iran University of Science and Technology, Tehran, Iran*
[2] *Semnan University, Semnan, Iran*
[3]*Islamic Azad University of Arak, Arak, Iran*
** Corresponding author. Tel: +989128021976, E-mail: rahbarii2@asme.org*

Abstract: wind as a significant renewable source of energy along with different ways for its optimum utilization is attended. At this paper, initially different types of wind turbine power control systems are introduced briefly, then advantages and disadvantages of them, are evaluated in practical and theoretical aspects. At the following, governing generated power formulation is proved briefly, then the effective parameters on power, e.g. wind velocity, wind temperature are studied and simulated in MATLAB software. Then practical data from an actual stall control wind turbine entered and related curves are investigated. Based on these data, performance of an actual pitch control wind turbine is estimated and related curves are investigated. At the following, using Weibull theory, real power-time curve and estimated power-time curve, monthly produced energy of turbines are estimated. And finally Specific Power Performance (SPP) is defined and shown that pitch control system produced energy more than stall control system at the same rotor swept area.

Keywords: *Wind Turbine, Power Control System, Pitch Control, Stall Control*

1. Introduction

The human progresses in various scientific and industrial fields have increased the need to generate energy and to investigate its various resources. Providing this energy from fossil sources like oil and gas is not reasonable because of various reasons such as environmental pollutions, reduction of reservoir of these resources and the next generation's requirements for them. These facts along with economic problems and the increment of fuel cost have encouraged the researchers in various countries to pay more attention to renewable energies. Therefore, the wind, as one of the renewable energy resources, and its optimal exploitation methods, have been noticed so that the predictions indicate that in 2020 the portion of wind in generating the energy required for human activities will be more than 375 TWh. The design of wind turbines depends on the conditions of the location they are installed, and most of them are designed to generate power with the minimum possible cost at low wind speeds. Thus, if the wind speed exceeds a specified limit, some of the important parts of turbine may be harmed. The designers use various control systems to prevent these harms and also to optimal exploitation of turbines. The most important control systems are stall control, pitch control, and yaw control, from which the pitch control is the most common system [1 to 3] .

Of course, some researches were also performed to design other control systems. One of them is "control of wind turbine using memory based method" by Song [4]. Using this method, the turbine chooses the optimal power control method based on the previous experienced conditions. Another new method was also presented in the paper titled as "multi variable control strategy for variable speed variable pitch" by Bakhezzar et al. [5] . Using the doubly fed induction generator to control the voltage induced by rotor in the generator has been noticed by the researchers in the recent years. Fernandez and Garcia investigated this subject in a paper titled as "comparative study on doubly fed induction generator (DFIG) wind turbines operating with power regulation" [6] . Modeling and controlling this type of generators were performed by Hee Song Ko [7] .

In this paper, the control systems of wind turbines were investigated comprehensively. In addition to theoretical facts, technical and empirical points were also involved. Furthermore, the power generated by different control systems was compared in this study. The effect of local conditions of the place considered for installing the turbine, such as wind blowing conditions, on the selection of the appropriate control system was also discussed in this paper.

2. Investigation of generated power

The one-dimensional BEM theory was used to investigate the power generation of wind turbines [3] . Based on this theory, the rotor of wind turbine can be modeled as an ideal impenetrable disk. Because there is no friction between air and the rotor, and the wake flow speed has no rotational component. The shape of stream lines thorough the rotor will be similar to figure (1). This disk decreases the speed from V_0 at the upstream to u at the rotor plate, and to u_1 at the back of rotor. At normal speeds, the flow can be assumed incompressible, and the speed and pressure variations can be assumed as shown in figure (1) .

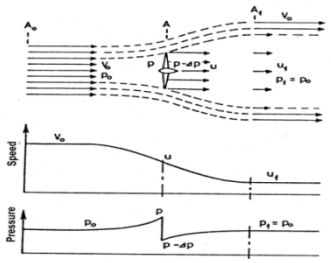

Fig. 1. Demonstration of streamlines, axial speed and pressure up- downstream of rotor.

Using axial momentum equation, it can be proved that:

$$u = \frac{1}{2}(V_0 + u_2) \tag{1}$$

Also, the usable power in a cross section area equal to the area swept by rotor (A) is:

$$P_{avail} = \frac{1}{2}\rho A V_0^3 \tag{2}$$

The dimensionless power coefficient is obtained by dividing the power by the usable power:

$$C_P = \frac{P}{\frac{1}{2}\rho V_0^3 A} \tag{3}$$

And finally, the induction factor is defined as:

$$u = (1-a)V_0 \tag{4}$$

It can be observed that for $a = 1/3$, $C_{P,\max} = 16/27$.

3. Investigation of power control systems

3.1. Stall control systems

Blade design of this type of turbines is so that they naturally control the power generated by turbine. These rotors with constant pitch are designed to operate near the optimal tip speed in moderate winds. In turbines with this type of control system, an asynchronous generator is often used by which the rotor rotational speed is kept approximately constant. A rotating tip located at the end of the rotor is usually used as the aerodynamic brake. This device which is activated by centrifugal force, is subjected against the wind flow with a 90° angle, and limits the rotor momentum by applying the opposite torque due to the drag force.

3.2. Pitch control systems

In a turbine with pitch control system, all blades can rotate about the root, and thus, the attack angle changes simultaneously throughout the rotor length. One of the most conventional mechanical mechanisms of the rotor pitch control contains a piston inserted inside the turbine main shaft. This piston changes the rotor pitch by its reciprocating movement using a mechanism installed forward the turbine hub. Obviously, the lift coefficient has a direct relation with the attack angle [1] . Therefore, decreasing the attack angle reduces the lift force and the power. Thus, pitch control system can control the output power by rotating the rotors. Also, referring the power curve of this type of turbines, it is obviously found that since the rotors can rotate slowly, the power curve is smoother and the power peaks are reduced [3] . To overcome the problem caused by great peaks in power for high speeds in a wind turbine with pitch control system, a system named as "OptiSlip" produced by Vestas was used.

From technical point of view, using pitch control mechanisms to control power necessitates the use of very strong hydraulic systems to generate and transfer very high pressures (120 Bar for medium wind turbines, and even more for greater turbines). Providing this hydraulic system affects the turbine total price. In places with high air turbulence, the pitch control system should operate harder. This results in overheating the hydraulic oil, and finally, lengthy turbine stops by safety system. This reduces the turbine productivity.

3.3. Active stall control systems

There is another method which uses the combination of pitch and stall control systems. In this system, to achieve the maximum efficiency at low wind speeds the rotors are repositioned like a wind turbine controlled by pitch. At high speeds, the rotors are rotated slowly against the wind to get stall. With this type of control, a smoother limited power is achieved compared with pitch control turbines. Combining both systems facilitates the required stops in emergency cases and restarting wind turbines compared with stall control. This type of system is less common today [2] .

3.4. Yaw control systems

In this control system, instead of limiting the output power using pitch or stall controls, the turbine yaw is controlled. The machines which use pitch and stall control systems usually have yaw control. This system receives the data related to wind flow direction from the turbine wind gauge and tries to turn the nacelle so that the maximum air flow rate enters the rotor disk. In a machine controlled by yaw system, at high wind speeds, the rotor turns against the wind direction to reduce the air flow rate in rotor, and thus, the generated power decreases.

4. Study procedure

4.1. Weibull distribution method theory and its application in estimating the available wind electricity energy generation

Considering the random nature of wind with long-term measurements in various time periods, Weibull Density Function was used to compute the wind energy [8] .

$$F(V) = \frac{k}{c}\left(\frac{V}{c}\right)^{k-1} e^{-\left(\frac{V}{c}\right)^{k}} \tag{5}$$

F (v), the cumulative distribution function, is:

$$F(V) = 1 - e^{-\left(\frac{V}{c}\right)^{k}} \tag{6}$$

Where V is the wind speed, c and k are scale parameter and shape parameter, respectively. These parameters can be computed using "Maximum likelihood" method with iteration from the following equations:

$$k = \left(\frac{\sum_{i=1}^{n} V_i^{k} Ln(V_i)}{\sum_{i=1}^{n} V_i^{k}} - \frac{\sum_{i=1}^{n} Ln(V_i)}{n} \right)^{-1} \tag{7}$$

$$c = \left(\frac{1}{n}\sum_{i=1}^{n} V_i^{k}\right)^{\frac{1}{k}} \tag{8}$$

Where V_i , is the speed at time period i and n is the number of the wind non-zero speeds. The continuous distribution of wind flow in the studied region is obtained using Weibull curve. The generated energy is estimated by combining this curve and the power curve of wind turbines. The energy of a wind turbine in a month is investigated by following equations:

$$E_{Month} = N_0 \int_{V_{Cut-In}}^{V_{Cut-Out}} P(u)\, f(u)\, du \tag{9}$$

Where N_0 is 744 hours/month, f(u) is Weibull function and P(u) is power curve.

4.2. Location of study

Location of the present study was Paskulan wind farm in Manjil, a city in Iran. Its pressure can be assumed about 1 Atmosphere with a good precision. The average air temperature during the test period was $13.67^{\circ}\mathrm{C}$. Therefore, the average air density was $1.231\,\mathrm{kg/m^3}$.

4.3. Wind blow condition

Since the wind patterns of a region repeat annually, the Weibull curve obtained in March 2003 [9] can be used to estimate the wind condition in March 2009 with a good accuracy. Based on this curve, weibull shape parameter (k) was 1.68, weibull scale parameter (A) was 11.7 m/s and average wind velocity was 10.4 m/s. As mentioned before, stall and pitch control

systems are more applicable compared with the other control systems. Thus, in the following was concentrated on the sample turbines with these two control system types.

First, based on Eq. (3), the effective parameters on the power generated by turbine considering the weather conditions of the studied region were simulated in MATLAB software for two turbines with different control systems.

The first turbine is of 550 kW type and was made by NEG-MICON Company. It uses stall control system. The second turbine is of V47-660 kW type and was made by Vestas Company. It uses pitch control system and is equipped with OptiSlip. The power curves of above turbines for the ideal case and for the air conditions of the mentioned wind farm were shown in figures (2).

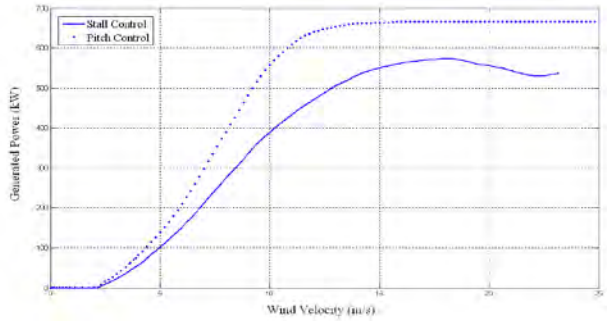

Fig. 2. Ideal power curve wind turbines.

For 550 kW wind turbine, it's obvious that maximum generated power, is 550 KW occurs at 18 m/s. Power curve after reaching to maximum point, will be decreased. In the following, this curve will be compared with practical curve. For 660 kW wind turbine, it can be obviously observed that the power generated by the turbine is uniform compared with the past and remains constant after reaching the maximum value. This maximum power value occurs at speed of 15 m/s.

In the following, the power generated by 550 kW turbine is investigated in the real mode. The values used in this section were recorded by the logger located on these turbines. This system measures and records the turbine generated power data, wind speed, wind temperature, and some other parameters with 10 minute time intervals, And during the studied time period 4463 time intervals were recorded that, the turbine was active only during 1501 intervals. During the other intervals, the turbine was in stop mode due to maintenance and blowing wind with very high speeds (cut-out), or other unforeseen characters. In figure (3), the real generated power was shown versus the active times.

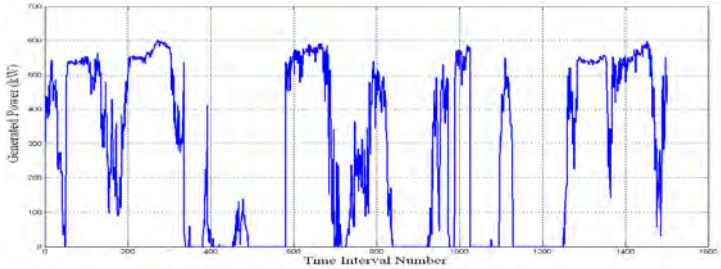

Fig. 3. Demonstration of Power vs. Time intervals for stall control wind turbine in real mode.

The power curve for active time intervals was shown in figure (4).

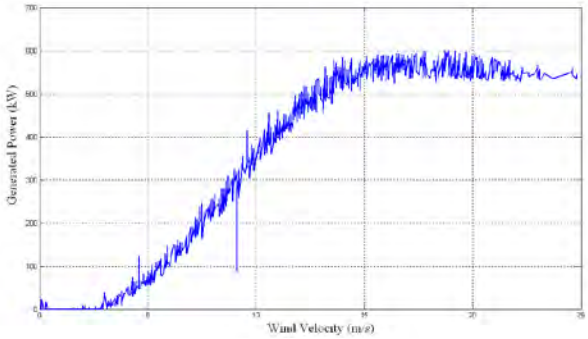

Fig. 4. Demonstration of Power curve for stall control wind turbine in real mode.

Comparing figures (2) and (4) reveals that there is a marked difference between the power generated in real mode and the power computed in ideal mode obtained with constant power values presented by the manufacturer and based on the weather conditions of the studied location.

The reason of this difference is that the turbine characteristics presented by the manufacturer (such as power coefficient and power curve based on standard DIN ISO 2533) are related to the generated power of 550 kW, but in fact, the turbine maximum mechanical power is 600 kW (about 10% more than the nominal power), and it was observed that with turbine optimum operation, this maximum value of power is exploitable.

The percentage error curve versus the wind speed was shown in figure (5).

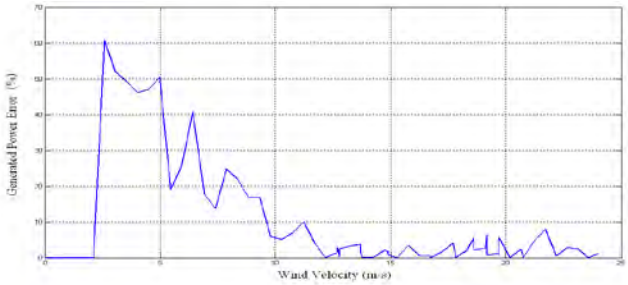

Fig. 5. The percentage error curve versus the wind speed for stall control wind turbine.

As shown in this figure, at speeds lower than 2.5 m/s the turbine does not start to operation to generate remarkable power, thus, there is no percentage error. At near cut-in speeds, the percentage error is very high. The reason is the small value of generated power; therefore, it's not noticeable. It can be observed that the percentage error reduces with increasing speed and remains lower than 10% after the speed of 10 m/s.

Based on equation (9) and using trapezoidal numerical integrating method for the studied time period, 224110 kWh of energy generation was estimated.

By computing the area under the power-real time curve by trapezoidal numerical integrating method, the real power generated during this time period reached 68672.9 kWh. Considering the fact that turbine was active only in 1/3 of the time period, if assumed the turbine will operate in such a way this time interval, estimated energy using this method and Weibull function has 9.758 % variations. Now assume the pitch regulated turbine installed in the previous location and subjected to the previous wind conditions. Assuming that the turbine

stop time, due to periodical repairs or possible malfunctions and not generating power at speeds more than cut-in value, is equal to the corresponding value of stall controlled turbine, and the turbine operates in ideal conditions, the power-time curve of this turbine was estimated by figure (6).

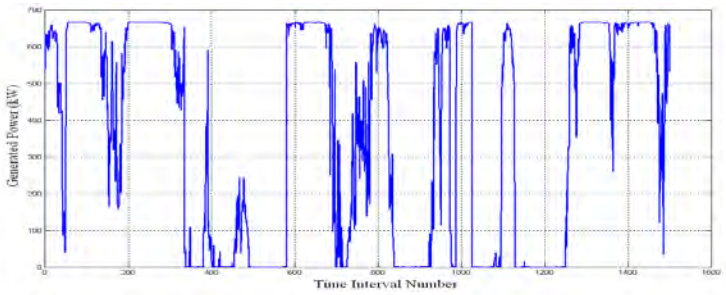

Fig. 6. Estimated Power Vs. Time intervals for pitch control wind turbine.

Comparing figures (6) and (3) obviously reveals that the variations of the power generated by pitch controlled turbine are very smaller than the corresponding values of stall controlled turbine. By numerical integrating in this period, it was found that 90670 kWh of energy is exploitable from this turbine.

Based on Weibull theory and using equation (6) and trapezoidal numerical integrating method for the studied time period, 299690 kWh of energy generation was estimated.

Considering the fact that the turbine was active during 1/3 of the period, the estimated value by Weibull theory has a good consistency with the value estimated using power curve. If assumed the turbine will operate in such a way this time interval, estimated energy using this method and Weibull function has 11.1634 % variations.

By defining Specific Power Performance (SPP) as follows, the value of this parameter for pitch controlled and stall controlled turbines were presented in table (1).

$$SPP = \frac{Generated\ Energy \quad (Kwh)}{Rotor\ Swept\ Area \quad (m^2)} \tag{10}$$

Table 1. Specific Power Performance for various turbines

Type of Power Control system	Rotor Swept Area	SPP based on Weibull function	SPP based on power-time curve
Stall Control	1325 m^2	169.13	154.1
Pitch Control	1735 m^2	172.73	155.38

As it can be observed, the value of Specific Power Performance for wind turbines using pitch control system is about 0.8 - 2.13% greater than the corresponding value of the wind turbines using stall control system.

5. Conclusion

In this study, the governing generated power formulation was first proved. Then, the types of power control systems were investigated theoretically and practically. It was found that selecting the appropriate power control system for optimum exploitation of turbine depends on the conditions of the intended location to install the turbine. It's possible that using pitch

control system results in turbine failures due to the numerous times of operation; and thus, it reduces the turbine efficiency. Then, Weibull theory for estimating the energy generated by turbine was introduced and investigated. Then, power curves of two different wind turbines under the wind conditions of the studied region sketched using MATLAB. Then, the practical values of energy and power generated by stall controlled turbine were obtained and investigated based on the data received from the turbine installed in the region. Then, the power and energy generated by pitch controlled turbine were estimated. Finally, by defining Specific Power Performance and comparing two different control systems, it was found that SPP Value for pitch controlled turbine is about 0.8-2.13% greater than the corresponding value of stall controlled turbine. In choosing the appropriate wind turbine for installation in a site, this low difference along with more prices also should be considered.

References

[1] Erich Hau, Wind turbines, fundamentals, technologies, applications, economics, Springer, 2nd Edition, 2005, pp. 73 – 88.

[2] Thomas Ackermann, Wind power in power system, John Wiley and Sons, 2005, pp. 13-20.

[3] Martin O. L. Hansen, Aerodynamics of wind turbine, EarthScan, 2008, pp. 39 – 48.

[4] Y. D. Song, Control of wind turbines using memory based method, journal of wind engineering and industrial aerodynamics 85, 2000, pp. 263-275.

[5] B. Boukhezzar, L. Lupu, H.Siguerdidjane, M. Hand, Multivariable control strategy for variable speed variable pitch wind turbine, Renewable energy journal 32, 2007, pp. 1273–1287.

[6] L. M. Fernandez, C. A. Garcia, Comparative study on performance of control systems for doubly fed induction generator (DFIG) wind turbines operating with power regulation, Energy journal 33, 2008, pp. 1438 – 1452.

[7] Hee - Song Ko, Gi- Gab Yoon, Won Pyo Hong, Modeling and control of a DFIG based variable speed wind turbine, Electric power research 78, pp. 1841 – 1849.

[8] Eyad S. Hrayshat, Wind availability and its potentials for electricity generation in Ta. la, Jordan, Renewable and Sustainable Energy Reviews Journal 9, 2005, pp. 111- 117.

[9] M. Sharifi, Application of Weibull function in estimation of produced energy by wind turbines in Iran, Proceedings of 21st International Power System Conference 2003, 2190-2197.